

**A 3D Morphological Analysis of the Ontogenetic Patterning of Human Subchondral
Bone Microarchitecture in the Proximal Tibia**

DISSERTATION

Presented in Partial Fulfillment of the Requirements for the Degree Doctor of Philosophy
in the Graduate School of The Ohio State University

By

Jesse Roberto Goliath, B.A, M.A.

Graduate Program in Anthropology

The Ohio State University

2017

Dissertation Committee:

Professor Samuel Stout, Advisor

Professor James Gosman

Professor Mark Hubbe

Professor Clark Larsen

Professor W. Scott McGraw

Copyrighted by
Jesse Roberto Goliath
2017

Abstract

The objective of this research was to test the hypotheses that ontogenetic patterns of change in tibial subchondral trabecular and cortical bone microstructure are age and condyle site-specific due to differential loading associated with changing joint kinetics and body mass. High-resolution computed tomography (HR-CT) images were acquired for 31 human tibiae, ranging in age from 8 to 37.5 years. The skeletal samples are from Norris Farms #36 site, a cemetery mound in the central Illinois River valley associated with the Oneota culture, dating to A.D. 1300. This bioarchaeological sample was chosen for this study because of its cultural and biological homogeneity, high number of subadult individuals, extensive archaeological context, and excellent preservation. Proximal epiphyses were digitally isolated for analysis as regions of interest (ROIs) using Avizo Fire 6.2 and 8.1.1. 3D resolution-corrected morphometric analysis of subchondral bone architecture was performed for 11 cubic volumes of interest (VOIs) using the BoneJ plugin for ImageJ. VOIs were positioned within and between the tibial condyles within the epiphyseal region. The analysis of the subchondral cortical plate was accomplished through dual-threshold cortical masking.

Ontogenetic patterns in the epiphysis of the proximal tibia were described using eight 3D morphological parameters: bone volume fraction (BV/TV), mean trabecular thickness (Tb.Th), mean trabecular spacing (Tb.Sp), structure model index (SMI),

connectivity density (Conn.D), degree of anisotropy (DA), trabecular number (Tb.N), and cortical thickness (Ct.Th) in the subchondral cortical plate. Kruskal-Wallis and Wilcoxon signed rank tests were used to examine the association between region, age, and each of the eight structural parameters. For analysis, individuals were divided into four age categories: child, adolescent, young adult, and middle age. The findings of this study indicate that age-related changes in mechanical loading have heterogeneous effects on trabecular bone morphology within the proximal tibia. Specifically, there were significant differences in BV/TV ($\alpha = 0.033$), Conn.D ($\alpha = 0.001$), DA ($\alpha = 0.012$), and Plate Ct.Th ($\alpha = 0.000$) across age. With age, subchondral trabecular microstructure increased in bone volume fraction and degree of anisotropy, and decreased in connectivity density. In the subchondral cortical plate, there is an age-related increase in thickness. When comparing condylar regions, only the degree of anisotropy significantly differed ($\alpha = 0.004$) between medial and lateral condyles. The trabeculae in the medial condyle were more anisotropic than the lateral region.

These results indicate that age-related changes in loading have varied effects on subchondral cortical and trabecular bone morphology within the proximal tibia. More specifically, trabeculae in the medial condyle are likely more directly influenced by loading than trabeculae in the lateral condyle during growth. Ultimately, trabeculae in the epiphyseal region are likely more directly influenced by mechanical forces during growth. The differential response of trabecular bone to changing mechanical loads during growth and development serves as a powerful tool to evaluate the significance of mechanical loading on adult trabecular bone morphology. Understanding the spatial

specifics of ontogenetic processes during subchondral bone development can offer insights into adult morphological variation in joint health and disease.

Dedication

To my family – everything I am I owe to you.

Acknowledgments

This research would not have been possible without the support of many individuals and institutions. First, I would like to acknowledge the members of my dissertation committee, whose mentorship and assistance have been essential to my success: Dr. Sam Stout (my advisor); Dr. James Gosman, Dr. Mark Hubbe, Dr. Clark Spencer Larsen, and Dr. W. Scott McGraw. I want to thank Dr. Stout for introducing me to the field of skeletal biology and for guiding me through my graduate career. I am also grateful to Dr. Gosman for giving me the opportunity to work with the TBLO project, and for his guidance and knowledge of the subjects of skeletal ontogeny and micro-CT analysis.

Dr. Timothy Ryan of Pennsylvania State University who allowed me the use the Norris Farms CT data for and several current and former members of his research laboratory (including Simone H. Sukhdeo, Colin Shaw, Bernadette Perchalski) contributed to this project by sharing data, co-developing methods, and providing general encouragement and general troubleshooting assistance.

Tim Stecko at the PSU Center for Quantitative Imaging who performed much of the CT scan acquisition that constitutes the raw data used in this study. As well as, Terrance Martin and Dee Ann Watt of the Illinois State Museum and Dr. George R

Milner of Pennsylvania State University who granted permission for CT scan acquisition of the Norris Farms skeletons.

Financial support from the National Science Foundation (awarded to Dr. James H. Gosman [BCS-1028793] and Dr. Timothy M. Ryan [BCS-1028904]) funded the original CT scan acquisition and my position as Graduate Research Associate on the Trabecular Bone Locomotor Ontogeny Project. Additional financial support in the form of travel and research awards was received from OSU Department of Anthropology, OSU Graduate School, American Association of Physical Anthropologists, American Anatomical Association, and American Society for Bone and Mineral Research.

Several thanks also go to the following individuals: Dr. Zac Hubbell for helping train me to use Avizo Fire and being a constant source of troubleshooting support. Dr. Meghan-Tomasita Cosgriff-Hernandez for her friendship, encouragement and support, since the beginning of my graduate school career. Cyndi Freeman for giving me the opportunity to mentor incredible students and becoming a life-long friend and member of the family. David Sweasey for all his technical support and computer restoration. Erin and Tim Sefczek for their friendship, support, and allowing me to be a part of their family as “Uncle Jesse” to Lucas and Owen. Aaron Comstock, Amy Koogler, Barbara Betz, David Carey, Eddie Walsh, Leigh Oldershaw, Marissa Stewart, Nate Patrick, Naveen Turlapati, Rama Gottumukkala, Saskia Richter, Victoria Dominguez and countless others for their friendship and constant cheerleading. Finally, I want to thank you Mami, Papi, Gabe, and Nick for your constant guidance, encouragement, and support.

Vita

- 2003.....Charleston Catholic High School,
Charleston, WV
- 2007.....B.A. Honors Anthropology, University of
Notre Dame
- 2010.....M.A. Anthropology, The Ohio State
University
- 2009 - 2012Graduate Teaching Associate, Department
of Anthropology, The Ohio State University
- 2013 - 2016Graduate Administrative Associate,
Graduate School, The Ohio State University
- 2015 - 2016Graduate Research Associate, Department
of Anthropology, The Ohio State University

Publications

Goliath JR, Stewart MC, Stout SD. 2016. Variation in Osteon Histomorphometrics and Their Impact on Age-at-Death Estimation in Older Individuals. *Forensic Sci Int* 262: 282.e1-282.e6.

Stewart MC, Goliath JR, Stout SD, Hubbe M. 2015. Intraskletal Variability of Relative Cortical Area in Humans. *Anat Rec* 298(9): 1635-1643.

Stewart M, McCormick L, Goliath JR, Sciulli P, Stout S. 2013. A Comparison of Histomorphometric Data Collection Methods. *J Forensic Sci* 58: 109-113.

Fields of Study

Major Field: Anthropology

Specializations and Interests: Skeletal Biology, Bone Histology, Bioarchaeology, Forensic Anthropology, Functional Morphology, Bone Histomorphometrics, Growth and Development

Table of Contents

Abstract.....	ii
Dedication.....	v
Acknowledgments.....	vi
Vita.....	viii
List of Tables	xvi
List of Figures.....	xviii
List of Abbreviations.....	xxii
Chapter 1: Research Considerations for Study of Subchondral Bone Microarchitecture .	1
Introduction.....	1
Morphology of the Subchondral Bone.....	3
Structure.....	3
Osteochondral Junction.....	4
Function of the Subchondral Bone.....	6
Cartilage-bone interface.....	7
Subchondral Bone Influence on Osteoarthritis (OA).....	8
Primary versus Secondary Osteoarthritis.....	9

Ontogeny.....	12
Growth Studies in Archaeological Skeletal Samples.....	14
Trabecular Bone.....	15
Cortical Bone.....	16
Growth Studies in Modern Humans.....	17
Studies in Subchondral Bone Ontogeny.....	19
Human Studies.....	19
Non-human Studies	
High Resolution X-Ray Computed Tomography.....	22
Micro-CT Analysis in Comparison to Traditional Histology.....	25
Aims and Hypotheses.....	26
Summary.....	29
Organization of Dissertation.....	29
Chapter 2: Skeletal Biology and Joint Morphogenesis.....	31
Skeletal Formation.....	31
Endochondral Ossification.....	32
Longitudinal Growth.....	33
Proximal Tibial Epiphysis Development.....	36
Influence of Mechanical Loading on Epiphyseal Morphology.....	38
Hierarchical Structure of Bone.....	39
Cortical and Trabecular Bone.....	40
Woven and Lamellar Bone.....	41

Bone Cells.....	42
Growth and Modeling.....	45
Bone Remodeling.....	45
Basic Multicellular Unit (BMU).....	47
Factors Affecting Bone Remodeling.....	49
Disease.....	49
Diet and Subsistence.....	49
Mechanical Load.....	50
Cortical bone mass.....	53
Age-Related Bone Loss.....	53
Joint Morphogenesis.....	54
Articular Cartilage.....	56
Structure and Function.....	56
Synovial Joints.....	60
Tibiofemoral Joint (Knee Joint).....	62
Impact of Knee Joint Kinematics and Locomotion on Skeletal Loading..	63
Determinants of Degenerative Joint Disease.....	66
Senescence.....	68
Inflammation.....	69
Trauma/Fracture.....	69
Genetics.....	70
Summary.....	70

Chapter 3: Theoretical Implications for Functional Interpretation of Bone	
Microstructure.....	72
Historical Perspectives in Bone Functional Adaptation.....	72
Mechanostat Theory.....	74
Utah Paradigm.....	75
Mechanical Properties of Bone and Cartilage.....	76
Cartilage.....	78
Mechanical Loading Effects on Bone Surfaces.....	81
Critiques of Bone Functional Adaptation.....	83
Summary.....	84
Chapter 4: The People of the Oneota Tradition.....	85
Oneota Tradition.....	85
Broad-Spectrum Subsistence.....	85
Oneota Settlement.....	86
Sociopolitical Organization and Division of Labor.....	87
Oneota Material Culture.....	88
Norris Farms 36 Cemetery (11F ^o 2167) and Morton Village (IAS 11F1).....	88
Bold Counselor Phase.....	90
Faunal and Floral Resources at Morton Village.....	93
Physical Anthropology of Norris Farms 36.....	97
Warfare and Lethal Trauma.....	97
Genetics of Norris Farms 36 Population.....	99

Summary.....	100
Chapter 5: Materials and Methods.....	102
Norris Farms Oneota Skeletal Sample.....	102
Age-at-death and Sex Estimation.....	103
Body Mass Estimation.....	104
Principles and Procedures of CT Data Acquisition.....	105
Segmentation Process and Thresholding.....	105
Limitations of CT reconstruction.....	107
Resolution effects.....	108
Artifacts.....	109
Pennsylvania State University CQI Scanning Protocol.....	110
Digital image rendering in Avizo Fire.....	111
Region of Interest (ROI) Placement.....	114
Volume of Interest (VOI) Placement and Extraction.....	115
Subchondral Bone Structural Analysis.....	120
Trabecular Bone Morphometric Parameters.....	120
Cortical Masking.....	122
Statistical Analysis.....	130
Hypothesis 1.....	130
Justification for Age Categories.....	131
Hypothesis 2.....	132
Influence of Sex on Structural Parameters.....	133

Summary.....	133
Chapter 6: Results.....	134
Quantification of Subchondral Bone Structure.....	136
Condyle Differences.....	137
Sex Differences.....	137
Visualization of Data.....	138
Summary.....	151
Chapter 7: Discussion and Conclusions	157
Characteristics of Subchondral Bone and Plate Ontogeny.....	159
Implications of this Study.....	162
Limitations.....	165
Conclusions and Future Directions.....	168
References	170
Appendix A: Supplemental Data Tables.....	206
Appendix B: Supplemental Tables from SPSS Statistics	231

List of Tables

Table A.1 Demographic information for individuals in this study.....	207
Table A.2 Body mass estimation calculations for individuals aged 8 to 11.99 years.....	209
Table A.3 Body mass estimation calculations for individuals 15 to 37.99 years.....	210
Table A.4 VOI size and position data.....	211
Table A.5 Postcranial metrics for all individuals in this study.....	212
Table A.6 Threshold and bone morphometric variables for all VOIs in each condylar region for all individuals.....	213
Table A.7 Average bone morphometric values in each condylar region for all individuals.....	224
Table A.8 Tibial threshold values used in the cortical masking procedure for steps 1-3 of dual thresholding/segmentation in Avizo Fire 8.1.1.....	227
Table A.9 Subchondral plate mean thickness and max thickness in all individuals.....	229
Table B.1 Shapiro-Wilk Test for Normality.....	232
Table B.2 Descriptive Statistics for Variables in Lateral and Medial Condylar Regions.....	233
Table B.3 Age Category Independent Sample Kruskal Wallis Test with Bonferroni correction.....	234
Table B.4 Mean Statistics for All Variables by Age Category.....	235

Table B.5 Pairwise Related Samples Wilcoxon Signed Ranks Test for All Structural Parameters.....	236
Table B.6 Mean Statistics for All Variables by Condyle Region.....	240
Table B.7 Mann Whitney Test Comparing Structural Parameters Between Sexes.....	241

List of Figures

Figure 1.1 Photomicrograph showing osteochondral junction in a medial tibial plateau...	5
Figure 2.1 Process of Endochondral Ossification.....	33
Figure 2.2 Zones of the Epiphyseal Growth Plate	36
Figure 2.3 Hierarchical scale in bone structure	40
Figure 2.4 Zones of Articular Cartilage with Chondrocyte Morphology and Collagen Fiber Orientation.....	58
Figure 2.5 Example of a synovial joint.....	61
Figure 2.6 Example of knee alignments	64
Figure 3.1 Stress (MPa)-Strain (%) curve for a ductile material	78
Figure 4.1 Norris Farms 36 Cemetery	90
Figure 4.2 Bold Counselor Phase Oneota Sites of the Central Illinois River Valley	92
Figure 4.3 Bold Counselor Phase Jar Fragment from Morton Village with example tall rim and curvilinear trailed lines	93
Figure 5.1 Example of visual segmentation procedure using ImageJ.....	107
Figure 5.2 Example of the isosurface properties menu in Avizo Fire 8.1.1	113
Figure 5.3 Isosurface rendering of a 16 year old posterior tibia.....	113
Figure 5.4 Example of the selected ROI with VOIs placed in the epiphyseal region	115
Figure 5.5 Placement of 11 VOIs in the proximal tibia.....	117

Figure 5.6 Example of an isolated trabecular (15.5 yr old) VOI using ImageJ	117
Figure 5.7 Proximal Tibia Half Scan VOI Placements	118
Figure 5.8 Example of compressive forces between distal femur and proximal tibia	118
Figure 5.9 Example of importing image stack into ImageJ	119
Figure 5.10 Example of set scale for quantifying bone parameters.....	120
Figure 5.11 Example of a proximal tibia CT half scan.....	124
Figure 5.12 Cortical masking script (TOP) and threshold properties (BOTTOM)	125
Figure 5.13 Step one of separation script execution (highlighting bone).....	126
Figure 5.14 Step two of separation script execution (highlighting air space)	127
Figure 5.15 Final product of cortical masking procedure (transverse view) with dataset output	129
Figure 5.16 Final isosurface rendering following the cortical masking procedure	129
Figure 6.1 VOI 1 Lateral Condyle (LEFT) and VOI 6 Between Condyles (RIGHT)	138
Figure 6.2 Medial Condyle Mid-Condyle Sagittal Rendering.....	139
Figure 6.3 Medial Condyle Posterior View Isosurface Rendering (TOP) and 2-D Micro- CT Image (BOTTOM).....	140
Figure 6.4 Lateral Condyle Superior View Isosurface Rendering (TOP) and 2-D Micro- CT Image (BOTTOM).....	141
Figure 6.5 VOI 1 Medial Condyle (LEFT) and VOI 5 Between Condyles (RIGHT)	142
Figure 6.6 Lateral Condyle Mid-Condyle Sagittal Rendering.....	142
Figure 6.7 Medial Condyle Posterior View Isosurface Rendering (TOP) and 2-D Micro- CT Image (BOTTOM).....	143

Figure 6.8 Lateral Condyle Superior View Isosurface Rendering (TOP) and 2-D Micro-CT Image (BOTTOM).....	144
Figure 6.9 VOI 2 Medial Condyle (LEFT) and VOI 7 Between Condyles (RIGHT)....	145
Figure 6.10 Medial Condyle Mid-Condyle Sagittal Rendering.....	145
Figure 6.11 Lateral Condyle Posterior View Isosurface Rendering (TOP) and 2-D Micro-CT Image (BOTTOM).....	146
Figure 6.12 Medial Condyle Superior View Isosurface Rendering (TOP) and 2-D Micro-CT Image (BOTTOM).....	147
Figure 6.13 VOI 3 Medial Condyle (LEFT) and VOI 7 Between Condyles (RIGHT)..	148
Figure 6.14 Lateral Condyle Mid-Condyle Sagittal Rendering.....	148
Figure 6.15 Lateral Condyle Posterior View Isosurface Rendering (TOP) and 2-D Micro-CT Image (BOTTOM).....	149
Figure 6.16 Lateral Condyle Superior View Isosurface Rendering (TOP) and 2-D Micro-CT Image (BOTTOM).....	150
Figure 6.17 Bone volume fraction (%) across age categories	152
Figure 6.18 Trabecular thickness (mm) across age categories	152
Figure 6.19 Trabecular separation (mm) across age categories.....	153
Figure 6.20 Structural mode index (-) across age categories.....	153
Figure 6.21 Connectivity Density (mm^{-3}) across age categories	154
Figure 6.22 Degree of anisotropy (-) across age categories.....	154
Figure 6.23 Trabecular number (mm^{-1}) across age categories.....	155
Figure 6.24 Subchondral plate thickness (mm) across age categories.....	155

Figure 6.25 Bone volume fraction (%) sex differences across age.....	156
Figure 6.26 Structural model index (-) sex differences across age.....	156

List of Abbreviations

American Association of Physical Anthropologists.....	AAPA
Anterior.....	A
Basic Multicellular Unit.....	BMU
Body Mass.....	BM
Bone Volume Fraction.....	BV/TV
Center for Quantitative Imaging.....	CQI
Computed Tomography.....	CT
Connectivity Density.....	Conn.D
Cortical Thickness.....	Ct.Th
Degree of Anisotropy.....	DA
Growth Hormone.....	GH
High Resolution Computed Tomography.....	HR-CT
Indian Hedgehog.....	IHH
Insulin-like Growth Factor-1.....	IGF-1
Lateral.....	L
Matrix Metalloproteinases.....	MMP
Medial.....	M
Micrometer.....	μm

Minimum Effective Strain.....	MES
Osteoarthritis.....	OA
Polar Second Moment of Area.....	J
Posterior.....	P
Region of Interest.....	ROI
Receptor Activator of Nuclear Factor κ B.....	RANK
Receptor Activator of Nuclear Factor κ B Ligand.....	RANK-L
Runt-Related Transcription Factor 2.....	Runx2
Second Moment of Area.....	I
Structural Model Index.....	SMI
Three-Dimensional.....	3D
Trabecular Number.....	Tb.N
Trabecular Separation.....	Tb.Sp
Trabecular Thickness.....	Tb.Th
Volume of Interest.....	VOI

CHAPTER 1: RESEARCH CONSIDERATIONS FOR STUDY OF SUBCHONDRAL BONE MICROARCHITECTURE

Introduction

The use of three-dimensional (3D) bone architecture for reconstructing the paleobiology of past humans and other primates has become popular in recent years (Fajardo and Müller 2001; MacLatchy and Müller 2002; Richmond et al., 2004; Maga et al. 2006; Gosman and Ketcham, 2009; Griffin, 2008; Mazurier et al., 2010; Ryan and Walker, 2010; Raichlen et al., 2015; Ryan and Shaw, 2015; Saers et al., 2016). The effectiveness of bone, especially subchondral bone, for reconstructing behavioral and locomotive patterns depends on a better understanding of the relationships among bone structure, biomechanical loading, and behavior as well as an understanding of the mechanical role of bone in various joints (Ahluwalia, 2000; Su, 2011). Adult bone morphology incorporates structural features established during ontogeny and modified by biological factors and functional adaptive changes during maturation (Wang et al., 2011; Rauch, 2012). The response of bone to mechanical loading, especially during development plays an important role in skeletal adaptation, and determines much of adult bone morphology (Turner and Robling, 2003; Duren et al., 2013). Experimental studies have demonstrated that the 3D arrangement of trabecular bone reflects variation in mechanical properties at specific anatomical locations (Huiskes et al., 2000; Mittra et al.,

2005; Ryan et al., 2007; Saporin et al., 2011; Raichlen et al., 2015; Goliath et al., 2016). Understanding the spatial specifics of ontogenetic processes during bone development, therefore, can offer insights into normal and pathognomonic morphological variation. This understanding also has implications in activity patterns, locomotion, and mechanical load within and between populations.

This dissertation examines subchondral bone microarchitecture changes during growth and development in subadult and young adult skeletal remains associated with the Oneota (Norris Farms) archaeological population. More specifically, this study aims to explain the trabecular and cortical tissue level changes that occur in proximal tibia subchondral bone in both the medial and lateral condylar regions. Structural parameters used to describe the bone microarchitecture include, bone volume fraction (BV/TV), degree of anisotropy (DA), trabecular thickness (Tb.Th) and trabecular spacing (Tb.Sp). These parameters are calculated directly from high-resolution computed tomography (HR-CT) scans using Avizo® Fire, a data analysis and visualization software, and BoneJ, a plugin of ImageJ. Derived structural variables, such as trabecular number (Tb.N), connectivity density (Conn.D), and structural model index (SMI) are calculated using BoneJ. These methods enable a quantification of the ontogenetic patterning that distinguishes the developmental timing and variation in subchondral bone. Bone volume fraction and degree of anisotropy serve as a reflection of the growth and development associated with onset and maturing of normal functional activities (i.e. walking), and changing body mass. Before addressing the goals and hypotheses of this study, a review

of the morphology and function of subchondral bone, previous ontogenetic studies, and micro-CT analysis, will be discussed.

Morphology of the Subchondral Bone

Structure

A number of studies (Müller-Gerbl, 1998; Carlson and Patel, 2006; Intema et al., 2010; Su, 2011; Bousson et al., 2012; Burr and Gallant, 2012; Henrotin et al., 2012; Hamann et al., 2013) have established that the anatomy of subchondral bone is highly variable. The term “subchondral bone” remains ambiguous. It has been used to refer to several structural features: the calcified tissue immediately below the tidemark of the articular cartilage; the thin cortical lamella directly underneath the radiologically visible joint space; the dense trabecular bone immediately adjacent to the cortical lamella; the subarticular tissue; and/or a combination of these features (Müller-Gerbl, 1998; Madry et al., 2010). Duncan et al. (1987) defined the subchondral plate as a zone which separates the articular cartilage from the marrow cavity and consists of two layers: the calcified region of the articular cartilage and a layer of lamellar bone. Müller-Gerbl (1998) further defined “the subchondral zone” or “subchondral bone plate” as the bony lamella lying beneath the calcified zone of the articular cartilage. Depending upon the joint, this varies in thickness. The trabeculae arising from this bony lamella are referred to as “supporting trabeculae” (Madry et al., 2010). In this study, “subchondral bone” is defined as both the cortical subchondral bone plate directly beneath the calcified cartilage of the articular cartilage and the underlying supporting trabeculae, referred to as subchondral trabecular bone (subarticular spongiosa).

Osteochondral Junction

Subchondral bone is a part of the osteochondral junction. In a normal joint, the osteochondral junction comprises the deeper non-calcified cartilage, calcified cartilage, and the underlying subchondral bone (Figure 1.1). The calcified zone interfaces with the non-mineralized cartilage and is separated by the tidemark and the subchondral region (Suri and Walsh, 2012; Martin et al., 2015). At the line of contact between the subchondral plate and the articular cartilage there is a discrete band of mineralized cartilage, which is more radio-dense than the adjacent bone. It is referred to as the tidemark. The tidemark is a three-dimensional structure having a distinct anatomical appearance from the calcified cartilage and subchondral bone plate (Lyons et al., 2005; Lyons et al., 2006). Immediately beneath the calcified cartilage is a 1–3 mm thick plate of highly vascularized bone that is physiologically similar to cortical bone but less stiff. Distal to the plate is the subchondral trabecular bone. It is more porous and has a lower volume and density than the cortical plate (Imhof et al., 2000; Henrotin et al., 2012; Burr and Gallant, 2012).

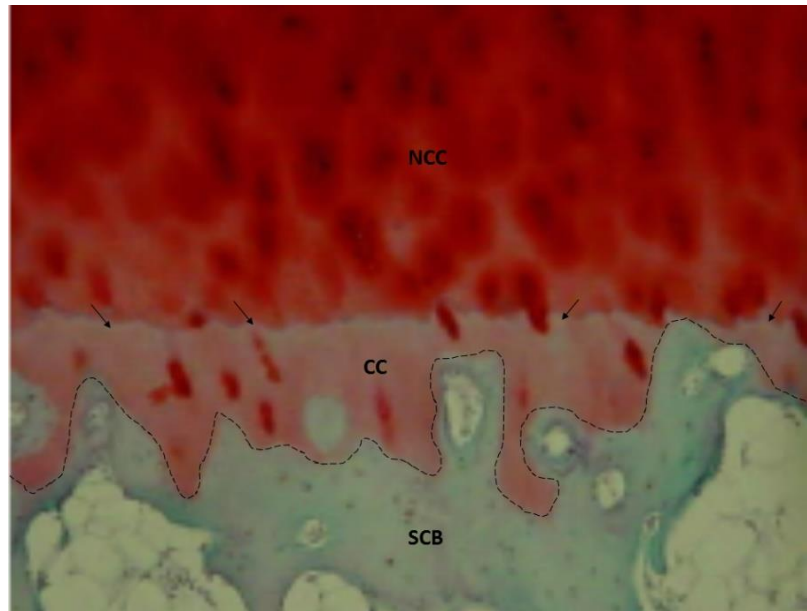


Figure 1.1: Photomicrograph showing osteochondral junction in a medial tibial plateau.
Note: NCC: non-calcified cartilage; CC: calcified cartilage; SCB: subchondral bone;
Arrows denote tidemark; Dashed line indicates the osteochondral junction (Modified
from Suri and Walsh, 2012).

In normal joint articular tissue, the subchondral bone is composed of large trabecula with little trabecular space (Martel-Pelletier et al., 2007). The thickness of the subchondral plate varies within and between joints. These variations include the contour of the tidemark, the composition of the subchondral bone plate, and differences in the trabecular structure and their mechanical properties. In most joints, the center of the cavity is associated with a much thicker subchondral plate than found peripherally (Dewire and Simkin, 1996). In the case of the tibial plateau, the subchondral bone is thicker in the center than at the periphery (Duncan et al., 1985). Regional differences in the density distribution (mineralization) of the subchondral bone can also be recognized

and greater density is regularly found in the more heavily loaded regions of the joint surface (Müller-Gerbl, 1998). Several studies (Noble and Alexander, 1985; Odgaard et al. 1989; Milz and Putz; 1994; Madry et al., 2010) have found greater subchondral bone and plate density in the medial rather than in the lateral part of the plateau. At places within the joint where the stress is assumed to be the greatest, the density is higher, the thickness is greater, and the vascularization is more strongly developed (Clark and Huber, 1990; Müller-Gerbl, 1998; Ahluwalia, 2000).

Function of the Subchondral Bone

The subchondral bone provides support and protection for its adjacent cartilage. Mechanical integrity of the cartilage and its resistance to injury depends on its communication with the underlying subchondral bone (Burr, 1998; Martin et al., 2015). Both structures, the cartilage and its supporting subchondral bone, have corresponding mechanical functions. The cartilage serves as the weight bearer and the subchondral bone serves as a structural support and shock absorber (Duncan et al. 1987; Layton et al. 1988; Lories and Luyten, 2011; Hamann et al., 2013; Hamann et al., 2014). According to Radin and Rose (1986), the subchondral bone absorbs a majority of the mechanical load transmitted by synovial joints. Due to the greater stiffness and strength of the subchondral bone in comparison with the articular cartilage (Gordon et al., 2003; Barr et al., 2015), it is generally established that the subchondral bone plays an important role in intra-articular load transmission (Choi et al. 1990; McKinley and Bay 2001; Gomoll et al., 2010; Suri and Walsh, 2012). The subchondral region exhibits the strongest architectural

response to differences in joint loading regimes (Pontzer et al., 2006) and serves to maintain joint shape.

Cartilage-bone interface

Articular cartilage and subchondral bone act as a functional unit. Each of these anatomically closely related tissues is affected by any alteration in the mechanical properties of the other. The purpose of the cartilage-bone interface is to maintain structural integrity of the osteochondral unit during which tensile, compressive, and shear forces are transmitted from the viscoelastic articular cartilage layer to the much stiffer mineralized end of the long bone. The biological interaction and mechanical mutual support make subchondral bone and cartilage a functional unit that cannot be separated (Hoemann et al., 2012; Zhang et al., 2012). The cartilage-bone interface is a boundary composed of mineralized blood vessels and type I and II collagen. Calcified cartilage and bone tissue in the adult subchondral bone have a similar mineral content (Hoemann et al., 2012). Cartilage and subchondral bone are in close proximity. Both the short diffusion distance and permeability of the calcified cartilage suggest that nutrients, cytokines, signal molecules (prostaglandin E₂, nitric oxide) and glucose exchange in either direction (Duncan et al. 1985; Lyons et al., 2006; Pan et al., 2009; Funck-Bretano and Cohen-Solal, 2011). Some authors have also suggested that deeper layers of the cartilage are metabolically influenced by subchondral capillaries (Milz and Putz, 1994; Müller-Gerbl, 1998). Taken together, these findings indicate that, the subchondral bone fulfills both mechanical and metabolic functions and is an active site of remodeling.

Subchondral Bone Influence on Osteoarthritis (OA)

Even though it is not the primary focus of this research, it is important to note the role of subchondral bone in osteoarthritis development and progression. Osteoarthritis is a multifactorial disease characterized by the degeneration of cartilage and modification of the structural and material properties of subchondral bone. Microarchitectural changes in subchondral bone influence the onset and progression of osteoarthritis in later life (Kamibayashi et al., 1995; Ding et al, 2003; Bobinac et al., 2003; Buckland-Wright, 2004; Suri and Walsh, 2012; Li et al., 2013; Funck-Bretano and Cohen-Sol, 2015). Osteoarthritis has been associated with a variety of causal factors, including physical activity (Jurmain, 1999), bone metabolism (Hunter and Spector, 2003), anatomical variation (Hunter et al., 2005), body size (Jurmain, 1999; Weiss, 2006), genetic predisposition (Chapman and Valdez, 2012), and hormonal levels (Dumond et al., 2003) (Weiss and Jurmain, 2007; Klaus et al., 2009).

In the development of osteoarthritis, there is increased subchondral osteoclast activity at the osteochondral junction, and increasing vascularity due to proteolysis (Suri and Walsh, 2012). Inoue (1981) suggested that initial changes occur around the tidemark and osteochondral junction because stresses are concentrated at these sites. Increased subchondral osteoclastic activity permits the cutting of vascular channels through the subchondral plate and into the non-calcified cartilage. As a result, subchondral and synovial compartments become compromised and resulting fracturing leads to structural change across the whole joint. Increases in subchondral bone thickness and reduced density of trabecular bone beneath the subchondral plate occur early (Kamibayashi et al.,

1995; Hayes et al., 2001; Buckland-Wright, 2004; Goldring, 2009; Suri and Walsh, 2012). As cartilage breaks down during osteoarthritic pathogenesis, cartilage thickness diminishes and radiographic joint space decreases (Mahjoub et al., 2012; Holland et al., 2013).

Primary versus Secondary Osteoarthritis

There are two types of osteoarthritis, primary and secondary. Primary osteoarthritis is generally associated with aging and mechanical stress, or the “stress hypothesis” (Jurmain, 1977a; Larsen et al., 1995; Klaus et al., 2009; Larsen, 2015). It is argued that osteoarthritis results from a long-term physiological imbalance between mechanical stress placed on joint tissue and the ability of joint tissues to withstand that stress (Radin, 1982). Under and over-loading in joints both increase enzyme production, especially matrix metalloproteinases (MMPs). Sclerotic subchondral bone stimulates MMP production (Suri and Walsh, 2012). MMPs attack the cartilaginous matrix and disrupt cartilage homeostasis. While enzyme inhibitors are produced, they cannot keep pace with the proteolytic process. The cartilage begins to erode and break down into fibrils allowing proteoglycans and collagen fragments to be released into the joint space. The presence of these breakdown products ultimately produces an inflammatory response in the synovial membrane involving increased production of enzymes and cytokines that destructively diffuse into the cartilage. Over time, bone overgrowth results from an attempt to repair the joint (Waldron, 2007; Suri and Walsh, 2012; Sharma et al., 2013).

Secondary osteoarthritis, in contrast, tends to develop relatively early in life after a specific cause, such as an injury to the joints (Jurmain, 1999). In cases of injury, the

normal vascular barrier between cartilage and subchondral bone can become breached by fibrillation. Capillaries then penetrate into the subchondral plate and the deep calcified zone of articular cartilage, which allows for the migration of osteocytes (Jurmain, 1999). When cartilage becomes denuded, subchondral bone is destroyed resulting in subchondral resorption and joint surface porosity (Ortner, 2003). It is difficult, if not impossible, to differentiate between primary and secondary osteoarthritis in an archaeologically-derived skeletal series. Both types of osteoarthritis leave very similar skeletal changes, including osteophytes (growth of new bone on margins), erosion of bone on joint surfaces, porosity, and severe surface polishing due to bone-on-bone contact (eburnation) (Ortner, 2003; Larsen, 2015). The best way to solve the problem of etiology of osteoarthritis is through more clinical research on living people. Studies of archaeological populations can be valuable, but they will never be able to match the diagnostic ability of clinical studies in which many more factors such as body mass, actual activity patterns, diet, patient history, genetics, and history of injuries can be accurately measured and taken into account (Pearson and Buikstra, 2006; Weiss and Jurmain, 2007). However, the clinical literature has conflicting and complex findings about the associations between osteoarthritis and activity. For example, it has been reported that many joints are able to maintain strenuous, long-term loading from distance running and other activities without developing osteoarthritis (Hoffman, 1993; Lane et al., 1993; Panush and Lane, 1994; Pearson and Buikstra, 2006). Also, part of the difficulty in applying clinical studies of osteoarthritis to bioarchaeological studies is the fact that physicians define osteoarthritis in different terms and conditions than

anthropologists. In clinical settings, the breakdown of cartilage in joints, damage to the subchondral bone, and narrowing of the joint capsule are all used to diagnose osteoarthritis (Jurmain, 1999; Weiss and Jurmain, 2007) However, many bioarchaeologists include the development of osteophytes and lipping around the joint capsule in their definitions of OA severity. This occurrence is not clinically relevant unless the osteophytes interfere with the joint's function (Jurmain, 1999; Pearson and Buikstra, 2006).

Jurmain (1977a; 1977b; 1999) urges anthropologists to pay special attention to the age of onset of osteoarthritis in specific joints in comparisons between sexes and populations. He concluded that investigating patterning in multiple joints, using the total available skeletal sample, is essential to accurate interpretations. A problem with studying age of onset arises from the fact that in clinical studies, injury to a joint, particularly in childhood, emerges as a major risk factor for OA later in adulthood (Micheli and Klein, 1991; Jurmain, 1999, Pearson and Buikstra, 2006), i.e. secondary osteoarthritis. Other concerns include non-standard data recording protocols (Buikstra and Ubelaker, 1994) and misinterpretations (Bridges, 1992). While osteoarthritis is clearly related to mechanical stress, it should be critically interpreted and not taken as a straightforward indicator of lifestyle (Bridges, 1992). A variety of studies suggest that different joints may develop osteoarthritis in response to dissimilar stimuli (Jurmain, 1999). The practice of inferring specific physical activities from OA patterns is improper and risky; rather, bioarchaeologists should be examining patterns of more habitual movements. These observations are more readily available and are the appropriate

conclusions gained from the study of osteoarthritis (Pearson and Buikstra, 2006).

Understanding the developmental patterns of subchondral bone microarchitecture can elucidate some of the questions that still exist regarding osteoarthritic onset in clinical joint research, as well as, disease classification in bioarchaeological studies.

Ontogeny

Bogin (1999: 155) defines ontogeny as “the process of growth, development, and maturation of an individual organism from conception to death.” Ontogenetic change in human and non-human bone has been a topic of considerable research (Kneissel et al., 1997; Glorieux et al., 2000; Ryan and Krovitz, 2006; Ryan et al., 2007; Cunningham and Black, 2009; Gosman and Ketcham, 2009; Gosman et al., 2013; Terhune et al., 2013; Acquaah et al., 2015; Goliath et al., 2016). Most studies of human and non-human ontogeny use micro-CT and geometric morphometric methods. These methods allow for quantification of complex 3D forms across body sizes and developmental ages. In studies of ontogeny, these methods are useful as they can be used to describe a trajectory of ontogenetic shape change in a particular sample population. In regards to bone microarchitecture, ontogenetic patterns provide major insights into the form and structure of bone. Growth is the most opportune time to modify the mass of the skeleton (Frost, 2003). More specifically, growing bone exhibits the greatest functional responsiveness to mechanical stimulation, with tissue sensitivity diminishing rapidly once skeletal maturity is attained (Gosman et al., 2011; Forwood, 2013). Infancy and childhood are periods of rapid bone growth and development. These early periods of ontogeny have a significant influence on bone strength during old age (Javaid et al., 2011; Acquaah et al., 2015).

Growth is a heavily regimented process controlled by hormones of the endocrine system (Bogin, 1999). Postnatal growth initiates rapidly and slowly stabilize at around 3 years of age. During puberty, there is a period of peak growth that slows until epiphyseal fusion occurs (Bogin, 1999). The development of secondary sexual characteristics is signaled by the adolescent growth spurt. It coincides with the onset of puberty and menarche in females. However, these processes do not exactly correspond to each other. Females begin their increase in the velocity of growth about 1 year (at 10 years of age) before they develop the external signs of developing maturity. The male growth spurt occurs at around 12 years of age, at least 6 months after their bodies have begun to develop (Cameron and Demerath, 2002). Growth is a highly sensitive indicator of health and it is affected by many factors (Gray and Wolfe, 1996; Larsen, 2015). The physical growth and development of children is an indicator of the social and economic environment in which they live in (Bogin and Loucky, 1997). It is important to note that the bone we acquire as children may have later effects on the adult bone structure and its ability to adapt to mechanical loads (Oliver et al., 2007). Size and shape have a strong genetic component but are also influenced by the environment in which individuals develop (Tanner, 1981; Goodman and Martin, 2002). Even in the same environment, there will be intrapopulation variation (Vercellotti et al., 2011). The final growth outcome of an individual is the result of a complex interaction between genetic and environmental factors. This is one of the main advantages in studying subadults (Bogin, 1999; Goodman and Martin, 2002).

Growth Studies in Archaeological Skeletal Samples

During the past decade, there has been an increase in the study of children and childhood in anthropology. The initial interest began with the rise of feminist approach in the 1970s (Baxter, 2008). Studies of past childhood growth have been used to provide valuable information on nutritional stress, prolonged skeletal growth, and delayed maturation (Saunders, 2008; Halcrow and Tayles, 2011). Johnston (1962) was the first to attempt to study growth using archaeological skeletal samples. These samples did not represent the normal healthy children, but those who had died. Saunders and Hoppa (1993) addressed this issue by examining the literature on survivors and non-survivors and found that mortality bias had little effect on bone measurements in juvenile skeletons. As mentioned earlier, bones undergo dramatic changes in size, shape, and organization. Different skeletal elements grow at different rates during the different phases of development (Bogin, 1999; Vercellotti, 2011). Lovejoy et al. (1990) developed a method to measure growth velocity in archaeological populations. This method estimated diaphyseal length in each age category and attempted to control for genetic variability in growth within each sample. However, factors such as disease and malnutrition can stop or alter these growth rates. The timing and duration of these growth perturbations can lead to short-term or permanent alterations. As a consequence, different growth histories can produce skeletal variation among individuals (Bogin, 1999). Despite the scale of analysis used in this study, growth histories can provide insight into epiphyseal architectural response to ontogenetic loading, especially, in association with increasing body mass.

Trabecular Bone

Ontogenetic studies of trabecular architecture in archaeological skeletal samples do have a presence in the anthropological literature. Kneissel et al. (1997) studied trabecular bone structure in both growing and aging lumbar spine in a Medieval Nubian population. They found that trabecular bone structure in children consisted of a dense network of small rod-like trabeculae. During adolescence came a period of the greatest bone volume with more small plate-like trabeculae and the adult form developed a large plate-like trabecular structure. Early postnatal development (0-3years) of the femur (Glorieux et al., 2000; Ryan and Krovitz, 2006) is characterized by an increase in trabecular thickness and bone volume, and a decrease in trabecular number with age. Ryan and Krovitz (2006) using the Norris Farms 36 skeletal series, demonstrated that bone volume fraction, trabecular number, and degree of anisotropy decrease between 6 months and 12 months old and by 2-3 years of age, the bone volume, thickness, and degree of anisotropy increase slightly in the femur. Moreover, Ryan et al. (2007) demonstrated mechanically significant structural differences between the femur and humerus during development. Gosman and Ketcham (2009) examined the ontogenetic patterning of trabecular bone microstructure in proximal tibiae of a subadult skeletal sample from SunWatch Village using various quantitative parameters of trabecular structure such as bone volume fraction (BV/TV), degree of anisotropy (DA), trabecular number (Tb.N), and trabecular thickness (Tb.Th). Gosman and Ketcham (2009) reported that bone volume fraction and degree of anisotropy are highest at birth, followed by a rapid decrease during the first year of life and a subsequent increase until late childhood.

Trabecular number was found to decrease continuously from birth to skeletal maturity. However, trabecular thickness increases continuously during development. Rauch (2012) suggests differential remodeling rates exist between the metaphysis and diaphysis during pubertal growth. He suggested that as growth in length accelerates, there is less time for cortical thickening through trabecular coalescence. With increasing load requirements, periosteal apposition rates in the diaphyses are only a fraction of the apposition rates in the more stagnant metaphysis. This leads to a differential remodeling rate between metaphyseal bone and diaphyseal bone.

Cortical bone

Cortical bone growth, measured by examining cortical thickness, provides complementary data for long-bone growth and health (Garn et al., 1964a; b; Larsen, 2015). However, Ruff (2000a) has argued that such interpretations are too simplistic and based on flawed methods. Cortical, periosteal, and medullary areas have been shown to follow very different growth trajectories, with cortical thickness being more influenced by mechanical loading than nutritional health (Daly et al., 2004). Goldman et al. (2009) examined mid-shaft cortical drift direction in 14 juvenile femoral shafts and identified with age a posterior and medial drift that later shifted to an antero-lateral direction similar to adult -like geometry. They suggested that cortical growth was more rapid during toddler stage and puberty and slowed in late childhood and later adolescence. Gosman et al. (2013) quantified diaphyseal cortex shape development of the tibia and femur using the Norris Farms 36 skeletal series. They noted that select locations in both the tibial and femoral diaphyses become increasingly less round (more asymmetrical) in cross section

in association with growth-related cortical drift and likely in response to increasing, location-specific, mechanical load-bearing demands. Long bone proportions can change constantly during growth, both externally and internally, due to differential sensitivity to mechanical influences. However, mechanical loads during adulthood have little effect on the external linear dimensions of long bone diaphyses (Frost, 2003; Ruff, 2005; Ruff et al., 2006). According to Ruff (2005), diaphyseal cross-sectional strength appears to be much more responsive to changes in mechanical loads.

Growth Studies in Modern Humans

Modern studies of growth are complicated by numerous variables, including socioeconomic status, genetics, environment, and cultural practices that are difficult to control for and add confusion to the picture (Larsen, 2015). However, modern growth studies do provide invaluable information that can be used to assess the health status of children in past populations. Stini (1969) examined the growth status of modern Colombian children who were under continual stress from protein-deficiency. He found that females had the ability to make up this growth (catch-up) in pre-adolescence, but that males were more severely delayed, resulting in less pronounced sexual dimorphism in the adult stature. In the 1970s, Garn et al. (1972) examined the surface-specific changes that accompany bone growth and development and advanced our understanding of sex differences in bone development using radiographic data. Garn et al. (1972) proposed that boys experienced more periosteal apposition compared with girls, and that girls experience more endocortical apposition. However, this theory cannot be applied to all skeletal sites because the study focused on non-weight bearing metacarpals. Bogin and

Loucky (1997) demonstrated the relationship between genetics and nutrition in growth attainment. They studied children born to Guatemalan immigrants in California. These children are genetically shorter than their African-American, Mexican-American and European-American peers but due to parental economic status, they are taller than children born in Guatemala (Goodman and Martin, 2002).

In regards to bone microstructure, Cunningham and Black (2009) examined trabecular bone structural organization in human newborn ilium and determined that a systematic and regional organization of internal architecture was established at a very early growth stage in the ilium. Glorieux et al. (2000) found similar results to Ryan and Krovitc (2006). They noted an increase in bone volume and trabecular thickness in modern human femora. Reissis and Abel (2012) demonstrated, using fetal stillborn aged between 4 and 9 months, that during fetal development an increase in trabecular thickness and a decrease in trabecular number is apparent in the humerus and femur. Duren et al (2013) found phenotypic sex differences in second metacarpal bone diameter and cortical thickness at an early age with males having wider and longer metacarpals compared to females throughout most of life. Acquaah et al. (2015) showed that gestation was characterized by increasing bone volume fraction while infancy had significant bone loss in vertebrae. Several studies (Ding and Hvid, 2000; Ding et al., 2003; Cui et al., 2008; Chen et al., 2013) have examined post maturity trabecular microstructural changes at the proximal tibia and proximal femur. These changes include a decrease in BV/TV, Tb.Th, and connectivity density (Conn.D), as well as an increase in trabecular separation (Tb.Sp) and structural model index (SMI). The decline in bone volume fraction (BV/TV) and

thickness (Tb.Th) with aging was similar for women and men. These studies noted that the age-related decrease in trabecular number (Tb.N) for women was nearly twice that in men. Age-related bone loss at the proximal tibia in women is considered to be due to decreases in both Tb.N and Tb.Th, whereas in men, the primary mechanism for the decrease in BV/TV was trabecular thinning.

The variable, age at peak height velocity (APHV), is also commonly used as an indicator of maturity in longitudinal studies of childhood and adolescent growth (Gabel et al., 2015) and is highly correlated with sexual maturation. APHV refers to age when maximum linear growth in height occurs and generally occurs in boys and girls when approximately 90-92% of adult stature has been achieved (Bailey, 1997; Bailey et al., 1999; Gabel et al., 2015). In a recent study, Gabel et al. (2015) noted that boys had greater cortical bone accrual rates on periosteal and endocortical surfaces compared with girls due to accelerated periosteal apposition during adolescence.

Studies in Subchondral Bone Ontogeny

Human Studies

Given that microarchitectural changes in subchondral bone influence joint maintenance in later life (Bobinac et al., 2003; Buckland-Wright, 2004; Li et al., 2013; Funck-Bretano and Cohen-Sol, 2015), it is surprising that so little research has been directed toward the structure and variation in human subchondral bone during ontogeny. Age-related alterations in the structure and material properties of subchondral trabecular bone in the proximal tibia have been investigated in a small number of studies (Ding et al., 1997; Ding et al., 2002; Gosman, 2007; Gosman and Ketcham 2009; Chen et al., 2011). Ding et

al. (2002) investigated normal age-related (16-85 years) changes in trabecular microstructural properties. Ding et al. (2002) demonstrated that the decrease in mechanical properties of trabecular bone in the proximal tibia with aging is a consequence of the loss of trabecular material. The study showed that bone volume fraction and mean trabecular volume decreased significantly with age; connectivity did not have a general relationship with age; and the degree of anisotropy increased with age. These age-related changes had the same trend and pattern for both the medial and lateral condyles of the tibia (Ding et al., 1997; Ding et al., 2002; Ding, 2010). Gosman and Ketcham (2009) found that in young adult individuals from SunWatch Village (16-20 years old), subchondral bone had a decrease in trabecular number and degree of anisotropy, and an increase in bone volume fraction with age. Chen et al. (2011) examined proximal tibia structural parameters in elderly Japanese populations. Similar to Ding and colleagues (2002), they found a decrease in BV/TV and Tb.Th with age in both women and men.

In a recent study by Goliath et al. (2016) using Norris Farms individuals, ontogenetic changes to trabecular bone structure in the metaphysis and epiphysis (subchondral) of the proximal tibia were compared using six morphological parameters: bone volume fraction (BV/TV), mean trabecular thickness (Tb.Th), mean trabecular spacing (Tb.Sp), structure model index (SMI), connectivity density (Conn.D), and degree of anisotropy (DA). These findings indicated that age-related changes in mechanical loading had heterogeneous effects on trabecular bone morphology within the proximal tibia. Specifically, there were significant differences in BV/TV, SMI, and DA between

epiphyseal and metaphyseal trabeculae. With age, trabecular microstructure is distinguished by higher values in BV/TV and Tb.Th in the epiphysis and shows that the epiphysis tolerates higher loads than the metaphysis. Trabeculae in the epiphyseal region are likely more directly influenced by mechanical forces than trabeculae in the metaphyseal region during growth. Differential rates of modeling and remodeling between the epiphyseal and metaphyseal trabecular bone may also contribute to the observed differences.

Non-human Studies

Researchers have primarily focused on cartilage morphogenesis and physical activity in non-human development (Tanck et al., 2001; Brama et al, 2002; Ding et al., 2006; Tanck et al., 2006; Isaksson et al., 2009; Jiao et al., 2010; Barak et al., 2011; Holland et al., 2011; Turunen et al., 2012; Hamann et al., 2013). Radin (1982) compared the effects of changes in loading impulse magnitude in the distal femora of sheep. Their results show that trabecular architecture became more longitudinally oriented (anisotropic) in response to the harder surface. Tanck et al. (2001) examined trabecular response to mechanical loading in the vertebrae and proximal tibiae of juvenile pigs and found bone volume increase occurred early in development but architecture adapted later. Brama et al. (2002) noted that equine subchondral bone biochemical and structural alterations of the collagen network develop during the first six months post-partum. Ding et al. (2006) showed in 3-6-month-old guinea pig samples that subchondral trabecular bone volume and cortical plate thickness increased significantly with age, while structural model index decreased, with trabeculae reflecting a more plate-like structure. Jiao et al.

(2010) demonstrated that the rapid developmental changes of rat subchondral bone primarily occurred before 4 months of age, resulting in thinner cartilage but larger and thicker subchondral bone. They also noted that formation of subchondral bone was faster in female than in male rats. Barak et al. (2011) examined trabecular bone adaptation in two sheep groups (active and sedentary) and found significantly higher bone volume fraction (BV/TV), trabecular number (Tb.N), and trabecular thickness (Tb.Th), lower trabecular separation (Tb.Sp), and less rod-shaped trabeculae in the exercised than sedentary sheep. Hamann et al. (2013) found that for both subchondral trabecular bone and its cortical plate, bone volume fraction (BV/TV) and trabecular thickness (Tb.Th) increased in the tibiae of rats. This study indicates that condensation of the subchondral bone does not solely occur during the development of osteoarthritis but is actually a physiological process during development. However, comparisons between studies are difficult due to differences in species, anatomical location, and experimental conditions. These ontogenetic studies establish a context for the present study, by showing that trabecular and cortical bone ontogeny, may be quantified, but cannot be characterized by any singular developmental trend, even within a skeletal element or region.

High Resolution X-Ray Computed Tomography

The method of Computed Tomography (CT) scans, originally named CAT (Computerized Axial/Assisted Tomography) scans, was established in 1972 by Godfrey Hounsfield following the invention of modern computers (Hounsfield, 1973; Bart and Wallace, 2013). Traditional CT scanners pass an x-ray beam through a specimen onto a detector that captures the x-ray image created by the scattered photons. Either the

specimen or the x-ray detection unit is rotated in such a way as to obtain multiple scans of the specimen at every angle. These x-ray scans are then processed using computer software and combined into multiple 2D image “slices” of the region of interest (ROI) of that specimen. The 2D image slices are stacked and converted into a 3D reconstruction. A voxel is the 3D discrete unit of the scan volume that is the result of the CT reconstruction. It is a 3D volume representing two dimensions within the slice and the slice thickness. The smallest voxel size (i.e., highest scan resolution) is ideal, however higher-resolution scans require longer acquisition times and create larger data sets. Additionally, differences in voxel size have little effect on the assessment of structures with relatively high thickness (i.e. 100 to 200 μm), such as cortical bone or trabeculae in humans (Bouxsein et al., 2010). High-resolution computed tomography (HR-CT) is an emerging non-invasive method with an average voxel (3D pixel) size of 50 μm . This method permits quantification of geometric, microstructural and mechanical properties of cortical and trabecular bone (Burghardt et al., 2013). The highest resolution (1 μm -10 μm) machines are Micro-Computed Tomography (Micro-CT) scanners (Burghardt et al., 2011; Bart and Wallace, 2013). The electromagnetic radiation from a CT scanner used to collect x-rays falls between 0.001 to 10 nanometers in wavelength. Because x-rays can detect differences in tissue density as photons pass through tissue, CT scans are particularly helpful as a diagnostic tool. More dense tissue prevents photons from passing through, and as such CT scanning is ideal to study bone (Burghardt et al., 2011; Bart and Wallace, 2013).

Bone exists as a multi-level material. Each level of structure is organized in a different fashion from the one above it. Bone is arranged hierarchically in size from collagen and mineral nanostructures, to bone cells, to trabecular and cortical tissue, and finally bone as a whole organ. These levels of structural hierarchy will be described in more detail in Chapter 2. Study of trabecular and cortical structures through micro-CT provides insight into the tissue scale structural properties. 3D analysis of the micro-CT images provides quantification of the morphometry, connectivity, and anisotropy in bone (Peyrin, 2011). In both anthropology and healthcare, CT scans are used to determine the 3D structure of opaque material. These studies track skeletal development, examine human growth and adaptation, examine the microstructures of bone and teeth, track bone damage, examine trabecular structures, evaluate bone health to study disease progression, study metabolic disease, and evaluate bone integrity. (Lazenby et al., 2011; Burghardt et al., 2011). This investigative technique involves analyzing a specific region of interest (ROI) with a larger bone sample and focused volumes of interest (VOIs) within that region. The three dimensional (3D) images obtained from high resolution CT are used to understand bone microarchitecture in several ways. Such methods include the use of computer assisted image processing to measure bone density or connectivity and to count trabeculae or other features directly from the image (Hildebrand and Rüesegger, 1997a;b). In anthropology, CT has primarily been used to analyze and measure many different variables related to bone structure including, bone volume fraction (BV/TV) trabecular thickness (Tb.Th), structure model index (SMI) trabecular spacing (Tb.Sp) trabecular number (Tb.N), and cortical architecture (e.g. thickness, density). Chen et al.

(2013) recently studied post maturity age-related changes in trabecular and cortical bone microstructure based primarily on HR-CT and micro-CT. Chen and colleagues focused on the vertebrae, femoral neck, and distal radius, which are common osteoporotic fracture sites. In older individuals, they found a decrease in trabecular bone is caused by thinning of the trabeculae and that trabecular bone loss over life was one-half at the vertebra and one-quarter at the femur, radius, and tibia (Chen et al, 2013).

Micro-CT Analysis in Comparison to Traditional Histology

The use of 2D histomorphometry is the gold standard for assessing bone microstructure because it is the only method for direct in situ analysis of bone cells and their activities but it does have limitations. Sectioning followed by histology can image bone interior but is destructive, lengthy and semi-quantitative, with some subjectivity in defining microstructural features. Moreover, it cannot discriminate an increase in the number of remodeling events from an individual event nor can a full 3D volumetric measurement be obtained (Parfitt, 2002; Vanderroost and van Lenthe, 2014). In contrast, Micro-CT is a fast and non-destructive technique allowing longitudinal studies of bone growth (Peyrin, 2011). It reduces the need to use bone histology for measuring interior microanatomy of bone, but histology is still necessary to image bone cells. Micro-CT cannot provide direct information on cellular function and remodeling activity because analysis is quantified using a reconstructed image (Burghardt et al., 2011; Particelli et al., 2012; Martin et al., 2015). Higher resolution micro-CT technology (synchrotron) has opened the possibility to examine bone structure from macro to nano and should be incorporated with current 2D histomorphometric techniques (Cooper et al., 2012).

Aims and Hypotheses

The specific aims of this study were to investigate normal age-related variations in the microstructural properties of human trabecular and cortical subchondral bone, to assess whether age-related trends in the properties differ for the medial and the lateral condyles, and to evaluate the relationship between microstructural properties and population.

Hypothesis 1: With the increase in body mass and developing adult gait, all subchondral bone structural parameters will be affected by age.

1A: In subchondral trabecular bone, there is an increase in bone volume fraction (BV/TV), anisotropy (DA), structural model index (SMI), and trabecular thickness (Tb.Th) with age.

1B: In trabecular subchondral bone, there is a decrease in connectivity (Conn.D), trabecular separation (Tb.Sp), and the number of trabeculae (Tb.N) with age.

1C: In cortical subchondral plate, there is an increase in the thickness (Plate Ct.Th) with age.

Subchondral trabecular bone is expected to follow the same ontogenetic processes as other trabecular regions of the skeleton, a subsequent functional condensation of the underlying subchondral bone due to endochondral ossification with an increase in the degree of anisotropy (Gosman, 2007). In assessing subchondral bone at different ages during growth, it would be expected that subchondral bone becomes denser with increasing age due to increasing trabecular thickness. Bone volume fraction will have a slight increase with decreases in trabecular number. These patterns have also been

reported by other researchers examining trabecular ontogeny (Ryan and Krovitz; 2006; Gosman, 2007; Gosman and Ketcham 2009; Gosman, 2012). Because the subchondral bone absorbs a majority of the joint mechanical load, loading is the primary factor in explaining its orientation (Wolff, 1892; Pearson and Lieberman, 2004; Sugiyama et al., 2010; Gosman, 2012). The ontogenetic changes seen in bone mass thickness and density occur with increases in load amount and duration. The changes seen in the distribution of trabeculae and their patterns are based on the direction of the load (Pearson and Lieberman, 2004; Gosman and Stout, 2010). The remodeling of trabecular architecture includes an increase in the bone volume fraction (BV/TV), an increase in trabecular thickness, and a decrease in the number of trabeculae (Ryan and Krovitz 2006; Gosman and Ketcham, 2009; Gosman, 2012).

In regards to the subchondral plate, there is an expected increase in thickness due to similar mechanical forces affecting the underlying subchondral trabecular region. Hvid (1988) claimed that the dense subchondral bone plate serves to distribute the forces transmitted through the menisci and cartilage to the subchondral trabecular bone. During growth and in the presence of increased loading, cortical bone increases to adapt to maintain equilibrium strain homeostasis (Frost, 2003; Ding et al., 2006).

Hypothesis 2: Due to increasing mechanical load and changing joint kinetics with development, there is a significant difference in subchondral trabecular bone and cortical plate structural parameters between the medial and lateral condyle.

2A: The medial condyle is better adapted to increasing load and body mass, with greater thickness, connectivity, bone volume fraction, and anisotropy than the lateral condyle.

2B: The lateral condyle will have greater trabecular separation and trabecular number.

It is well established that development of the knee angle shifts from bowlegged (varus) in the infant stage to knocked knees (valgus) in early childhood and stabilizes to a less valgus alignment as part of normal and physiological development (Engel and Staheli, 1974; Salenius and Vankka, 1975; Cheng et al., 1991; Heath and Staheli, 1993; Saini et al., 2010). The development of the tibiofemoral angle (TFA) can be divided into three phases: Phase I: knee alignment changes from an infantile varus alignment to maximum valgus; Phase II: valgus knee alignment decreases in amount; and Phase III: knee alignment remains stationary and the adult pattern of genu valgus is established. However, the age ranges at which these phases come in children and adolescents has been found to differ with different ethnic groups (Cheng et al., 1991; Heath and Staheli, 1993; Cahuzac, 1995; Arazi et al., 2001; Oginni et al., 2004; Yoo et al., 2008; Saini et al., 2010). These age-related changes in the limb alignment at the knee shifts weight from medial condyle to lateral condyle and then back to medial (Hurwitz, et al., 1998). Because of the genu valgus knee alignment, it has been argued that the medial condyle is stronger and denser than the lateral condyle. As mentioned earlier, several studies (Hvid et al, 1985; Hvid and Hansen 1985; Harada et al., 1988; Milz and Putz, 1994; Ding et al., 1997; Müller-Gerbl, 1998; Ding et al., 2002) have shown that the medial condyle of the tibial plateau is much stronger than the lateral condyle, and that in both regions the strength decreases rapidly with the distance from the surface. On average, the maximum density in the medial compartment is about 200 HU (Hounsfield unit) greater than the lateral (Müller-Gerbl, 1998). Gosman et al. (2011) suggested that a

higher bone volume fraction (BV/TV) in the lower limb is influenced by the load-bearing mechanical forces. These mechanical forces may be stronger on the medial condyle due to the anatomical positions of the distal femur and proximal tibia.

Summary

In this introductory chapter, the theoretical and experimental bases for an ontogenetic subchondral bone research project have been discussed. The principles behind the use of high resolution and micro-CT technology for quantifying and analyzing skeletal microarchitecture were also discussed. Hypotheses were developed based on bone functional theory, recent animal models, and human studies. These methods are applied to an archaeological subadult and young adult skeletal series from Norris Farms 36 skeletal collection, an Oneota cemetery assemblage. The results of this study are expected to contribute to the development of new quantitative reference data for the ontogenetic patterning of human subchondral bone.

Organization of Dissertation

This dissertation consists of seven chapters including this general introduction and statement of hypotheses. Chapter 2 places subchondral bone into the broader context of skeletal biology and cartilage morphogenesis. Chapter 3 is the historical bone biology background chapter, including the origins and development of the theory of bone functional adaptation, the tenets of the Utah Paradigm of skeletal physiology, and the principles of the mechanostat theory. Chapter 4 provides a review of the Oneota culture, an examination of relevant archaeological investigations of Morton Village and Norris Farms 36 and also presents a summary of the bioarchaeological research data on Norris

Farms skeletal remains. Chapter 5 discusses the materials (Norris Farms 36 tibiae) that form the basis for this investigation, age-at-death estimation, and body mass calculation. It also details the methods of the research including high resolution CT scanning acquisition and protocol, the structural analysis program Avizo Fire, and statistical procedures/tests used for hypothesis testing. Chapter 6 is a compilation of the results with a visual interpretation of the quantitative data. Chapter 7 provides an interpretative framework for an understanding of the meaning of the quantitative patterns of subchondral bone ontogeny and the various potential sources of error, strengths, and limitations of the study design and execution. The Conclusion summarizes the results of this project and places them into the broader context and significance of skeletal research. Two appendices are included for reference: Appendix A includes tables of all data collected and calculated for all specimens included in the study. Appendix B includes all supplemental SPSS statistical output tables.

CHAPTER 2: SKELETAL BIOLOGY AND JOINT MORPHOGENESIS

Skeletal Formation

Throughout childhood, adolescence, and early adulthood our bones undergo changes in size, shape, and organization through the process of modeling and remodeling (Goldman et al., 2009). The development of the adult skeleton is achieved by longitudinal growth, modeling, and remodeling. In bone, both growth hormone (GH) and insulin-like growth factor-1 (IGF-1) are essential for the development, longitudinal growth of the skeleton, and maintenance of bone mass. IGF-1 mediates most of the effects of GH on skeletal metabolism, promotes chondrogenesis, and increases bone formation by regulating the functions of the differentiated osteoblasts. GH regulates somatic growth and development as well as carbohydrate and lipid metabolism (Giustina et al, 2008). Notch is also a critical regulator of skeletal development, but its role in remodeling of the adult skeleton is unclear (Liu et al., 2016). During the 3rd to 8th week of embryonic development, the mesodermal layer of the embryo forms the beginnings of the skeletal system (Yang, 2013). Skeletal formation proceeds through two major mechanisms: intramembranous and endochondral ossification. In intramembranous ossification, osteochondral progenitors differentiate directly into osteoblasts to form membranous bone. The development of cortical and trabecular bone in the long bones is a result of the

endochondral ossification process in the presence of loading (Frost and Jee, 1994; Gosman, 2012; Martin et al., 2015).

Endochondral Ossification

During endochondral ossification, osteochondral progenitors differentiate into chondrocytes (cartilage cells) to form a cartilage template of the developing bone. (Yang, 2013). Indian hedgehog (IHH) and bone morphogenetic proteins (BMP2) are essential for function in endochondral ossification. IHH and BMP2 are proteins that regulate proliferation and differentiation of chondrocytes and induces osteoblast differentiation in the perichondrium (Yang, 2013). During endochondral ossification, a cartilaginous model (anlagen) is converted into bone. This cartilage model is formed from chondroblasts and is surrounded by connective tissue (perichondrium), except at its ends. In a long bone, the primary center of ossification is in the middle of the cartilage model. At almost the same time, three events occur: 1) mesenchymal cells form osteoblasts, which lay down bone just outside the cartilage core, creating a periosteal collar, 2) the chondrocytes within the cartilage core undergo hypertrophy and as their lacunae enlarge, the matrix is compressed to thin septa, which calcify; 3) blood vessels form the periosteum and penetrate the cartilage core accompanied by hematopoietic cells, osteoprogenitor cells, and osteoclasts. In the interior of the cartilage model, the osteoprogenitor cells differentiate to become osteoblasts, which begin to deposit bone on the septa of calcified cartilage, creating trabeculae. These primary trabeculae (primary spongiosa) soon become remodeled and replaced by secondary trabeculae (secondary

spongiosa) of lamellar bone or are replaced by marrow (Mackie et al., 2011; Martin et al., 2015) (Figure 2.1).

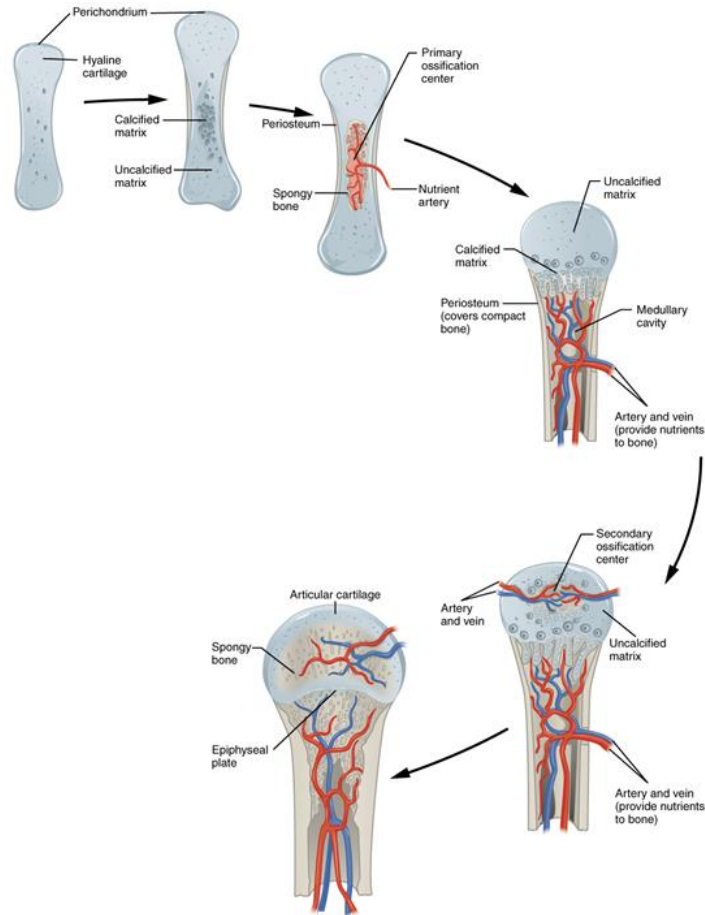


Figure 2.1: Process of Endochondral Ossification. (Anatomy & Physiology, Connexions. <http://cnx.org/content/col11496/1.6>).

Longitudinal Growth

Longitudinal growth of bones occurs in a nonmineralized region of growth near the end the bone. This region is referred to as the growth plate or physis. The physis separates the bony epiphysis from the bony metaphysis. New cartilage is constantly

formed by chondrocytes within the growth plate. The growth plate is divided into zones, each representing a stage in the life cycle of chondrocytes. The processes that occur during this temporal sequence through the growth plate are largely directed by a protein called *Sox9*, in collaboration with Indian hedgehog (*Ihh*) and parathyroid hormone (PTH) proteins (Leung et al., 2011). *Sox9* is the master regulator for chondrogenesis (Hino et al., 2014). The hedgehog family of proteins are important for tissue differentiation during limb development. Parathyroid hormone related protein (PTHrP) regulates endochondral bone growth by proliferating chondrocytes and delaying their differentiation (Kronenberg, 2006; Yang, 2013).

The process of longitudinal length occurs in 4 zones, each zone representing a different stage in the life cycle of the chondrocytes. These zones include: the reserve zone, proliferative zone, hypertrophic zone, and the zone of calcification (Figure 2.2). In the reserve zone, stem cells differentiate into chondrocytes. Cells of moderate size are scattered irregularly throughout this zone, which is anchored to the bone of the epiphysis and receives nourishment from epiphyseal blood vessels. These cells are not resting, but are dividing slowly to provide chondrocytes for the remainder of the growth plate. Type II collagen content is high in this region, and the fibrils are randomly arranged (Martin et al., 2015).

In the proliferative zone, these chondrocytes divide repeatedly and arrange themselves into columns. They also become disk-like, similar to a stack of coins. In this zone, the chondrocytes produce collagen and molecules needed in the development of the extracellular matrix. This is the region where most of the growth in length occurs in the

bone, primarily due to cell proliferation rather than cellular activity itself (Hunziker et al., 1987). Chondrocyte proliferation and maturation is permitted by suppression of Type X collagen production by the protein *Sox9* (Leung et al., 2011; Hino et al., 2014). Each chondrocyte produces about two times its own volume in new matrix during its lifetime (Hunziker et al., 1987). The collagen fibers are aligned parallel to the cell columns. The chondrocytes produce large amounts of proteoglycan and other molecules needed for the mechanical integrity of the surrounding extracellular matrix (ECM). As chondrocytes decline in proliferation, they mature and increase in size due to glycogen accumulation in the hypertrophic zone. They also increasing their volume and surface area by 4–10 times (Horton, 1993; Horton et al., 1998). Chondrocytes in this zone are in the early stages of apoptosis (programmed cell death). They stop producing cartilage matrix and begin producing molecules that prepare the adjacent cartilage for calcification. Eventually, they begin the process of apoptosis while preparing adjacent cartilage for calcification. In the zone of calcification, the degenerative chondrocytes continue to hypertrophy and the surrounding cartilage matrix begins to calcify (Martin et al., 2015). As they reach the limit of this zone, where the growth plate ends and the metaphysis begins, the chondrocytes go through apoptosis. Simultaneously, the surrounding cartilage matrix is calcified (Mackie et al., 2011; Martin et al., 2015). Longitudinal growth ceases with the closure of the growth plates at the end of the growing period (Robling and Stout, 2008).

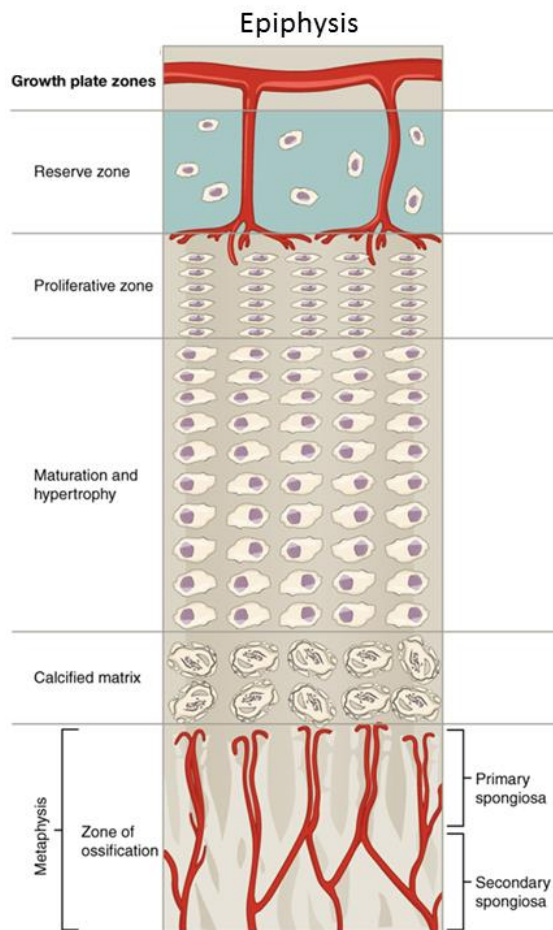


Figure 2.2: Zones of the Epiphyseal Growth Plate (Anatomy & Physiology, Connexions. <http://cnx.org/content/col11496/1.6>).

Proximal Tibial Epiphysis Development

During the first trimester, the tibia begins as cartilage model and starts to ossify during the eighth week in utero (O’Rahilly et al., 1957). Toward the end of the third trimester the proximal epiphysis begins to ossify. Epiphyseal trabeculae are formed from the secondary ossification center. Kuhns and Finnstrom (1976) reported that in North American and Swedish populations the epiphysis is radiographically visible between 2 and 5 postnatal weeks. It is always present by 3 months postpartum (Paterson, 1929;

Francis et al., 1939; Pyle and Hoerr, 1955; Hansman, 1962; Scheuer and Black, 2004).

Girls advance faster than boys during the whole of postnatal development of the proximal epiphysis. At birth, the proximal epiphysis appears as a porous, oval nodule similar in morphology to the mature shape. During the second year, the osseous expansion causes inferior flattening and the growth plate becomes established, while superiorly there is an extension towards the tibial spines. By 3-4 years of age, the articular surfaces begin to become distinct with a rounded, pitted superior surface and a roughly oval outline. The intercondylar eminence also becomes observable around this time. These features become more distinct as rapid growth continues and the articular surfaces become smoother throughout childhood (Scheller, 1960). By 6-7 years old, the condyles have reached their characteristic adult shape, the lateral being circular and the medial elongated anteroposteriorly. By 7 years in girls and 9 years in boys, the epiphyseal and metaphyseal diameters are equal in width (Pyle and Hoerr, 1955). By 11-13 years, the epiphysis is very substantial in size. Both the medial and lateral sides of the epiphysis cap the metaphysis. During early adolescence, the proximal epiphysis is identified by the presence of a large tuberosity that extends perpendicular to the condylar surface. The distal portion of the tibial tuberosity unites with the proximal epiphysis at 12 to 14 years of age. The proximal epiphysis fuses between 13 and 17 years in females and between 15 and 19 in males (Scheuer and Black, 2004; Baker et al., 2005). The proximal epiphysis is responsible for about 57% of growth in length of the bone (Digby, 1915; Gill and Abbott, 1942; Anderson et al., 1963). The commencement of fusion is 13 years in females and 15.5 years in males, with completion about 1.5 years later (Pyle and Hoerr, 1955). Other

observations have rather later times for complete fusion extending to 17 years in females and 19.5 years in males. McKern and Stewart (1957), reported, in males, early stages of union at 17-19 years old and that complete fusion did not occur until 23 years (Scheuer and Black, 2004).

Influence of Mechanical Loading on Epiphyseal Morphology

Mechanical loading during ontogeny plays a significant role in the development of epiphyseal morphology (Carter, 1987; Carter and Wong, 1988; Carter et al., 1989; Carter et al., 1996; Shefelbine et al., 2002; Ruff, 2003; Ryan and Krovitz, 2006; Garzon-Alvarado et al., 2010; Barak et al., 2011; Mirtz et al., 2011; Peinado Cortes et al., 2011; Guevara et al., 2016). There are mechanical influences on the rate of endochondral ossification fronts, the appearance of secondary ossification centers, and the geometry of the growth plates. Cartilage loading at the bone ends are also responsible for the stabilization of the subchondral growth at skeletal maturity and are a key factor in establishing the thickness of the articular cartilage covering the joint surfaces (Carter et al., 1996; Hamrick, 1999; Peinado Cortes et al., 2011). By the end of gestation, the epiphyses undergo a series of developmental changes with the formation of secondary ossification center. Finally, between the ages of five and six secondary ossification center enlarges until a complete epiphyseal ossification is achieved (Long and Ornitz, 2013; Guevara et al., 2016). There is a clear shift from highly variable to highly predictable joint angles with locomotive maturity that lead to a significant change in load orientations (anisotropy) throughout growth and development (Raichlen et al., 2015). However, some studies suggest that the joint response to loading patterns depends on the bone/region

(Carlson et al., 2008; Wallace et al, 2013). Carlson et al. (2008) and Wallace et al. (2013) suggested that joints more constrained in their range of motion show lower trabecular response in anisotropy to loading patterns than joints that have higher degrees of freedom/motion in murine studies (Wallace et al., 2013).

Hierarchical Structure of Bone

Bone is a hierarchically organized material that is constructed as a fiber-reinforced composite material. Bone is arranged hierarchically according to structure at size scales ranging from nanometers (collagen and minerals) to microns (trabecular plates) to milli- and centimeters (bone as an organ) (Figure 2.3). Structure at each level imparts a unique mechanical adaptation (Fratzl and Weinkamer, 2007). At the histological level, bone is either dense cortical (compact) bone, or more porous trabecular (cancellous) bone. The tissue that forms these microscopic architectures can be lamellar (sheet-like) or completely disorganized. Bone microstructure is often in layers, alternating between regions with highly oriented mineral and adjacent interlamellar regions (Martin et al., 2015). At the microscopic level, secondary osteons (Haversian systems) about 200 μm in diameter can act as strong fibers embedded in a matrix composed of interstitial lamellae. At the nanoscale, bone matrix is composed of cross-linked collagen fibers interspersed with mineral platelets, with non-collagenous proteins that control the assembly and size of these components. This organizational structure produces a composite material with mechanical properties superior to those of any of its constituents, including an ability to resist structural failure through the fatigue process incurred by a lifetime of repetitive loading (Martin et al., 2015).

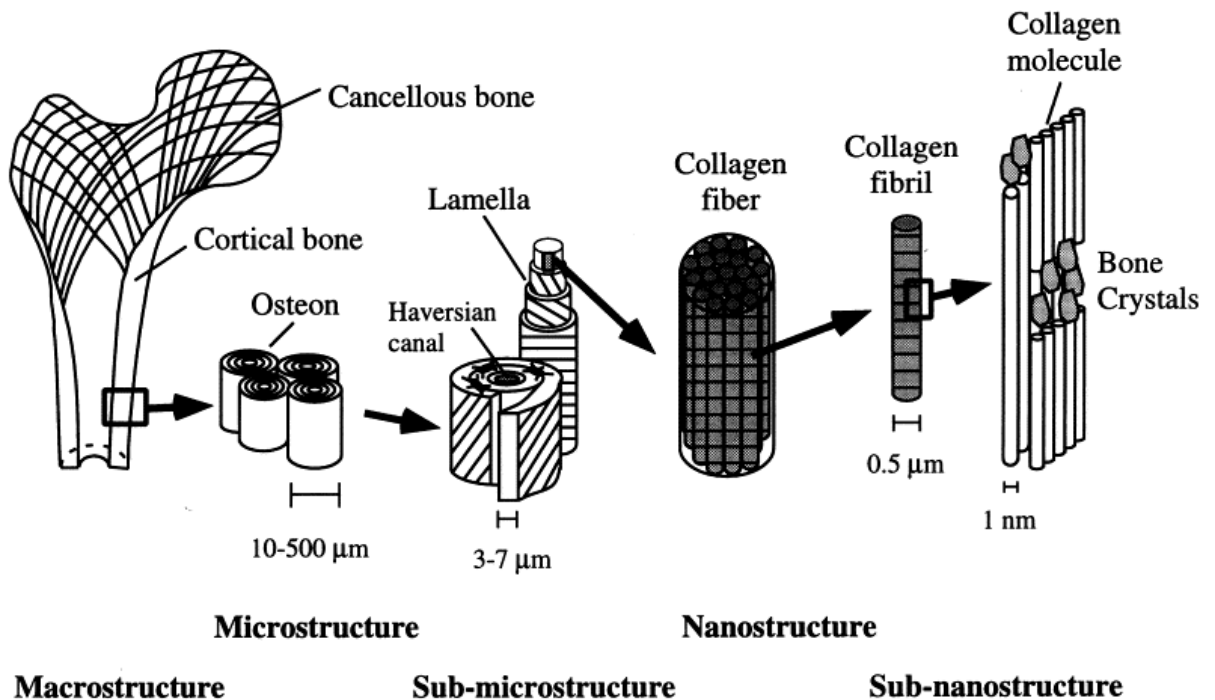


Figure 2.3: Hierarchical scale in bone structure. (Modified from Cowin et al., 1987)

Cortical and Trabecular bone

Cortical bone (compact bone) is the dense bone found in shafts of long bones and the cortex around vertebral bodies and flat bones. It is strong and provides both support and protection. It is less porous than trabecular bone but porosity increases with age and with osteoporotic changes to the skeleton. It consists of Haversian canals that are aligned to the long axis of the bone and contain blood vessels and nerve fibers. They are about 50 μm in diameter. Volkmann's canals are short, transverse canals connecting Haversian

canals to each other and to the outside surfaces of the bone. These canals also contain blood vessels and nerve fibers.

Trabecular bone (cancellous bone) is porous bone found inside vertebrae, carpal bones, flat bones, and the ends of long bones. The pores are interconnected and filled with blood marrow. The trabecular bone presents a porous structure of which the microarchitecture is characterized by a complex arrangement of thin (100 – 200 μm) strong plates and struts or rods (Raux et al., 1975; Singh 1978; Hayes and Snyder, 1981; Odgaard, 1997). The bony structures recognizable in a single section through this network, give a qualitative impression of the alignment of the plates and rods in trabecular bone (Eckstein et al., 2000). Trabecular bone tissue has much lower density than cortical bone and allows the skeleton to build large but lightweight conical volumes of bone at the end of long bones that carry the large loads of the joints. (Martin et al., 2015).

Woven and Lamellar Bone

Bone can be further characterized as primary and secondary bone. Cortical and trabecular bone contain two types of bone tissue: woven and lamellar. Woven bone is quickly formed and poorly organized tissue with collagen fibers and mineral crystals are more randomly arranged. Woven bone is common in a fracture callus and is formed early in the healing process to help stabilize the broken bone. In general, woven bone can be made more quickly than lamellar bone, but it is weaker (Stout and Crowder, 2012; Martin et al., 2015). Lamellar bone is slowly formed and highly organized. It consists of parallel layers of lamellae comprising a matrix of collagen fibers with mineral plates. Primary lamellar bone results from the resorption of existing bone and replacement by new

lamellar bone. There may be a variety of patterns of lamellar arrangement at the level of the collagen fibrils, and likely each have important mechanical implications (Ascenzi and Bonucci, 1970; 1976; Reisinger et al., 2011; Stout and Crowder, 2012)

Bone Cells

There are four types of bone cells: osteoclasts, osteoblasts, osteocytes, and bone lining cells. Osteoclasts are the cells that resorb bone. They are multinucleated cells that are derived from the monocyte/macrophage lineage under the stimulation of RANKL (Receptor Activator of NF κ B Ligand) and M-CSF (Macrophage-Colony Stimulating Factor). The molecule RANKL that binds to the RANK receptor is produced by osteoblasts, thus, osteoclasts differentiation and function is regulated by osteoblasts or osteoblast progenitors. Parathyroid hormone (PTH) and 1,25 hydroxyl vitamin D also stimulate RANKL production. Resorption occurs along a ruffled border of the cell, which is sealed to the bone surface by a peripheral clear zone. Osteoclasts erode their way through bone by demineralizing the adjacent bone through acidification of the bone mineral. This exposes the collagen which is then decomposed by the enzymes cathepsin k and matrix metalloproteinases (MMPs). These enzymes are produced by the osteoclasts. Once resorption is complete, osteoclasts die by apoptosis and disappear (Boyce and Xing, 2008; Teti, 2011; Martin et al., 2015).

Osteoblasts are mononuclear cells that produce osteoid, the organic portion (Type I collagen) of the bone matrix. Osteoblasts develop from mesenchymal precursor cells from the bone marrow that differentiate under the influence of bone morphogenetic proteins (BMPs), Runx2 and osterix, which regulate osteoblasts function by coordinating

Wnt-signaling pathway, transcription growth factor beta (TGF- β) and BMPs. Wnt signaling stimulates Runx2 gene expression. Runx2 is the master transcription factor that stimulates osteoblast differentiation and regulates bone formation (Boyce and Xing, 2008). Full differentiation of osteoblasts also requires some level of mechanical stress, one reason that bone formation is impaired in cases of disuse or during spaceflight (Robling and Turner, 2009). Osteoblasts express osteocalcin (OC) and alkaline phosphatase (AP) which can be measured in blood serum. Osteoblasts also express osteoprotegerin (OPG) which is the naturally occurring inhibitor of RANKL. OPG when bound to the RANKL receptor halts osteoclasts differentiation and prevents bone resorption. The concentrations of these molecules are indicative of the rate of bone formation and mineralization. Osteoblasts have extensive communications with each other and cells on bone surfaces (bone lining cells), within the bone matrix (osteocytes) and in the bone marrow through cellular processes that connect at gap junctions (inter-cellular channels) with processes from neighboring cells (Boyce and Xing 2008; Robling and Turner, 2009; Teti, 2011).

Osteocytes, which make up 90-95% of all cells in bone, are former osteoblasts that have become buried in the bone which they and their neighbors have made. Osteocytes sit in cavities called lacunae and communicate with each other and with osteoblasts via narrow canals called canaliculi. Canaliculi cover a large surface area of bone and with osteocytes are important for both transporting mineral into and out of bone, and also in transduction of mechanical signals (mechanotransduction) (Bonewald, 2011; Bonewald, 2013; Martin et al., 2015). Osteocytes form a functional group of cells

that connects cells on the bone surface with those in bone marrow and with those in blood cells. They form a mechanosensory network that is able to detect and respond to changes in mechanical stress. They detect load through strain induced fluid flow within the canaliculi which alters the cell processes. During normal physical activity, osteocytes produce a protein called sclerostin that inhibits Wnt signaling and suppresses bone formation. When high levels of mechanical loading are detected, sclerostin expression is suppressed, stimulating osteoblast differentiation and increasing bone formation (Robling and Turner, 2009; Bonewald, 2013; Martin et al., 2015). When bone is damaged or non-loaded, osteocytes begin to die by apoptosis. Either the apoptotic osteocytes (Kennedy et al., 2012), or healthy osteocytes adjacent to the dying ones produce RANKL, which, as previously mentioned, is important for the differentiation and activation of osteoclasts. These osteoclasts remove the damaged/non-loaded bone.

Bone lining cells are quiescent (dormant) osteoblasts. These are the osteoblasts that escaped being buried in newly formed bone and remained on the surface when bone formation ceased. As production of bone matrix stops, bone lining cells become quiescent and flattened against the bone surface. They maintain communication with osteocytes and each other via gap junctions and also maintain their receptors for hormones and other chemical signals. Like osteocytes, they are also responsible for transfer of mineral into and out of bone (Robling et al., 2006; Martin et al., 2015).

Growth and Modeling

Growth is defined as the accrual of bone mass through processes of bone formation during development. It does not account for bone shape, except in length, and does not involve resorption of tissue. During the growth phase, portions of the endosteal and periosteal surfaces are under continuous resorption and other portions are under continuous formation, a process known as modeling. Bone modeling sculpts the shape (architecture) and size (mass) of bone via modeling drifts by adding bone in some places and removing it in others (Frost 1992; Robling and Stout, 2008). Growth and modeling result in the production of organized parallel sheets of primary bone, circumferential, and endosteal lamellae (Robling and Stout, 2008). During modeling, some blood vessels in the periosteum become incorporated into the circumferential lamellae being deposited, producing primary vascular canals (Robling and Stout, 2008). Modeling is necessary because the longitudinal growth process does not produce a bone with the correct shape for an adult. Modeling occurs by activation-formation (A-F) or activation-resorption (A-R) sequence. Modeling is defined as either bone formation or bone resorption, but not both, at a given site. Modeling is continuous and prolonged during growth but is greatly reduced after skeletal maturity (Seeman, 2009; Martin et al., 2015). Modeling also occurs during fracture healing occurs occasionally.

Bone Remodeling

Remodeling is the process by which the skeleton is continuously renewed. It results in the turnover of lamellar bone without causing large changes in bone quantity, geometry, or size (Frost, 1969). The purpose of remodeling is to adjust the skeleton to changes in

mechanical demands, to prevent accumulation of fatigue damage, to repair micro fractures, to ensure the viability of the osteocytes, and to allow the skeleton to participate in the calcium homeostasis (Parfitt 1983; Burr, 1993; Stout and Crowder, 2012). Bone remodeling is a surface phenomenon and occurs on all bone surfaces. In bone, four different surfaces or envelopes can be identified: the periosteal, intracortical, endosteal, and the trabecular surfaces. Besides a variation in remodeling activity between different skeletal sites, there is also variation in the remodeling activity and bone balance between the different envelopes in individual bones (Parfitt, 2002). In healthy individuals, remodeling is a uniform process that begins in early childhood and continues throughout life. Remodeling is considered to exist in two basic forms: systemic and targeted. Systemic remodeling is stochastic and serves a metabolic function (e.g., mineral homeostasis). The second form of bone remodeling is primarily biomechanical in function and targeted to repair microdamage in bone (Parfitt 1983; Burr, 1993; Bentolila et al., 1998). The breakdown and renewal of bone that occurs during remodeling aids in skeletal maintenance, and helps bone adapt to mechanical stresses such as weight, posture, and physical activity (Wolff, 1892; Woo et al., 1981; Kumar et al., 2005). Bone remodeling occurs as a sequence of events (ARF sequence) performed by a team of cells called the basic multicellular unit (BMU) of remodeling (Frost 1969; Stout and Crowder, 2012).

Basic Multicellular Unit (BMU)

The basic multicellular unit (BMU) consists of two coupled cells (osteoclasts and osteoblasts). A BMU consists of about ten osteoclasts and several hundred osteoblasts. There are three principal stages in a BMU's lifetime: activation (A), resorption (R), and formation (F). The A-R-F process can be divided into six sequential phases. Activation, Resorption, Reversal, Formation, Mineralization, Quiescence. The osteoclasts resorb a volume of bone in the form of a cutting cone (cortical) or bone compartment (trabecular). In cortical bone, the BMU forms a complex structure, which bores holes through the bone, creating a longitudinal tunnel. In front is the cutting cone, where osteoclasts resorb bone during the resorption phase. In between the resorption and formation phases, there is a reversal period. During this period, at the edges of the resorptive bay, mononuclear cells lining the resorptive bay and deposit a special thin layer of matrix called a reversal (cement) line. Closely following the osteoclasts comes a capillary loop with endothelial cells and mesenchymal cells, which are osteoblast progenitors. This initiates the closing cone, in which the longitudinal tunnel is refilled by new bone. During the formation phase, osteoblasts then move in and begin to lay down new matrix in concentric lamellae, starting from the edges of the resorptive bay is left (Frost, 1969; Parfitt, 1990; 1994; Stout and Crowder, 2012; Martin et al. 2015). Cortical bone canals are known as Haversian canals, and they house blood vessels and nerves. The entire structural unit of reversal line, lamellae, and Haversian canal formed by this process is known as an osteon or Haversian system (Cooper et al., 1966; Frost, 1969; Widmaier et al., 2001). The amount of remodeling and the basic structural units (BSUs) created (osteons) help us to

predict age (Stout and Simmons, 1979). Through the process of bone remodeling several types of secondary osteons develop, such as type I, type II, double zonal, and drifting osteons. (Stout and Crowder, 2012). These units form the basis for most histomorphometric age estimation techniques. Formation is much slower than resorption. Resorption period is about 3 weeks and the formation period is about 3 months. Completed BMU's create secondary osteons in cortical bone and hemi-osteons in trabecular bone. This process is about 4–6 months (Sims and Martin, 2014; Harrison and Cooper, 2015; Martin et al., 2015).

In trabecular bone, the BMU is similar, but moves across the trabecular surface, where the osteoclasts dig a trench (bone remodeling compartment) rather than a tunnel. In trabecular bone, the BMU can be viewed as a cortical BMU cut through the middle and are referred to as a hemi-osteon in this process (Stout and Crowder, 2012). Remodeling of individual trabeculae within trabecular bone, which occurs frequently in both children and adults, rarely produces a complete osteon because the 200 μm diameter osteon is too large to fit within most trabecula which have an average diameter of 100–150 μm . One surface of the hemi-osteon borders the marrow cavity, and the remaining surface is separated from older bone within the trabeculae by a cement line just as whole osteons are separated from their surroundings in cortical bone (Sims and Martin, 2014; Martin et al., 2015).

Factors Affecting Bone Remodeling

Disease

Numerous pathological conditions can affect remodeling rates and, in turn, age estimations. Histological research on archaeological human remains focuses on histomorphological features that reflect remodeling rates to determine systemic disturbances and pathologies (Schultz, 2001). These patterns help bioarchaeologists reconstruct past behaviors and life histories (Stout, 1989). Remodeling rates are influenced by a variety of diseases and nutritional disorders. For example, diabetes tends to slow down remodeling, while secondary hyperparathyroidism tends to accelerate it (Robling and Stout, 2008). Histologically determined ages are only reliable when the individual is free from metabolic disturbances. These factors have received considerable attention in the literature, and a number of researchers have attempted to account for pathological conditions in age estimations (Ericksen, 1991; Paine and Brenton, 2006; Robling and Stout, 2008).

Diet and Subsistence

Diet may also be a factor affecting remodeling rates. Using mice, Cao et al. (2010) suggest that obesity induced by a high fat diet increases bone resorption, which may dampen any positive effects of increased body weight on bone. Paine and Brenton (2006) reported that malnutrition also influences age estimation by creating an underestimated age for black South Africans. Overall, osteon size and Haversian canals were larger in the malnourished individuals. Greater remodeling rates have been found in maize agriculturalists when compared to hunter-gatherers (Stout, 1978; 1983; 1989; Stout

and Lueck, 1995). Stout (1983) suggested that the greater remodeling rates in the maize agriculturalists might be due to low calcium serum ratios. This is a result of overproduction of the parathyroid hormone and is a characteristic of maize-based diets in modern populations (Stout, 1983). These same results were found in a study done by Ericksen (1980). Ericksen performed a comparative histomorphometric study on three populations with varying subsistence strategies. Ericksen examined the Eskimo (carnivores), Arikara (horticulturalists), and Pueblo Indians (intensive agriculturalists). Ericksen (1980) found a high degree of variability in osteon morphology and structure between these populations, especially in the frequency of Type II osteons. Type II osteons are structures that represent sites of hyper-calcification. They include a smaller complete Haversian system within a larger parent osteon (Robling and Stout, 2008). Ericksen (1980) argues that this variation is due to diet. Eskimos, who consumed mostly meat, had higher frequencies of Type II osteons when compared to the Arikara and Pueblo Indians who subsisted on a more plant-based diet.

Mechanical Load

This section provides a general overview of the influence of mechanical loading on bone. Its influence on bone and cartilage properties are discussed in more detail in Chapter 3. It is well established that mechanical factors play a fundamental role in both fetal and postnatal skeletal ontogeny (Schoenau et al., 2003). Several studies have provided evidence that growing bone has a greater response to increased mechanical loading than adult skeletons (Forwood, 2013). Like the overall size and morphology of skeletal elements, the mechanical environment also influences cortical and trabecular

remodeling at the microscopic level. The peak attained bone mass and final architecture are controlled by adaptive mechanisms sensitive to mechanical factors (Forwood, 2013). Mechanical loading history itself is a major factor in regulating skeletogenesis and factors which regulate musculoskeletal developmental mechanics persist throughout life (Carter et al., 1996). Hamrick (1999) suggests that mechanical loading associated with the postnatal onset of locomotor and postural development may provide an important stimulus for the progression of ossification and the formation of articular cartilage in the epiphyses of growing mammals. In a computational study, Guevara et al., (2016) suggested that mechanical stimuli may affect growth plate and epiphyseal ossification. Within the growth plate, variations due to stimuli appear during each stage of bone development. Therefore, they suggest that mechanical stimuli may play different regulation roles on growth plate behavior through normal long bone development.

Trabecular architecture is both responsive and highly sensitive to its mechanical loading environment (Ryan and Ketcham, 2002; Pontzer et al., 2006; Barak et al., 2011; Wallace et al., 2013; Raichlen et al., 2015). One of the primary functions of trabecular bone is to transmit loads generated during activity/movement through struts oriented to best resist these loads (Raichlen et al., 2015). Researchers have suggested a relationship between limb usage, loading patterns and trabecular architecture in human and non-human primates (MacLachy and Müller, 2002; Ryan and Ketcham, 2002; Richmond et al., 2004; Fajardo et al., 2007; Gosman and Ketcham, 2009; Scherf et al., 2013; Su et al., 2013; Raichlen et al., 2015), and experimentally in guinea fowl (Pontzer et al., 2006), mice (Carlson et al., 2008; Wallace et al., 2013), and sheep (Barak et al., 2011).

However, there is some evidence that loading patterns are not always reflected in trabecular architecture (e.g., Carlson et al., 2008; Wallace et al., 2013). With increased mechanical loading in cortical bone, osteocytes act as strain receptors and transducers (Bonewald, 2011). They communicate with each other through a system of canaliculi at gap junctions. Together, osteocytes throughout a bone form a complex cellular network (CCN) that includes cells along the periosteal and endosteal membranes which surround the external and internal surface of surfaces of the bone (Pearson and Lieberman, 2004; Bonewald, 2011). The potential outcomes are either quiescence, modeling, (periosteal and/or endosteal deposition or resorption), or Haversian remodeling (bone turnover) (Pearson and Lieberman, 2004). Low levels of loading can lead either to no response (quiescence) or to resorption through activation of osteoclasts.

Mechanical load, in and of itself is not a cultural factor, but can be influenced by cultural factors that can differ between cultural groups. Heavy mechanical loading, for example can accelerate remodeling rates in certain bones and thus potentially yield estimates above actual age (Wolff, 1892; Woo et al., 1981, Kumar et al., 2005). Additionally, remodeling rates can be altered through decreased levels of physical activity or decreased responsiveness to loading (Kohrt, 2001; Pearson and Lieberman, 2004). Moreover, individuals with high levels of mechanical loading have higher osteonal densities (Robling and Stout, 2003). When comparing archaic Pecos Pueblo Indian femora with other modern humans (20th century Euro-Americans), Burr et al. (1990) found distinct patterns of variation between the two groups. Pecos adult females had smaller Haversian canals and males had higher osteon densities when compared to

the modern American groups. Burr and colleagues (1990) hypothesized that these Pecos Indians had a more active lifestyle than individuals in the modern population.

Cortical bone mass

Several studies have found an association between delayed growth, indicators of nutritional stress, and reduced cortical mass (Huss-Ashmore et al., 1982; Saunders and Melbye, 1990; Mays, 2000). Cortical bone growth, measured by examining cortical thickness, provides complementary data for long-bone growth and health (Garn et al., 1964a; b; Larsen, 2015). However, Ruff (2000a) has argued that such interpretations are too simplistic and based on flawed methods. Cortical, periosteal, and medullary areas have been shown to follow very different growth trajectories, with cortical thickness being more influenced by mechanical loading than nutritional health (Daly et al., 2004). In order to truly examine bone loss as the result of malnutrition, Ruff (2000b) suggests that non-weight-bearing bones of the upper limb and body mass also need to be taken into account. Sciulli (1994) has also pointed out that long bones will react differently to external stimuli, with the rapidly growing bones of the lower limb showing greater developmental delay than the upper limbs in periods of stress (Chapskie, 2006).

Age-Related Bone Loss

Normal bone mass in humans, after growth has ceased, is maintained by the balance between bone formation by osteoblasts and bone resorption by osteoclasts. With age, starting around the third decade of life, after peak bone mass has been reached there is a slow and steady loss of bone that occurs in all mammalian species. Females lose more bone and at a faster rate than males (Grynpas, 2003). Both cortical and trabecular bone

are loss with age. Cortical loss is indicated by reduction in the thickness of the cortex. Trabecular reduction in the fraction of marrow space occupied by bone (trabecular bone volume) Previous work suggests that the ability of adult bone to remodel in response to applied loads is diminished not only in cortical bone (Lieberman et al., 2003; Pearson and Lieberman, 2004), but also in trabecular bone. There is a conversion of trabecular plates to rods (Christiansen et al., 2000; Keaveny and Yeh, 2002; Knopp et al., 2005; Pontzer et al., 2006; Jacobs et al., 2010; Wu et al., 2011). The surface/volume increases progressively as bone becomes more porous and is always higher in trabecular than in cortical bone, but a decrease in surface area in trabecular bone (Parfitt, 1983; Seeman 2008). An increase in activation frequency leads to an increase in the number of ongoing remodeling cycles. This increases the remodeling space and proportionally decreases the amount of bone. A negative balance leads to cortical and trabecular thinning (Seeman 2008). In trabecular bone, there is a decrease in the number of trabeculae with age; this decrease leads to a loss of connectivity in the trabecular network. In cortical bone, the thinning leads to trabecularization along the interior surface (Parfitt, 1984; Seeman 2008; Morse et al., 2014).

Joint Morphogenesis

In the limbs, mesenchyme accumulations within the growing limb bud will become a hyaline cartilage model for each of the limb bones. A joint interzone will develop between these areas of cartilage. Mesenchyme cells at the margins of the interzone will give rise to the articular capsule, while cell death at the center forms the space that will become the joint cavity of the future synovial joint. The hyaline cartilage

model of each limb bone will eventually be converted into bone via endochondral ossification. However, hyaline cartilage will remain, covering the ends of the adult bone as the articular cartilage. Joints form during embryonic development in conjunction with the formation and growth of the associated bones. The first sign of joint formation is the appearance of an interzone at a potential joint site. Synovial joints arise through a non-cartilaginous region called the interzone. The interzone becomes an important signaling center which regulates growth through such factors as GDF-5. The interzone also expresses bone morphogenetic proteins (BMPs) and their antagonist, noggin. Overexpression of BMPs, or the loss of noggin leads to joint fusions. The interzone also expresses Wnt-14, which appears to be specific for the developing anlagen, and regulates its non-chondrogenic nature (Archer et al., 2003; Decker et al., 2014).

The interzone is made of mesenchymal cells that are in close proximity to each other and connected by gap junctions. With time, the interzone thickens and the interzone cells give rise to chondrocytes that are at each epiphyseal end (Pacifci et al., 2006). Joints are formed in the cartilaginous condensations when chondrogenesis is arrested, and a joint interzone is induced. One of the earliest gene markers of interzone cells is growth and differentiation factor-5 (*Gdf-5*), whose expression becomes strong at each presumptive synovial joint limb site (Storm and Kingsley, 1996; Decker et al., 2015). Several mice studies (Rountree et al., 2004; Koyama et al., 2008; Decker et al., 2015) have showed that joint progenitor cells with a *Gdf-5* lineage, including those within and surrounding the histological interzone, gave rise to multiple joint tissues over time, including the articular cartilage, synovial lining, and intrajoint ligaments.

Articular Cartilage

There are three types of cartilage: hyaline, elastic, and fibrocartilage. Hyaline cartilage is the most prevalent type of cartilage. It is found in the ventral ends of ribs, tracheal rings, and covering the joint surfaces of bones (articular cartilage). In addition, the growth plates are composed of this type of cartilage. Elastic cartilage is found in the external ear, eustachian tubes, and epiglottis. It has greater flexibility and elasticity than hyaline cartilage. Fibrocartilage is the type of cartilage occurring in intervertebral disks, pubic symphysis, menisci, and in the body attachments of certain tendons. It also may form when hyaline cartilage is damaged (Fox et al., 2009; Martin et al., 2015). For the purposes of this study, the primary focus will be on hyaline (articular) cartilage.

Adult cartilage is avascular, and chondrocytes obtain nutrients through diffusion. The nutrients are derived from the synovial fluid whose diffusion is facilitated during joint loading. With joint loading, some of the water in cartilage is squeezed out into the synovial space. When the joint is unloaded, the hydrophilic properties of the cartilage proteoglycans cause the water to be sucked back into the cartilage. As the water returns to the cartilage, diffusion of nutrients from the synovial fluid is facilitated (Fox et al., 2009; Martin et al., 2015).

Structure and Function

Articular cartilage is highly specialized connective tissue of synovial (diarthrodial) joints. The purpose of this tissue is not to serve as a shock absorber, but to provide a suitable surface for lubrication and wear prevention. Its principal function is to provide a smooth, lubricated surface for low friction articulation and to facilitate the transmission of loads

to the underlying subchondral bone. Articular cartilage is unique in its ability to withstand high cyclic loads, demonstrating little or no evidence of damage or degenerative change (Mankin, 1982; Buckwalter, 1998; Fox et al., 2009). It is composed of an extracellular matrix (ECM) with a sparse distribution of chondrocytes. The ECM is made up of water, collagen, and proteoglycans. Water is the most abundant component of articular cartilage. The relative water concentration decreases from about 80% at the superficial zone to 65% in the deep zone (Buckwalter and Mankin, 1997). The flow of water through the cartilage and across the articular surface helps to transport and distribute nutrients to chondrocytes, in addition to providing lubrication (Fox et al., 2009). Articular cartilage is lubricated by hydrodynamic loading, lubricin, and hyaluronic acid. Hydrodynamic loading is loading of the articular cartilage that forces water out of the cartilage. This fluid forms an aqueous layer that separates and protects the opposing surfaces. Lubricin, a glycoprotein, is produced by synovial lining cells and binds to articular cartilage to create a protective layer of water molecules. Hyaluronic acid is also produced by synovial lining cells and lubricates the contact surface between synovium and cartilage (Moore et al., 2011).

Water makes up 65% to 80% of mass of the cartilage and accounts for 80% of the weight near the surface. At deep zone, it is about 65%. Water content decreases with normal aging and increases with osteoarthritis. Increased water content leads to increased permeability and decreased strength/ Collagen makes up 10 to 20% of total cartilage mass. Type II is most abundant, collagen accounting for 90% to 95% of the total collagen content. Small amounts of types V, VI, IX, X, and XI collagen are also present. Collagen

provides the framework and tensile strength. Proteoglycans make up 10 to 15% of cartilage and provide compressive strength. Proteoglycans also retain water and aggrecan is the most responsible for hydrophilic behavior. Proteoglycans are produced by chondrocytes and are composed of glycoaminoglycans subunits which are mainly chondroitin sulfate and keratin sulfate.

Articular cartilage is composed of four zones (layers): superficial (tangential) zone, middle (transitional) zone, deep (radial) zone, and calcified zone (Fox et al., 2009) (Figure 2.4).

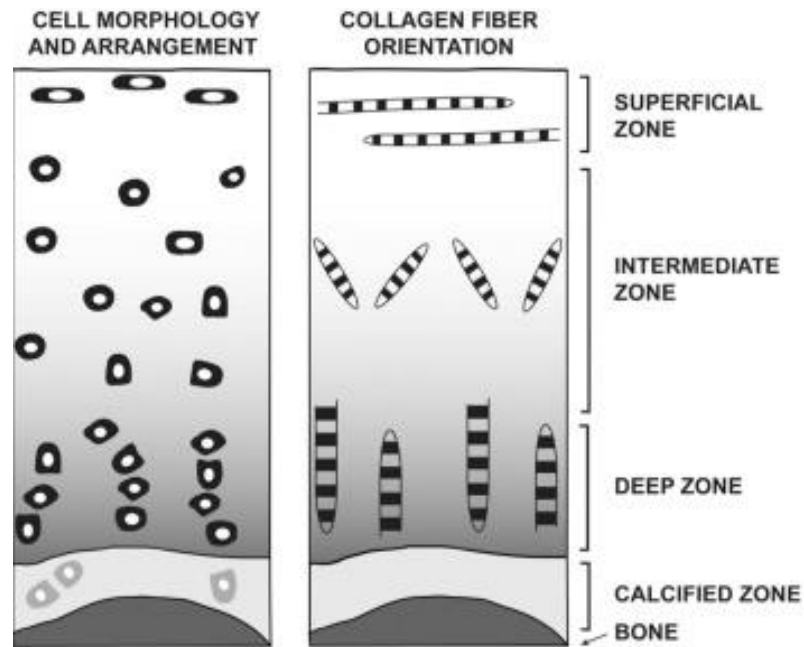


Figure 2.4: Zones of Articular Cartilage with Chondrocyte Morphology and Collagen Fiber Orientation. (Modified from Müller et al., 2014).

The superficial (tangential) zone is a thin layer that protects deeper layers from shear stresses and makes up approximately 10-20% of articular cartilage thickness. The collagen fibers of this zone (primarily, type II and IX collagen) are packed tightly and aligned parallel to the articular surface (Figure 4). The superficial layer contains a relatively high number of flattened chondrocytes, and the integrity of this layer is imperative in the protection and maintenance of deeper layers. This zone is in contact with synovial fluid and is responsible for most of the tensile properties of cartilage, which enable it to resist the sheer, tensile, and compressive forces imposed by articulation (Fox et al., 2009).

Immediately deep to the superficial zone is the middle (transitional) zone, which provides an anatomic and functional bridge between the superficial and deep zones. The middle zone represents 40-60% of the total cartilage volume, and it contains proteoglycans and thicker collagen fibrils. In this layer, the collagen is organized obliquely, and the chondrocytes are spherical and at low density. Functionally, the middle zone is the first line of resistance to compressive forces (Fox et al., 2009).

The deep zone is responsible for providing the greatest resistance to compressive forces, given that collagen fibrils are arranged perpendicular to the articular surface. The deep zone contains the largest diameter collagen fibrils in a radial disposition, the highest proteoglycan content, and the lowest water concentration. The chondrocytes are typically arranged in columnar orientation, parallel to the collagen fibers and perpendicular to the joint line. The deep zone represents approximately 30% of articular cartilage volume. The

tide mark distinguishes the deep zone from the calcified cartilage. The calcified layer plays an integral role in securing the cartilage to bone, by anchoring the collagen fibrils of the deep zone to subchondral bone (Buckwalter and Mankin, 1998; Hayes et al., 2001; Fox et al., 2009; Müller et al., 2014).

Synovial Joints

Synovial joints provide essentially frictionless motion between limb segments while transmitting relatively high loads between them (Mow et al., 1992; Martin et al., 2015). The synovial fluid is manufactured by cells in the synovial membrane, which lines the interior of the fibrous joint capsule. The articular capsule consists of an external fibrous layer and an internal synovial membrane that lines the internal surfaces of the articular cavity not covered with cartilage. Fatty deposits separate these layers. The capsule is attached to the margins of the articular surface. This fibrous layer creates a tight seal preventing the release of synovial fluid. The synovial membrane lines the internal aspect of the fibrous capsule (Figure 2.5). The synovial tissue secretes synovial fluid to lubricate the joint and nourishes the avascular structures. Inside the synovial membrane are fluid-filled sacs called bursae. Generally, these bursae aid in the movement of tendons that glide over bone or over other tendons (Moore et al., 2011). Since most muscles have a much shorter lever arm than the forces exerted from outside, the joint reaction force is in general several times higher than the body weight. Therefore, the tissues which form the joints are subjected to considerable mechanical stresses and strains. However, the structure of the joints and the material properties of the connective tissues allow them, under ideal conditions, to maintain their mechanical functions

adequately for decades in spite of the high loading. This is at least in part achieved by the growth, differentiation and regeneration processes being under the control of regulatory feedback mechanisms which guarantee their dynamic adaptation to the mechanical requirements, and an optimization of their functions during daily use (Eckstein et al., 2000).

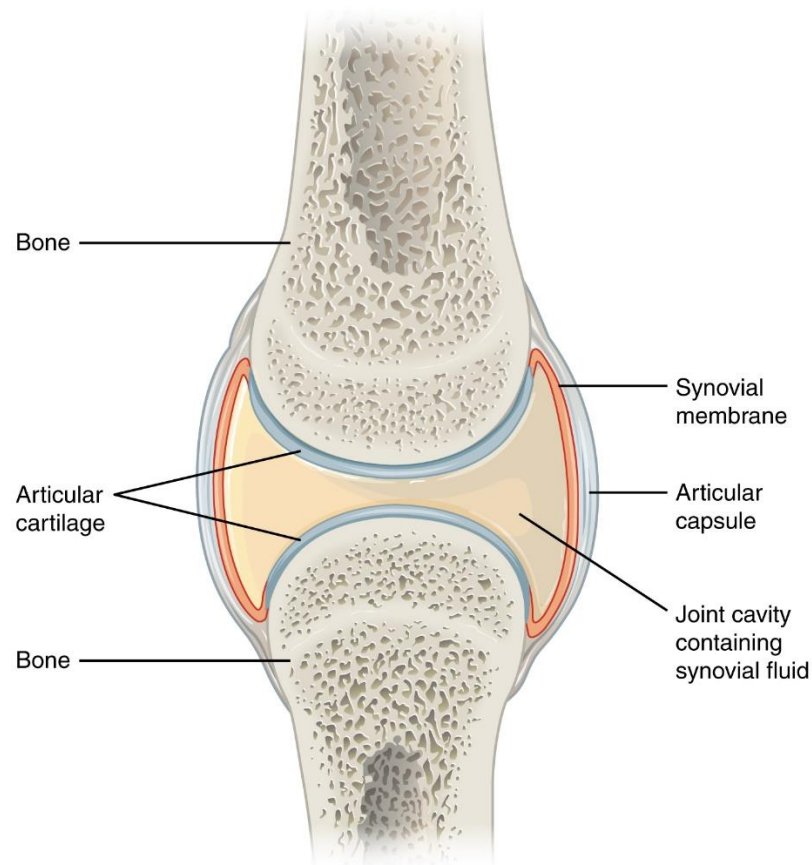


Figure 2.5: Example of a synovial joint. (Anatomy and Physiology, Connexions. <http://cnx.org/content/col11496/1.6/>).

Tibiofemoral Joint (Knee Joint)

The tibiofemoral joint is a modified hinge type of synovial joint. It is made up of an articular capsule, which surrounds three bones, the distal end of the femur, proximal end of the tibia, and the patella, as well as joints between these skeletal structures. The tibiofemoral joint is a hinge joint between the tibia and the femur. The joint contains three articulations, two articulations between the lateral and the medial femoral and tibial condyles and one articulation between the patella and the femur along the patellar groove. During flexion and extension of the knee, facets on the posterior surface of the patella articulate with the patellar surface of the femur. On the articular surface of the tibia, lies the medial meniscus and lateral meniscus. They deepen the articular surface and serve as shock absorbers. The most important muscle in stabilizing the knee joint is the quadriceps femoris, particularly the fibers of the vastus medialis and vastus lateralis. Flexion and extension are the main knee movements. The modified hinge movement of flexion and extension is combined with gliding and rolling, and with rotation. When the leg is fully extended with the foot on the ground, the knee locks because of the medial rotation of the femur on the tibia. This position makes the lower limb a solid beam and more adapted for weight bearing. When the knee is locked, the thigh and leg muscles can relax briefly without making the knee joint too unstable. To unlock the knee, the popliteus muscle contracts, rotating the femur laterally on the tibial plateau so that flexion of the knee can occur. The menisci must be able to move on the tibial plateau as the points of contact between the femur and the tibia change. The popliteus, semimembranosus, and pes anserinus (semitendinosus, gracilis, sartorius) muscles are important structures in

resisting excessive external tibial rotation and maintaining the neutral tibial rotation (Moore et al., 2011).

Impact of Knee Joint Kinematics and Locomotion on Skeletal Loading

As infants grow into children and eventually into adults, normal knee alignment changes occur. Because of varied feet and hip positions, there are valgus/varus alignments at the knee (Han et al., 2013). The “normal knee” tibial joint line is in varus (toward midline) and the “normal knee” femoral joint line is in valgus (away from midline) (Figure 2.6). As varus alignment increases there is an increase in medial tibiofemoral compartment load, while an increase in valgus alignment leads to an increase in lateral tibiofemoral compartment load (Sharma et al., 2010). The development of the knee can be divided into three phases: Phase I: knee alignment changes from an infantile varus alignment to maximum valgus; Phase II: valgus knee alignment decreases in amount; and Phase III: knee alignment remains stationary and the adult pattern of genu valgus is established (Saini et al., 2010). Most children have varus alignment when they start to walk. Usually by the age of 2-3 years, the knee alignment becomes more valgus. The valgus alignment peaks in the next 1-2 years. After six years of age, the knees will assume a straighter alignment. By 12 years of age, the genu valgus alignment adult configuration will be attained (Saini et al., 2010). These shifts in knee alignment create a mechanical shift in skeletal loading from medial to lateral during early childhood and back to medial in the adult configuration.

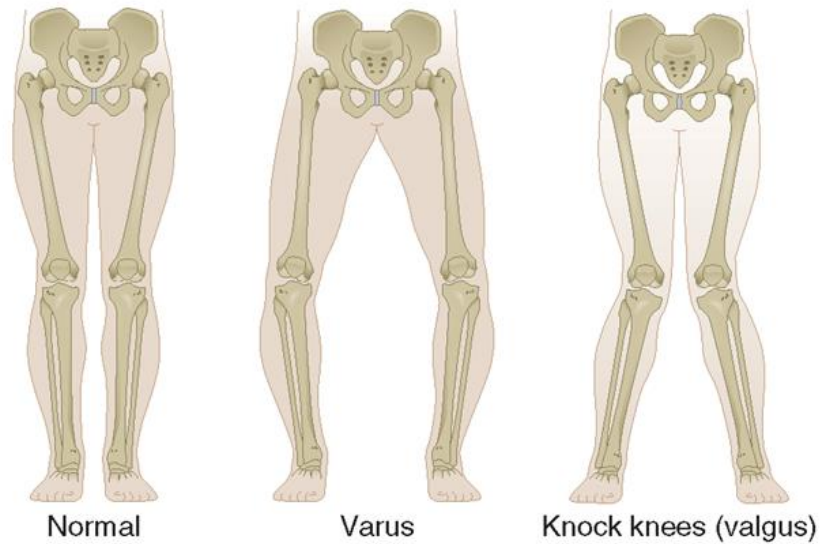


Figure 2.6: Example of knee alignments. (http://what-when-how.com/wp-content/uploads/2012/05/tmpa83a73_thumb2.png).

Locomotion has a major impact on skeletal loading and bone growth during development (Raichlen et al., 2015). Modern human locomotor behavior undergoes major modifications from infancy to adulthood. Early in locomotor development there is an inherent instability in bipeds (Sutherland et al., 1980; Adolph et al., 2003; Raichlen et al., 2015). Researchers agree that increased strength and postural control are the primary cause of improvement in the development of walking. Changes in body growth affect strength and balance by changing the biomechanical constraints on movement (Adolph et al., 2003). Walking infants take small unsteady steps with their legs spread apart and their toes pointing externally to the sides. There is high variability from step to step, and the distance each leg travels is not symmetrical. Because of their instability on one foot, most new walkers plant their entire foot down immediately or walk on their toes. As walking improves, infants take larger steps, maintain a smaller lateral distance between their feet,

and display a heel-toe progression (Adolph et al., 2003). As gait matures, stance width diminishes, normal arm swing appears, and step length and walking velocity increase (Sutherland et al., 1980; Cowgill et al., 2010). Movement of the lower limb during walking is divided into alternating swing and stance phases. The stance phase begins with a heel strike, when the heel hits the ground and begins to adopt the body's full weight and ends with a push-off from the forefoot. The swing phase begins after push-off, when the toes leave the ground, and ends when the heel strikes the ground. The primary muscles involved are of the lower leg (gastrocnemius, soleus, tibialis anterior/posterior, and peroneals), and the thigh/knee (vastus lateralis/medialis, obliques, and rectus femoris). (Moore et al., 2011).

Key stages in locomotor development include the adoption of an upright stance and bipedal locomotion at about 12–14 months (Hallemans et al., 2005), and the attainment of an adult patterns of locomotion between 5 and 9 years old (Sutherland et al., 1980; Adolph et al., 2003). These shifts in positional and locomotor behaviors coincide with, or are preceded by, morphological changes in the pelvis (Abel and Macho, 2011). Since both cortical bone and trabecular bone respond to changes in loading patterns, the response of bone structure to early irregular loading and then to more predictable loading during late childhood provide a unique morphological indicator of development in mature and stable gaits (Raichlen et al., 2015). Past research has indicated that the ontogenetic patterns of change in tibial trabecular bone microarchitecture can be associated with locomotor behavior. Shifts from unstable to stable locomotion leave markers on bone during growth and development (Raichlen et

al., 2015). Cowgill et al (2010) found that mediolateral forces are significantly higher in young children than in adults, reflecting mediolateral instability in early walkers.

Raichlen et al. (2015) compared locomotor kinematics with trabecular bone measurements in the distal tibia found less intra-individual variation and higher values in anisotropy as age increased (Raichlen et al., 2015).

Therefore, normal changes in gait patterns across ontogeny are linked to changes in long bone shape during growth. The biomechanical loading produced during early walking likely differs from that of mature gait, and differences between the loads result in differential modeling of the lower limb in young children and adults (Cowgill et al., 2010).

Additionally, recent work shows that trabecular architecture in the tibia differentiates loading patterns in bipedalism and quadrupedalism (MacLatchy and Muller, 2002; Ryan and Ketcham, 2002; Ryan and Shaw 2012; Barak et al., 2013; Raichlen et al., 2015). In guinea fowl, femora are clearly altered following experimentally induced changes due to their locomotor behavior (Pontzer et al., 2006). Barak et al. (2011) examined BV/TV and DA of trabecular bone in the head and neck of the proximal femur and the proximal humerus in bipedal humans and other primates. They found significant differences in trabecular orientation and DA in species with different locomotor repertoires. Species who load their joints primarily in one direction have more anisotropic trabecular structure and less with more generalized locomotor behaviors (Barak et al., 2011). Trabecular morphology may provide a sensitive marker of changes in locomotor stability, since the architecture of trabecular struts may hold more detailed information

regarding both the magnitude and orientation of loading patterns during development (Pontzer et al., 2006; Barak et al., 2011).

Determinants of Degenerative Joint Disease

Degenerative diseases of the joints have become tremendously more common during the twentieth century as a result of the considerable elongation of life expectancy (Eckstein et al., 2000). Degenerative joint disease, specifically osteoarthritis, is a multifactorial disorder characterized by degeneration of cartilage and modification of the structural and material properties of subchondral bone. Multiple risk factors for the development of osteoarthritis have been identified, including age, sex, prior joint injury, obesity, genetic factors, mechanical influences (mal-alignment), and abnormal joint shape (Oliveria et al., 1995; Hashimoto et al., 1998; Chapman and Valdes, 2012). Defining arthritic changes to joint surfaces can encompass a variety of chronic, age-progressive, inflammatory, and degenerative processes. Osteoarthritis is the result of intricate biochemical alterations to normal cell metabolism, which promote altered cartilage repair and cartilage loss (Lajeunesse, 2002). Moreover, it is probable that both genetic and environmental factors play some part in the etiology of most cases of degenerative joint disease (Weiss and Jurmain, 2007). While aging-related changes occur in joint tissues of all individuals, osteoarthritis does not manifest in all individuals, even at advanced age (Temple-Wong et al., 2009; Goekoop et al., 2011). Aging is not the cause for osteoarthritis, however the risk factors for osteoarthritis do increase with age. Ortnier (2003) notes that older individuals are more likely to manifest aspects of the disorder. Aging-related changes provide a basis upon which osteoarthritis can be initiated. Aging

creates an imbalance between stressors that cause damage and the mechanisms that repair or protect against damage (Kirkwood, 2005). For these reasons, degenerative joint disease is both a disease process, as well as, a product of senescence.

It has been previously stated that osteoarthritis is a disorder that hinders and distorts the function of articular cartilage. However, the effects of senescence can also alter many of the factors influencing articular cartilage function.

Senescence

Senescence is a process of decline in the ability to adapt to environmental stress (Bogin, 1999). The pattern of decline varies greatly between individuals, but specific molecular, cellular, and organ level changes can be measured and described. There are many effects of aging on the cellular and extracellular level of articular cartilage (Lotz and Loeser 2012). Aging-associated cellular changes in articular cartilage include cell density depletion due to apoptosis and non-programmed cell death, impaired response to extracellular stimuli, and abnormal gene expression and cell differentiation.

Chondrocytes are required for cartilage tissue homeostasis, and cell dysfunction could be a primary factor leading to cartilage failure. With increasing age, chondrocytes become less responsive to growth factors, develop anomalies due to reactive oxygen species, and lose their ability to cope with mechanical stress (Lotz and Loeser, 2012). Senescent chondrocytes are more vulnerable to accumulation of aberrant proteins and metabolic waste (Vicencio et al., 2008) and decrease in proteoglycan content. The ability of the joint to withstand compressive load is primarily due to proteoglycans. Senescent chondrocytes stimulate pro-inflammatory factors and excessive production of matrix

metalloproteinases (MMPs) due to SASP (senescence-associated secretory phenotype) (Kraan and Berg, 2012). Because of this, there is increased proteolytic activity, which increases collagen molecule degradation. AGE (advanced glycation end products), promoted by elevated glucose levels, increase with age, increase stiffness and increased susceptibility to fatigue failure. AGE receptors on articular chondrocytes stimulate catabolic signaling, upregulation of MMP, and chondrocyte hypertrophy (Cecil et al., 2005; Yammani et al., 2006; Steenvoorden et al., 2006).

Inflammation

Inflammation may be another factor influencing articular cartilage function. Subchondral osteoclastic activity is associated with replacement of the subchondral bone marrow by fibrovascular tissue including macrophages and lymphocytes. This immune response is driven by cytokine expression in the subchondral bone spaces. Interleukin-1 is an enzyme expressed in the subchondral bone spaces. It inhibits proteoglycan production, mediates inflammatory response, and stimulates matrix metalloproteinases (MMPs). Moreover, there is greater stimulation of chondrocyte production of inflammatory mediators and ECM degrading enzymes (Lotz and Loeser, 2012). There is also an up-regulation of vascular endothelial growth factor, which exposes chondrocytes to differentiation factors from tissue (Pan et al., 2012).

Trauma/Fracture

In cases of injury, the normal vascular barrier between cartilage and bone can become breached by fibrillation. Capillaries then penetrate into the subchondral plate and the deep calcified zone of articular cartilage, which allows for the migration of

osteocytes. When cartilage has eroded, subchondral bone is destroyed resulting in subchondral resorption and joint surface porosity (Ortner, 2003). With disruption in the tidemark, subchondral tissues become exposed to factors produced by articular chondrocytes nearer the joint surface, such as vascular endothelial growth factor (VEGF) (Pan et al., 2012). Abnormal force on normal articular cartilage due to trauma is responsible for ‘surface irregularities’ (Mitchell and Cruess, 1977). Injurious mechanical loading may be a stimulus for excessive reactive oxygen species production in cartilage. The superficial zone is where the earliest changes occur in human articular cartilage aging (Temple-Wong et al., 2009) and is also the most susceptible to mechanical injury (Otsuki et al., 2008; Carames et al., 2012).

Genetics

Genetics also plays a role in the development of OA. It appears from molecular studies that genetic influences have no or little heritability in the presence versus absence of osteoarthritis, but genes affect the severity of the osteoarthritis present (Spector and MacGregor, 2004). Geneticists have identified some single gene disorders of the hip, but have had difficulty in identifying the genetics of many of the common causes of degenerative hip diseases. The heterogeneity of the phenotypes studied is part of the problem (Hamilton and Jamieson, 2012). Two genes significantly associated with OA: MCF2L and GPR22/7q22. The MCF2L gene is significantly associated with large joint OA and GPR22/7q22 are several genes found to be associated with OA (Hamilton and Jamieson 2012; Meulenbelt, 2012).

Summary

This chapter has provided background on current concepts in skeletal ontogenetics, with special focus on the role of mechanics in development of the long bones. The highly sensitive process of long bone formation and longitudinal growth is responsible not only for the general process of bone enlargement, but also the origins of several fundamental characteristics of long bone geometry and microarchitecture. The ongoing modification of bone tissue via cellular mechanisms (modeling and remodeling) of independent and coupled deposition and resorption is subject to a complex system of controlled feedback mechanisms that are governed by mechanical loading, genetic pre-programming, diet, age, anatomical site, hormones, and other factors.

CHAPTER 3: THEORETICAL IMPLICATIONS FOR FUNCTIONAL INTERPRETATION OF BONE MICROARCHITECTURE

Historical Perspectives in Bone Functional Adaptation

As mentioned in Chapter 2, bone models and remodels in response to the mechanical stresses it experiences, resulting in a lightweight structure that is adapted to its applied loads (bone functional adaptation). Therefore, bone form reflects its mechanical loading history during life. The idea that bone senses and adapts to its mechanical environment is an old concept. In 1638, Galileo first noted that mechanical stimuli contributed to bone shape and bone strength regulation. In 1827, Sir Charles Bell observed that trabecular structure had forces acting on it. Both Sir Bell and Jean Baptiste Marc Bourguery (1832) recognized that trabecular architecture was influenced by mechanical forces and maximum strength efficiency. In 1838, F.O. Ward compared the trabecular arrangement in the femoral neck to a street lamp and its holding bracket. Ward's comparison is significant because he recognized that bone structure can be analogous to engineered structures (Martin et al., 2015).

In the mid-1800s, Hermann Von Meyer (1867) and Karl Culmann (1866) observed that trabeculae were orientated along principal stress lines. Von Meyer proposed the concept that trabecular architecture followed the direction of principle compressive and tensile stresses in a similarly shaped trabecular structure. Culmann developed a graphical method to calculate principal stress directions using a Fairbairn

steam crane. He found that trabeculae are oriented in the principal direction of stresses in a curved crane-like shape of adaptation along the stresses. Later John Koch (1917), resolved some of the issues regarding the comparison of Culmann's stress trajectories for the Fairbairn crane with a human femur. Koch calculated the stress trajectories in a human femur based on actual anatomic measurements. He was able to demonstrate that trabecular orientations are similar to mathematical calculations of stress trajectories for a homogeneous structure of the same shape; density should be highest in areas of highest shear stress.

At the end of the nineteenth century, Wilhelm Roux (1885), influenced by Darwin, hypothesized that organisms possessed the ability to adapt to changes in their living conditions. Roux proposed that the ability of bone to align trabeculae with stress trajectories was accomplished by cells forming and resorbing bone according to variations in a functional stimulus (mechanical load). He proposed that bone obtains maximum mechanical efficiency with minimum mass and in summary bone changes in relation to the loading stresses placed on it. Independent of Roux, Julius Wolff (1892) introduced a theory (Wolff's Law) that states the final mass and trabecular architecture of bone is determined by a bone's mechanical environment. The form of bone follows its function in a mathematically manner, and adapts to its mechanical environment. However, the mechanisms by which this change occurs was not stated by Roux or Wolff (Frost, 2004; Ruff et al., 2006). It was not until Alfred Glücksmann (1942) that evidence for these theories was produced. Glücksmann constrained the growing limbs of chick embryos to create bending loads and found increased ossification along principal lines of

tensile stress. Wolff's Law relied on a mathematical model that bone was similar to a metal beam and has now been falsified but the general idea influenced later researchers and the concept of bone functional adaptation (Ruff et al., 2006).

In summary, nineteenth-century researchers provided three key concepts regarding bone's ability to adapt to changing mechanical loads: bone structure optimizes strength with respect to the amount of material used; trabeculae line up with principal stress directions; and these things are accomplished by a self-regulating system of bone cells responding to a mechanical stimulus.

Mechanostat Theory

More recently, the mechanism of bone functional adaptation was introduced by Frost (1987; 2003) and several others (Lanyon and Rubin, 1984; Skerry, 2006; Martin, 2007). Harold Frost (1987), an orthopaedic surgeon, proposed the mechanism that controls changes in mass during longitudinal growth, modeling, and remodeling is a mechanical feedback system called the mechanostat. Similar to a thermostat, the mechanism that controlled bone mass would be turned on or off in response to strain from an applied load. Frost argued that the aim of bone adaptation is to keep habitual strain within the bone within defined thresholds. The strain thresholds, called minimum effective strains (MES) can initiate or suppress remodeling and modeling and also determine when and where these activities are activated or deactivated (Frost 1987) and a subsequent increase in bone mass. Strains below the minimum effect strain for modeling (MES_m) suppress the activation of bone modeling and result in no additional formation of bone. Above another threshold, in which bone is exposed to greater than typical peak

mechanical loads, bone formation occurs on the existing structure to increase bone strength (Frost, 2003). However, minimum effective strain for remodeling (MES_r) keeps remodeling in a conservation state and bone is retained. If the strains fall below the MES_r , as in immobilization or hypogravity, bone remodeling increases, permanently removing bone, primarily from the endosteal envelope (Frost, 1998). The thresholds separating these zones or ranges are termed “setpoints.” As with any homeostatic control system, bone’s mechanostat is constrained by several independent components, hormones, nutrition, behavior and environmental factors all influence the regulator. These setpoints are determined by those factors, and so cannot be viewed as fixed at a particular strain level. However, Frost does not explain how skeletal sites are regulated differently. Thus, bone tissue has an intrinsic “mechanostat” which regulates bone functional adaptation. With increasing load, modeling is increased and remodeling is inhibited and with decreased loading, modeling is inhibited and remodeling is increased based on mechanical strain and set points in a hormonal and metabolic environment.

Utah Paradigm

Supplementing the 1960 paradigm of skeletal physiology, the University of Utah hosted a series of Hard Tissue Workshops in the mid-1990’s focused on biomechanics and tissue level mechanisms (Frost, 2000). These workshops established an agreement between the subfields of skeletal biology and addressed the lack of a multidisciplinary approach to skeletal research. As a result of these workshops, the Utah Paradigm was created. This paradigm proposed that bone effector cells (osteoblasts and osteoclasts) ultimately determined bone health (Frost, 1998; 2000). This paradigm also focused on the

topics of bone mechanical property and how the mechanostat could be used to explain how load-bearing skeletal elements attain mechanical competency. This paradigm also specified that mechanical factors, especially voluntary loads and strains that come from muscle forces rather than body weight, are the driving force behind load-bearing skeletal architecture and that non-mechanical factors (hormones, sex, age), alter how, when, and where bone is deposited (Frost, 2000). It is important to note that these non-mechanical factors do not control bone strength, and that bone strength is ultimately controlled by mechanical loads (Morse et al., 2014).

Mechanical Properties of Bone and Cartilage

The mechanical properties of a structure depend on both its geometry and the properties of the material inside. The primary mechanical function of bone is to provide a rigid attachment for muscles, and to remain as light as possible for movement. To accomplish this bones must adapt their shape and architecture (Turner and Pavalko, 1998). However, there are many extrinsic and intrinsic factors that affect bone's mechanical properties in response to loading. Extrinsic factors include the mode of strain, the duration of the strain, and the rate of the strain. Intrinsic factors include the degree of mineralization, and the organization of the tissue (Pearson and Lieberman, 2004). Age is also a factor in how bones deal with mechanical forces. Younger individuals, generally exhibit strong modeling and remodeling responses to loading, while older individuals exhibit a weaker response (Pearson and Lieberman, 2004) In older individuals, osteoblasts are less responsive to strains than osteoblasts in growing individuals (Stanford et al., 2000; Donahue et al., 2001; Jacobs et al., 2010; Wu et al., 2011). Additionally,

comparative studies reveal that after exercise mechanical loading only stimulates periosteal growth in mostly individuals prior to skeletal maturity, and acts to slow down the rate of bone loss in older individuals (Kohrt, 2001). Mechanical loading also affects bone structural features differently. Case in point, loading magnifies the structural changes produced during growth (Bass et al., 2002).

The skeletal system is anisotropic and subject to a variety of different types of forces in such a way that the bone receives loads in different directions. There are loads produced by weight, gravity, muscle forces, and external forces. The loads are applied in different directions producing forces that may vary from five different types: compression, tension, shear, curvature and torsion. Bone is considered viscoelastic because it responds differently when it receives loads in different speeds. When it receives the load quickly, the bone responds more rigidly, and may handle a higher load before it breaks. When it receives the load slowly, the bone is not so rigid or strong, breaking under lesser loads. The bone tissue starts to deform permanently and eventually breaks if the load continues in the non-elastic phase. Thus, when the load is removed, the bone tissue does not retake the original extent and is permanently elongated (Holtrop, 1975). Another way to assess the behavior of the bone or any other material when subjected to load is to measure the stress, or the load by area, and deformation (strain) or change in the length or angle. When bones are loaded in compression, tension, or torsion, bone tissue is deformed. Deformation of tissue, or the relative change in length of bone tissue, is referred to as strain. The stress-strain curve and the load-deformation curve illustrate the performance strength characteristic of a material when subjected to the load.

When the load is applied, there is an initial elastic response that eventually reaches a yield point, getting into the plastic response where the material is deformed permanently or is broken. The strength of the material is determined by the energy or area under the curve. The hardness of a material, called elasticity module (Young's modulus) is determined by the inclination of the curve during the elastic response phase (Figure 3.1).

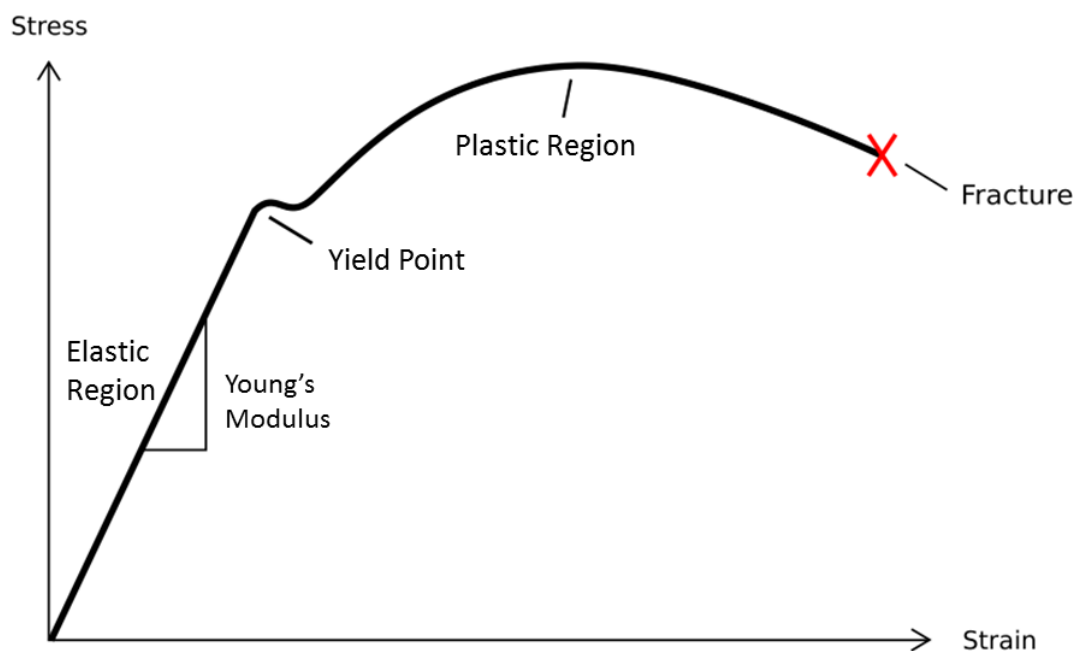


Figure 3.1: Stress (MPa)-Strain (%) curve for a ductile material.

Cartilage

Bone is sensitive to its mechanical environment. Cartilage is less adaptive (Martin et al., 2015). Articular cartilage is a thin layer of specialized connective tissue with unique viscoelastic properties. Its principal function is to provide a smooth, lubricated surface for low friction articulation and to facilitate the transmission of loads to the

underlying subchondral bone. It is able to transfer loads from one bone to another while simultaneously allowing the load-bearing surface to articulate with very low friction (Martin et al., 2015). The biomechanical behavior of articular cartilage is best understood when the tissue is viewed as a two-phase medium. Articular cartilage consists of 2 phases: a fluid phase and a solid phase. Water is the principal component of the fluid phase, contributing up to 80% of the weight of the tissue. Inorganic ions such as sodium, calcium, chloride, and potassium are also found in the fluid phase. The solid phase is characterized by the extracellular matrix, which is porous and permeable (Fox et al., 2009).

The relationship between proteoglycan aggregates and interstitial fluid provides compressive resilience to cartilage through negative electrostatic repulsion forces. The initial and rapid application of articular contact forces during joint loading causes an immediate increase in interstitial fluid pressure. This local increase in pressure causes the fluid to flow out of the extracellular matrix generating a large frictional drag on the matrix. When the compressive load is removed, interstitial fluid flows back into the tissue. The low permeability of articular cartilage prevents fluid from being quickly squeezed out of the matrix. The 2 opposing bones and surrounding cartilage confine the cartilage under the contact surface. These boundaries are designed to restrict mechanical deformation.

It is well established that bone responds to mechanical loading during growth however the specific role of mechanical loading in determining articular surface area is unclear. The development and maintenance of cartilage structure and mechanical

characteristics are tied directly to the effect of mechanical loading on the biology of the cartilage cells and their ECM. Patterns of stress, strain, and fluid flow created in the joint can affect the micro and macro morphology of articular cartilage (Wong and Carter, 2003). Compared to congenitally or neonatally paralyzed limbs, joints in normal limbs developed greater diameters, greater radii of curvature and surface areas, thicker capsules and ligaments, and more subchondral bone to support their articular cartilage (Frost, 1999). Plochocki and Organ (2003) tested the hypothesis that a growth mechanism responsive to mechanical stresses allows articular surface area to adapt to its mechanical environment. Their data supported the hypothesis that articular surface area is responsive to differential loading during growth. Articular surface area at the proximal femur and proximal tibiae are significantly greater in exercised pigs relative to controls. Plochocki et al. (2009) propose that the joint surface growth is regulated by hydrostatic compressive stress in articular cartilage. In this study, they used a computational approach to evaluate the theory. Their results indicated that magnitude showed increased joint congruence, increased articular cartilage stresses, and enlarged articular contact. The chondral modeling theory may allow scientists to more accurately infer the magnitude and direction of habitual peak joint loadings. During growth, epiphyseal trabeculae are usually thicker, fewer, and farther apart than the secondary spongiosa. Throughout life, the loads on epiphyseal spongiosa transfer to the metaphyseal spongiosa (Frost and Jee, 1994)

Articular cartilage is viscoelastic and exhibits time-dependent behavior when subjected to a constant load or deformation. Two types of mechanisms are responsible for

viscoelasticity in articular cartilage: flow dependent and flow independent. Articular cartilage also exhibits a creep and stress-relaxation response. When a constant compressive stress is applied to the tissue, its deformation increases with time, and it will deform or creep until an equilibrium value is reached (Fox et al., 2009). Under loading and elevated loading in joints increases enzyme production, especially matrix metalloproteinases (MMPs). MMPs attack the cartilaginous matrix and disrupt cartilage homeostasis. While enzyme inhibitors are produced, they cannot keep pace with the proteolytic process. The cartilage begins to erode and break down into fibrils allowing proteoglycans and collagen fragments to be released into the joint space. The presence of these breakdown products ultimately produces an inflammatory response in the synovial membrane involving increased production of enzymes and cytokines that destructively diffuse into the cartilage. Over time, bone overgrowth results from an attempt to repair the joint (Waldron, 2007; Suri and Walsh, 2012).

Mechanical Loading Effects on Bone Surfaces

The competing architectural demands of remodeling and modeling show that mechanical adaptation occurs at both the structural level and at the tissue level, and these processes must be somehow coordinated. Shape and size changes are effected on external (i.e., periosteal and endosteal) bone surfaces, where there is more modeling than remodeling during growth, and less capacity for change in adults (Frost, 1986). On the other hand, changes in material properties are effected on internal (i.e., Haversian and trabecular) bone surfaces. Internal bone surfaces are governed primarily by remodeling throughout life (Frost, 1986; Martin et al., 2015). Carpenter and Carter (2008) argue that

periosteal surface loads may be an important component of a group of mechanical stimuli, which has implications for the development of bone cross-sectional shapes. In response to mechanical loading the periosteal cells respond by increased cell proliferation, angiogenic response, and release of nitric oxide and PGE2 (Prostaglandin E2) production. This response stimulates bone formation (Turner and Robling, 2004; Robling et al., 2006; Gosman et al., 2011). Increased mechanical loading leads to greater subperiosteal expansion of long bone cortices prior to puberty, and greater endosteal narrowing afterward (Bass et al., 2002; Ruff, 2005). This process changes with the onset of puberty; estrogen production begins to inhibit periosteal apposition and stimulates new bone acquisition on the internal surface (Bass et al, 2002). Ausk and colleagues (2012) reported that in the absence of loading (transient muscle paralysis), the periosteal surface maintains its morphology. However, cortical bone loss is achieved through rapid endosteal expansion. Szulc and Delmas (2007) reported these same findings in elderly men. With age, there was higher endosteal bone loss and the periosteal apposition rate remained constant.

Biomechanically, morphological variation in both cortical (Bass et al., 2002; Shaw, 2011; Stock, 2006) and trabecular bone (Lambers et al., 2013b; Morgan et al., 2003; Schulte et al., 2013) strongly correlates with the loading environment (Christen et al., 2014). Osteons affect the mechanical properties of the cortex in several ways: replacing highly mineralized bone matrix with less calcified material, increasing cortical porosity, and introducing cement line interfaces that have different mechanical properties. If a cement line is disrupted by stress in cortical bone, the disruption is contained within

the bone, but in trabecular bone it may propagate to the surface, disconnecting the structural unit from the parent trabecula. Thus, remodeled cortical bone structure may be inherently more damage resistant than remodeled trabecular bone structure. Three determinants of trabecular bone mechanical properties are the magnitude of the porosity, anisotropy of the trabecular architecture, and the material properties of the tissue in the individual trabeculae (Martin et al., 2015). In trabecular bone, soft tissue dominates the space, and anisotropy is governed by trabecular orientation. The relative numbers and sizes of trabeculae oriented in different directions control the anisotropy of the macroscopically measured material properties.

Critiques of Bone Functional Adaptation

Although many of these studies have some idea for how bone responds to loading, it is clear that the mechanisms underlying bone functional adaptation are not fully understood (Currey, 2012) and that many other factors may contribute to changes in bone morphology. The general concept that bone adapts to its mechanical environment during life can be used to explore differences in past mechanical environments. However, debate exists about the potential systemic impact on other areas of the skeleton when one bone/region is loaded (Lieberman, 1996; Sample et al., 2008; Sugiyama et al., 2010; Wallace et al., 2010; Cresswell et al., 2016), and how bone remodeling changes in response to differences in age (Pearson and Lieberman, 2004; Ruff et al., 2006; Nikander et al., 2010), muscle (Robling, 2009) versus joint reaction loading (Judex and Carlson, 2009; Schipilow et al., 2013) force (Christen et al., 2014; Schulte et al., 2013), and even how these factors are balanced against the role of the bone in maintaining homeostasis

(Currey, 2003; Dempster and Raisz, 2015; Stephens et al., 2016). Moreover, bone is not an idealized isolated unit in response to mechanical load ii is also affected by surrounding muscles and connective tissue.

Summary

This chapter provided background information regarding the historical context of bone biology research, including the origins and development of the theory of bone functional adaptation, the key concepts of the Utah Paradigm of skeletal physiology, and the principles of the mechanostat theory. Moreover, the impact of mechanical loading on bone and cartilage development is elucidated. Finally, this chapter ends with a critical review of bone functional adaptation and its use in bone biology research.

CHAPTER 4: THE PEOPLE OF THE ONEOTA TRADITION

Oneota Tradition

The Oneota people occupied much of the Midwestern United States from the late 10th through early 17th centuries A.D. Evidence of this culture can be found throughout the country, including portions of Illinois, southern Michigan, northwestern Indiana, Iowa, Wisconsin, southern Minnesota, northern Missouri, and eastern Nebraska (Green, 1995; Berres, 2001). Oneota groups are distinguished from surrounding Mississippian societies, such as Cahokia of the American Bottom and the Fort Ancient tradition of the Middle Ohio River region, by their horticultural adaptation to the Prairie Peninsula, a distinct region exhibiting a mosaic of grassland, forest, and aquatic/wetland resources (Transeau, 1935; Geis and Boggess, 1968; Berres, 2001). The Oneota were more reliant on wild resources than is the case for Mississippian peoples (Schroeder, 2004).

Broad-Spectrum Subsistence

The Oneota villagers were horticulturalists who maintained broad-spectrum subsistence economies that involved slash-and-burn cultivation of maize supplemented by a wide range of seasonally available wild foods from the forest and prairie. A vital part of Oneota emergence was the efficient exploitation of forests, prairies, and wetlands and areas conducive to horticulture. Their hunting, gathering, and fishing economy was supplemented by horticultural strategies combining cultivation of C3 plants, such as

squash and small-seeded annuals, with limited maize horticulture (Brown, 1982; 1990). Maize agriculture intensified through time (Overstreet, 1981), giving rise to elaborate ridged fields in southeastern Wisconsin to promote cultivation (Boszhardt et al., 1985; Overstreet, 1981). At the same time, reliance of maize seems less intense in some other areas, possibly because of lower population densities or greater dependence on wild resources (Gibbon, 1972). Animal procurement (hunting and fishing) was geared to the exploitation of a wide variety of species. Large terrestrial species, such as white-tailed deer and elk, were viewed as representing important components in Oneota economy (Gibbon, 1986: 332), but the varied aquatic/wetland resources near the villages (e.g., fish, waterfowl, mussel, and turtle species) were the main target of exploitation (Gibbon, 1986; Berres, 2001). Among Oneota in general, small mammals (e.g. squirrels, beaver, and muskrat) as well as birds, amphibians, reptiles, fishes, and freshwater mussels were likely as important as upland game such as deer and elk (Emerson and Brown, 1992; Berres, 2001). In terms of plant food remains, Oneota sites reflect relatively diverse plant exploitation with three distinct components: wild-plant gathering, nut collecting, and plant cultivation (Gibbon, 1986: 333). Gathered wild plants, such as wild fruits and American lotus, were collected from a variety of environmental contexts (woodland, wetland, and disturbed habitats) and represented an important secondary food source (Santure et al., 1990).

Oneota Settlement

The broad-spectrum subsistence strategies often involved settlement movements in response to wide seasonal fluctuations in food availability and unpredictable migration

patterns of elk and bison (Arzigian et al., 1989). The general Oneota settlement subsistence system has two distinct phases of an annual seasonal cycle: relatively large, semi-permanent horticultural villages, which were usually in riverine settings and were occupied from spring through the late fall or early winter, and outlying hunting camps, found in upland settings, which were occupied by nuclear family units during the winter (Berres, 2001). Whether near a lake or river, the Oneota main settlements were never far from forest, prairie, and aquatic/wetland resources (Brown, 1982; 1990). Villages were located on elevated terraces within proximity of extremely productive aquatic/wetland environments and prairie-forest ecotones as well as highly fertile horticultural forest soils that could be easily worked with a digging stick or hoe (Stoltman, 1986; Schroeder, 2004). The village inhabitants had access to local chert sources (for tools) exposed as glacial cobbles in stream beds or present in beds of limestone along the valley of bluffs (Santure et al., 1990; Kreisa, 1993; Berres, 2001). Oneota peoples were more sedentary than Late Woodland societies but moved their settlements more frequently than appears to have been the case for the people living at the large Mississippian mound sites further to the south (Schroeder, 2004).

Sociopolitical Organization and Division of Labor

Oneota societies are characterized as having a tribal level of sociopolitical integration, much like Woodland societies. Oneota villages had access to similar resources, making them relatively self-sufficient, which may explain, the limited power of leaders. Politico-economic systems were embedded in kin-based social organizations (Green, 1995). Male and female Oneota leaders helped direct many ritual and economic activities, while group

consensus played a vital role in decision-making matters. Such shared decisions resulted in behavioral uniformity within social groups (Berres, 2001). Among Oneota peoples, men did most of the hunting and fishing, butchering, quarrying, metalworking, land clearing, raiding, boatbuilding, housebuilding, and work in bone, horn, shell, and wood. Women were engaged in such activities as pottery production, cooking, gardening, gathering shellfish, hide-working, preservation of meat and fish, burying the dead, child care, and producing clothing (Benn, 1995).

Oneota Material Culture

The Oneota material culture consists of a variety of worked bone, antler, shell, and lithic artifacts. Oneota made distinctive globular jars with tall (high) rims, tempered with crushed shell from freshwater mollusks. They were often decorated with curvilinear trailed lines and chevrons and are distinctly different from the grit tempered cord-marked vessels that are classified as Late Woodland. Artifact assemblages from Oneota sites are also characterized by relatively large numbers of end scrapers that were used for processing and cleaning hides (Boszhardt and McCarthy, 1999; Schroeder, 2004), as well as, small triangular projectile points with some miscellaneous stemmed and un-stemmed knives (Overstreet, 1995; Esarey and Conrad, 1998; Berres, 2001).

Norris Farms 36 Cemetery (11F⁰2167) and Morton Village (IAS 11F1)

Norris Farms 36 cemetery is the burial mound associated with Morton village, a Bold Counselor Phase habitation site (A.D. 1300-1450). The proximity of the village to the burial mound suggests that the individuals interred at Norris Farms 36 resided at the Morton village site. The duplication of many domestic pottery design elements on burial

vessels strongly supports this theory (Santure, 1990a). Both Norris Farms 36 cemetery and Morton Village make up the Morton site complex. The Morton site complex is located in Liverpool Township of Fulton County, Illinois. The site is situated on a 1.6km long section of the western bluff of the Illinois River valley. Norris Farms 36 cemetery was completely excavated in 1984 and 1985 by the Illinois State Museum, and approximately 264 well-preserved skeletons (122 adults, 142 children) were recovered. In this study, 31 of the 264 skeletons were used. Most of the graves were located in a low mound in slightly alkaline loess soil. The excavated mound is approximately a 2,078m² area (Figure 4.1). The age and sex distribution of the skeletons correspond to expected human mortality patterns in traditional societies (Milner et al., 1989), which suggests that most community members were buried in this cemetery (Santure et al., 1990). It is one of the earliest Oneota sites discovered in the area, and is thought to represent an intrusive population that originated from Oneota groups in the Upper Mississippi River Valley (Esarey and Santure, 1990). There is little evidence of biological interaction between the Bold Counselor Phase Oneota and surrounding Mississippian groups (Steadman, 1998). However, there is strong ceramic evidence of coexistence and cohabitation of both Oneota and Mississippian peoples (Esarey and Conrad, 1998; Steadman, 2008).

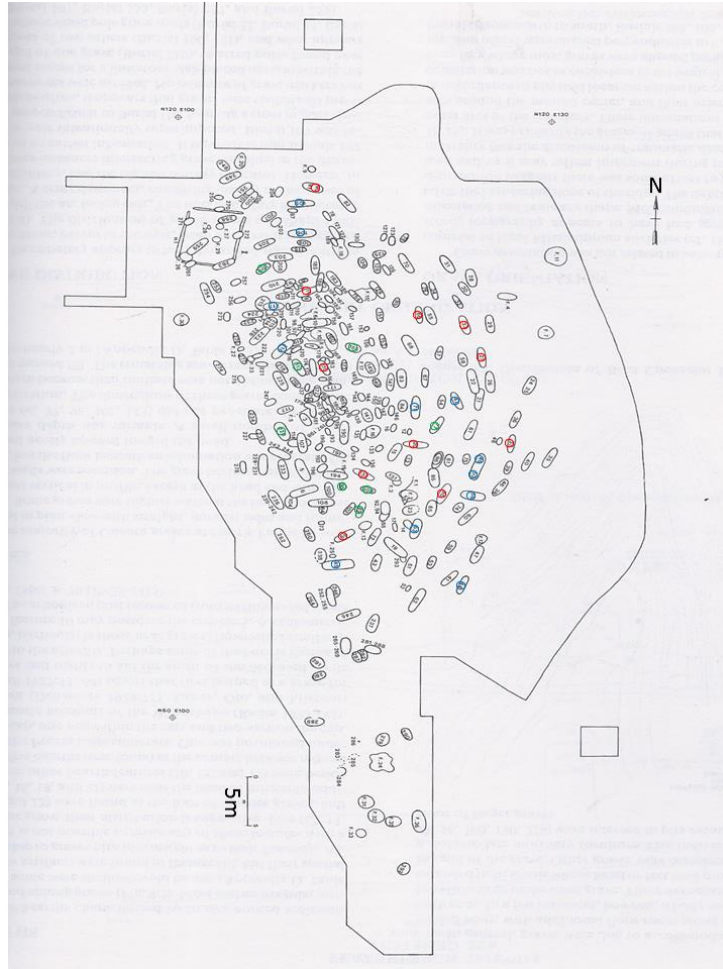


Figure 4.1: Norris Farms 36 Cemetery.

Note: Burials of the individuals used in this study are indicated. Males (Blue), Females (Red), Juveniles (Green) (Adapted from Santure et al., 1990)

Bold Counselor Phase

The Bold Counselor phase is the occupation of a spatially restricted section of the central Illinois River valley by an intrusive, Oneota-derived population. Five Bold Counselor Phase components are presently known in the central Illinois River valley (Figure 4.2). Bold Counselor Phase refers to the evidence for an Oneota group that migrated from somewhere in the upper Mississippi River valley to the central Illinois

River valley during the middle to late 13th century. While artifacts are used as the primary means of identifying this shift in cultural identity, the Oneota society does not seem to have been as organizationally complex as its Mississippian predecessor. Regional specialists interpret the Oneota sites as an intrusion of people into the valley, and this particular ceramic tradition persisted into the 15th century A.D. (Esarey and Santure, 1990; Milner et al., 1991a). Other than the use of shell-tempering in pottery, little similarity in material culture can be seen between the 14th and 15th century Bold Counselor Phase and late Middle Mississippian occupations of the region. The hallmarks of the Bold Counselor ceramics are: 1) a high frequency of jars with horizontal trailing, 2) low incidence of lip stamping on jars, 3) production of bowls which have lip stamping, 4) the presence of a broad, shallow bowl formed with flared, concave handles, and 5) the presence of Mississippian style plates with Oneota motif decorations (Esarey and Conrad, 1998) (Figure 4.3). The close spacing of the Bold Counselor Phase villages and the lack of secondary sites were strongly dictated by social factors. The concentration of most of the population into intensively occupied villages certainly had a debilitating impact upon general health. Constrained zones due to constant threat of violence, as well as, immediately sequential sites, may have restricted their availability of local faunal and floral resources and their efficient exploitation. Morton, C.W. Cooper, and Sleeth, sites were found to be coexisting, and therefore increased intercommunity contact may have further contributed to a decline in the health of the population by facilitating the spread of disease (Esarey and Santure, 1990; Esarey and Conrad, 1998). There is evidence indicating total abandonment of the Illinois River by A.D. 1450. Morse and Morse (1983:

282) suggest that after about A.D. 1400 further nucleation of populations in the central Mississippi Valley took place, leaving many areas empty (Esarey and Santure, 1990). Given the evidence for major changes in the lifeways of the Illinois River valley between A.D. 1250-1400 and the lack of any evidence for continued Bold Counselor Phase or Middle Mississippian occupation of the area after A.D. 1450, it seems likely that both groups finally withdrew from the valley and/or disappeared as distinct cultural entities altogether. There is no local evidence of post A.D. 1450 cultural activities, and continuity of populations is very unlikely. It seems most likely that the various disruptive factors affecting the inhabitants of the central Illinois River valley caused an end to the former lifeway by A.D. 1450 (Esarey and Santure, 1990).

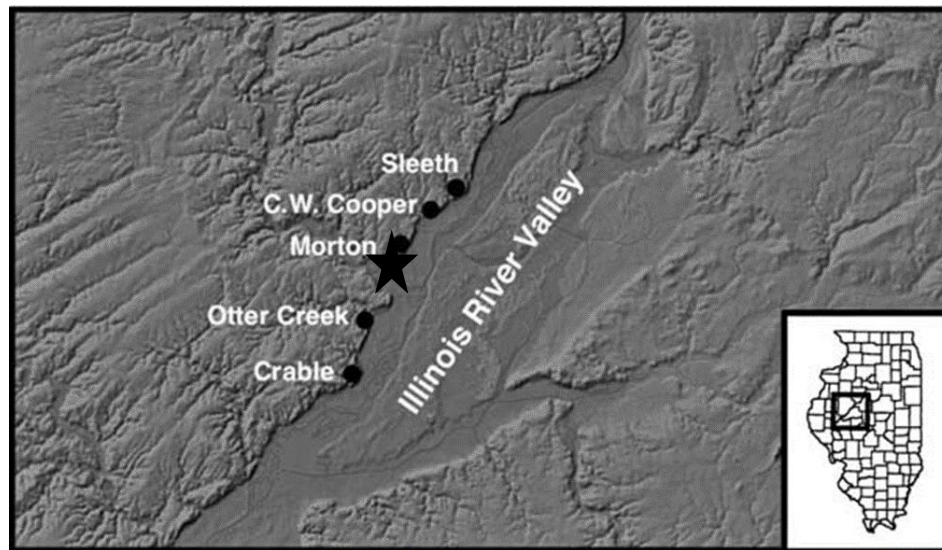


Figure 4.2: Bold Counselor Phase Oneota Sites of the Central Illinois River Valley.
Note: ★ = Norris Farms 36 Cemetery (Adapted from Lieto and O’Gorman, 2014).



Figure 4.3: Bold Counselor Phase Jar Fragment from Morton Village with example tall rim and curvilinear trailed lines. (Morton Village Archaeological Project).

Faunal and Floral Resources at Morton Village

Regionally, the subsistence economy of the late prehistoric Oneota peoples is comprised of a broad spectrum of wild and cultivated resources (Styles and King, 1990). The diversity of available resources at Morton Village is consistent with Oneota sites but unlike other Oneota groups, early floral and faunal analyses suggested a relatively restricted subsistence base, with an emphasis on maize cultivation and white-tailed deer. In comparison to the preceding Mississippian component at Morton site, the Oneota component appears to have more acorn nutmeats, more maize, and a greater number of other domestic plants and potential cultigens, and more wild fruit.

Faunal remains from Morton village suggest a focus on woodland and Illinois River flood plain resources, particularly deer and fish. Bone artifacts from woodland and aquatic/semi-aquatic taxa were present. Marine gastropods (*Marginella apicina*), freshwater pelecypods (*Campeloma sp*), domestic dog (*Canis familiaris*), turkey, freshwater drum (*Aplodinotus grunniens*), white-tailed deer, goshawk (*Accipiter gentilis*), freshwater mussels (*Anodonta spp*), trumpeter swan (*Cygnus buccinator*), channel catfish (*Ictalurus punctatus*), bowfin (*Amia calva*), common snapping turtle (*Chelydra serpentina*), softshell turtle (*Trionyx sp*), and elk were represented. The absence of bones from migratory waterfowl in village refuse and the large proportion of fish, suggest a warm weather occupation occurring between the spring and fall waterfowl migrations (Styles and King, 1990).

Plant remains from Morton village indicate diverse plant usage. Small wild seeds of native taxa knotweed (*Polygonum erectum*), chenopod (*Chenopodium spp.*), little barley (*Hordeum pusillum*) occur in small quantities at Morton site. Wild fruits are well represented in Oneota sites, particularly American plum (*Prunus americana*) and nuts were common. These include hickory nuts (*Carya spp.*), acorns (*Quercus spp.*), black walnut, butternut (*Juglans cinerea*), and hazelnut. The relatively large amount of acorn nutmeats recovered from the Morton site is unique among the Oneota sites (Styles and King, 1990). However, it is clear that Oneota agriculture was well established and included the cultivation of corn (*Zea mays*), beans (*Phaseolus vulgaris*), squash (*Curcubita pepo*), and sunflower (*Helianthus annuus*) (Tubbs and O’Gorman, 2005; Tubbs, 2013).

Isotopic samples from Norris Farms 36 suggested that maize was slightly less important than it was to the nearby Mississippians (Hollinger, 1995; Buikstra and Milner, 1991). There is lower consumption of maize by the Bold Counselor Oneota population interred at Norris Farms 36 in relation to the Middle Mississippians. Oneota were getting less of their dietary protein from maize than the Middle Mississippians at Orendorf (Steadman, 1998; Tubbs, 2013). Isotopic values also suggest that the diet at Norris Farms 36 was much more diverse in food resources, similar to traditional Oneota diet. The increased maize consumption at Morton Village relative to other Upper Mississippian groups may be a response to cultural contact with Middle Mississippians. Moreover, there is a general trend for higher consumption of maize by females (Tubbs, 2013).

Mortuary Behavior and Grave Distribution of Norris Farms 36

The Norris Farms 36 cemetery consisted of many graves, most containing single individuals that collectively formed an elongated asymmetrical oval. Grave shape was elliptical, and depth varied from 31 centimeters to almost 2 meters below surface level. Another meaningful pattern is the presence of burned areas or hearths near some graves. They represent the remains of graveside fires that aided the spirit of the deceased on its journey to the otherworld (Santure, 1990b). Skeletal orientation was dependent on topography rather than celestial orientation, although groups of individuals are oriented alike. The center of the cemetery was preferred for infants, while the outer rings of graves primarily held adults. The distribution of males and females appears to represent time of death rather than specific burial precincts, although females were more common in outer rows on the eastern edge of the cemetery. The preferred location for the internment of

warfare victims was at the cemetery edge in reopened graves. Most individuals were buried in a fully articulated (95%), extended (86%), and supine (81%) position (Santure, 1990c; Emerson and Brown, 1992). There are more adult females than males in the cemetery sample; however, this difference between the sexes is not significant. The overall demographic picture is consistent with the interment of most or all of the village dead in a community cemetery.

The pattern of mortuary behavior at Norris Farms 36 reflected both group and individual emphases. In some instances, individuals were treated in terms of their group affiliations. Such an example includes simple familial relationships, where relatives were buried either together or in close proximity to one another. Individualized emphasis seemed to be expressed by the placement of several burials with little indication of clans or moieties (Santure and Esarey, 1990). Grave goods were associated with individuals of all ages and both sexes and generally consisted of common artifacts such as shell spoons with complete ceramic vessels. The association of shell spoons with complete vessels indicates that pots were filled with food at the time of burial (Santure and Esarey, 1990: 106). Based on the distribution of artifacts, males were important members of Bold Counselor Phase society. Artifacts reflective of daily tasks (weapons, lithic tools, processing tools, and raw materials) were almost exclusively associated with males, as were status ornaments and ritual equipment. There is also a widespread age distribution of individuals with arrow points. At Norris Farms 36, individuals from 8 to 50+ years old were buried with arrow points. Seventy percent of adult males had arrow points in their graves. The high frequency of arrow points combined with the wide age range of

individuals perhaps emphasized the significance this weapon had to ensure day-to-day group survival (Santure and Esarey, 1990).

Physical Anthropology of Norris Farms 36

The human remains from Norris Farms 36 represent the largest existing well-preserved and adequately documented Oneota skeletal collection. The Norris Farms 36 skeletal series was derived from a completely excavated cemetery. The Oneota burial sample consists of 42% adults (n = 112), 4% adolescents (n = 10), and 54% children and infants (n = 142). In general, the Oneota skeletons were complete and well preserved. However, osteological and archaeological evidence indicates that the Oneota were victims of local warfare in the form of malnutrition, nutrition-related disease, and warfare-related trauma such as cut marks from scalping and projectile points embedded in bone (Santure, 1990b; Milner et al., 1991a). Of the 264 individuals buried in this cemetery, 50 show evidence of violent death. The violent deaths were probably the result of intermittent raids upon the associated Oneota village that left the dead mutilated for status-enhancing trophies (Milner et al., 1991a: 594) and further supports the claim that the Oneota were an intrusive population that was in conflict with neighboring Mississippian villages. This conflict may have affected the frequency and/or range of physical activity among the Oneota. With constant raiding, there was limited movement to obtain geographically available resources. Moreover, the danger with venturing away from the settlement prevented parents from bringing their children during food obtaining activities. These precautionary behaviors and sedentary lifestyle may have influenced the locomotive patterns of the group as a whole.

Warfare and Lethal Trauma

One of the more notable aspects of the Norris Farms 36 skeletal series is the high level of social conflict documented by skeletal evidence of lethal trauma. The victims tended to die in small-scale surprise attacks. Fifty individuals (19 males, 23 females, 2, children, 1 adolescent, 5 indeterminate), or 19% of the burial population, were victims of intermittent raids. Among the adult victims, females and males are equally represented. The low frequency of children may indicate that children were rarely killed or they were killed without impacting the skeleton. Evidence of violence consisting of arrow wounds, parry fractures, scalping, decapitation, and other mutilation was observed on the skeletal remains of these individuals. Complete or partially articulated remains were interpreted as raid victims who were not immediately recovered for burial at their death. In general, victims of violent death were interred in peripheral areas of the cemetery, and buried with other victims in mass or reopened graves (Santure et al., 1990)

The Oneota population from Norris Farms 36 differ from modern groups in that both males and females experienced an equivalent risk of violent death. The nature of the wounds and the dispersal of the graves are suggestive of a pattern of warfare featuring opportunistic raids. These findings are consistent with death occurring as a result of the ambush of solitary individuals or small groups of people who were at some distance from the protection of the main settlement. Moreover, two patterns were present: 1) more adult victims than juveniles and 2) victims with skeletal evidence of old age or debilitating conditions often occurred in the violent death category (Milner and Smith, 1990; Milner et al., 1991a).

The ever-present threat of raids and warfare adversely affected their ability to exploit the abundant edible plant and animal species in the region. This is particularly true of resources that were most efficiently exploited by small groups or people or those located some distance from the protection of the main settlement. The impact of conflict on the adaptive success of this population is perhaps best reflected by a comparatively low level of community health, as indicated by various markers of disease stress, including dental disease, porotic hyperostosis, and periosteal lesions (Milner et al., 1991a). These interpretations are coupled with Milner and Smith's (1990) observations of the high incidence of dental caries and evidence of vitamin deficiency (Styles and King, 1990). It is possible that a socially induced disruption of subsistence practices contributed to circumstances favoring considerable disease load experienced by the Norris Farms 36 community members (Milner et al., 1991b). This community must have also participated in interactions with other social groups. The existence of such intergroup ties is indicated by Mississippian-style burial goods (Santure and Esarey, 1990; Milner et al., 1991b).

Genetics of Norris Farms 36 Population

Genetics is a significant component when understanding joint and bone ontogenetic development. Genetic studies also provide the strongest evidence for reconstructing prehistoric residence (Hollinger, 1995). In regards to the Norris Farms 36 collection, previous studies have extracted both mitochondrial DNA (mtDNA) and nuclear DNA from this collection (Stone and Stoneking, 1993; 1998; 1999; Stone et al., 1996). DNA preservation was excellent, with about 70% of the samples producing mtDNA results and approximately 15% yielding nuclear DNA data from 108 individuals

in this collection. (Stone and Stoneking, 1998). There is a fairly high number of related lineages, due to inbreeding, but a large amount of mtDNA diversity was found in the prehistoric Norris Farms population (Stone and Stoneking, 1998). All four of the major Amerindian mtDNA haplogroups were found, in addition, to a fifth Mongolian haplogroup in Norris Farms. Sequences of the first hypervariable region of the mtDNA control region revealed a high level of diversity in the Norris Farms population (Stone and Stoneking, 1999). The mtDNA haplogroup and sequence diversity at Norris Farms are similar to those found in other Amerind populations (Stone and Stoneking, 1999). Despite the probable inclusion of related individuals in the sample, the Norris Farms population has a high level of mtDNA diversity, equivalent to that found in such modern groups as the Nuu Chah Nulth, Embera, and Mapuche (Stone and Stoneking, 1999). The Norris Farms population does have a high percentage of singleton mtDNA types (73.9%) compared to other modern Amerindian populations (Avg. = 45.4%). This could reflect some loss of diversity in modern populations due to the decrease in population size associated with European contact (Thornton, 1987; Ubelaker, 1988; 1992). Additionally, Stone and Stoneking (1993) found genetic evidence suggesting that at least some of the males may have come into the group by marriage or by being captured in conflict. Perhaps these sites were involved in some of the earliest movements toward matrilineal residence.

Summary

The Norris Farms 36 skeletal series provides physical anthropologists and archaeologists alike with an unparalleled opportunity to identify the demographic

structure of a late prehistoric Midwestern population. It also allows us to determine the level of community health, and to evaluate the correspondence between health and the adaptive stance of this particular society. Studies of the human skeletal remains from Oneota contexts at Norris Farms 36 suggest that sociopolitical stress may have been an important factor influencing subsistence and other activities locally. Maize cultivation is clearly important; but the diversity of wild plant foods, including both upland and aquatic resources, and apparently nuts, fruits, seeds, indicates that collecting of wild resources was also an important part of subsistence. Subsistence pursuits may have been limited by the threat of raids. Reduced red-meat consumption, coupled with heavy utilization of maize, could have contributed to the poor health of these people. Overall, this was a highly-stressed population when compared with many other groups reported in the literature on the health of the prehistoric peoples of the Eastern Woodland (Milner and Smith, 1990). Despite being a stressed population, the scale of analysis used to interpret subchondral bone microarchitecture should not be affected. Moreover, the Norris Farms skeletal series has a semi-permanent village lifestyle for subadults which is closer to modern groups than compared to hunter gatherer populations which makes this ideal for future data comparison with clinical studies.

CHAPTER 5: MATERIALS AND METHODS

Norris Farms Oneota Skeletal Sample

High-resolution computed tomography (HR-CT) scans of Norris Farms tibiae specimens from 31 individuals (12 males, 11 females, 8 subadults), ranging in age from 8 to 37.5 years old, (Average: 22.6 years), were used to examine subchondral trabecular bone and cortical plate ontogenetic changes. Demographic information for the selected samples is found in Table A.1 in Appendix A. The skeletal series was chosen for this study because of its cultural and biological homogeneity, high number of subadult individuals, extensive archaeological context, and excellent preservation. The proximal tibia has been chosen for this study because it is a skeletal region that is primarily controlled by axial compressive and tensile stresses and is commonly used in clinical and research studies of joint development and disease. As previously mentioned, the Norris Farms 36 site is an Oneota cemetery from the central Illinois River Valley dating to approximately A.D. 1300 with graves containing individuals associated with the Oneota cultural tradition of village agriculturalists (Santure et al., 1990). The burial population consists of 264 individuals. The individuals range in age from fetal to 50+ years as determined by dental formation, sequence of epiphyseal closure, and age-associated changes (Milner and Smith, 1990). No physical analysis of the actual skeletal samples was conducted in the present investigation; all work was conducted via analysis of HR-

CT images. Data analysis was performed using Avizo® Fire versions 6.2 and 8.1.1, a data analysis and visualization software from FEI, and the macros BoneJ. BoneJ is a macros plugin for bone image analysis in java-based ImageJ (v. 1.51f) (National Institutes of Health, <http://rsbweb.nih.gov/ij/>). BoneJ provides open source tools for trabecular geometry and whole bone shape analysis (Kontulainen et al., 2007; Doube et al., 2010).

Age-at-death and Sex Estimation

All age-at-death and sex estimations for the Norris Farms 36 skeletal series were determined in a previous project (Milner et al., 1989). Age-at-death for individuals in the Norris Farms 36 samples was estimated according to standard methods for macroscopic skeletal age estimation (Milner et al., 1989; Milner and Smith, 1990). Milner et al. (1989) relied upon dental development (Moorrees et al., 1963a; 1963b; Thoma and Goldman, 1960; Ubelaker, 1978) and epiphyseal closure (Ubelaker, 1978) to estimate age-at-death in subadults, while adult ages were assessed via pubic symphysis morphology, endocranial suture closure, and auricular surface morphology (Milner et al., 1989). The Norris Farms 36 series was also seriated according to developmental and maturity stages. Adult skeletons were sexed using aspects of skeletal morphology described in Krogman (1962), Brothwell (1963), Acsadi and Nemeskeri (1970), Bass (1971), Ubelaker (1978), and Stewart (1979). Most adult Oneota skeletons were estimated as either male or female. Sixty-two (54.4%) were females and 52 (45.6%) were males (Milner and Smith, 1990).

Body Mass Estimation

Skeletal measurements used to calculate subadult body mass estimates in this study are based on past Norris Farms 36 skeletal series research carried out by Bernadette Perchalski, Dr. Zac Hubbell, and Dr. Colin Shaw. Femoral head diameter measurements, used for adult body mass calculations, were performed by Dr. Colin Shaw, using digital calipers on the actual skeletal material. Polar second moments of area (J) used for body mass estimation of sub-adults aged 8 to 11.99 years were previously acquired by Hubbell (2016) using the BoneJ plugin for ImageJ (Doube et al., 2010), which provides maximum (I_{\max}) and minimum (I_{\min}) second moments of area. The sum of these values equals the J value of the cross-section (Larsen, 2015; Hubbell, 2016).

While established methods for adult body mass estimation from skeletal remains exist (Ruff et al., 1991; Ruff et al., 1997; Auerbach and Ruff, 2004), only recently have reliable methods been established for body mass estimation in subadults skeletons (Ruff, 2007; Robbins et al., 2010; Robbins Schug et al., 2013). Ruff (2007) developed the first reliable protocol for subadult body mass estimation using geometric properties of the lower limb and pelvis. Ruff created regression equations for estimating body mass for individuals aged 1 to 17 years using femoral head diameter, distal femoral metaphysis breadth and bi-iliac pelvic dimensions from the longitudinal Denver Child Growth Study data (McCammon, 1970). These individuals were of European ancestry and of upper and middle socioeconomic classes (Ruff, 2007; Hubbell, 2016). Ruff's (2007) equation is age-specific in order to account for the changing body proportions during stages of growth and development. Robbins Schug et al. (2013) published a related study using the

Denver Child Growth Study data and presented a series of regression-derived subadult body mass estimation equations that produced results without reference to independent age data, thus eliminating a potential source of error with skeletal age-at-death estimates. For this research study, Robbins Schug et al. (2013) subadult regression formulae were used to estimate subadult body mass and femoral head diameter (FHD) regression formulae from Ruff et al., 1997 were used for estimating adult body mass.

The actual regression formulae used for the Norris Farms Oneota sample body mass (BM) calculations are provided here.

For subadults aged 8 to 11.99 years: $\ln\{BM\} = 2.0683 - 0.3126*\ln\{J\} + 0.0477*\ln\{J\}^2$ (Robbins Schug et al., 2013; J is the mean of the right and left sides polar second moments of area) (Robbins Schug et al., 2013).

For individuals aged 15 to 37.99 years, body mass estimations are based on the mean of values from three formulae (two for sex-pooled samples and a sex-specific formula) from Ruff et al. 1997. The formulae are as follows: **Equation 1)** $BM = 2.239 \times FHD - 39.9$; **Equation 2)** $BM = 2.268 \times FHD - 36.5$; **Equation 3: males)** $BM = 2.741 \times FHD - 54.9$; **Equation 4: females)** $BM = 2.426 \times FHD - 35.1$.

Tables A.2 (subadults aged 8 to 11.99 years), and A.3 (individuals aged 15 to 37.99 years) in Appendix A show the relevant measurements and corresponding body masses for each individual.

Principles and Procedures for CT Data Acquisition

Segmentation Process and Thresholding

The segmentation process (thresholding) is an essential step in the analysis of CT scan images. It involves separating bone from non-bone structures for subsequent

quantitative analyses. This technique allows for visualizing and quantifying CT scan images by establishing a grayscale value to represent the density between bone (white) and non-bone (black) in a CT reconstructed image (Coleman and Colbert, 2007). The goal of selecting a threshold is to obtain results that are physically accurate (i.e. similar to the original structure). Threshold values used during the post-acquisition phase for image segmentation have major effects on quantitative analyses (i.e. calculating thickness, connectivity, and volume) (Hara et al., 2002; Buie et al., 2007; Buxsein et al., 2010; Christiansen, 2016). Errors due to inaccurate segmentation artifacts can cause misinterpretation of volume or connectivity morphometric data in trabecular bone (Buie et al., 2007; Buxsein et al., 2010; Christiansen, 2016). Care must be taken when selecting a threshold in studies where bone mineralization may not be constant (i.e. growth and development). Thus, it is necessary to use specimen specific thresholds or local segmentation methods (Buxsein et al., 2010). In this study, grayscale values were determined using specimen specific auto thresholding in ImageJ (Optimise Threshold) for standardization of each specimen and to remove possible subjectivity. However, in some scans, bone and deeply embedded loess (soil) were not always sufficiently distinguished to allow for auto thresholding. These thresholds were adjusted and optimized by visual inspection. When necessary, manual thresholding of a binary scan image was done to ensure that no loess was included in the segmentation (Figure 5.1) (Buie et al., 2007; Particelli et al., 2012). Threshold values were determined for all subchondral trabecular VOIs extracted from the epiphyseal region and for the subchondral cortical plate during the process of cortical

masking. The process of VOI extraction and cortical masking will be discussed later in this chapter. All threshold values are reported in Tables A.6 and A.8 in Appendix A.

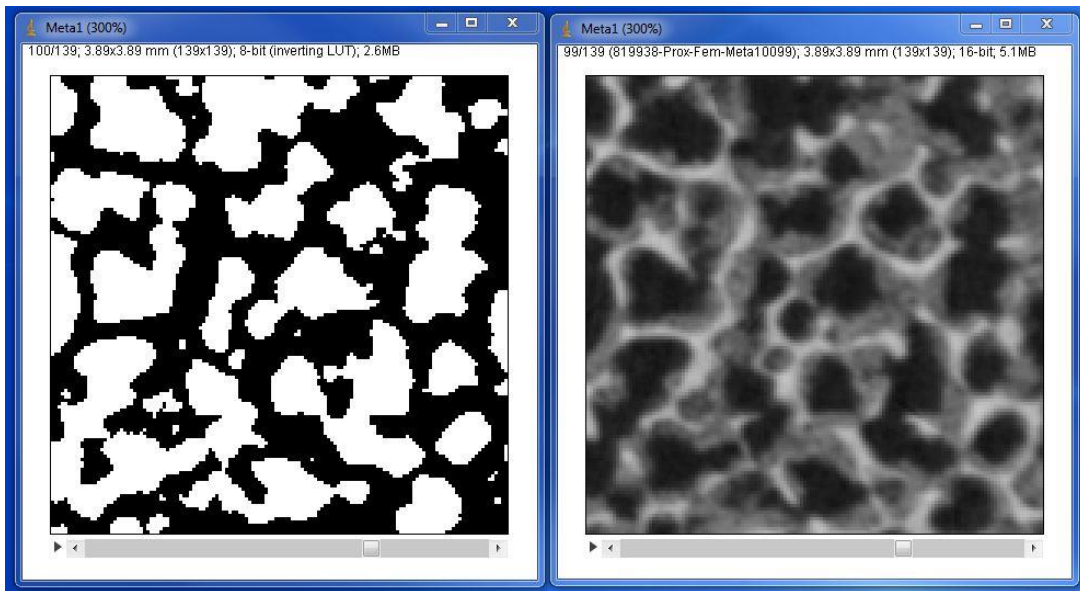


Figure 5.1: Example of visual segmentation procedure using ImageJ. Binarized (left image), Grayscale (right image).

Limitations of CT reconstruction

While the use of CT scans in anthropology is not without its benefits, there are disadvantages and limitations for its use. Extraction of quantitative structural information can be difficult in CT scans; result vary depending on the threshold of the instrumentation used, the image processing techniques, or resolution issues.

Resolution effects

As previously mentioned, the resolution can greatly affect the quality of a scanned image and more specifically, the smaller the specimen, the higher the resolution that is needed (Bouxsein et al. 2010). Industrial scanners can accommodate objects with a wide range of sizes, shapes, and materials but the resolution in a CT image is determined by the size and number of detectors, the size of the X-ray focal point, and the source to object and source to detector distances (Badea and Panetta, 2014; Rueckel et al., 2014). Resolution choice is a compromise between the detail of the reconstructed image and the amount of data obtained and time needed for processing (Bouxsein et al. 2010). Selection of voxel size/resolution for image acquisition should be based upon the size and detail of the specimen being scanned and adjusted based on time and/or data storage constraints (Badea and Panetta, 2014). The effect of different scanning and reconstruction/voxel size on trabecular parameters was examined by Kim et al. (2004). This study found a large difference in trabecular thickness between resolution/voxel size quality in the same instrument and they suggested that morphometry studies using low resolution systems need to be reevaluated (Stock, 2011). Thick structures like human cortical and trabecular bone are unaffected by low resolutions because even large voxels are much smaller than cortical and trabecular minimum thickness in adults (Bouxsein et al. 2010). In contrast, Gosman and Ketcham (2009) found significant differences in trabecular bone properties between lower- and higher-resolution scans while analyzing micro-CT resolution effects. For these reasons, scan resolutions used for the Norris Farms No. 36 skeletal series vary

by specimen size. In this study, proximal tibiae for each individual were scanned as two halves (medial and lateral) for the best possible resolution.

Artifacts

Artifacts can also seriously degrade the quality of CT images. These are any discrepancies between the reconstructed image and the true object. CT images are more prone to artifacts than conventional radiographs because the image is reconstructed from several independent detector measurements. The reconstruction technique assumes that all the measurements are consistent, so any error of measurement will reflect as an error in the reconstructed image (Bouxsein et al., 2010). The most frequently encountered artifact in CT scanning is beam hardening, which causes the edges of an object to appear brighter than the center, even if the material is the same composition throughout. The artifact is caused by the increase in mean X-ray energy, or “hardening” of the X-ray beam as it passes through the scanned object (Ketcham and Carlson, 2001). Beam-hardening artifacts are also frequently manifested in the air that surrounds an attenuating object, creating dark or occasionally light streaks (Ketcham and Hanna, 2014). Ring artifacts are caused by errors in output from individual detectors or sets of detectors, and appear as full or partial circles on the CT reconstruction. A number of factors can cause these such as, changes in temperature or beam strength, too much dust on the detector, or damaged pixels in camera capture (Ketcham and Carlson, 2001; Bouxsein et al., 2010). A variety of other artifacts can also arise: streaking, star-burst, and shading. Streaking is due to an inconsistency in a single measurement (i.e. beam hardening, metal exposure). Metal exposure in the scan causes total absorption of the X-ray beam, yielding star-shaped

artifacts in the reconstructed image. Shading is due to a group of views deviating from the true measurement (i.e. patient/specimen motion). (Ketcham and Carlson, 2001; Barrett and Keat, 2004; Ketcham and Hanna, 2014). Only very faint ring artifacts were noted in a few of the Norris Farms 36 scan samples. These were so minor that once the scans were binarized and segmented in ImageJ for measurement they had little impact on quantitative data in this project.

Pennsylvania State University CQI Scanning Protocol

All skeletal analysis for this project was performed using three-dimensional (3D) digital models derived from high resolution CT scans. All Norris Farms specimens were scanned at the Center for Quantitative X-Ray Imaging (CQI) at Pennsylvania State University using a Universal OMNI-X HD-600 Industrial High Resolution X-ray CT system (Bio-Imaging Research, Inc., Lincolnshire, IL). The Norris Farms 36 skeletal series was scanned by Tim Stecko at the Pennsylvania State University Center for Quantitative X-ray Imaging under the direction of Dr. Tim Ryan. Both full (whole plateau) and half (condyle) scans of the proximal tibia were created. Resulting scans had voxel sizes ranging from 0.013 to 0.117 mm depending on specimen size (with the larger, adult bones having the largest voxel dimensions). For better resolution and quality, initial whole bone scans were divided into half scans by condylar region when possible. In all cases, scans were collected at the maximum resolution obtainable based on size (Ryan and Milner, 2006; Ryan and Krovitz, 2006). Scanning procedure involved foam mounting each specimen with foam to stabilize the bone inside a thin-walled plastic tube. With energy settings of 180 kilovolts (kV), 0.11 milliamps (mA), 2,800 projections, and using

a Feldkamp reconstruction algorithm, transverse cross-sectional slice images were collected for each whole tibia Image reconstructions resulted in 1,024 by 1,024 pixel, 16-bit TIFF images (Gosman et al., 2013; Hubbell, 2016). Following scan data collection, the 16-bit images were converted to 8-bit TIFFs using ImageJ, ensuring that the grayscale values were in the same way for all images in each specimen's dataset. Image stacks (which comprise whole-bone datasets) include between 860 and 3,707 slices per bone (depending upon bone size and scan resolution). Most voxel dimensions resulting from the scans are isotropic (i.e. voxels are perfect cubes), but some larger bones were reconstructed with anisotropic voxel dimensions (i.e. voxels are not cubes; voxel height is different from length and depth measurements). All voxel dimensions are reported in Table A.4 in Appendix A.

Digital image rendering in Avizo Fire

Once scan data were acquired, it was necessary to render digital images from the raw CT scans for examination of specimen condition. During this stage of the process, any scanned skeletal element found to be damaged or corrupted such that the anatomical region of interest was affected was marked for exclusion from the study. Images were sample in Avizo® Fire versions 6.2 and 8.1.1, a material science data analysis and visualization software package from FEI. This section details the steps used for digital model rendering. All Norris Farms 36 CT scans used in this study were originally acquired as part of an NSF funded project (BCS-1028793 and BCS-1028904) investigating trabecular bone ontogeny in association with locomotor development. This was designed and executed by co-principal investigators James Gosman, Tim Ryan, and

David Raichlen. As such, scan data received from Pennsylvania State University had in some cases already been converted to various data formats. Most acquired scan data were in the form of DICOM files, which can be loaded in Avizo Fire as image stacks. Some scan data was in raw format, which requires that scan information (e.g. x/y/z voxel dimensions) be provided when the raw scan file is opened in Avizo Fire.

Regardless of data format, once a bone scan dataset is successfully loaded in Avizo Fire, an isosurface rendering, an image reconstruction, must be generated in order to visualize the external surface of the bone image. For this study, isosurface properties were set at a threshold of 2800 (determined previously to be the best level for showing the bone surface and eliminating noise in the rendering) and with the downsample option checked and set to 4 in each dimension (Figure 5.2). Once an isosurface rendering was complete, a three-dimensional image of the scanned bone would appear in the Avizo Fire viewer window (Figure 5.3)

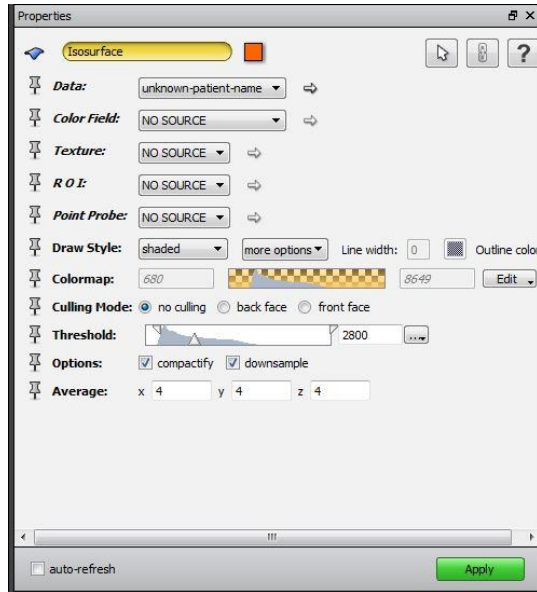


Figure 5.2: Example of the isosurface properties menu in Avizo Fire 8.1.1.

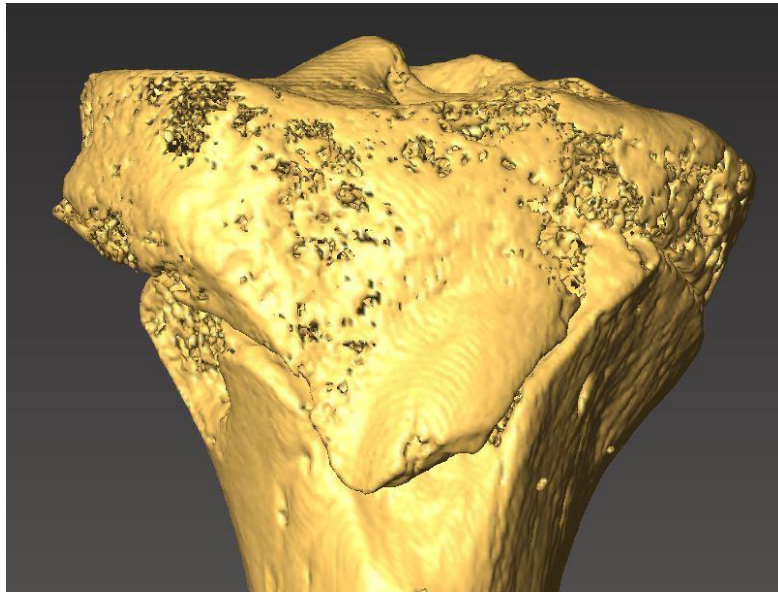


Figure 5.3: Isosurface rendering of a 16 year old proximal tibia (anterior view).

Region of Interest (ROI) Placement

The region of interest (ROI) is the portion of a bone that was identified as containing the structural features of interest. When setting up the scan acquisition, it is critical to ensure that a sufficient amount of the sample is scanned to allow for reliable and reproducible morphology and density measurements. The region of interest (ROI) should be defined based on the location of the start point of the scan or the contoured region of interest and the size (ie, length) of the region. Because any 3D model generated from CT scan data is made of stack of images (slices), scan datasets are stored as a sequence of individual files comprised essentially of 2D images (with a resolution-based height that makes up the voxels' "z" dimensions) that are numbered, distally to proximally. Thus, ROIs can be identified in terms of the number of slices that comprise them and their place in the slice stack sequence. In the case of this study, the ROI is the proximal epiphyseal region of the tibia. All samples comprised the subchondral cortical bone immediately under cartilage and subchondral trabecular bone. ROI length and number of slices are reported in Table A.4 in the Appendix A of this document (Bouxsein et al., 2010; Hubbell, 2016).

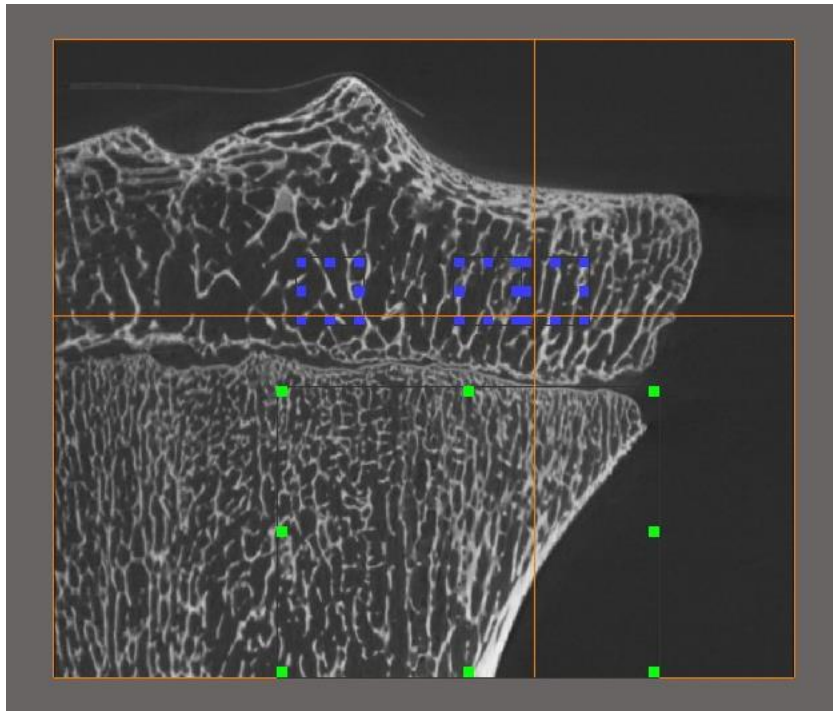


Figure 5.4: Example of the selected ROI (orange box) with VOIs (blue boxes) placed in the epiphyseal region.

Volume of Interest (VOI) Placement and Extraction

For analysis of the subchondral trabecular bone, eleven cubic volumes of interest (VOIs) were collected from the medial and lateral condyle of the proximal tibia using Avizo Fire 6.2 (Figures 5.5 & 5.6). For half scans, the number of VOIs were divided in half (Figure 5.7) Bone morphometric measurements were obtained for each VOI in the sample using the java-based ImageJ (v. 1.51f) (National Institute of Health) and BoneJ macros plug-in (Doubé et al., 2010). (Figure 5.3). VOIs were positioned within and between tibial condyles within the epiphyseal region, just inferior to the proximal tibia's contact area with the distal femur. There are compressive forces in the proximal tibia

during bipedal stance and locomotion (Figure 5.8). By contrast, no direct compression is exerted upon VOIs between the condyles (i.e. central unloaded VOIs) during weight-bearing. Previous researchers (Kim et al., 2004; Kivell et al. 2011; Saers et al., 2016) have noted the importance of VOI size and location and on trabecular properties, so the largest VOI possible was placed in order to ensure that each VOI is reflective of structural variation between joints. Because certain properties (connectivity and structure) are impacted by VOI size, each specimen's VOI was adjusted to the individual (Lazenby et al., 2011) by using epiphyseal condylar breadth and the anteroposterior breadth of the proximal femoral metaphysis as the size standard. Each VOI size was calculated as 25% of the anteroposterior breadth of the proximal femoral metaphysis, resulting in cubic VOIs ranging in size from 4.0 to 8.178 mm, reflecting size increases in growth of the tibia across age (Raichlen et al., 2015). Epiphyseal breadth dimensions and VOI cube sizes are reported (Tables A.4 and A.5) in Appendix A. Multiple VOIs are used because the microarchitecture of trabecular and cortical bone is spatially mixed and is highly dependent on VOI position and size (Gosman and Ketcham, 2009). Once created, the cubic VOI was saved as a stack of DICOM and TIFF files and imported into ImageJ (version 1.51f) (National Institutes of Health, <http://rsbweb.nih.gov/ij/>) to calculate the trabecular properties. The sequence of CT image slices (DICOM format) corresponding to the ROI of the bone is imported into ImageJ, with the image sequence option selected in the pop-up window (Figure 5.9).

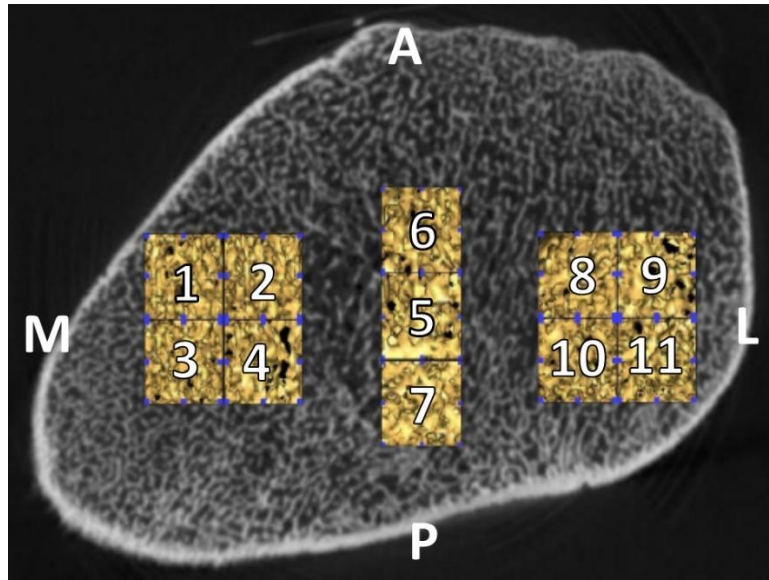


Figure 5.5: Placement of 11 VOIs in the proximal tibia (superior view).
Note: VOIs 1-4 are within the medial condyle; VOIs 8-11 are within the lateral condyle;
 VOIs 5-7 are between the condyles. A = Anterior; P = Posterior; M = Medial; L = Lateral

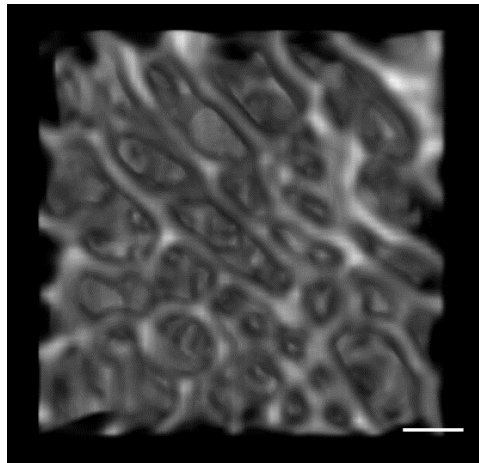


Figure 5.6: Example of an isolated trabecular (15.5 yr old) VOI using ImageJ.
Note: Scale: 1mm

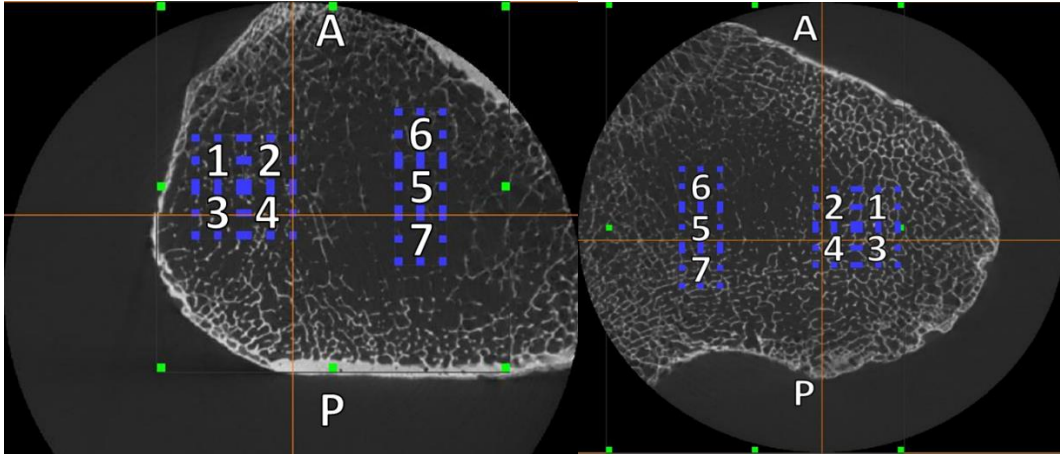


Figure 5.7: Proximal Tibia Half Scan VOI Placements.
 Note:(Left Image – Lateral Condyle, Right Image – Medial Condyle
 19.5 yr old Left Tibia, Superior View
 A = Anterior; P = Posterior

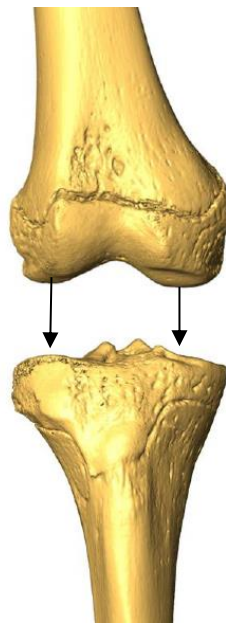


Figure 5.8: Example of compressive forces between distal femur and proximal tibia.
Note: anterior view.

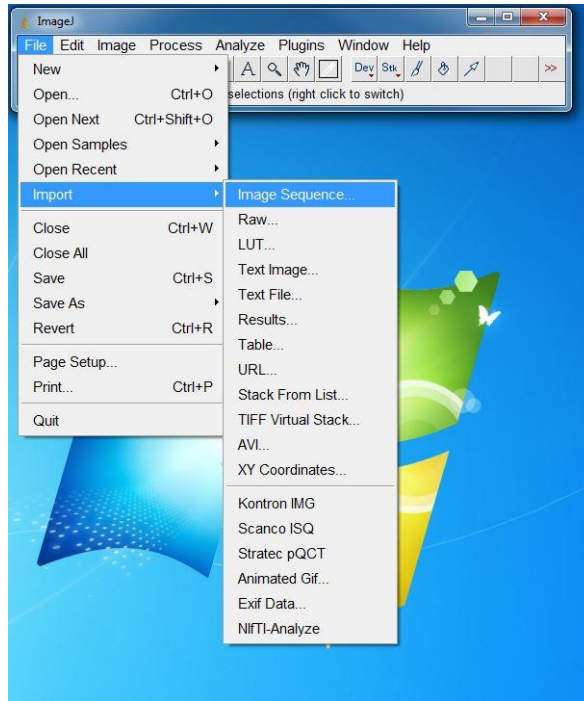


Figure 5.9: Example of importing image stack into ImageJ.

Once the image stack was imported, the stack was then converted into an 8-bit binary for subsequent analyses. Once binarized, a “set scale” using an individual scan voxel size was added for quantification of the trabecular bone morphometric parameters (Figure 5.10). Using BoneJ, bone volume fraction, mean trabecular thickness, mean trabecular separation, connectivity density, degree of anisotropy, and structural model index were quantified. One parameter (trabecular number) was derived from the variables, bone volume fraction and trabecular thickness.

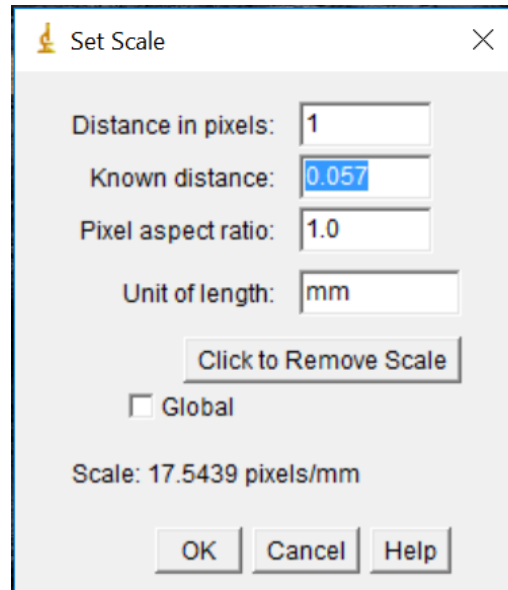


Figure 5.10: Example of set scale for quantifying bone parameters.

Subchondral Bone Structural Analysis

Trabecular Bone Morphometric Parameters

For analysis of the ontogenetic patterns in the subchondral trabecular bone, eight bone morphometric variables were quantified using the ImageJ bone analysis macros plugin BoneJ (Doubé, 2010). The morphometric parameters used are indicators of bone mechanical properties, microarchitecture, and functional adaptation to loading history (Burghardt et al., 2011).

Bone volume fraction (BV/TV, %)

Bone volume fraction is the amount of trabecular bone volume in proportion to the total reference VOI. It is represented as a percentage (Hildebrand et al., 1999; Lazenby et al., 2011). The material comprising the bone volume fraction is often referred to as bone

tissue. Trabecular BV/TV is one of the most important and fundamental architectural properties of trabecular bone (Ding et al., 2002).

Trabecular Thickness (Tb.Th, mm)

Trabecular thickness is a measure of the average thickness of trabecular struts as defined by binarization within the VOI (Hildebrand and Rüegsegger, 1997a; Lazenby et al., 2011). Trabecular thickness (Tb.Th) and trabecular separation (Tb.Sp) are calculated using mode independent distance transform methods (Hildebrand and Rüegsegger, 1997a; Dougherty and Kunzelmann, 2007).

Trabecular Separation (Tb.Sp, mm)

Trabecular separation is a measure of the average width of space between trabecular struts as defined by binarization within the VOI. Trabecular separation is calculated independently in three dimensions using the same method outlined for trabecular thickness. The average width of spaces between adjacent trabeculae in a VOI (Hildebrand and Rüegsegger, 1997a; Dougherty and Kunzelmann, 2007; Lazenby et al., 2011).

Connectivity Density (Conn.D, mm⁻³)

Connectivity Density is a measure of the ‘connectedness’ of trabeculae to one another within the VOI. Connectivity density was calculated using the Euler characteristic, a topological approach that incorporates both the number of particles (components) of a structure and the number of enclosed cavities to determine connectivity (Odgaard and Gundersen, 1993; Toriwaki and Yonekura, 2002).

Degree of anisotropy (DA, unitless)

Degree of anisotropy is a measure of the directional orientation of trabeculae. Anisotropy values are reported as a dimensionless value ranging from 0 (fully isotropic) to 1 (fully anisotropic). Anisotropic structures have a preferred orientation while isotropic structures demonstrate symmetry of orientation in 3D space (Lazenby et al., 2011). Degree of anisotropy (DA) was determined using the mean intercept length (MIL) method (Odgaard, 1997).

Structural Model Index (SMI (unitless))

Structure model index is a dimensionless measure of the plate-like or rod-like geometry in respect to trabecular strut morphology within in a VOI. A value of 0 indicates plate-like shape; while a value of 3 indicates rod-like shape. The SMI is calculated by means of three-dimensional image analysis based on a differential analysis of the triangulated bone surface in relation to bone volume (Hildebrand and Rüegsegger, 1997b; Lazenby et al., 2011). However, Salmon et al. (2015) has demonstrated that the commonly used parameter may not be suitable for use on real bone geometries because it is strongly influenced by BV/TV.

$$\text{Trabecular Number (Tb.N, mm}^{-1}\text{)} \quad \text{Tb.N} = (\text{BV/TV})/\text{Tb.Th}$$

Trabecular number is the ratio of bone volume fraction to trabecular thickness a measure of the number of traversals across a trabecular or solid structure made per unit length on a linear path through a trabecular bone region (Lazenby et al., 2011).

Cortical Masking

For analysis of the subchondral plate, a cortical mask was necessary to ascertain cortical subchondral properties. Proximal tibia half scans for each individual were used to

examine thickness in each condylar region (Figure 5.11). Once a range of slices was identified as the ROI for a particular bone, a truncated image stack comprised only those slices numbers was imported into Avizo Fire version 8.1.1. for masking of the cortical component of the bone image. This procedure was necessary in order to facilitate a later step in the data collection process to ascertain subchondral bone cortical plate properties. Dr. Tim Ryan developed a custom separation script, which serves the purpose of digitally separating the cortical region from the rest of the volume, such that any ROI may be separated into trabecular and cortical volumes which may be saved as independent datasets. This script is similar to the dual threshold technique developed by Buie et al. (2007), which automatically segments cortical and trabecular compartments. The script works through a 3-step manual process of visually distinguishing bone verse non-bone in the digital image by referencing transverse slices. It is executed on the basis of grayscale thresholds that are defined by the user as belonging either to bone or non-bone (Figure 5.12). This was accomplished by adjusting the threshold levels pertaining to each step in the script execution process. This required multiple attempts to ensure the proper material was not excluded from the separation. Table A.8 (Appendix A) provide threshold values in steps 1-3 of the masking process for each specimen (Hubbell, 2016).

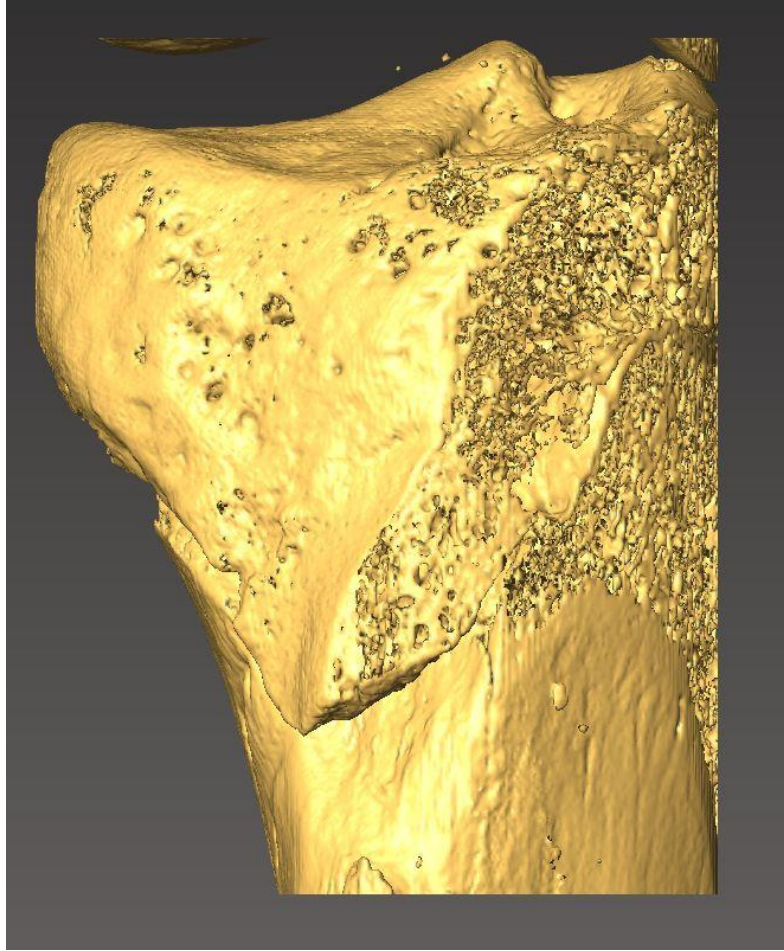


Figure 5.11: Example of a proximal tibia CT half scan.
Note: 16 year old Lateral Condyle, Anterior View

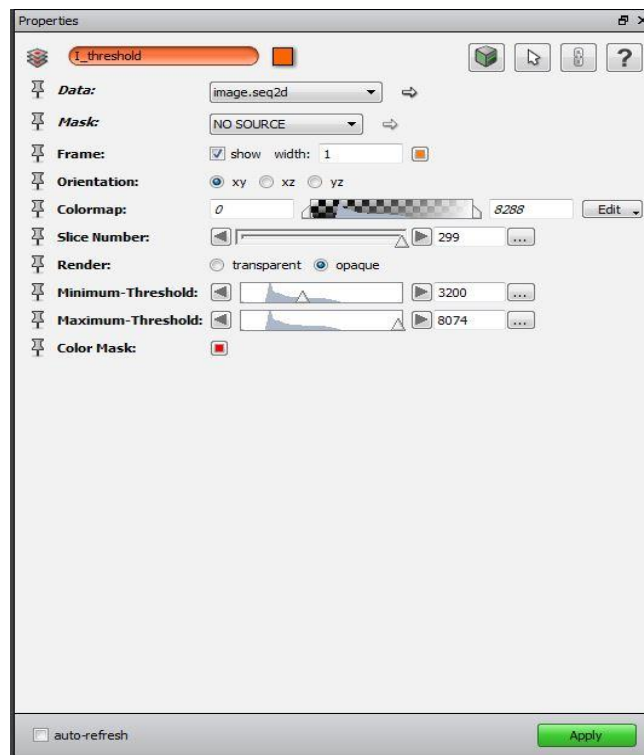
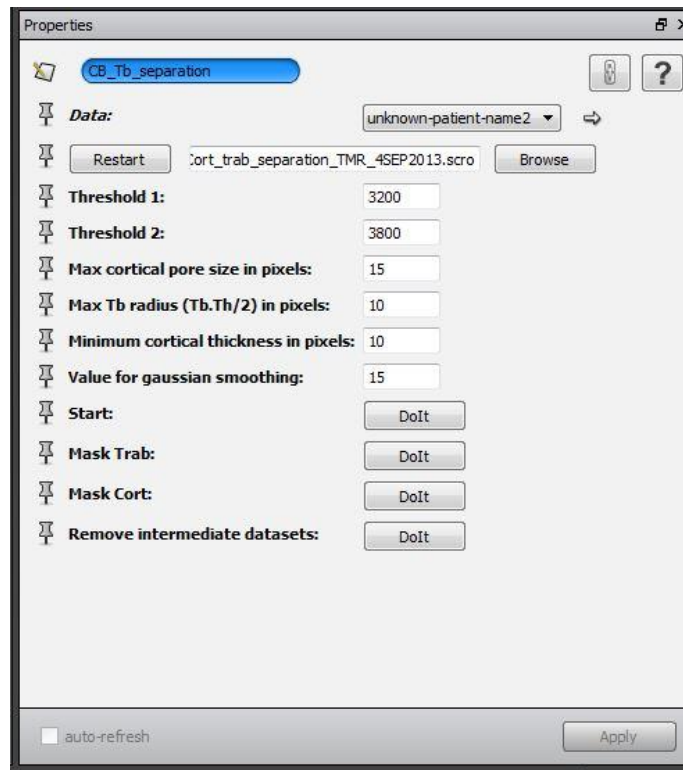


Figure 5.12: Cortical masking script (TOP) and threshold (BOTTOM) properties.

The ROI separation process begins by loading the ROI image stack in Avizo Fire 8.1.1, orienting the image with the distal margin visible (XY plane orientation) and loading Dr. Ryan's script into the program. The Avizo Fire properties window displays all options and commands for an active script or tool. The first step is to adjust the threshold maximum and minimum values such that only bone was highlighted in the viewer window (Figure 5.12). In this step, it is allowable to leave some of the less dense trabeculae unselected. Once the levels are properly set, "OK" is selected in the dialogue box. Next, non-bone area inside the cortical margins is highlighted in the viewer window by the same threshold adjustment technique as in the first step (Figure 5.13).

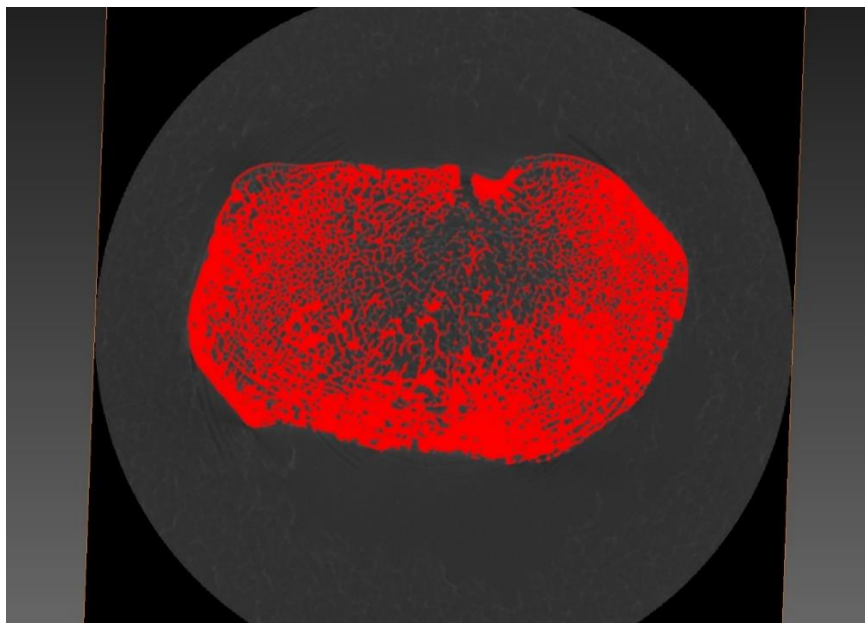


Figure 5.13: Step one of separation script execution (highlighting bone)
Note: Bone material selected via threshold adjustments; 16.5 year old tibia cross-section shown

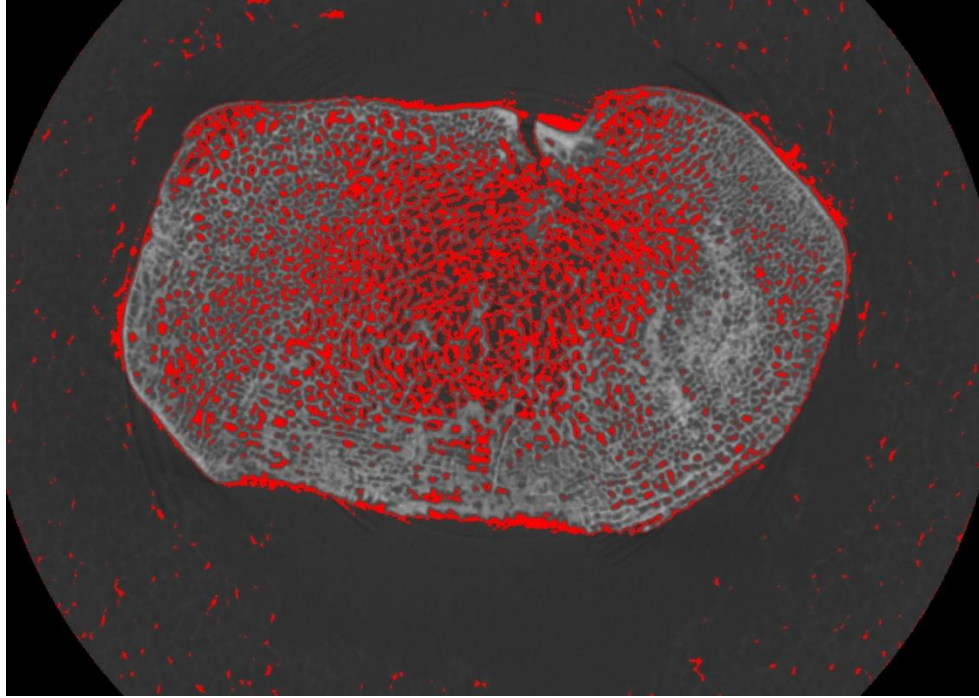


Figure 5.14: Step two of separation script execution (highlighting air space).
Note: Air space selected via a second set of threshold adjustments. 16.5 year old tibia cross-section shown

During the second step of the cortical masking procedure, it is usually not possible to select all the air space in the image without also selecting some bone, but it is important to leave some air space unselected if necessary so that no bone is highlighted in this step. Once these levels are properly set, “OK” is again selected in the dialogue box. After processing is completed following this step, the viewer window displays an outline of the ROI cross-section, filled in entirely in red (Figure 5.14). At this point in the process, no additional threshold adjustments are necessary; the filled cross-section serves to highlight the entire ROI volume (including bone and non-bone), and will automatically

have a lower threshold set to 1 and an upper threshold set to 53. These numbers remain and “OK” is selected in the dialogue box for the final time (Hubbell, 2016).

Once lengthy processing finishes in the final step of the separation protocol, a new image appears onscreen, showing the original grayscale cross-section with a partially transparent blue overlay that delineates the newly isolated trabecular ROI (Figure 5.15). In the Avizo “Main Panel” or pool window, teal modules represent newly created datasets; one for the cortical and one for the trabecular ROI and these can be saved as a new image dataset. It is also possible to create an isosurface rendering created with the cortical dataset (Figure 5.16). In BoneJ, the cortical dataset can be imported as an image sequence to determine thickness. Once the dataset is loaded, the brightness of the image stack is adjusted for the purpose of visualizing the bone VOI; this is done by selecting “Image” from the ImageJ menu bar, then “Adjust” then “Brightness/Contrast.” The stack was then converted into an 8-bit binary for subsequent analyses. Once binarized, a “set scale” using an individual scan voxel size was added for quantification of the plate mean cortical thickness (Ct.Th). Cortical thickness mean values for each individual are reported in Table A.9 in Appendix A of this document.

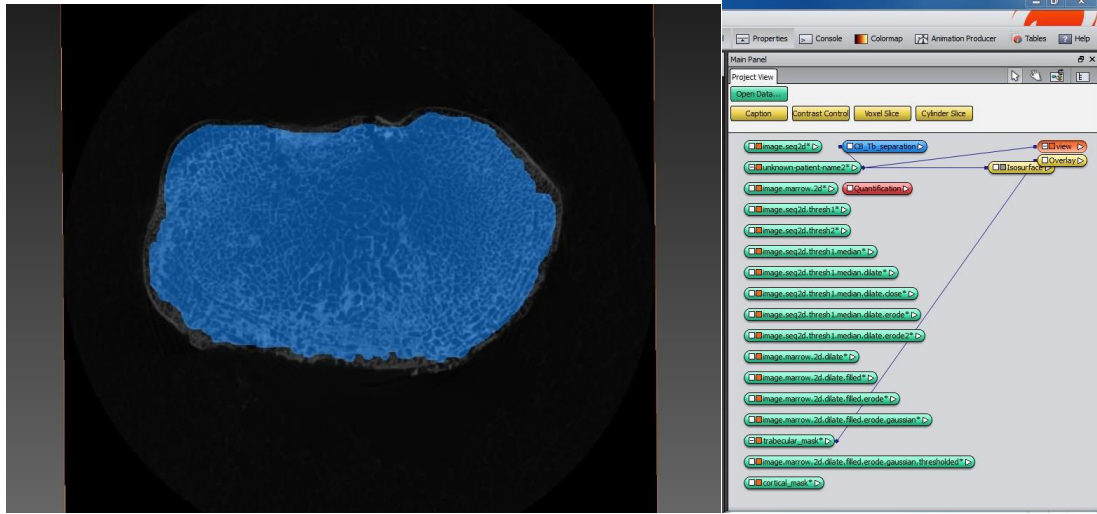


Figure 5.15: Final product of cortical masking procedure (transverse view) with dataset output.

Note: Blue area represents the isolated trabecular bone section of the original ROI. 16.5 year old tibia cross-section shown

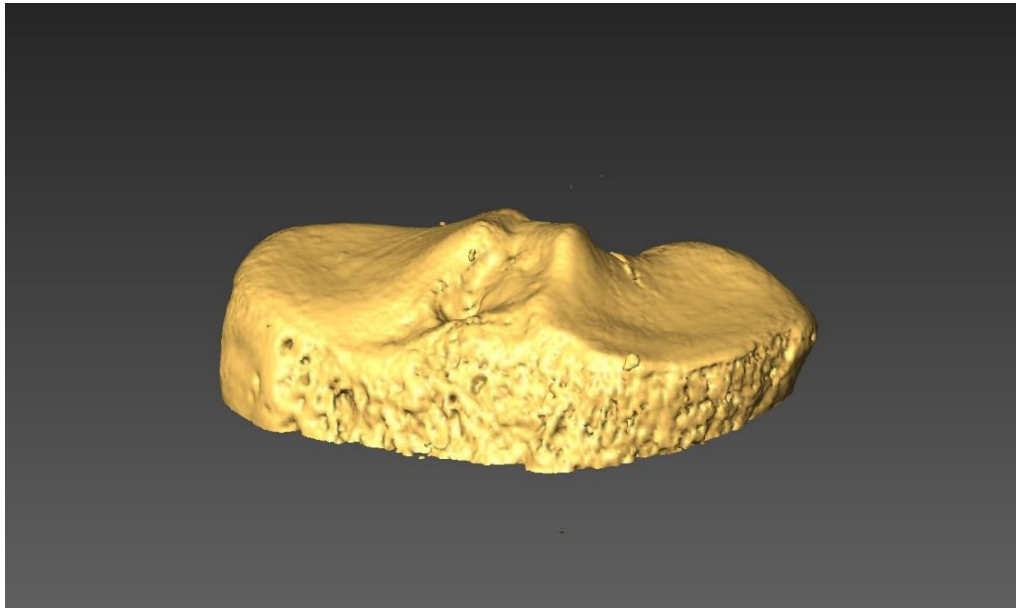


Figure 5.16: Final isosurface rendering following the cortical masking procedure
Note: 16.5 year old full tibia cortical shell

Statistical Analysis

Statistical analyses were performed using SPSS version 24 (IBM SPSS Statistics 24.0 IBM, Armonk, NY). For the purpose of statistical analysis, age-at-death estimates given as a range (e.g. 10 to 12 years) were converted to their mid-range value (e.g. 11 years). Based on prior research studies, all VOIS located in between condyles (VOIs 5, 6, 7) were removed from further analyses. The VOIs associated with each region (Lateral and Medial) were averaged for each individual for analyses. All variables were tested for normality using the Shapiro-Wilk test (Table B.1). Of the nine variables, three (Age, Tb.Sp, Conn.D) were not normally distributed and therefore nonparametric test were used for all further analyses. Significance level was set at alpha (α) = 0.05 for all statistical tests. Any outliers that were more than two standard deviations away from the mean were removed from further analyses. Descriptive statistics for all variables are reported in Table B.2 in Appendix B.

Hypothesis 1

With the increase in body mass and developing adult gait, all subchondral bone structural parameters will be affected by age.

To test age-related influences on all structural parameters, the sample was divided into four age groups/categories:

- 1.) Child (8 – 13.99 years, N = 6)
- 2.) Adolescent (14 – 19.99 years, N = 10)
- 3.) Young Adult (20 – 30.99 years, N = 4)
- 4.) Middle Age (31 – 37.99 years, N = 11)

Justification for Age Categories

Age categories are based on sample demographics, tibial development, and previous growth studies.

Child

In humans, trabecular structure of the tibia reaches an adult-like pattern (BV/TV, anisotropy) at approximately 8 years old (Ryan and Krovitz, 2006; Gosman and Ketcham, 2009; Raichlen et al., 2015). Thus, overall trabecular architecture appears to be optimized later in life (Huiskes et al., 2000; Tanck et al., 2001; Ryan and Krovitz, 2006; Cunningham and Black, 2009; Kivell, 2016). At ages 8-13 the distal part of the tuberosity starts to ossify from one or more centers (Scheuer and Black, 2004). At approximately 8 years, the pattern of BV/TV and DA settle into the range of adult values (Gosman and Ketcham, 2009). Individuals of this category have increased body mass, adult gait pattern, and independent activity.

Adolescent

Individuals in this category have increased body mass related to pubertal growth spurt with a fully active adult lifestyle (Gosman, 2007). The proximal epiphysis begins to fuse in 13 years in females and 15.5 years in males, with later times extending to 17 years in females and 19.5 years in males (Scheuer and Black, 2004).

Young Adult

Individuals in this category have reached their peak attained bone mass and final attained height. Individuals have increased body mass with cessation of growth.

Middle Age

Individuals in this category continue to maintain their final attained height and body mass but there are decreases in bone mass due to endo-trabecular deficit of bone replacement during remodeling. Normal, age-related bone loss in trabecular bone begins to occur in men and women after age 30–35 (Martin et al., 2015).

Body mass estimations are provided in Table A.3 in Appendix A of this document.

Mean differences for each bone structural parameter were tested across age categories by using an independent samples Kruskal-Wallis Test and a Bonferroni correction post-hoc test. A Kruskal-Wallis test is a rank-based nonparametric test that can be used to determine if there are statistically significant differences between two or more groups of an independent variable on a continuous or ordinal dependent variable. A Kruskal-Wallis test cannot differentiate which specific groups of independent variables are statistically significantly different from each other; so, a post hoc test must be performed.

Hypothesis 2

Due to increasing mechanical load and changing joint kinematics with development, there is a significant difference in subchondral trabecular bone and cortical plate structural parameters between the medial and lateral condyle.

To test regional differences in parameters, mean bone structural differences were tested across condyle location using related samples pairwise Wilcoxon Signed Rank test. The Wilcoxon signed rank test shows if observed difference between locations (Lateral and Medial) are significant for all structural variables.

Influence of Sex on Structural Parameters

Sex is another variable examined in this sample. For analyses between parameters and sex the Mann Whitney test was used. It is a non-parametric test that is used to determine if the mean of two groups are different from each other. This test was used to determine if subchondral bone architecture differs between males and females in the later age categories.

Summary

In this chapter, the details of all Norris Farms 36 CT data collection procedures, including materials preparation and statistical evaluations have been explained. Methods pertaining to the age-at-death estimations, as well as details regarding body mass estimations and bone measurements. This chapter as provided the protocols for CT acquisition as well as, the advantages and limitations of HR-CT scanning technology. Additionally, bone morphometric structural parameters were defined. Moreover, step-by-step procedures for Avizo Fire and ImageJ were provided for digital image manipulation, ROI and VOI identifications and extraction, and cortical masking. Finally, Chapter 5 included a discussion of the statistical methods used for evaluation of this research, the results of which are presented in the following chapter.

CHAPTER 6: RESULTS

The structural parameter values that come from VOIs located in the loaded condylar regions, including BV/TV ($\alpha = 0.033$), Conn.D ($\alpha = 0.001$), DA ($\alpha = 0.012$), and Plate Ct.Th ($\alpha = 0.000$) significantly differed across age categories (Table B.3). When comparing age categories, BV/TV was higher in Age Category 3 (20.0-30.99 years) compared to Age Category 1 (8.0-13.99 years). Bone volume fraction increased with age from childhood to adult and then remained constant in middle age. DA was also greater in Age Category 4 (31.0-37.99 years) compared to Age Category 1. Trabecular subchondral bone became more anisotropic with the adult form. Conn.D was less in both Age Categories 3 & 4 compared to Age Category 1. A decline in overall trabecular connectivity density is present in both adult categories. Subchondral plate cortical thickness was greater in the Age Categories 3 & 4 (20.0 -37.99 years) when compared to Age Categories 1 & 2 (8.0-19.99 years). This trend was present also between Age Categories 2 & 3. This represents an increase in subchondral plate cortical thickness with age. Mean values of all variables across age categories are reported in Table B.4. Pairwise related-samples Wilcoxon signed ranks tests were performed on all structural parameters means comparing medial and lateral condylar regions. In the subchondral cortical plate, the medial condyle was thicker in average than the lateral condyle, but there was no significant difference ($\alpha = 0.638$) found. In regards to the subchondral

trabecular bone, only DA significantly differed ($\alpha = 0.04$) between medial and lateral condylar regions (Table B.5). Wilcoxon signed-rank test, revealed that the medial condyle ranked higher than the lateral condyle in the majority of paired cases for degree of anisotropy. Overall, the medial condyle had a larger mean value for BV/TV and Tb.Th compared to the lateral. The lateral condyle had a larger mean value in Tb.Sp, SMI, and Conn.D. Mean values for all variables based on condyle location are reported in Table B.6.

As predicted, age and condyle specific variation does occur in the subchondral bone and plate, however, all structural parameters did not refute the null hypothesis of no change with age and location. These results indicate that statistical change only occurred with BV/TV ($\alpha = 0.033$), Conn.D ($\alpha = 0.001$), DA ($\alpha = 0.012$), and Plate Ct.Th ($\alpha = 0.000$) with age. Additionally, only DA significantly differed ($\alpha = 0.04$) between medial and lateral condylar regions.

Sex was also examined as a possible variable in the later age categories. A Mann Whitney U test was performed to examine the relationship between subchondral bone architecture and sex in the loaded condylar regions. SMI ($\alpha = 0.007$) was found to differ between males and females. BV/TV had a weak ($\alpha = 0.056$) statistical relationship. Overall, males had a higher bone volume fraction (i.e. more bone tissue) while women had higher SMI (i.e. more rod-like morphology) in the later age categories (Table B.7).

Quantification of Subchondral Bone Structure

Child

The child age group is typified by having the lowest mean bone volume fraction (0.234 mm), mean trabecular thickness (0.282 mm), mean degree of anisotropy (0.6155), mean structural model index, and mean trabecular number (0.826 mm^{-1}) of the four age groups. This group has the highest mean trabecular separation (0.858 mm) and mean connectivity density (4.132 mm^{-3}) and thinnest mean subchondral cortical plate (0.887 mm).

Adolescent

The adolescent age group is typified by an increase in trabecular thickness, bone volume fraction, anisotropy, and subchondral plate thickness when compared to the child age group. There is a general decline in connectivity density.

Young Age

The young adult age group is typified by having the highest mean bone volume fraction (0.290 mm), highest mean trabecular thickness (0.332 mm), highest mean trabecular number (0.8733 mm^{-1}), and highest degree of anisotropy (0.686) There is a decline in connectivity and an increase in subchondral plate thickness.

Middle Age

The middle age group is typified by the highest mean structure model index (1.29) with a decline in bone volume fraction and trabecular thickness from the young adult group. The subchondral plate mean thickness (1.644 mm) is highest in this group.

Condyle Differences

The medial condyle had a higher mean bone volume fraction (0.275 mm), trabeculae thickness (0.317 mm), degree of anisotropy (0.694), and thicker cortical plate (1.339 mm). However, the condyles only statically differed in degree of anisotropy, with the medial condylar region being more anisotropic. Lateral condyle had higher mean values in trabecular separation (0.853 mm), structural model index (1.16), and connectivity density (3.08 mm^{-3}). These results are similar to Ding and colleagues (Ding and Hvid, 2000; Ding et al., 2002). A majority of this study's samples fit in the young age range (16-39 yrs.) from Ding's research. They found that all the microarchitectural properties from the medial and lateral condyles had the same age-related trends. In normal individuals, the strength and density of the medial condyle are significantly greater than those of the lateral condyle (Hvid and Hansen, 1985). These results are consistent with higher loading at the medial condyle (Ding et al., 1997).

Sex Differences

Males and females statistically differ in only structural model index, and to a lesser extent bone volume fraction. Adult men had greater bone volume fraction than adult women. Adult women had trabeculae that were more rod-like in structure. This greater BV/TV has been found in other studies (Harada et al., 1988; Chen et al., 2011). Harada et al. (1988) found that in both condyles, the mean bone strength is greater in men than in women (Muller-Gerbl, 1998). Chen et al. (2011) showed that men had higher BV/TV and lower trabecular separation (Tb.Sp) in the old age and elderly groups compared to women.

Visualization of Data

The next section provides visual representations from each age category (Figures 6.1 – 6.16). The aim of this section is to provide visual examples of the microarchitectural changes that are occurring across the age categories.

AGE CATEGORY 1: 9.0-year-old (821006)

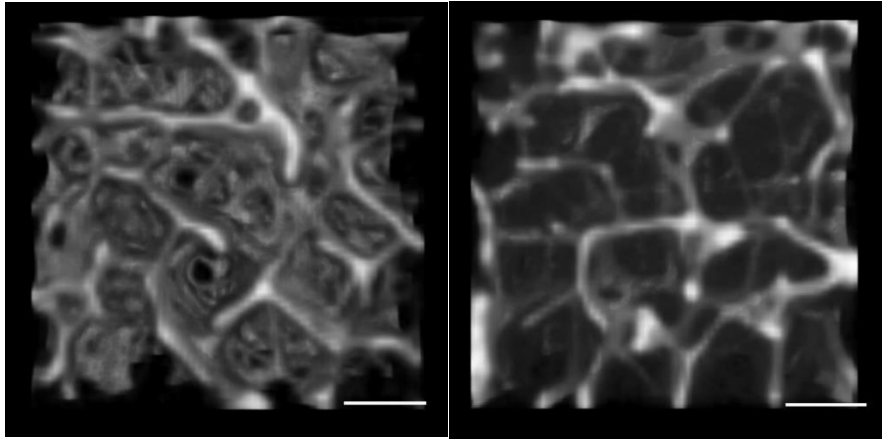


Figure 6.1: VOI 1 Lateral Condyle (LEFT) and VOI 6 Between Condyles (RIGHT).
Note: Scale: 1mm.

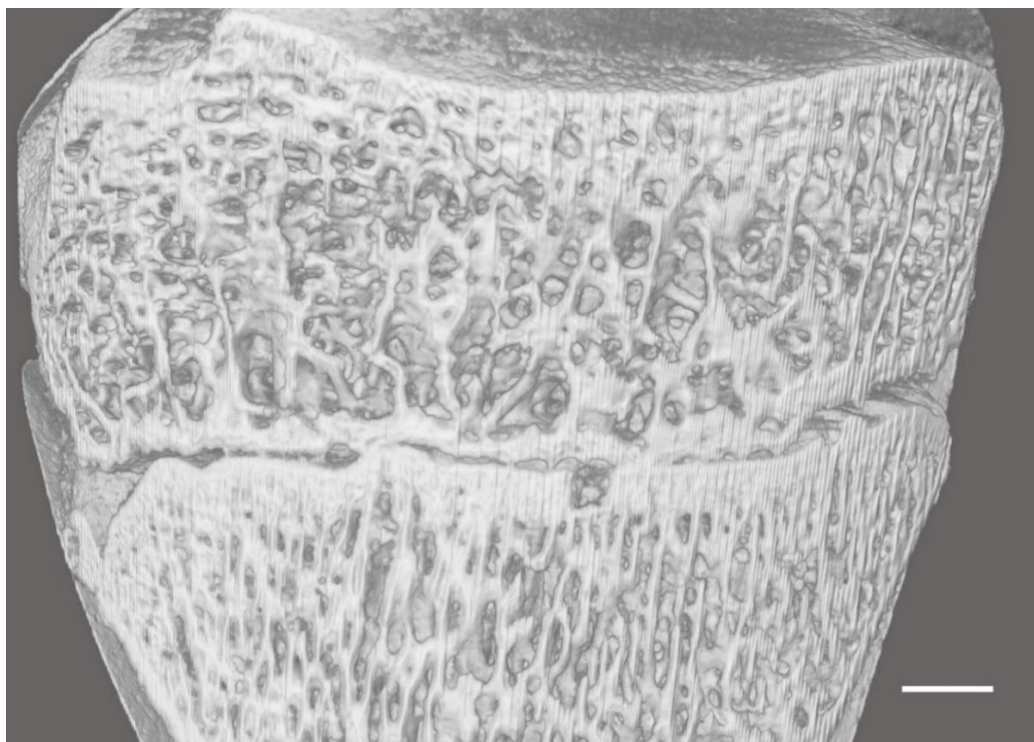


Figure 6.2: Medial Condyle Mid-Condyle Sagittal Rendering.
Note: Scale: 5mm.

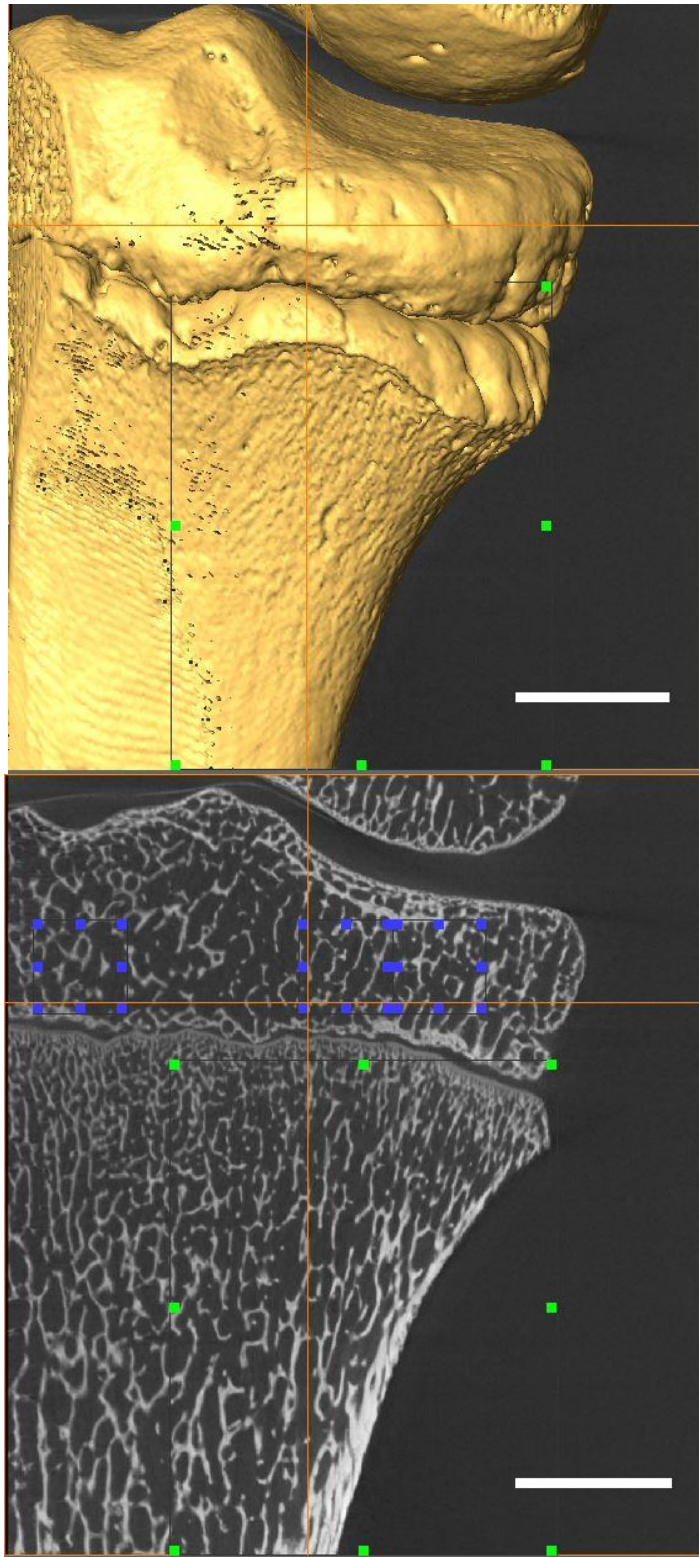


Figure 6.3: Medial Condyle Posterior View Isosurface Rendering (TOP) and 2-D Micro-CT Image (BOTTOM). *Note:* Scale: 5mm.

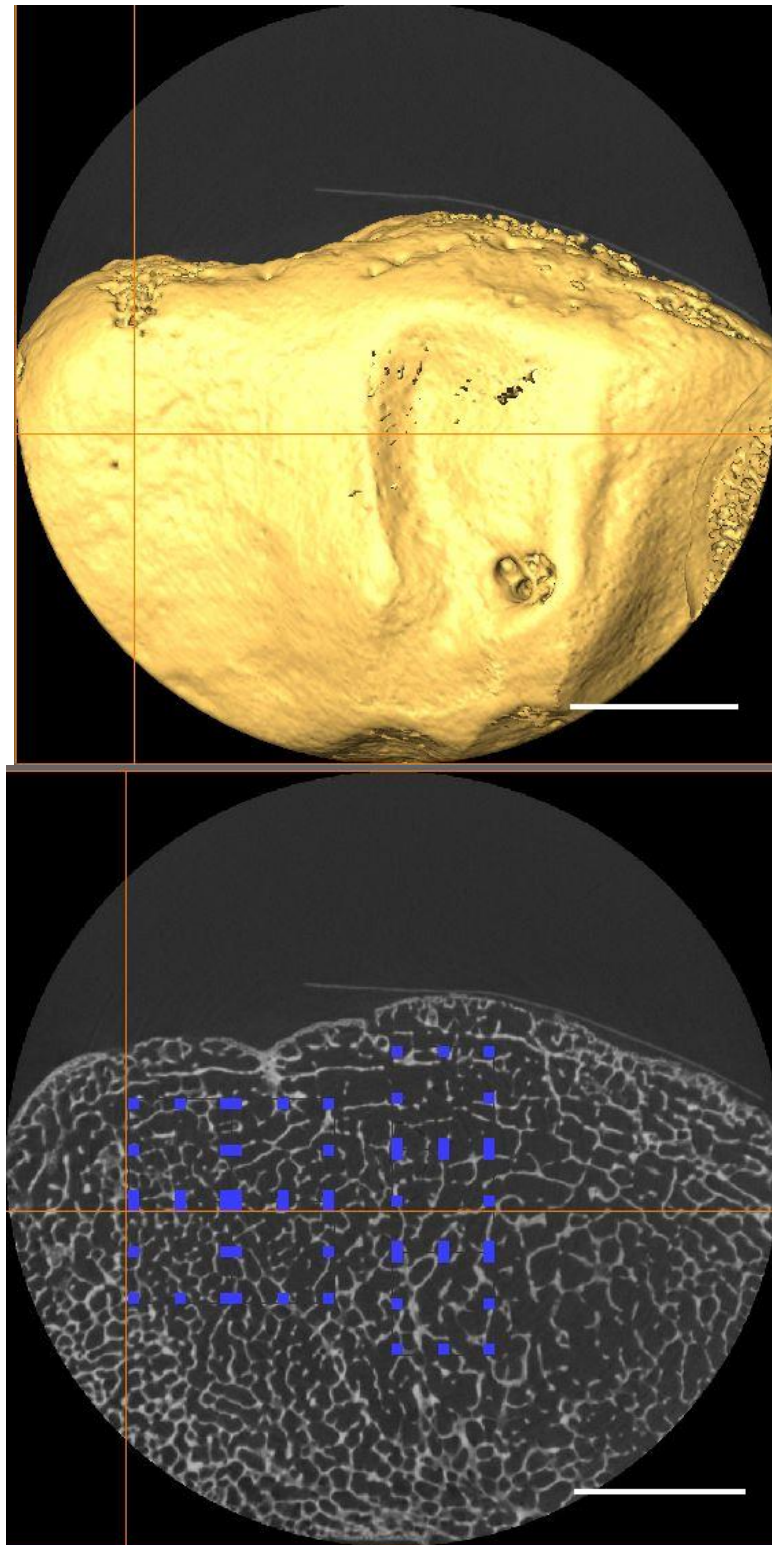


Figure 6.4: Lateral Condyle Superior View Isosurface Rendering (TOP) and 2-D Micro-CT Image (BOTTOM). *Note:* Scale: 5mm.

AGE CATEGORY 2
16-year-old male (819964)

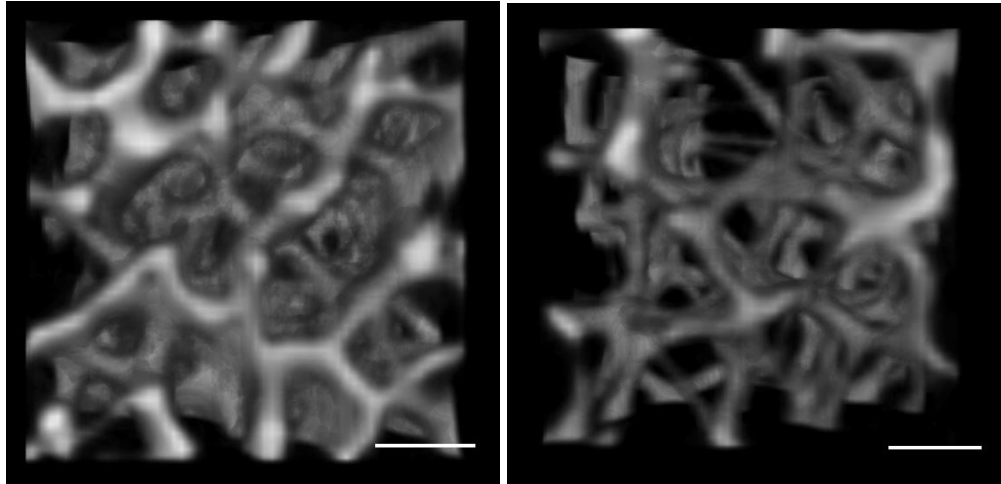


Figure 6.5: VOI 1 Medial Condyle (LEFT) and VOI 5 Between Condyles (RIGHT).
Note: Scale: 1mm.

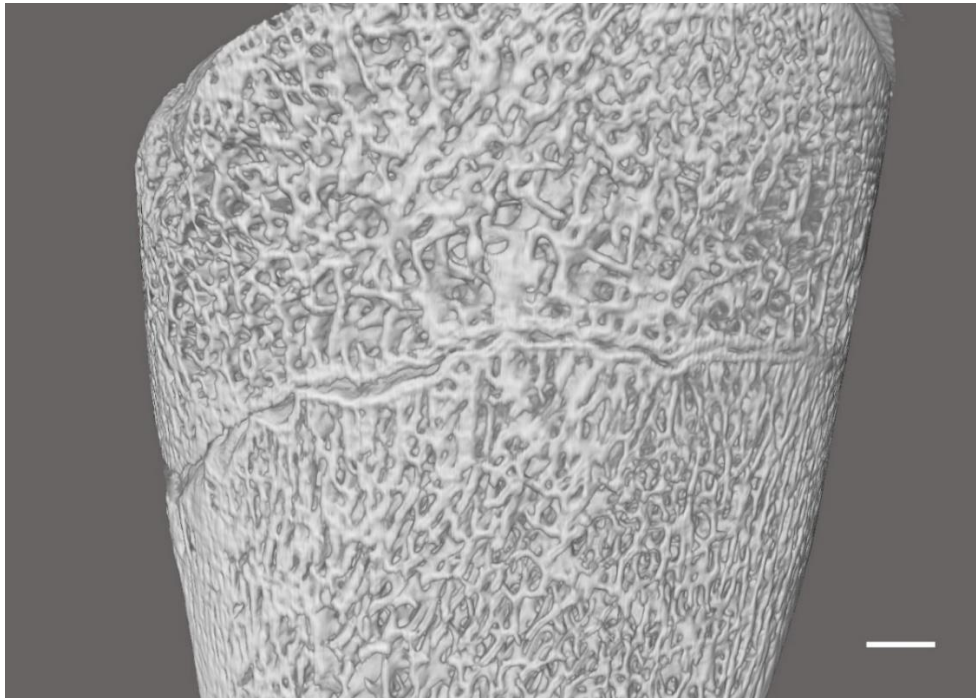


Figure 6.6: Lateral Condyle Mid-Condyle Sagittal Rendering. *Note:* Scale: 5mm.

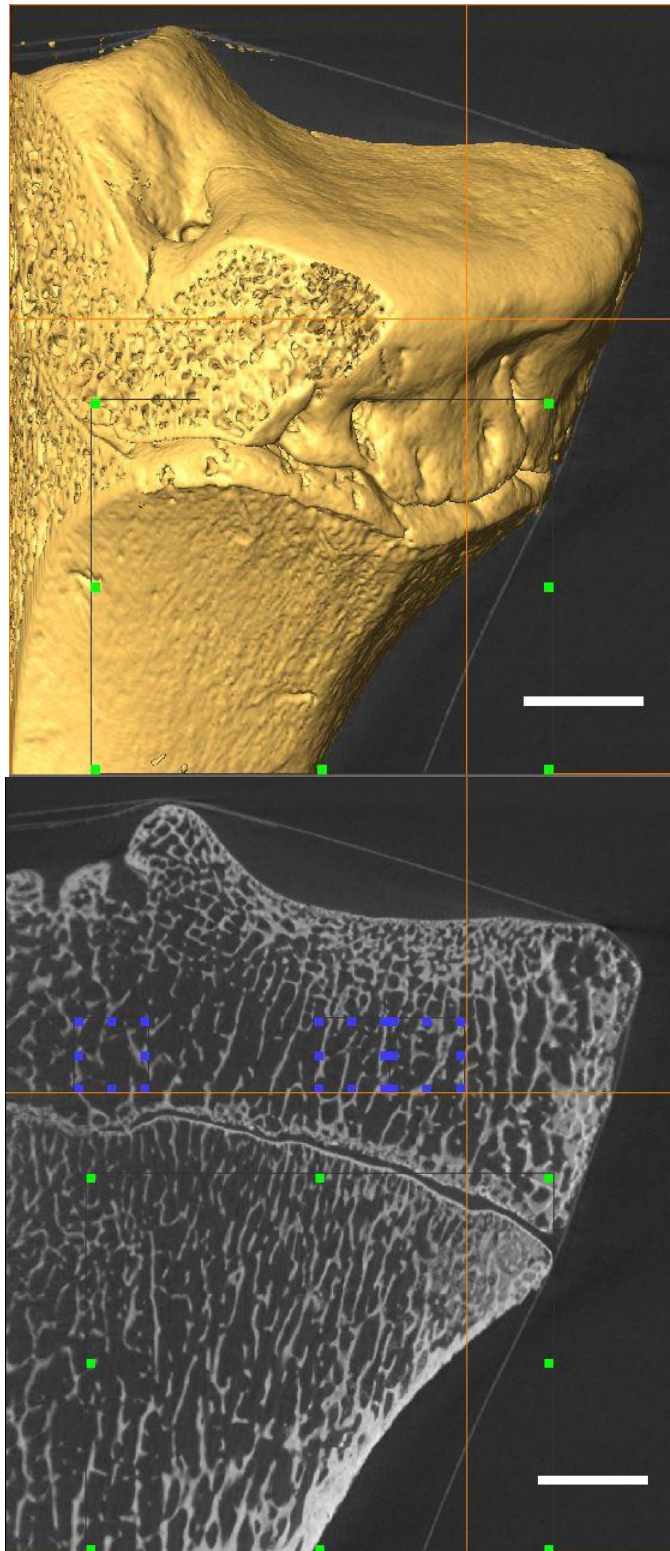


Figure 6.7: Medial Condyle Posterior View Isosurface Rendering (TOP) and 2-D Micro-CT Image (BOTTOM). *Note:* Scale: 5mm.

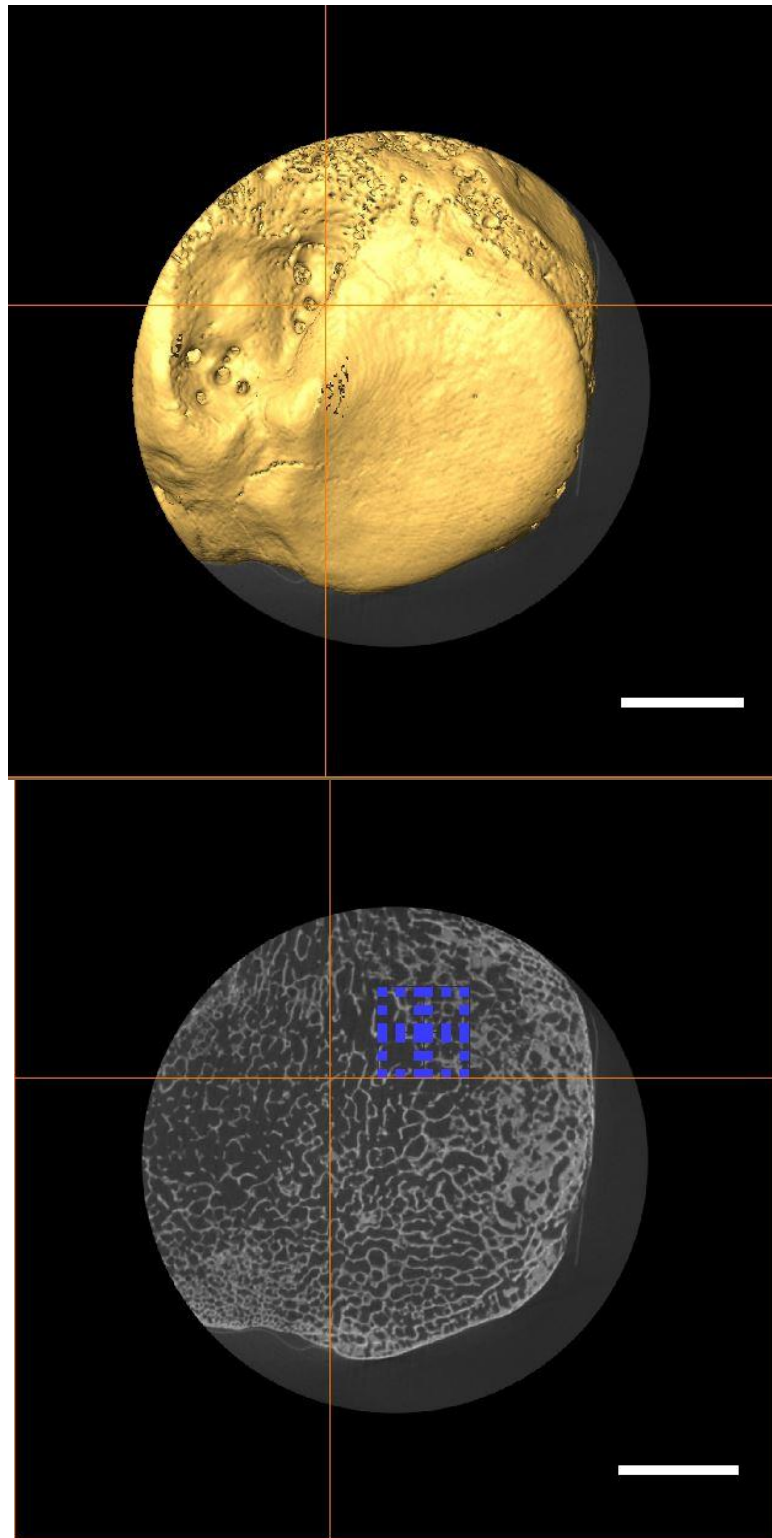


Figure 6.8: Lateral Condyle Superior View Isosurface Rendering (TOP) and 2-D Micro-CT Image (BOTTOM). *Note:* Scale: 5mm.

AGE CATEGORY 3
26-year-old 820735 male

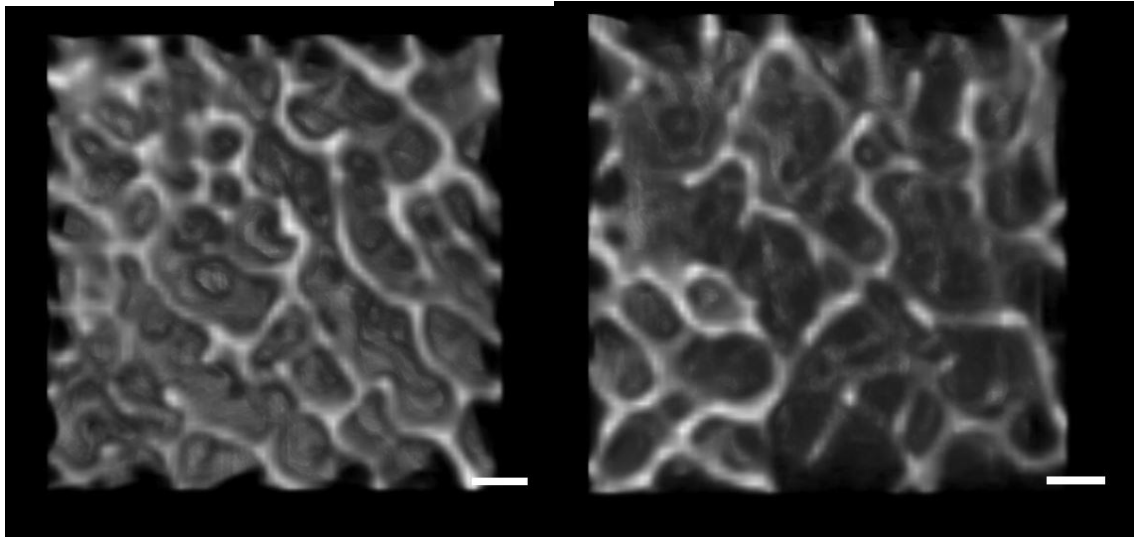


Figure 6.9: VOI 2 Medial Condyle (LEFT) and VOI 7 Between Condyles (RIGHT).
Note: Scale: 1mm.

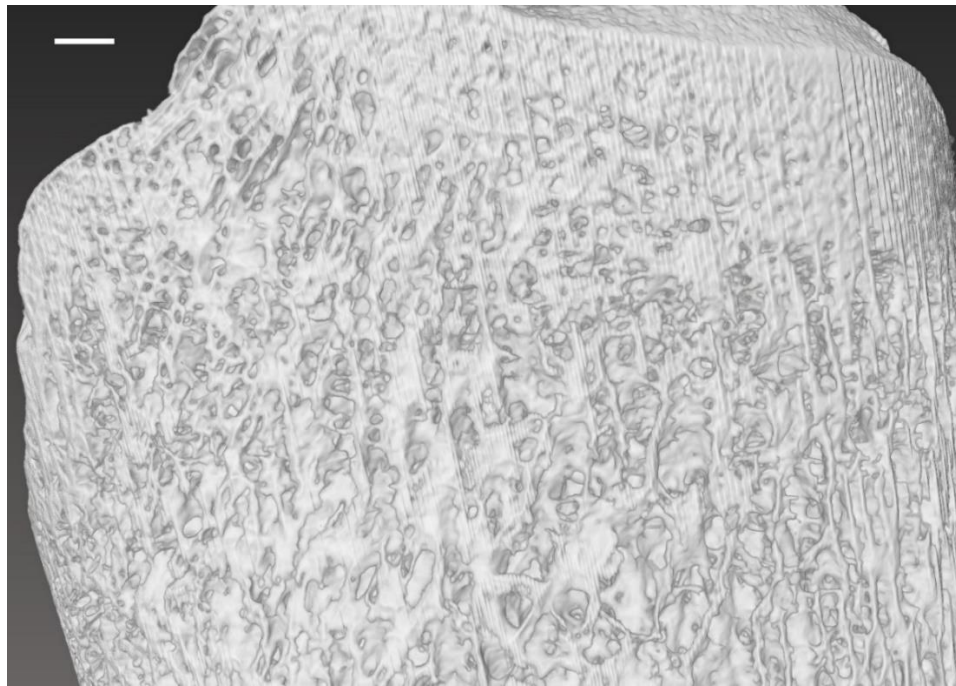


Figure 6.10: Medial Condyle Mid-Condyle Sagittal Rendering. *Note: Scale: 5mm.*

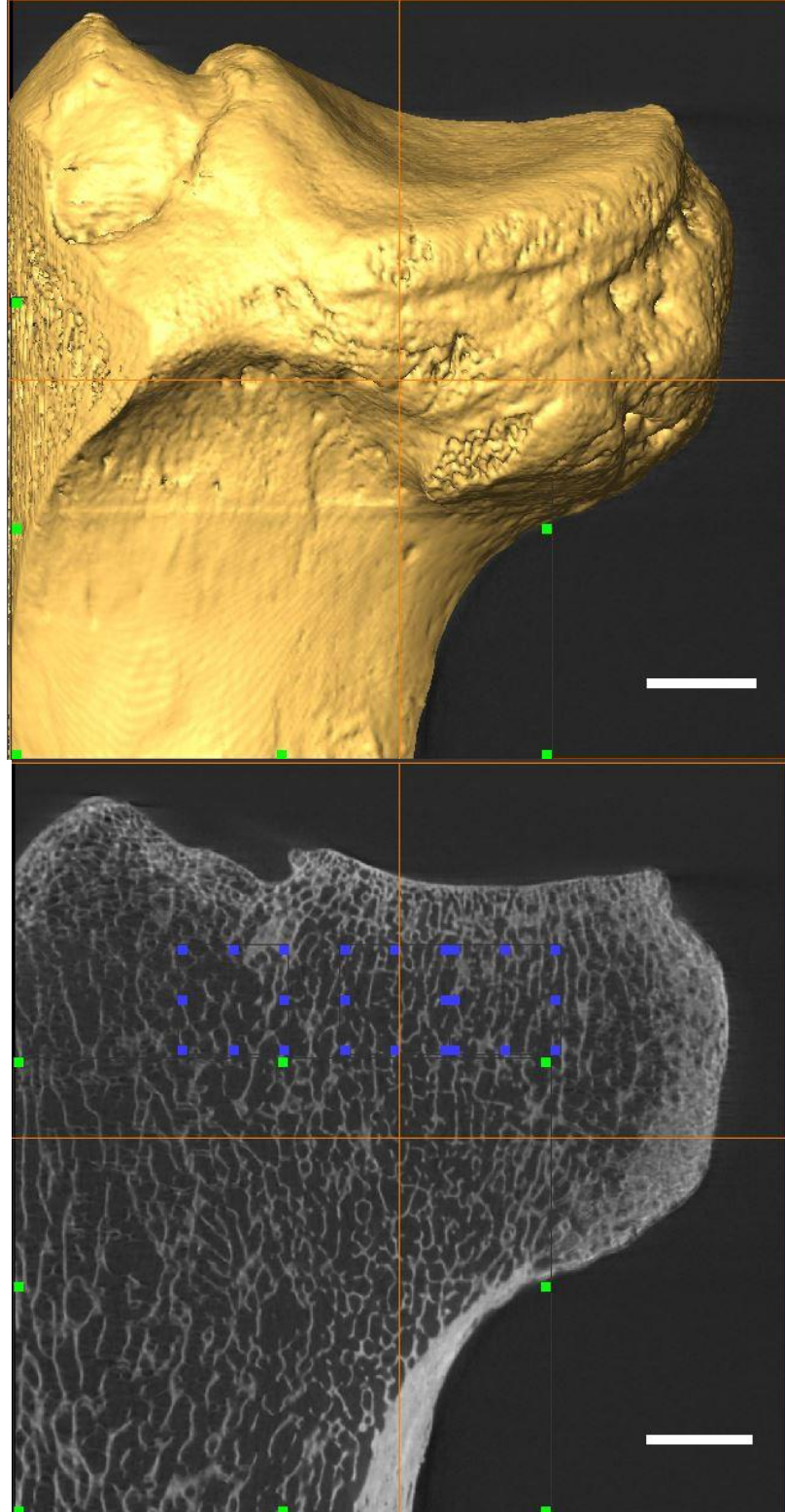


Figure 6.11: Lateral Condyle Posterior View Isosurface Rendering (TOP) and 2-D Micro-CT Image (BOTTOM). *Note:* Scale: 5mm.

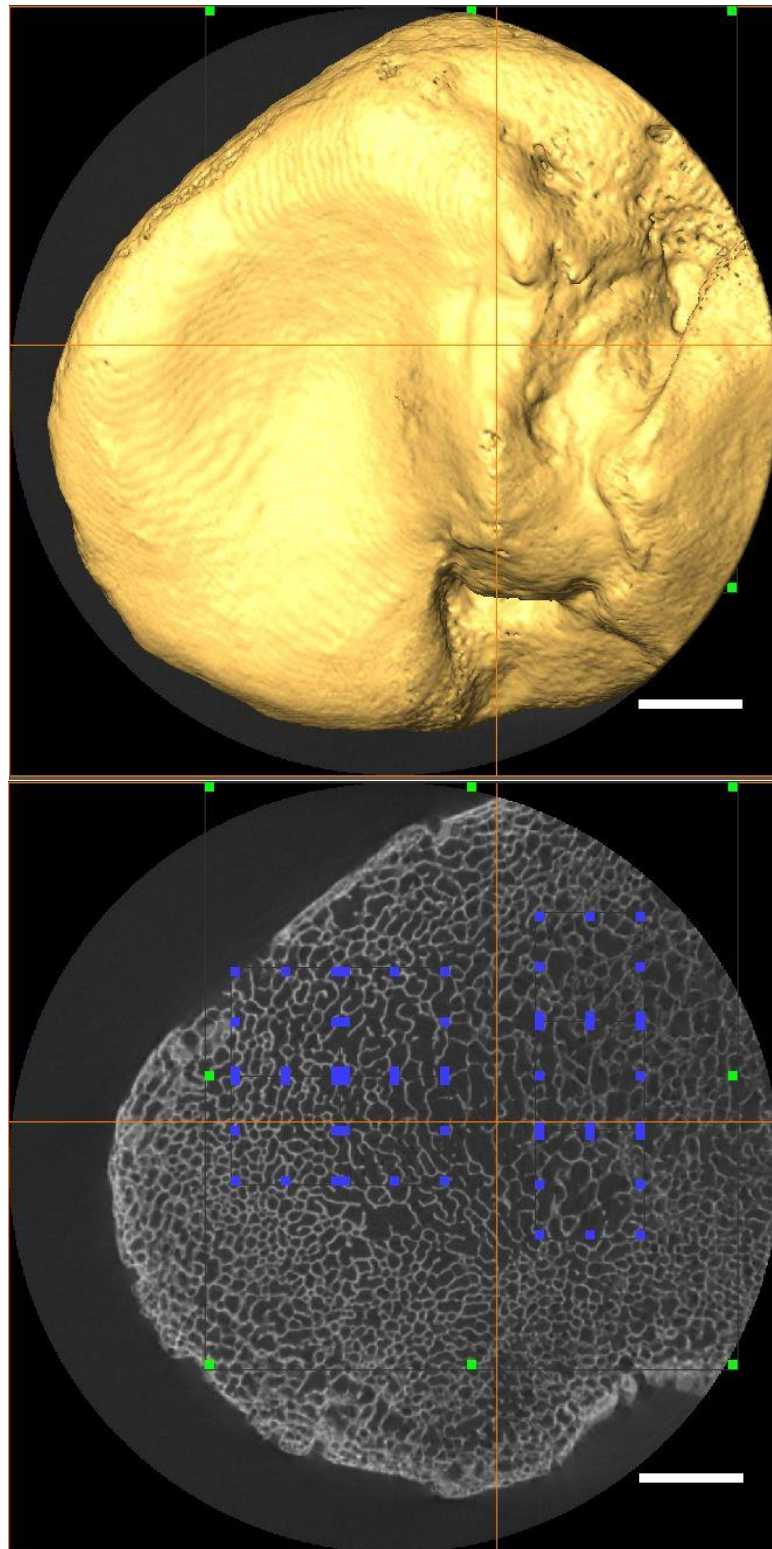


Figure 6.12: Medial Condyle Superior View Isosurface Rendering (TOP) and 2-D Micro-CT Image (BOTTOM). *Note:* Scale: 5mm.

AGE CATEGORY 4
37.5-year-old male (820740)

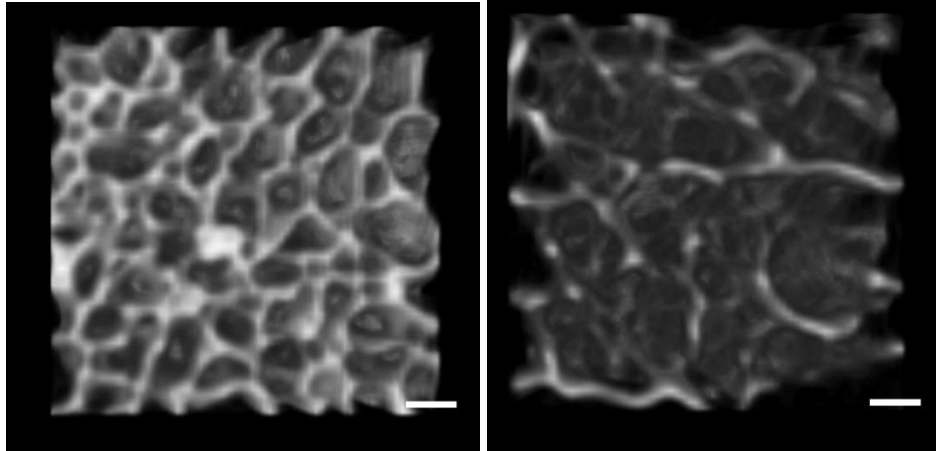


Figure 6.13 VOI 3 Medial Condyle (LEFT) and VOI 7 Between Condyles (RIGHT)
Note: Scale: 1mm.

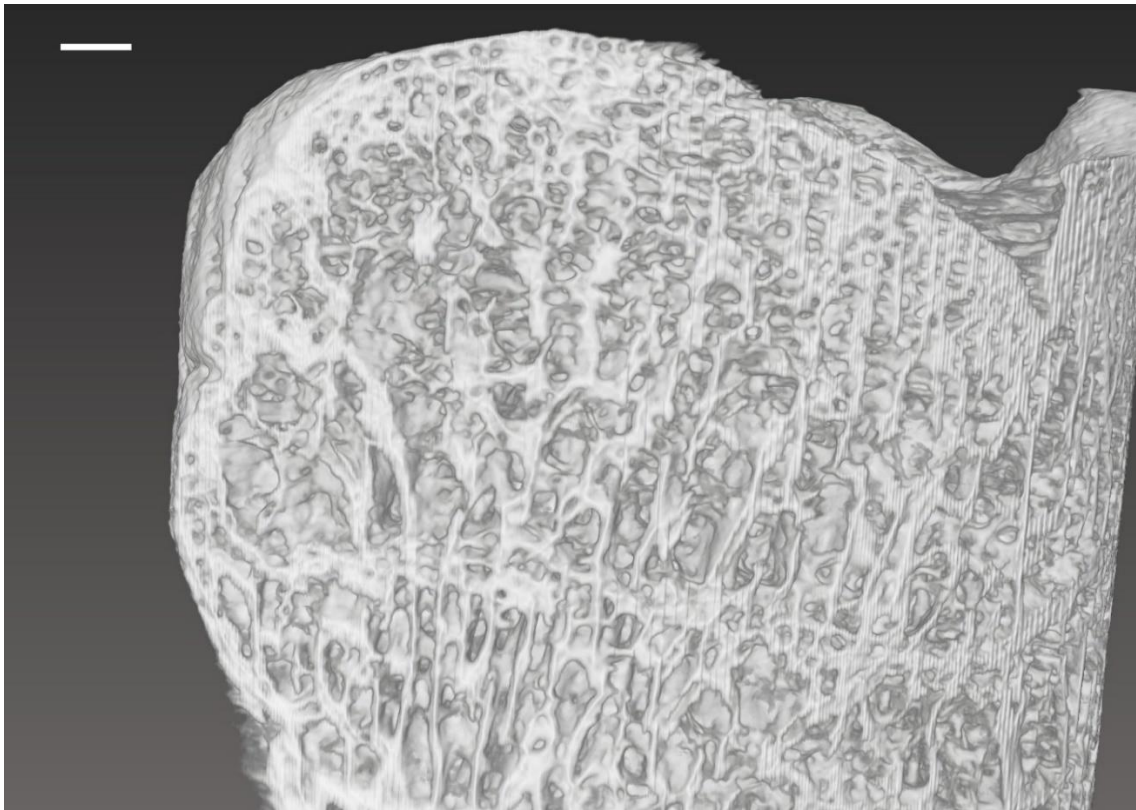


Figure 6.14: Lateral Condyle Mid-Condyle Sagittal Rendering. *Note: Scale: 5mm.*

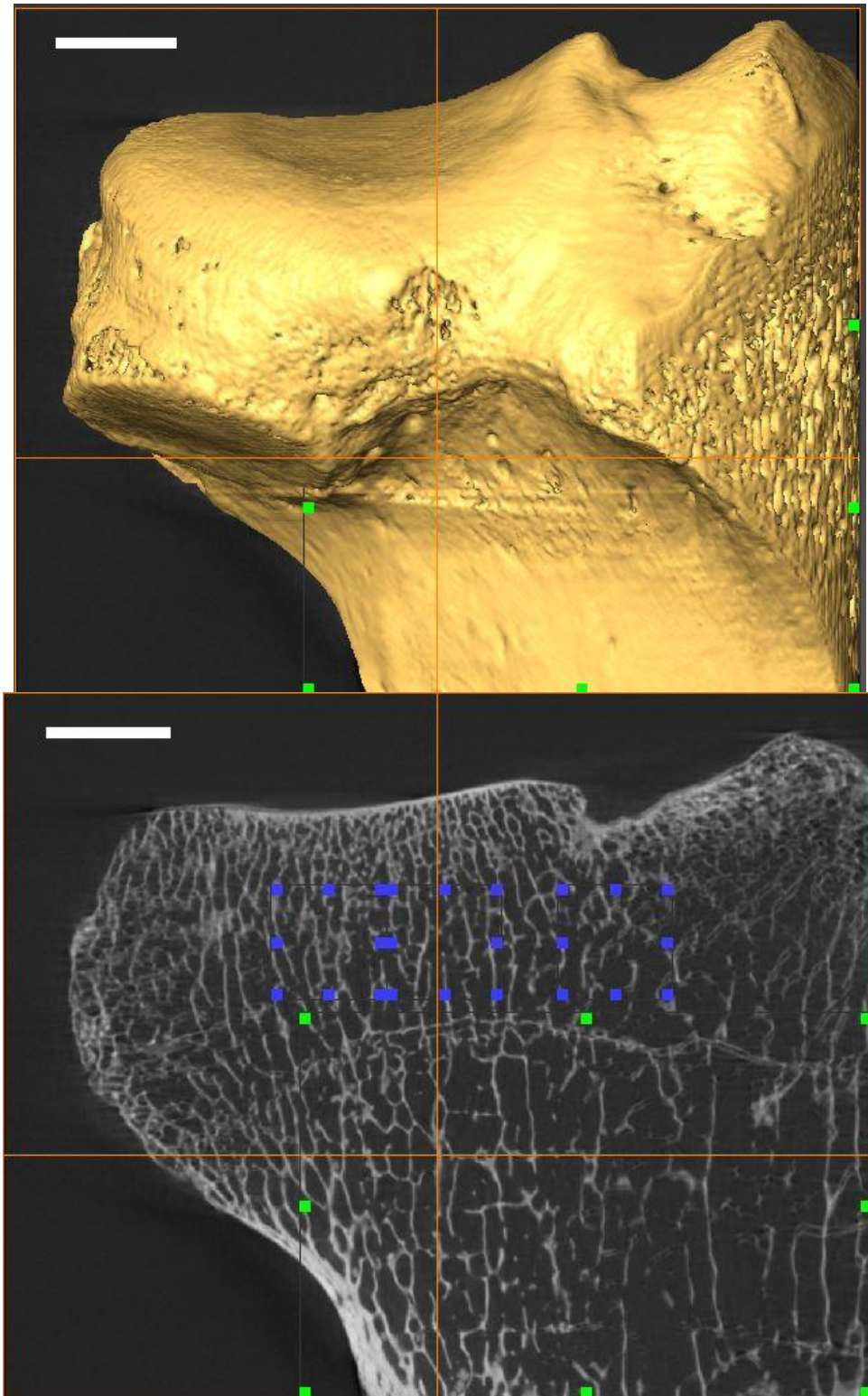


Figure 6.15: Lateral Condyle Posterior View Isosurface Rendering (TOP) and 2-D Micro-CT Image (BOTTOM). *Note:* Scale: 5mm.

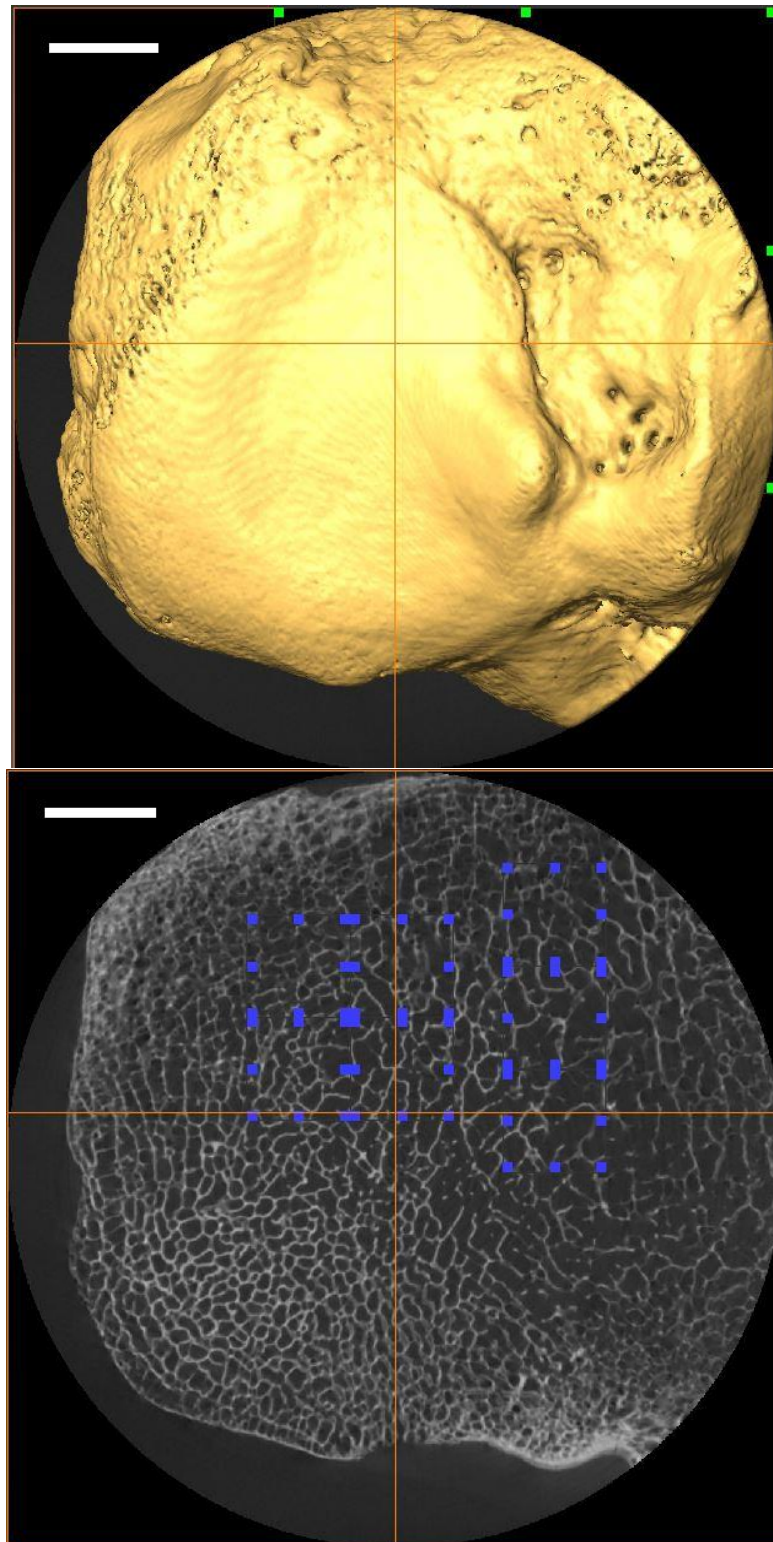


Figure 6.16: Lateral Condyle Superior View Isosurface Rendering (TOP) and 2-D Micro-CT Image (BOTTOM). *Note:* Scale: 5mm.

Summary

Subchondral bone structural parameters results across condyle location, age category, and sex are graphed in boxplots (95% CI) (Figures 6.17 – 6.26). When examining all structural parameter differences across the age categories in the loaded condylar regions, BV/TV ($\alpha = 0.033$), Conn.D ($\alpha = 0.001$), DA ($\alpha = 0.012$), and Plate Ct.Th ($\alpha = 0.000$) significantly differed with age. Bone volume fraction increased with age from childhood to adult and then remained constant in the middle age category. Trabecular subchondral bone became more anisotropic with the adult form. Moreover, a decline in overall trabecular connectivity density is present in both adult categories. Additionally, there was an increase in subchondral plate cortical thickness with age.

Pairwise related-samples Wilcoxon signed ranks tests were performed on all structural parameters means comparing medial and lateral condylar regions. The average mean thickness was greater in the medial condyle however, no significant difference ($\alpha = 0.638$) between medial and lateral condyle subchondral plate thickness was found. In regards to the subchondral trabecular bone, only DA significantly differed ($\alpha = 0.004$) between medial and lateral condylar regions, with the medial condyle being more anisotropic than the lateral condyle.

Finally, using a Mann Whitney test, SMI and to a lesser extent BV/TV were found to differ between males and females. Males had higher bone volume fraction (i.e. more bone tissue) while women had higher SMI (i.e. more rod-like morphology) in the later age categories.

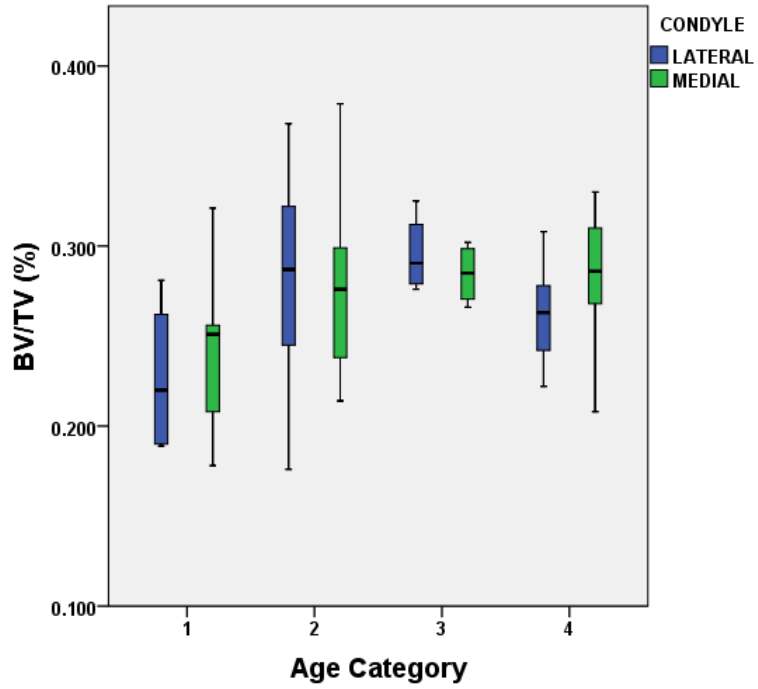


Figure 6.17: Bone volume fraction (%) across age categories.

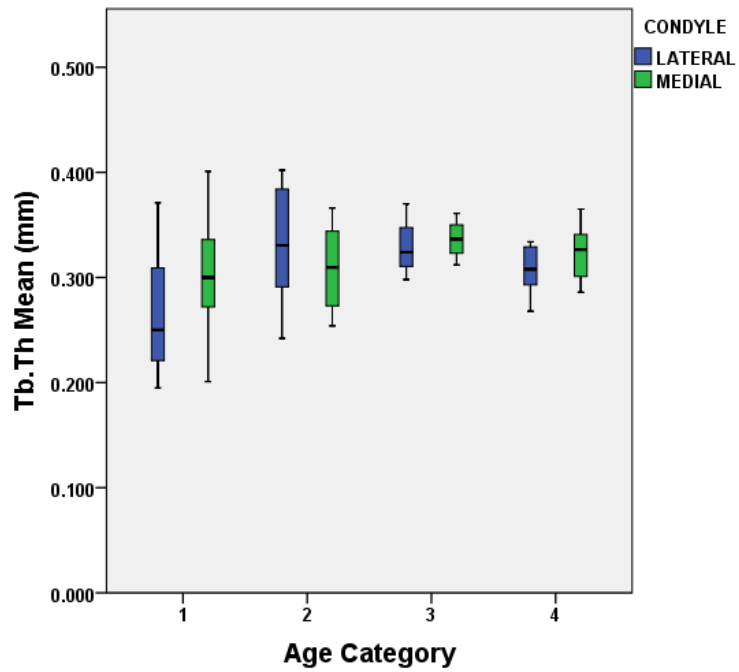


Figure 6.18: Trabecular Thickness (mm) across age categories

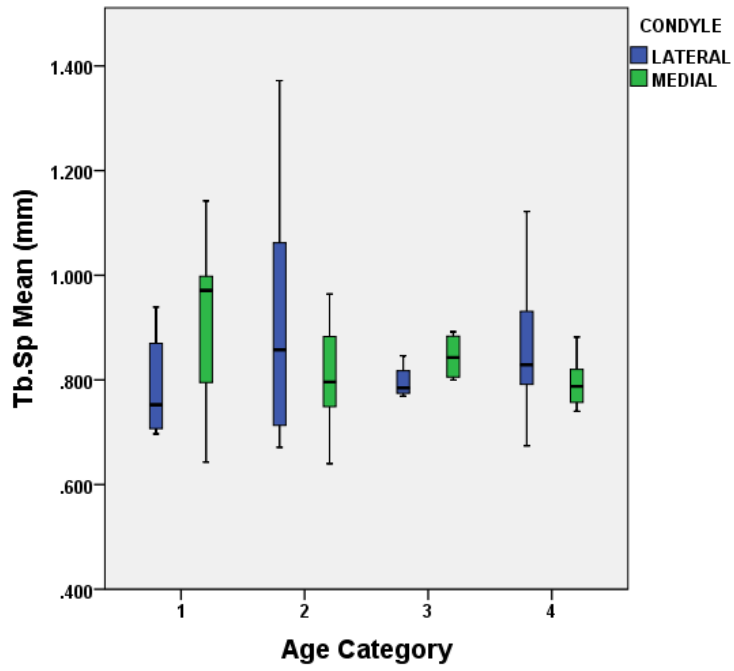


Figure 6.19: Trabecular separation (mm) across age categories.

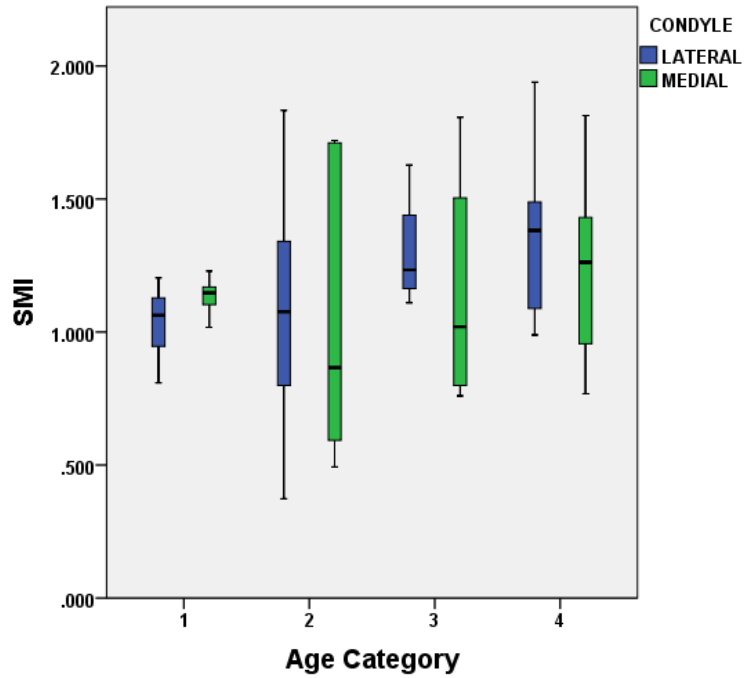


Figure 6.20: Structural model index (-) across age categories.

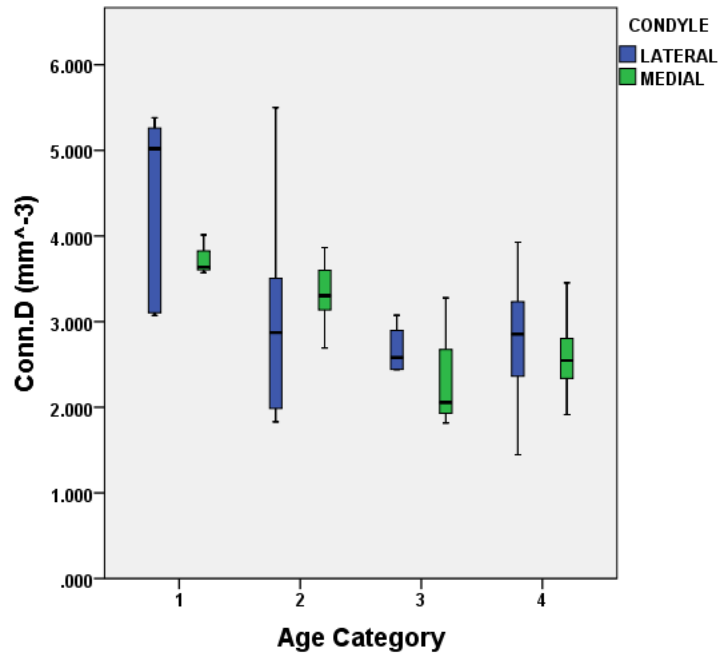


Figure 6.21: Connectivity Density (mm⁻³) across age categories.

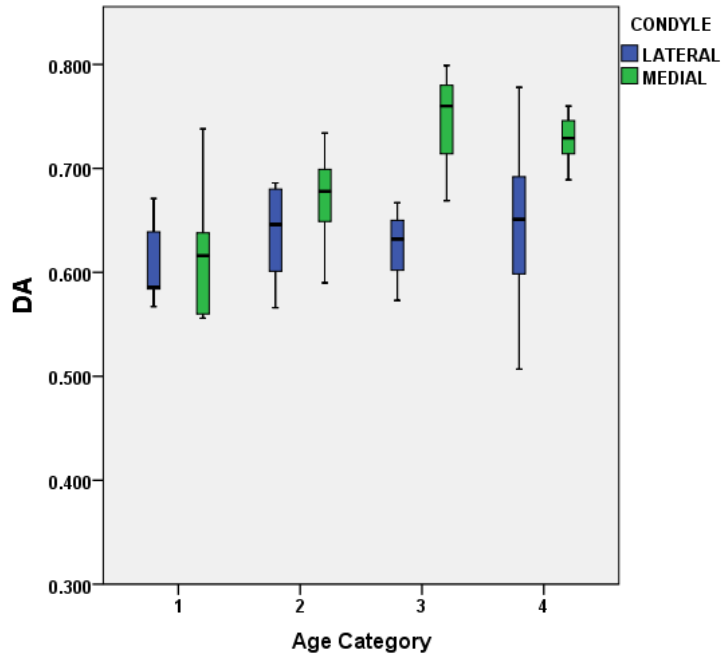


Figure 6.22: Degree of anisotropy (-) across age categories.

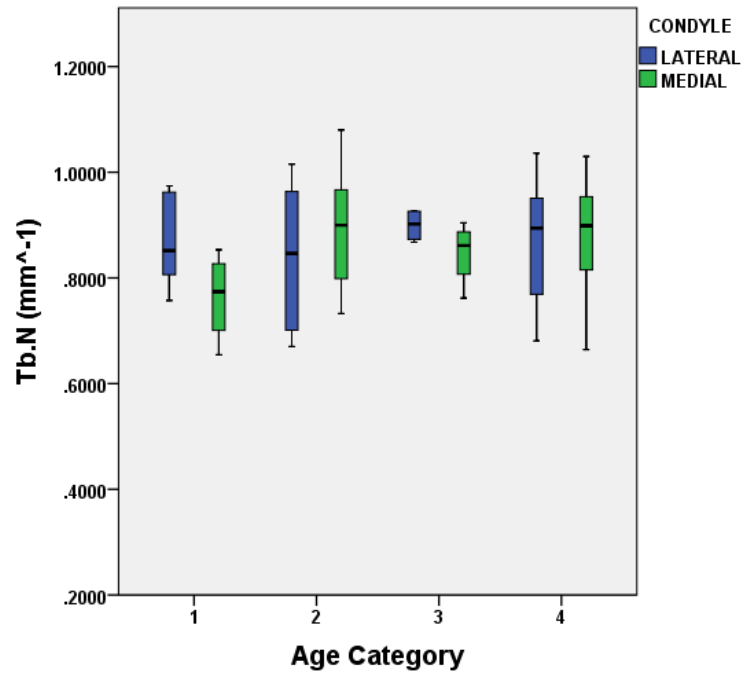


Figure 6.23: Trabecular number (mm^{-1}) across age categories.

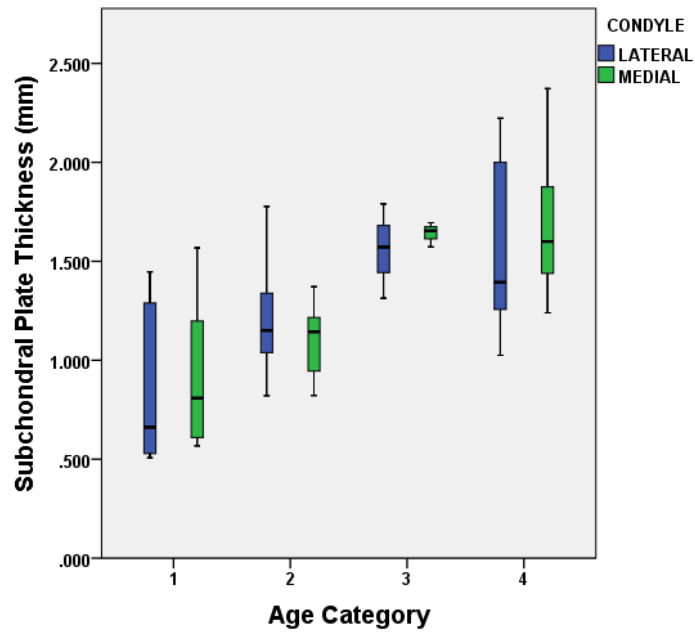


Figure 6.24: Subchondral plate thickness (mm) across age categories

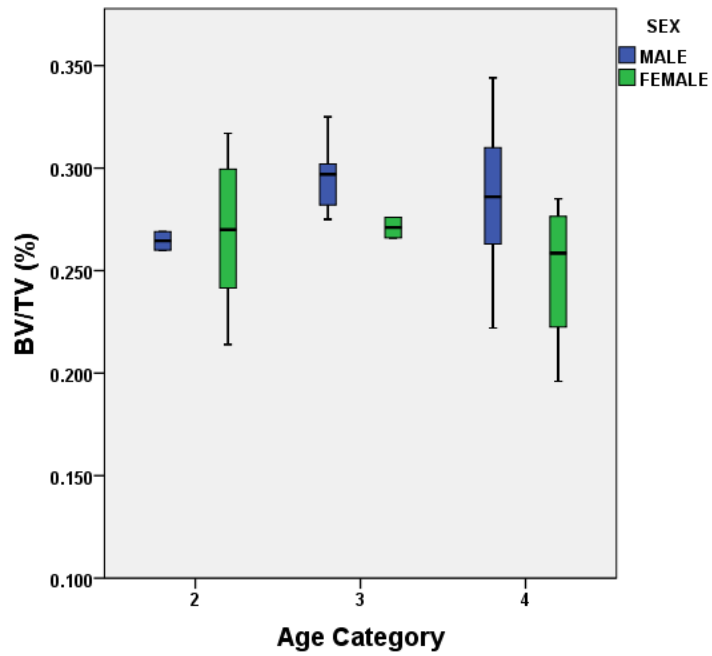


Figure 6.25: Bone volume fraction (%) sex differences across age

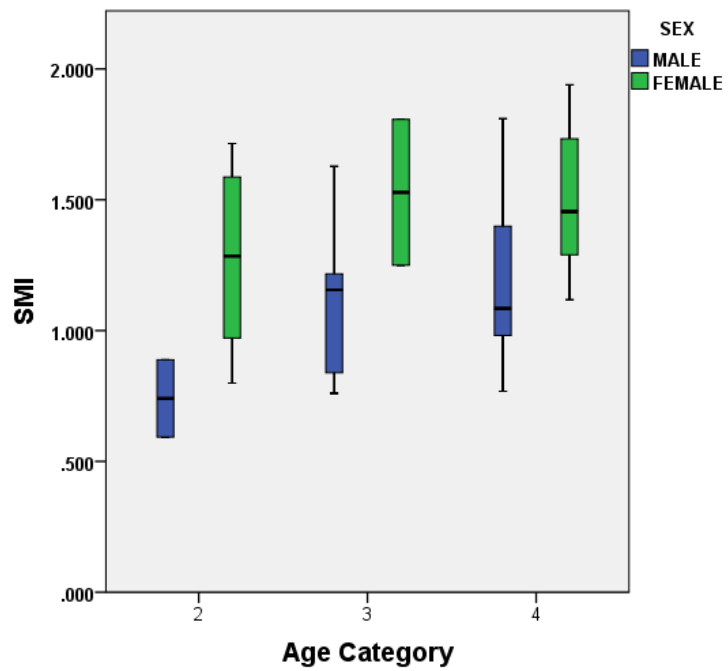


Figure 6.26: Structural model index (-) sex differences across age.

CHAPTER 7: DISCUSSION AND CONCLUSIONS

In comparing these cortical and trabecular bone quantifications with other proximal tibia subchondral studies (Ding et al., 2002; Gosman and Ketcham, 2009; Chen et al., 2011) there are some general similarities but due to differences in sample demographics and population there are differences. Ding and colleagues (2002) observations were geared toward much older individuals than are present in this study. In their younger individuals, they found no major changes in any structural parameters, but noted bone volume fraction and trabecular thickness decrease significantly after the age of 60, with an increase in structural model index (i.e. trabeculae shifting to a rod-like microstructure). Gosman and Ketcham (2009) found that in young adult individuals from the Fort Ancient site, SunWatch Village (16-20 years old), subchondral bone had an increase in bone volume fraction with age and decrease in trabecular number. However, this study also noted a decrease with degree of anisotropy. Chen and colleagues (2011) focused on a much older population with Japanese subjects ranging in age from 57-98 years old. They noted trabecular bone mineral density, bone volume fraction (BV/TV), and trabecular thickness (Tb.Th) decreased between the middle-aged and elderly groups in both men and women. In comparison with non-human tibial subchondral studies, similar results were found in rats (Hamann et al., 2013). Hamann et al. (2013) found that for both subchondral trabecular bone and its cortical plate, bone volume fraction

(BV/TV) and trabecular thickness (Tb.Th) increased in the tibiae of rats. Studies of trabecular bone growth and development in pigs have also demonstrated gradual increases in bone volume fraction, anisotropy, trabecular number, and trabecular thickness with age (Tanck et al., 2001).

When looking broader at trabecular ontogenetic studies, there are similar patterns. Abel and Macho (2011) examined ontogenetic variation in modern human iliac trabecular anisotropy and found that ilia trabecular tissue in infants is relatively isotropic, while that of adults is highly anisotropic. Acquah et al (2015) examined the ontogeny of vertebral trabecular architecture during the developmental period between 6 months prenatal and 2.5 years postnatal in a 19th century juvenile skeletal collection. In early childhood, a pattern of development appeared where BV/TV remained constant but the DA continued to increase. In the proximal femur (Ryan and Krovit, 2006), changes in trabecular number, thickness, and degree of anisotropy propose a gradual change from varying loading patterns to the more stable morphology associated with bipedal walking (Ryan and Krovit, 2006). The proximal tibia (Gosman and Ketcham, 2009) also shows a change in trabecular number and thickness, along with more highly oriented struts, with age. These structural alterations are along with more predictable loading patterns associated with locomotor maturation (Gosman and Ketcham, 2009).

The results of this research bolster previous findings by other studies of trabecular bone local responses to changes in loading patterns. The loss of tissue during infancy may be essential for developing a highly-orientated structure that can resist loads efficiently with minimal bone mass. It is easier to take away surplus material than add

new bone tissue, which also provides greater phenotypic plasticity and may be a response to developing postural and locomotor loads (Acquaah et al., 2015). It is expected that both trabeculae and overall bone shape probably respond in tandem to mechanical loads during ontogeny (Ruff et al., 2006), but that microstructural properties may continue after the adult shape has been attained. Moreover, these results suggest that subchondral bone microstructural properties are remarkably heterogenous.

Sex was another variable examined but only SMI was found to differ significantly between males and females, with women having a more rod-like structure. Eckstein et al., (2007) compared sex differences in trabecular bone microstructure across multiple skeletal sites and found males had thicker trabeculae, higher connectivity, and a higher degree of anisotropy in the femoral trochanter, but these results were not found in other skeletal sites in the same sample. However, Salmon et al. (2015) has demonstrated that the commonly used parameter of SMI may not be suitable for use on real bone geometries because it is strongly influenced by BV/TV.

Characteristics of Subchondral Bone and Plate Ontogeny

The human skeleton optimizes its microarchitecture by elaborate adaptations to mechanical loading during growth and development. During skeletal development, the processes of growth, modeling (shape change) and remodeling (turnover) work together to adapt bone for its typical peak biomechanical demands (Stout and Crowder, 2012). This concept can be applied to subchondral bone growth. The spatial distribution of the strength across the planes of the tibia seems to be consistent with the expected pattern of the load distribution and with contiguity of the trabecular bone. With age, both mineral

crystal and collagen undergo biochemical changes that diminish their capacity to provide the strength and toughness that bones need (Akkus et al., 2004; Pearson and Lieberman, 2004). With increasing body mass (Table A.3), the subchondral bone increases in bone volume with age. Because of this additional loading, trabecular thickness also increases. Lereim et al. (1974) noted that the strength of a normal tibial condyle increases with age. A decline in overall trabecular connectivity density is present in both adult categories. There is also an observed increase in anisotropy.

As a consequence of aging and decline in connectivity, the aging trabeculae seem to align more strongly to the primary direction, becoming more anisotropic. Highly anisotropic trabecular bone is thought to signify a locomotor pattern that restricts joint mobility to a particular direction, whereas more isotropic trabecular structure is considered to signal locomotor behavior involving greater joint mobility (Wallace et al., 2013). The degree of trabecular anisotropy reflects repetitive joint loading and, by extension, locomotor repertoire variability (Ryan and Ketcham, 2002; Ruff, 2005; Griffin et al., 2010; Wallace et al., 2013). These results support the hypothesis that trabecular struts grow to align with the orientation of peak compressive forces, at least in growing juveniles. Further, these results lend support to previous studies proposing the orientation of trabeculae in adults is a function of repeated loading during ontogeny (Hert, 1992), and that trabecular orientation reflects the orientation of peak compressive stress (Biewener et al., 1996; Carter and Beaupre, 2001; Pontzer et al., 2006). The structure adapts in response to an altered loading regime; allowing it to become more efficient at resisting compressive loads along an inferior–superior axis (Acquaah et al, 2015).

Bone volume fraction increased with age from childhood to adult and then remained constant in the middle age category. Trabecular thickness follows the same trend and begins to decline in middle age group. Chen et al. (2011) noted that bone volume fraction (BV/TV) and trabecular thickness (Tb.Th) decreased between the middle-aged and elderly groups similarly in women and men. There was an increase in subchondral plate cortical thickness with age. Age-related plate thickness has been found in non-human studies (Ding et al al, 2006) in guinea pigs, but thickening of subchondral bone plate has also been associated with the onset of osteoarthritis (Zamil et al., 2014; Zamil et al., 2016). Because of its relatively greater stiffness and strength in comparison with the overlying cartilage (Brown and Vrahas 1984; Choi et al. 1990; Lotz et al. 1991), the subchondral plate is generally believed to play an important role in juxta articular load transmission. It appears to be the result of the greater potential for modelling of trabecular tissue during later stages of development (and into adulthood perhaps), i.e. once modelling of external bone shape has slowed/ceased (Abel and Macho, 2011). Since both cortical bone and trabecular bone respond to changes in loading patterns, the response of bone structure to early irregular loading and then to more predictable loading during late childhood provide a unique morphological indicator of development in mature and stable gaits (Raichlen et al., 2015). Past research has indicated that the ontogenetic patterns of change in tibial trabecular bone microarchitecture can be associated with locomotor behavior. Shifts from unstable to stable locomotion leave markers on bone during growth and development (Raichlen et al., 2015). Distal tibia gait studies conducted by Raichlen et al. (2015) found intra-individual variation in DA was generally

high at young ages, likely reflecting variation in loading due to kinematic instability. With increasing age, mean DA converges on higher values and becomes less variable across the distal tibia. Similar to Raichlen et al. (2015), these results suggest that early in development, subchondral bone seems well structured to manage the disorganized loading patterns created by variation in lower limb segment angles from step to step. It is only after maturation occurs, and individuals become more stable and consistent walkers, that trabecular struts and cortex become consistently more highly oriented and that orientation converges on a single more vertical direction across the joint. It is also noteworthy, that the most substantial increase in muscle mass occurs after the pubertal growth spurt (Bogin, 1999), mediated by an increase in growth hormones and after linear growth has ceased. Implications are that morphological shape changes observed during late adolescence/early adulthood are mainly accepted by the internal structures (Abel and Macho, 2011).

Implications of this Study

This research represents a novel approach to quantifying subchondral bone microarchitecture and can potentially inform multiple areas of human skeletal research, including bioarchaeology and skeletal mechanobiology, the ontogeny of bone structure maturation, and clinical studies of skeletal health and joint disease. The present study builds on recent research that highlights the complex nature of trabecular and cortical development. Bioarchaeologists who employ the principles of bone functional adaptation theory to the study of human skeletons as indicators of physical activity often analyze cortical and trabecular bone separately. For example, Gosman and et al., (2013) examined

diaphyseal cortex shape development of the tibia and femur using the Norris Farms skeletal series. Gosman et al. (2013) identified site-specific patterns in cross-sectional cortical bone shape change across ontogeny, noting that both the tibial and femoral diaphyses become increasingly asymmetrical in cross section in association with growth-related cortical mechanical load-bearing demands. However, little is known about the intimate intersection present in the subchondral bone. In order to assess mechanical loading history in archaeological bone, it is vital that modern technological advancements that capitalize on methods of non-destructive analysis be implemented in the study of internal bone structures. High resolution CT is perfectly suited to this task, and directly quantifying mechanical integrity of skeletal microstructures represents a powerful new direction for bioarchaeological research. With the advances in technology it is possible to analyze multiple VOIs (Su et al., 2013) or the entire internal trabecular structure (Gross et al., 2014) to gain a greater understanding of how trabecular bone varies throughout an epiphysis.

This study provides a significant advance in our understanding of the complexities of tissue level growth dynamics in the proximal tibia. The sample provides a rare opportunity to study the effects of childhood bone growth on subchondral microstructural organization that may have effects on bone's mechanical properties well into adulthood. This study provides both consistencies and variability in patterns and tissue type distribution within age categories, and demonstrate their relationship to changing microarchitectural properties of tibial subchondral bone through ontogeny. The trends highlighted in the current study provide important baseline information that can be

used in future comparative studies of subchondral bone growth, important in both archaeological and orthopaedic contexts.

A review of the literature, establishes that physiological distribution of the structural parameters (thickness, mineralization, and density) of the subchondral region may reflect the long-term stresses with a joint surface imposed by the loading acting upon it. This leads to the conclusion that the evaluation of any one of these parameters is able to provide information on how a particular joint is stressed. Quantitative distribution of both subchondral bone density and cartilage thickness is a direct indication of local adaptation to the pressure transmitted through the joint (Müller-Gerbl, 1998). It has been argued that during growth, a joint's size is directly proportional to the size of its total loads. Therefore, its size at skeletal maturity is an indicator of those loads at the time of maturity. Once mature, the joint tissue does not increase in size but throughout life their supporting subchondral bone can decrease or increase in strength and mass to adapt to the changing loads that occur after skeletal maturity. An adult joint's size reflects the size of the loads it adapted to at skeletal maturity, while the cross-sectional area of its supporting bone at any later age could reveal the size of those loads at the time of death (Lanyon, 1992; Frost, 1999). Results of this study have lent support to previous clinical reports of architectural differences in the subchondral region and allow for comparisons in degenerative joint disease between living and archaeological populations. This study provides a novel age range of childhood to middle age, which is not found in other studies of subchondral bone. Moreover, the Norris Farms skeletal series represents a semi-sedentary population whose activity patterns are closer to contemporary groups

which can bridge clinical research. However, the lack of consensus among studies suggests we must use caution when interpreting trabecular bone.

Limitations

The most significant potential limitation to this study is the size and positioning of the volumes of interest. Previous analyses have clearly shown significant variation in bone structure within a single bone (Ryan and Krovitz, 2006; Ryan and Walker, 2010). However, this study provides an alternative approach by positioning multiple volumes throughout the epiphyseal region with the idea of characterizing structure across the entire region. Moreover, the VOIs created were scaled to the size of each individual. The use of multiple volumes has been successful in previous analyses (Fajardo et al., 2007), but presents a challenge in comparing different bones with distinctly different shapes and sizes (Ryan and Walker, 2010). Christiansen (2016) found in mice that parameters such as trabecular thickness and connectivity density are strongly affected by scan voxel size, while other parameters such as trabecular number and trabecular separation are less dependent on voxel size.

There are inherent biases in examining human remains in an archaeological context. Human remains from archaeological sites may represent a biased portion of the population from which they came. These are usually groups containing multiple generations of individuals and not biological populations. These groups typically include individuals who died at different times and under different circumstances, and individual remains are from different segments of the population (Larsen, 2015). For example, individuals may represent different class statuses, sexes, or age groups. Moreover,

taphonomic processes can lead to differential rates of preservation within these assemblages on the microscopic and macroscopic scale (Bell, 2012). Additionally, inaccuracies in age estimation and sex identification can result in distorted demographic profiles (Jackes, 1993). All of these biases are of concern to bioarchaeologists attempting to reconstruct and interpret past behavior based on human remains.

Understanding the developmental and morphological variation that exists in humans can help bioarchaeologists better define stress and lifestyle in past populations. However, there are inherent assumptions in interpreting growth and development in archaeological populations. There is the assumption of biological uniformitarianism, stationary populations, and the ability to determine accurate age estimates from skeletal material (Saunders, 2008; Roksandic and Armstrong, 2011). Moreover, there are biases in sample size, aging methodology, sex estimation, and preservation status that need to be addressed when performing analyses. Unfortunately, this and other similar studies are hindered by a scarcity of data. Few children die in the older age categories and until puberty, it is not possible to accurately determine the sex of skeletal remains. Therefore, developmental studies of older age categories are often based on small sample sizes and are potentially biased by a disproportionate number of males or females in one or other of the samples (Saunders, 2008; Larsen, 2015).

Growth studies provide invaluable information on the health status of children in past populations. They indicate how the differences in environment and exposure to stress can affect the growth outcome of these individuals. For those who survive into adulthood, the childhood stress will have an impact on the general health of that

population as adults. Despite being an informative area of research, growth studies present a number of challenges. By comparing modern growth standards with archaeological samples, we are comparing the growth of children who died to that of healthy living children from populations known to have had secular increases in height in recent decades. Also, it is difficult to determine if the growth of the children in the archaeological record accurately reflects the growth of those who became adults. In regards to methodology, when comparisons of growth are made between different archaeological samples it is important to limit inter-observer error by using the same aging criteria. In order to limit some of the errors inherent in regression formulae derived from archaeological populations, only comparisons between samples, of similar genetic backgrounds, should be implemented when trying to assess environmental impact on growth. In archaeological samples, growth data is obtained by measurements of the diaphyseal length (cross-sectional data), before epiphyseal fusion of the long bones. However, due to the nature of archaeological data, studies of deceased individuals do not provide true growth curves, nor can they provide information on a child's growth velocity. Rather, we compare the growth profiles of individuals who died within each age category to a modern healthy population, or with the growth profiles of a contrasting archaeological group (Chapskie, 2006; Saunders, 2008).

Behavioral reconstructions using subchondral bone structure in archaeological populations require a fundamental understanding of the link between ontogenetic changes in bone architecture and the mechanical loads experienced during locomotion and other behaviors. The response of trabecular bone to changing mechanical loads during growth

and development serves as a powerful experiment to evaluate both the significance of mechanical loading on adult trabecular bone morphology and ultimately the utility of trabecular bone structure for behavioral reconstruction. Moreover, there are still concerns regarding making expectations based solely on subchondral bone, such as what role does the articular cartilage play in the initial development, as well as, should we examine these regions of the body as a functional joint-subchondral bone unit or as separate components.

Conclusion and Future Directions

Age-related changes in mechanical loading have varied effects on subchondral bone morphology within the proximal tibia. This research uses bone functional adaptation theory to focus on the structural changes that occur at the cartilage-bone interface. The proposed application of 3D morphological analysis in a skeletal series with a wide range of ages is a novel means of explaining mechanical adaptedness within the context of skeletal growth, when bones are most sensitive to mechanical stimuli. Additionally, this research provides insights into the interrelationship between genetic control and functional response in cortical and trabecular microarchitecture. Thus, this study will advance knowledge on the role of mechanical loading in the bone microstructure development and augment the analytical repertoire of bioarchaeologists and bone scientists investigating the relationship between skeletal form and function.

The nature of the structural response to mechanical stimuli may also provide valuable information about the relationship between joint disease and bone microstructure, especially in the weight-bearing skeleton. This project established a

baseline for future investigations of the role of physical lifestyle in shaping skeletal morphology. Through elucidation of the general pattern of developmental and mid-life trends associated with trabecular and cortical structural change, the findings of the study can be compared with other archaeological skeletal samples with differing physical lifestyles (i.e. more mobile groups) in order to further clarify the mechanical sensitivity and functionality adaptive nature of subchondral bone in the weight-bearing skeleton. With ongoing conflict with the Mississippians and constant raiding, the Oneota of Norris Farms had limited mobility and limited frequency/range in physical activity and food procurement activities. This sedentary lifestyle and precautionary behavior provide a context for the overall locomotive patterns present among the group. Further, this study can lend an additional perspective to the impact of physiological and nutritional stress on skeletal development, as the Norris Farms people are known to have experienced chronic warfare and considerable hardship.

Future investigations include comparing the results of proximal tibia subchondral research to other skeletal regions in the Norris Farms #36 skeletons. Moreover, the comparison of this research with other groups can allow us to begin to characterize the role environment may play in the development and maintenance of skeletal microstructures. Finally, implementing Geographic Information Systems (GIS) analysis for mapping structural parameter patterns for all volumes of interest across time and regions, would provide another perspective of ontogenetic patterning in this region. It is clear that new methods for detecting variances in bone morphology must be added to pre-

existing ones to refine our understanding of the relationship between behavior, loading environment, function, and skeletal response.

REFERENCES

Abel R, Macho GA. 2011. Ontogenetic changes in the internal and external morphology of the ilium in modern humans. *Journal of Anatomy* 218: 324-335.

Acquaah F, Robson Brown KA, Ahmed F, Jeffery N, Abel RL. 2015. Early trabecular development in human vertebrae: overproduction, constructive regression, and refinement. *Frontiers in Endocrinology* 6:67.

Acsadi G, Nemeskeri I. 1970. *History of Human Life Span and Mortality*. Budapest: Akademiai Kiado.

Adolph KE, Vereijken B, ShROUT PE. 2003. What Changes in Infant Walking and Why. *Child Development* 74(2): 475-497.

Ahluwalia K. 2000. *Knee Joint Load as Determined by Tibial Subchondral Bone Density: It's Relationship to Gross Morphology and Locomotor Behavior in Catarrhines*. PhD Dissertation, Stony Brook University.

Akkus O, Adar F, Schaffler MB. 2004. Age-related changes in physicochemical properties of mineral crystals are related to impaired mechanical function of cortical bone. *Bone* 34: 443–453.

Anderson M, Green WT, Messner MB. 1963. Growth and the predictions of growth in the lower extremities. *Journal of Bone and Joint Surgery* 45A:1-14.

Arazi M, Ogun TC, Memik R. 2001. Normal development of the tibiofemoral angle in children: a clinical study of 590 normal subjects from 3 to 17 years of age. *Journal of Pediatric Orthopaedics* 21(2): 264-267.

Archer CW, Douthwaite GP, Francis-West P. 2003. Development of Synovial Joints. *Birth Defects Research (Part C)* 69: 144-155.

Arzigian CM, Boszhardt RF, Theler JL, Rodell RL, Scott MJ. 1989. Summary of the Pammel Creek Site Analysis and a Proposed Oneota Seasonal Round. *Wisconsin Archaeologist* 70.

Ascenzi A, Bonucci E. 1970. The mechanical properties of the osteon in relation to its structural organization. In: Balazs EA, editor. *Chemistry and Molecular Biology of the Intercellular Matrix*. New York: Academic Press. p. 1341–1359.

- Ascenzi A, Bonucci E. 1976. Mechanical similarities between alternate osteons and cross-ply laminates. *Journal of Biomechanics* 121: 275–294.
- Auerbach BM, Ruff CB. 2004. Human Body Mass estimation: A comparison of “Morphometric” and “Mechanical” Methods. *American Journal of Physical Anthropology* 125: 331-342.
- Ausk BJ, Huber P, Poliachik SL, Bain SD, Srinivasan S, Gross TS. 2012. Cortical bone resorption following muscle paralysis is spatially heterogeneous. *Bone* 50(1): 14-22.
- Badea CT, Panetta D. 2014. High-Resolution CT for Small-Animal Imaging Research. In: Brahme A, editor. *Comprehensive Biomedical Physics*, vol. 2. Amsterdam: Elsevier. p. 221-242.
- Bailey DA. 1997. The Saskatchewan Pediatric Bone Mineral Accrual Study: bone mineral acquisition during the growing years. *International Journal of Sports Medicine* 18(Supplemental 3): S191–S194.
- Bailey DA, McKay HA, Mirwald RL, Crocker PR, Faulkner RA. 1999. A six-year longitudinal study of the relationship of physical activity to bone mineral accrual in growing children: the University of Saskatchewan bone mineral accrual study. *Journal of Bone and Mineral Research* 14(10): 1672–1679.
- Baker BJ, Dupras TL, Tocheri MW. 2005. *The Osteology of Infants and Children*. College Station: Texas A&M University Press.
- Barak MM, Lieberman DE, Hublin J-J. 2011. A Wolff in sheep’s clothing: Trabecular bone adaptation in response to changes in joint loading orientation. *Bone* 49:1141-1151.
- Barr AJ, Campbell TM, Hopkinson D, Kingsbury SR, Bowes MA, Conaghan PG. 2015. A systematic review of the relationship between subchondral bone features, pain and structural pathology in peripheral joint osteoarthritis. *Arthritis Research and Therapy* 17:228.
- Barrett JF, Keat N. 2004. Artifacts in CT: Recognition and Avoidance. *Radiographics* 24(6): 1679-1691.
- Bart ZR, Wallace JM. 2013. Microcomputed Tomography Applications in Bone and Mineral Research. *Advances in Computed Tomography* 2:121-127.
- Bass SL, Saxon L, Daly RM, Turner CH, Robling AG, Seeman E, Stuckey S. 2002. The effect of mechanical loading on the size and shape of bone in pre-, peri-, and postpubertal girls: A study in tennis players. *Journal of Bone and Mineral Research* 17: 2274-2280.

- Bass WM. 1971. *Human Osteology: A Laboratory and Field Manual of the Human Skeleton*. Columbia: Missouri Archaeological Society.
- Baxter JE. 2008. The Archaeology of Childhood. *Annual Review of Anthropology* 37:159-175.
- Bell C. *Animal mechanics, or proofs of design in the animal frame*. Cambridge, MA: Morrill Wyman; 1827.
- Bell LS. 2012. Histotaphonomy. In: Crowder CM, Stout SD, editors. *Bone Histology, An Anthropological Perspective*. Boca Raton: CRC Press, p 241-251.
- Benn DW. 1995. Woodland People and the Roots of the Oneota. In: Green, W, editor. *Oneota Archaeology: Past, Present, and Future*. Office of the State Archaeologist Report 20. Iowa City: Office of the State Archaeologist. p. 91-140.
- Bentolila V, Boyce TM, Fyhrie DP, Drumb R, Skerry TM, Schaffler MB. 1998. Intracortical remodeling in adult rat long bones after fatigue loading. *Bone* 23:275-281.
- Berres TE. 2001. *Power and Gender in Oneota Culture: A Study of a Late Prehistoric People*. Dekalb: Northern Illinois University Press.
- Biewener AA, Fazzalari NL, Konieczynski DD, Baudinette RV. 1996. Adaptive changes in trabecular architecture in relation to functional strain patterns and disuse. *Bone* 19(1): 1-8.
- Bobinac D, Spanjol J, Zoricic S, Maric I. 2003. Changes in articular cartilage and subchondral bone in osteoarthritic knee joints in humans. *Bone* 32:284-290.
- Bogin, B. 1999. *Patterns of Human Growth*. 2nd edition. Cambridge: Cambridge University Press.
- Bogin B, Loucky J. 1997. Plasticity, Political Economy, and Physical Growth Status of Guatemala Maya Children Living in the United States. *American Journal of Physical Anthropology* 102: 17-32.
- Bonewald LF. 2011. The Amazing Osteocyte. *Journal of Bone and Mineral Research* 26(2): 229-238.
- Bonewald LF. 2013. Osteocytes. In: Rosen CJ, editor. *Primer on the Metabolic Bone Diseases and Disorders of Mineral Metabolism*, 8th Edition. Ames: John Wiley & Sons. p. 34-41.
- Boszhardt RF, Bailey TW, Gallagher JP. 1985. Oneota Ridged Fields at the Sand Lake Site (47Lc44), LaCrosse County, Wisconsin. *The Wisconsin Archeologist* 66(1): 47-67.

- Boszhardt RF, McCarthy J. 1999. Oneota end scrapers and experiments in hide dressing: An analysis from the LaCrosse locality. *Midcontinental Journal of Archaeology* 24: 177-199.
- Bourguery JM. 1832. *Traite Complet de l'Anatomie de l'Homme*. Paris: I. Osteologie.
- Bousson V, Lowitz T, Laouisset L, Engelke K, Laredo JD. 2012. CT imaging for the investigation of subchondral bone in knee osteoarthritis. *Osteoporosis International* 23(Supplemental 8): S861-S865.
- Bouxsein ML, Boyd SK, Christiansen BA, Guldberg RE, Jepsen KJ, Müller R. 2010. Guidelines for Assessment of Bone Microstructure in Rodents Using Micro-Computed Tomography. *Journal of Bone and Mineral Research* 25(7):1468-1486.
- Boyce BF, Xing L. 2008. Functions of RANKL/RANK/OPG in bone modeling and remodeling. *Archives of Biochemistry and Biophysics* 473: 139-146.
- Brama PA, TeKoppele JM, Bank RA, Barneveld A, van Weeren PR. 2002. Biochemical development of subchondral bone from birth until age eleven months and the influence of physical activity. *Equine Veterinary Journal* 34:143-149.
- Bridges PS. 1992. Prehistoric Arthritis in the Americas. *Annual Review of Anthropology* 21:67-91.
- Brothwell DR. 1963. *Digging Up Bones*. London: British Museum of National History.
- Brown JA. 1982. What Kind of Economy Did the Oneota Have? In: Gibbon GE, editor. *Oneota Studies*. Minneapolis: University of Minnesota Publications in Anthropology No.1. p. 107-112.
- Brown JA. 1990. The Oak Forest Site: Investigations into Oneota Subsistence Settlement in the Cal-Sag Area of Cook County, Illinois. In: Brown JA, O'Brien PJ, editors. *At the Edge of Prehistory: Huber Phase Archaeology in the Chicago Area*. Kampsville: Center for American Archaeology. p. 123-308.
- Brown TD, Vrahas MS. 1984. The apparent elastic modulus of the juxtarticular subchondral bone of the femoral head. *Journal of Orthopaedic Research* 2: 32-38.
- Buckland-Wright 2004. Subchondral bone changes in hand and knee osteoarthritis detected by radiography. *Osteoarthritis and Cartilage* 12: S10-S19.
- Buckwalter JA. 1998. Articular cartilage: injuries and potential for healing. *Journal of Orthopaedic and Sports Physical Therapy* 28: 192-202.
- Buckwalter JA, Mankin HJ. 1997. Articular cartilage, part 1: tissue design and chondrocyte-matrix interaction. *Journal of Bone and Joint Surgery* 79: 600-611.

- Buckwalter JA, Mankin HJ. 1998. Articular cartilage: tissue design and chondrocytes-matrix interactions. *Instructional Course Lectures* 47: 477-486.
- Buie HR, Campbell GM, Klinck RJ, MacNeil JA, Boyd SK. 2007. Automatic segmentation of cortical and trabecular compartments based on a dual threshold technique for in vivo micro-CT bone analysis. *Bone* 41(4): 505-515.
- Buikstra JE, Milner GR. 1991. Isotopic and Archaeological Interpretations of Diet in the Central Mississippian Valley. *Journal of Archaeological Sciences* 18: 319-329.
- Buikstra JE, Ubelaker DH. 1994. Standards for Data Collection from Human Skeletal Remains: Proceedings of a Seminar at the Field Museum of Natural History, Arkansas Archaeological Survey Research Series No. 44. Fayetteville: Arkansas Archaeological Survey.
- Burghardt AJ, Link TM, Majumdar S. 2011. High-resolution Computed Tomography for Clinical Imaging of Bone Microarchitecture. *Clinical Orthopaedics and Related Research* 469: 2179-2193.
- Burghardt AJ, Pialat J-P, Kazakia GJ, Boutroy S, et al. 2013. Multi-center Precision of Cortical and Trabecular Bone Quality Measures Assessed by HR-pQCT. *Journal of Bone and Mineral Research* 28(3):524-536.
- Burr DB. 1993. Remodeling and the repair of fatigue damage. *Calcified Tissue International* 53: S75-S81.
- Burr, DB. 1998. The importance of subchondral bone in osteoarthritis. *Current Opinion in Rheumatology* 10(3):256-262.
- Burr DB, Gallant MA. 2012. Bone remodeling in osteoarthritis. *Nature reviews: Rheumatology* 8(11):665-673.
- Burr DB, Martin RB. 1989. Errors in bone remodeling: toward a unified theory of metabolic bone disease. *American Journal of Anatomy* 186(2): 186-216.
- Burr DB, Ruff CB, Thompson DD. 1990. Patterns of skeletal histologic change through time: comparison of an archaic Native American population with modern populations. *Anatomical Record* 226: 307-314.
- Cameron N, Demerath E. 2002. Critical periods in human growth and their relationship to diseases of aging. *Yearbook of Physical Anthropology* 45: 159-184
- Cao JJ, Sun L, Gao H. 2010. Diet-induced obesity alters bone remodeling leading to decreased femoral trabecular bone mass in mice. *Annals of the New York Academy of Sciences* 1192:292-297.

- Carames B, Taniguchi N, Seino D, Blanco FJ, D’Lima D, Lotz M. 2012. Mechanical injury suppresses autophagy regulators and pharmacologic activation of autophagy results in chondroprotection. *Arthritis and Rheumatology* 64(4): 1182-1192.
- Carlson KJ, Lublinksy S, Judex S. 2008. Do different locomotor modes during growth modulate trabecular architecture in the murine hind limb? *Integrative and Comparative Biology* 48: 385-393.
- Carlson KJ, Patel BA. 2006. Habitual use of the primate forelimb is reflected in the material properties of subchondral bone in the distal radius. *Journal of Anatomy* 208:659–670.
- Carpenter RD, Carter DR. 2008. The mechanobiological effects of periosteal surface loads. *Biomechanics and Modeling in Mechanobiology* 7(3): 227-242.
- Carter DH, Beaupre GS. 2001. Skeleton function and form
- Carter DR. 1987. Mechanical loading history and skeletal biology. *Journal of Biomechanics* 20: 1095-1109.
- Carter DR, Orr TE, Fyrhie DP. 1989. Relationships between loading history and femoral cancellous bone architecture. *Journal of Biomechanics* 22: 231-244.
- Carter DR, Van Der Meulen MCH, Beaupre GS. 1996. Mechanical Factors in Bone Growth and Development. *Bone* 18(1): 5S-10S.
- Carter DR, Wong M. 1988. The role of mechanical loading histories in the development of diarthrodial joints. *Journal of Orthopaedic Research* 6(6): 804-816.
- Cecil DL, Johnson K, Rediske J, et al. 2005. Inflammation-induced chondrocyte hypertrophy is driven by receptor for advanced glycation end products. *Journal of Immunology* 175: 8296-8302.
- Chapman K., Valdes A. 2012. Genetic factors in OA pathogenesis. *Bone* 51(2): 258-264.
- Chapskie A. 2006. Sub-Adults in the Bioarchaeological Record. *Nexus* 19: 32-51.
- Chen H, Washimi Y, Kubo K, Onozuka M. 2011. Gender-related changes in three-dimensional microstructure of trabecular bone at the human proximal tibia with aging. *Histology and Histopathology* 26: 563-570.
- Chen H, Zhou X, Fujita H, Onozuka M, Kubo K-Y. 2013. Age-Related Changes in Trabecular and Cortical Bone Microstructure. *International Journal of Endocrinology* 2013:213-234.

- Cheng JC, Chan PS, Chiang SC, Hui PW. 1991. Angular and rotational profile of the lower limb in 2,630 Chinese children. *Journal of Pediatric Orthopaedics* 11(2):154–161.
- Choi K, Kuhn JL, Ciarelli MJ, et al. 1990. The elastic moduli of human subchondral, trabecular, and cortical bone tissue and the size-dependency of cortical bone modulus. *Journal of Biomechanics* 23: 1103–1113.
- Christiansen BA. 2016. Effects of micro-computed tomography voxel size and segmentation method on trabecular bone microstructure measures in mice. *Bone Reports* 5: 136-140.
- Christiansen M, Kveiborg M, Kassem M, Clark BF, Rattan SI. 2000. CBFA1 and topoisomerase I mRNA levels decline during cellular aging of human trabecular osteoblasts. *Journal of Gerontology* 55: B194-B200.
- Christen P, Ito K, Ellouz R, Boutroy S, Sornay-Rendu E, Chapurlat RD, van Rietbergen B. 2014. Bone remodeling in humans is load-driven but not lazy. *Nature Communications* 5: 4855.
- Clark JM, Huber JD. 1990. The structure of the human subchondral plate. *Journal of Bone and Joint Surgery* 72: 866–873.
- Coleman MN, Colbert MW. 2007. Technical Note: CT thresholding protocols for taking measurements on three-dimensional models. *American Journal of Physical Anthropology* 133(1): 723-725.
- Cooper DML, Thomas CDL, Clement JG. 2012. Technological Developments in the Analysis of Cortical Bone Histology. In: Crowder C, Stout SD, editors. *Bone Histology: An Anthropological Perspective*. Boca Raton: CRC Press. p 361-375.
- Cooper RR, Milgram JW, Robinson RA. 1966. Morphology of the osteon. An electron microscope study. *Journal of Bone and Joint Surgery* 48: 1239-1271.
- Cowin SC, Van Buskirk WC, Ashman RB. 1987. Properties of Bone. In: Skalak R, Chien S, editors. *Handbook of Bioengineering*. New York: McGraw Hill. p. 2.1-2.25.
- Cresswell EN, Goff MG, Nguyen TM, Lee WX, Hernandez CJ. 2016. Spatial relationships between bone formation and mechanical stress within cancellous bone. *Journal of Biomechanics* 49: 222-228.
- Cui W-Q, Won Y-Y, Baek M-H, Lee D-H, Chung Y-S, Hur J-H, Ma Y-Z. 2008. Age-and region-dependent changes in three dimensional microstructural properties of proximal femoral trabeculae. *Osteoporosis International* 19: 1579-1587.
- Culmann K. 1866. *Die Graphische Statik*. Zurich: Verlag von Meyer & Zeller.

- Cunningham CA, Black SM. 2009. Anticipating bipedalism; trabecular organization in the newborn ilium. *Journal of Anatomy* 214: 817-829.
- Currey JD. 2003. The many adaptations of bone. *Journal of Biomechanics* 36: 1487-1495.
- Currey JD. 2012. The structure and mechanics of bone. *Journal of Materials Science* 47: 41-54.
- Daly RM, Saxon L, Turner CH, Robling AG, Bass SL. 2004. The relationship between muscle size and bone geometry during growth and in response to exercise. *Bone* 34: 281-287.
- Decker RS, Koyama E, Pacifici M. 2014. Genesis and morphogenesis of limb synovial joints and articular cartilage. *Matrix Biology* 39: 5-10.
- Decker RS, Koyama E, Pacifici M. 2015. Articular Cartilage: Structural and Developmental Intricacies and Questions. *Current Osteoporosis Research* 13: 407-414.
- Dempster DW, Raisz LG. 2015. Bone physiology: Bone cells, modeling, and remodeling. In: Holick FM, Nieves WJ, editors. *Nutrition and Bone Health*. New York: Springer. p. 37-56.
- Dewire P, Simkin PA. 1996. Subchondral plate thickness reflects tensile stress in the primate acetabulum. *Journal of Orthopaedic Research* 14(5): 838 -841.
- Digby KH. 1915. The measurement of diaphysial growth in proximal and distal directions. *Journal of Anatomy* 50:187-188.
- Ding M. 2010. Microarchitectural adaptations in aging and osteoarthritic subchondral bone tissues. *Acta Orthopaedica Supplementum No. 340*. Vol. 81.
- Ding M, Dalstra M, Danielsen CC, Kabel J, Hvid I, Linde F. 1997. Age Variations in the Properties of Human Tibial Trabecular Bone. *Journal of Bone and Joint Surgery* 79(B): 995-1002.
- Ding M, Danielsen CC, Hvid I. 2006. Age-related three-dimensional microarchitectural adaptations of subchondral bone tissues in guinea pig primary osteoarthritis. *Calcified Tissue International* 78: 113-22.
- Ding M, Hvid I. 2000. Quantification of Age-Related Changes in the Structure Model Type and Trabecular Thickness of Human Tibial Cancellous Bone. *Bone* 26(3): 291-295.
- Ding M, Odgaard A, Hvid I. 2003. Changes in the three-dimensional microstructure of human tibial cancellous bone in early OA. *Journal of Bone and Joint Surgery* 85(B): 906-912.

- Ding M, Odgaard A, Linde F, Hvid I. 2002. Age-related variations in the microstructure of human tibial cancellous bone. *Journal of Orthopaedic Research* 20: 615-621.
- Donahue SW, Jacobs CR, Donahue HJ. 2001. Flow-induced calcium oscillations in rat osteoblasts are age, loading frequency, and shear stress dependent. *American Journal of Physiology. Cell Physiology* 281(5): 1635-1641.
- Doube M, Klosowski MM, Arganda-Carreras I, Cordelieres FP, Dougherty RP, et al. 2010. BoneJ: Free and extensible bone image analysis in ImageJ. *Bone* 47(6): 1076-1079.
- Dougherty R, Kunzelmann K. 2007. Computing local thickness of 3D structures with ImageJ. *Microscopy and Microanalysis* 13: 1678-1679.
- Dumond H, Presle N, Terlain B, Mainard D, Loeuille D, Netter P, Pottier P. 2003. Evidence for a key role of leptin in osteoarthritis. *Arthritis and Rheumatism* 48: 3118–3129.
- Duncan H, Jundt J, Riddle JM, Pitchford W, Christopherson T. 1987. The tibial subchondral plate. A scanning electron microscope study. *Journal of Bone and Joint Surgery* 69(8) 1212-1220.
- Duren DL, Seselj M, Froehle AW, Nahhas RW, Sherwood RJ. 2013. Skeletal Growth and the Changing Genetic Landscape during Childhood and Adulthood. *American Journal of Physical Anthropology* 150(1): 48-57.
- Eckstein F, Matsuura M, Kuhn V, Priemel M, Muller R, Link TM, Lochmuller E-M. 2007. Sex Differences of Human Trabecular Bone Microstructure in Aging Are Site-Dependent. *Journal of Bone and Mineral Research* 22(6): 817-824.
- Eckstein F, Merz B, Jacobs CR. 2000. Effects of Joint Incongruity on Articular Pressure and Distribution and Subchondral Bone Remodeling. *Advances in anatomy, embryology and cell biology*, Vol. 152. Berlin: Springer.
- Emerson TE, Brown JA. 1992. The Late Prehistory and Protohistory of Illinois. In: Walthall JA, Emerson TE, editors. *Calumet Fleur-De-Lys: Archaeology of Indian and French Contact in the Midcontinent*. Washington D.C.: Smithsonian Institution Press. p. 77-128.
- Engel GM, Staheli LT. 1974. The natural history of torsion and other factors influencing gait in childhood. A study of the angle of gait, tibial torsion, knee angle, hip rotation, and development of the arch in normal children. *Clinical Orthopaedics and Related Research*. 99:12–17.

- Ericksen MF. 1980. Patterns of microscopic bone remodeling in three aboriginal American populations. In: Browman DL, editor. *Early Native Americans: Prehistoric Demography, Economy, and Technology*. The Hague: Mouton. p. 239-270.
- Ericksen MF. 1991. Histologic Estimation of Age at Death Using the Anterior Cortex of the Femur. *American Journal of Physical Anthropology* 84:171-179.
- Esarey D, Conrad LA. 1998. The Bold Counselor Phase of the Central Illinois River Valley: Oneota's Middle Mississippian Margin. *The Wisconsin Archeologist* 79(2): 38-61.
- Esarey D, Santure SK. 1990. The Morton Site Oneota Component and the Bold Counselor Phase. In: Santure S, Harn AD, Esarey D, editors. *Archaeological Investigations at the Morton Village and Norris Farms 36 Cemetery*. Springfield: Illinois State Museum. p. 162-166.
- Fajardo RJ, Muller R, Ketcham RA, Colbert M. 2007. Nonhuman anthropoid primate femoral neck trabecular architecture and its relationship to locomotor mode. *Anatomical Record* 290(4):422-436.
- Forwood MR. 2013. Growing a Healthy Skeleton: The Importance of Mechanical Loading. In: Rosen CJ, editor. *Primer on the Metabolic Bone Diseases and Disorders of Mineral Metabolism*, 8th Edition. Ames: John Wiley & Sons. p. 149-155.
- Fox AJS, Bedi A, Rodeo SA. 2009. The Basic Science of Articular Cartilage: Structure, Composition, and Function. *Sports Health* 1(6): 461-468.
- Francis CC, Werle PP, Behm A. 1939. The appearance of centers of ossification from birth to 5 years. *American Journal of Physical Anthropology* 24:273-299.
- Fratzl P, Weinkamer R. 2007. Nature's hierarchical materials. *Progress in Materials Science* 52:1263-1334.
- Frost HM. 1969. Tetracycline-based histological analysis of bone remodeling. *Calcified Tissue Research* 3:211-237.
- Frost HM. 1986. *Intermediary Organization of the Skeleton*. Boca Raton: CRC Press.
- Frost HM. 1987. Bone "Mass" and the "Mechanostat": A Proposal. *Anatomical Record* 219: 1-9.
- Frost HM. 1992. Perspectives: bone's mechanical usage windows. *Bone and Mineral* 19(3): 257-271.
- Frost HM. 1998. Changing concepts in skeletal physiology: Wolff's law, the mechanostat, and the "Utah paradigm". *American Journal of Human Biology* 11: 437-455.

- Frost HM. 1999. An approach to estimating bone and joint loads and muscle strength in living subjects and skeletal remains. *American Journal of Human Biology* 11(4): 437-455.
- Frost HM. 2000. The Utah paradigm of skeletal physiology. An overview of its insights for bone, cartilage, and collagenous tissue organs. *Journal of Bone and Mineral Metabolism* 18: 305-316.
- Frost HM. 2003. Bone's Mechanostat: A 2003 Update. *Anatomical Record* 275A: 1081-1101.
- Frost HM. 2004. A 2003 Update of Bone Physiology and Wolff's Law for Clinicians. *Angle Orthodontist* 74(1): 3-15.
- Frost HM, Jee WSS. 1994. Perspectives: Applications of a biomechanical model of the endochondral ossification mechanism. *Anatomical Record* 240(4): 447-455.
- Funck-Bretano T, Cohen-Solal M. 2011. Crosstalk between cartilage and bone: where bone cytokines matter. *Cytokine Growth Factor Reviews* 22(2): 91-97.
- Funck-Bretano T, Cohen-Solal M. 2015. Subchondral Bone and Osteoarthritis. *Current Opinion in Rheumatology* 27(4): 420-426.
- Gabel L, Nettlefold, Brasher PM, Moore SA, Ahamed Y, Macdonald HM, McKay HA. 2015. Reexamining the Surfaces of Bone in Boys and Girls during Adolescent Growth: A 12-Year Mixed Longitudinal pQCT Study. *Journal of Bone and Mineral Research* 30(12): 2158-2167.
- Galileo G. 1638. *Discorsi e dimonstrazioni matematiche, intorno a due nuove scienze attentanti alla meccanica ed a muovimenti locali*. Madison: University of Wisconsin Press.
- Garn SM, Frisancho AR, Sandusky ST, McCann MB. 1972. Confirmation of the sex difference in continuing subperiosteal apposition. *American Journal of Physical Anthropology* 36: 377-380.
- Garn SM, Rohnmann CG, Behar M, Viteri F, Guzman MA. 1964a. Compact Bone Deficiency in Protein-Calorie Malnutrition. *Science* 25(145): 1444-1445.
- Garn SM, Rohnmann CG, Nolan Jr P. 1964b. The developmental nature of bone changes during aging. In: Birren JE, editor. *Relation of Development and Aging*. Springfield: Charles C. Thomas. p 41-61.
- Garzon-Alvarado DA, Peinado Cortes LM, Cardenas Sandoval RP. 2010. A mathematical model of epiphyseal development: hypothesis on the cartilage canals

- growth. *Computer Methods in Biomechanics and Biomedical Engineering* 13(6): 765-772.
- Geis JW, Boggess WR. 1968. The Prairie Peninsula: Its Origin and Significance in the Vegetational History of Central Illinois. In: Bergstrom RE, editor. *The Quarternary of Illinois*. Urbana: University of Illinois College of Agriculture. p. 89-95.
- Gibbon GE. 1972. Cultural Dynamics and Development of the Oneota Life-way in Wisconsin. *American Antiquity* 37(2): 166-185.
- Gibbon GE. 1986. The Mississippian Tradition: Oneota Culture. *Wisconsin Archaeologist* 67(3-4): 314-338.
- Gill GG, Abbott LC. 1942. Practical method of predicting the growth of the femur and tibia in the child. *Archives of Surgery* 45:286-315.
- Giustina A, Mazziotti G, Canalis E. 2008. Growth Hormone, Insulin-Like Growth Factors, and the Skeleton. *Endocrine Reviews* 29(5):535-559.
- Glorieux F, Travers R, Taylor A, et al. 2000. Normative data for iliac bone histomorphometry in growing children. *Bone* 26: 103-109.
- Glücksmann, Alfred. 1942. The role of mechanical stresses in born formation in vitro. *Journal of Anatomy* 76: 231-239.
- Goekoop RJ, Kloppenburg M, Kroon HM, et al. 2011. Determinants of absence of osteoarthritis in old age. *Scandinavian Journal of Rheumatology* 40: 68-73.
- Goldman HM, McFarlin SC, Cooper DML, Thomas CDL, and Clement JG. 2009. Ontogenetic Patterning of Cortical Bone Microstructure and Geometry at the Human Mid-Shaft Femur. *Anatomical Record* 292(1):48-64.
- Goldring SR. 2009. Role of bone in osteoarthritis pathogenesis. *Medical Clinics of North America* 93(1): 25-35.
- Goliath JR, Gosman JH, Hubbell ZR, Ryan TM. 2016. Epiphyseal versus Metaphyseal Trabecular Microarchitecture: Regional Ontogenetic Patterns in the Human Proximal Tibia. *Journal of Bone and Mineral Research* 31 (Supp. 1). [Abstract]
- Gomoll AH, Madry H, Knutsen G, et al. 2010. The subchondral bone in articular cartilage repair: current problems in the surgical management. *Knee Surgery, Sports Traumatology, Arthroscopy* 18(4): 434-447.
- Goodman AH, Martin DL. 2002. Reconstructing health profiles from skeletal remains. In: Steckel RH, Rose JC, editors. *The backbone of history: health and nutrition in the Western Hemisphere*. Cambridge: Cambridge University Press. p 61-93.

- Gordon KD, Duck TR, King GJ, Johnson JA. 2003. Mechanical properties of subchondral cancellous bone of the radial head. *Journal of Orthopaedic Trauma* 17: 285-289.
- Gosman JH. 2007. Patterns in ontogeny of human trabecular bone from SunWatch Village in prehistoric Ohio Valley. PhD Dissertation, Ohio State University, Columbus.
- Gosman JH. 2012. Growth and Development: Morphology, Mechanics, and Abnormalities. In: Crowder C, Stout SD, editors. *Bone Histology: An Anthropological Perspective*. Boca Raton: CRC Press. p 23-45.
- Gosman JH, Hubbell ZH, Shaw CN, Ryan TM. 2013. Development of Cortical Bone Geometry in the Human Femoral and Tibial Diaphysis. *Anatomical Record* 296: 774-787.
- Gosman JH, Ketcham RA. 2009. Patterns in Ontogeny of Human Trabecular Bone from SunWatch Village in the Prehistoric Ohio Valley: General Features of Microarchitectural Change. *American Journal of Physical Anthropology* 138: 318–332.
- Gosman JH, Stout SD. 2010. Current concepts in bone biology. In: Larsen CS, editor. *A companion to biological anthropology*. Malden, MA: Blackwell. p 465-484.
- Gosman JH, Stout SD, Larsen CS. 2011. Skeletal biology over the life span: a view from the surfaces. *Yearbook of Physical Anthropology* 54:86–98.
- Gray JP, Wolfe LD. 1996. What accounts for population variation in height? In: Ember CR, Ember M, Peregrine PN, editors. *Research Frontiers in Anthropology*. Upper Saddle River: Prentice Hall. p 103-120.
- Green W. 1995. *Oneota Archaeology: Past, Present, and Future*. Office of the State Archaeologist Report 20. Iowa City: Office of the State Archaeologist.
- Griffin NL. 2008. Bone architecture of the hominin second proximal pedal phalanx: a preliminary investigation. *Journal of Human Evolution* 54(1):162-168.
- Griffin NL, D’Aout K, Ryan TM, Richmond BG, Ketcham RA, Postnov A. 2010. Comparative forefoot trabecular bone architecture in extant hominids. *Journal of Human Evolution* 59: 202-213.
- Gross T, Kivell TL, Skinner MM, et al. 2014. A CT-image-based framework for the holistic analysis of cortical and trabecular bone morphology. *Paleontologia Electronica* 17: A17333.
- Grynopas MD. 2003. The role of bone quality on bone loss and bone fragility. In: Agarwal S, Stout SD, editors. *Bone loss and osteoporosis: An anthropological perspective*. New York: Kluwer Academic. p 33-44.

- Guevara JM, Gutierrez Gomez ML, Barrera La LA, Garzon-Alvarado DA. 2016. Developmental Scenarios of the Epiphysis and Growth Plate Upon Mechanical Loading: A Computational Model. *Journal of Mechanics in Medicine and Biology* 16(2): 1-13.
- Halcrow SE, Tayles N. 2011. The Bioarchaeological Investigation of Children and Childhood. In: Agarwal SC, Glencross BA, editors. *Social Bioarchaeology*. Hoboken: Blackwell Publishing p 333-359.
- Hamann N, Zaucke F, Dayakli M, et al. 2013. Growth-related structural, biochemical, and mechanical properties of the functional bone-cartilage unit. *Journal of Anatomy* 222: 248-259.
- Hamann N, Brüggemann, Niehoff A. 2014. Topographical variations in articular cartilage and subchondral bone of the normal rat knee are age-related. *Annals of Anatomy* 196(5): 278-285.
- Hamilton HW, Jamieson J. 2012. The classification of degenerative hip disease. *Journal of Bone and Joint Surgery* 94: 1193-1201.
- Hamrick MW. 1999. Development of epiphyseal structure and function in *Didelphis virginiana* (Marsupialia, Didelphidae). *Journal of Morphology* 239: 283-296.
- Han S, Ge S, Liu H, Liu R. 2013. Alterations in Three-dimensional Knee Kinematics and Kinetics during Neutral, Squeeze, and Outward Squat. *Journal of Human Kinetics* 39: 59-66.
- Hansman CF. 1962. Appearance and fusion of ossification centers in the human skeleton. *American Journal of Roentgenology* 88:476-482.
- Hara T, Tanck E, Homminga J, Huiskes R. 2002. The influence of microcomputed tomography threshold variations on the assessment of structural and mechanical trabecular bone properties. *Bone* 31(1): 107-109.
- Harada Y, Wevers HW, Cooke TD. 1988. Distribution of bone strength in the proximal tibia. *Journal of Anthropology* 3(2):167-175.
- Harrison KD, Cooper DML. 2015. Modalities for visualization of cortical bone remodeling: the past, present, and future. *Frontiers in Endocrinology* 6:122.
- Hashimoto S, Ochs RL, Komiya S, Lotz M. 1998. Linkage of chondrocyte apoptosis and cartilage degradation in human osteoarthritis. *Arthritis and Rheumatology* 41: 1632-1638.
- Hayes DW, Brower RL, John KJ. 2001. Articular Cartilage: Anatomy, Injury, and Repair. *Clinics in Podiatric Medicine and Surgery* 18(1): 35-53.

- Heath CH, Staheli LT. 1993. Normal limits of knee angle in white children—genu varum and genu valgum. *Journal of Pediatric Orthopaedics* 13(2):259–262.
- Henrotin Y, Pesesse L, Sanchez C. 2012. Subchondral bone and osteoarthritis: biological and cellular aspects. *Osteoporosis International* 23(Supplemental 8): S847-S851.
- Hert J. 1992. A new explanation of the cancellous bone architecture. *Functional and Developmental Morphology* 2: 17-24.
- Hildebrand T, Laib A, Müller R, Dequeker J, Rüeegsegger P. 1999. Direct three-dimensional morphometric analysis of human cancellous bone: microstructural data from spine, femur, iliac crest, and calcaneus. *Journal of Bone and Mineral Research* 14(7): 1167-1174.
- Hildebrand T, Rüeegsegger P. 1997a. A new method for the model-independent assessment of thickness in three-dimensional images. *Journal of Microscopy* 185:67-75.
- Hildebrand T, Rüeegsegger P. 1997b. Quantification of bone microarchitecture with the structure model index. *Computer Methods in Biomechanics and Biomedical Engineering* 1: 15-23.
- Hino K, Saito A, Kido M, Kanemoto S, Asada R, Takai T, Cui M, Cui X, Imaizumi K. 2014. Master Regulator for Chondrogenesis, Sox9, Regulates Transcriptional Activation of the Endoplasmic Reticulum Stress Transducer BBF2H7/CREB3L2 in Chondrocytes. *Journal of Biological Chemistry* 289(20):13810-13820.
- Hoemann CD, Lafantaisie-Favreau C-H, Lascau-Coman V, Chen G, Guzman-Morales J. 2012. The Cartilage-Bone Interface. *Journal of Knee Surgery* 25(2): 85-97.
- Hoffman DF. 1993. Arthritis and Exercise. *Primary Care* 20: 895-910.
- Holland JC, Brennan O, Kennedy OD, Mahony NJ, Rackard S, O'Brien FJ, Lee TC. 2013. Examination of osteoarthritis and subchondral bone alterations within the stifle joint of an ovariectomised ovine model. *Journal of Anatomy* 222: 588-597.
- Holland JC, Brennan O, Kennedy OD, Rackard SM, O'Brien FJ, Lee TC. 2011. Subchondral trabecular structural changes in the proximal tibia in an ovine model of increased bone turnover. *Journal of Anatomy* 218: 619-624.
- Hollinger HE. 1995. Residence Patterns and Oneota Culture Dynamics. In: Green, W, editor. *Oneota Archaeology: Past, Present, and Future*. Office of the State Archaeologist Report 20. Iowa City: Office of the State Archaeologist. p. 141-174.
- Holltrop ME. 1975. The ultrastructure of bone. *Annals of Clinical and Laboratory Science* 5(4): 264-271.

- Horton, WE. 1993. Morphology of connective tissue: cartilage. In: Royce PM, Steinmanns B, editors. *Connective Tissue and Its Heritable Disorders*. New York: Wiley-Liss, Inc. p 73–84.
- Horton WE, Feng L, Adams C. 1998. Chondrocyte Apoptosis in Development, Aging and Disease. *Matrix Biology* 17:107-115.
- Hounsfield GN. 1973. Computerized Traverse Axial Scanning (Tomography): Part 1. Description of System. *British Journal of Radiology* 46(552):1016-1022.
- Hubbell ZR. 2016. Developmental Mechanobiology of the Metaphyseal Cortical-Trabecular Interface in the Human Proximal Tibia and Proximal Humerus. PhD Dissertation: The Ohio State University.
- Huiskes R, Ruimerman R, van Lenthe GH, Janssen JD. 2000. Effects of mechanical forces on the maintenance and adaptation of form in trabecular bone. *Nature* 405:704-706.
- Hunter DJ, Spector TD. 2003. The role of bone metabolism in osteoarthritis. *Current Rheumatology Reports* 5: 15-19.
- Hunter DJ, Niu J, Zhang Y, Nevitt MC, Xu L, Lui LY, Yu W, Aliabadi P, Buchanan TS, Felson DT. 2005. Knee height, knee pain, and knee osteoarthritis. *Arthritis and Rheumatism* 52: 1418–1423.
- Hunziker EB, Schenk RK, Cruz-Orive, LM. 1987. Quantitation of chondrocyte performance in growth plate cartilage during longitudinal bone growth. *Journal of Bone and Joint Surgery* 69(A):162-173.
- Hurwitz DE, Sumner DR, Andriacchi TP, Sugar DA. 1998. Dynamic knee loads during gait predict proximal tibial bone distribution. *Journal of Biomechanics* 31 (5): 423–30.
- Huss-Ashmore R, Goodman A, Armelagos G. 1982. Nutritional inference from paleopathology. In: Schiffer B, editor. *Advances in Archaeological Method and Theory*. New York: Academic Press, p 395–474.
- Hvid I. 1988. Trabecular Bone Strength at the Knee. *Clinical Orthopaedics and Related Research* 227:210-221.
- Hvid I, Hansen SL. 1985. Trabecular bone strength patterns at the proximal tibial epiphysis. *Journal of Orthopaedic Research* 3(4):464-472.
- Hvid I, Jensen J, Nielsen S. 1985. Contribution of the cortex to epiphyseal strength. The upper tibia studied in cadavers. *Acta Orthopaedica Scandinavica* 56(3):256-259.

- Imhof H, Sulzbacher I, Grampp S, Czerny C, Youssefzadeh S, Kainberger F. 2000. Subchondral bone and cartilage disease: a rediscovered functional unit. *Investigative Radiology* 35: 581–588.
- Intema F, Sniekers YH, Weinans H, Vianen ME, Yocum SA, Zuurmond AM, DeGroot J, Lafeber FP, Mastbergen SC. 2010. Similarities and discrepancies in subchondral bone structure in two differently induced canine models of osteoarthritis. *Journal of Bone Mineral Research* 25 (7): 1650-1657.
- Isaksson H, Tolvanen V, Finnila MAJ, Iivarinen J, Tuukkanen J, Seppanen K et al. 2009. Physical Exercise Improves Properties of Bone and Its Collagen Network in Growing and Maturing Mice. *Calcified Tissue International* 85: 247–256.
- Jackes M. 1993. On Paradox and Osteology. *Current Anthropology* 34(4): 434-439.
- Jacobs CR, Temiyasathit S, Castillo AB. 2010. Osteocyte Mechanobiology and Pericellular Mechanics. *Annual Review of Biomedical Engineering* 12: 369-400.
- Javaid MK, Eriksson JG, Kajantie E, Forsén T, Osmond C, Barker DJ, et al. 2011. Growth in childhood predicts hip fracture risk in later life. *Osteoporosis International* 22:69–73.
- Jiao K, Dai J, Wang M-Q, Niu L-N, Yu S-B, Liu X-D. 2010. Age and sex-related changes of mandibular condylar cartilage and subchondral bone: A histomorphometric and micro-CT study in rats. *Archives of Oral Biology* 55: 155-163.
- Johnston FE. 1962. Growth of the Long Bones of Infants and Young Children at Indian Knoll. *American Journal of Physical Anthropology* 20: 249-254.
- Judex S, Carlson KJ. 2009. Is bone's response to mechanical signals dominated by gravitational loading? *Medicine and Science in Sports and Exercise* 41: 2037-2043.
- Jurmain RD. 1977a. Stress and the Etiology of Osteoarthritis. *American Journal of Physical Anthropology* 46: 353-366.
- Jurmain RD. 1977b. Paleoepidemiology of Degenerative Knee Disease. *Medical Anthropology* 1: 1-14.
- Jurmain RD. 1999. *Stories from the Skeleton: Behavioral Reconstructions in Human Osteology*. Vol. 1, Interpreting the Remains of the Past. Toronto and Amsterdam: Gordon and Beach.
- Kamibayashi L, Wyss UP, Cooke TD, Zee B. 1995. Trabecular microstructure in the medial condyle of the proximal tibia of patients with knee osteoarthritis. *Bone* 17:27–35.

- Keaveny TM, Yeh OC. 2002. Architecture and trabecular bone toward an improved understanding of the biomechanical effects of age, sex and osteoporosis. *Journal of Musculoskeletal and Neuronal Interactions* 2: 205-208.
- Kennedy OD, Herman BC, Laudier DM, Majeska RJ, Sun HB, Schaffler MB. 2012. Activation of resorption and active pro-osteoclastogenic signaling by distinct osteocyte populations. *Bone* 50(5): 1115-1122.
- Ketcham RA, Carlson WD. 2001. Acquisition, optimization and interpretation of x-ray computed tomography: Applications to the geosciences. *Computers and Geosciences* 27: 381-400.
- Ketcham RA, Hanna RD. 2014. Beam hardening correction for X-ray computed tomography of heterogeneous natural materials. *Computers and Geosciences* 67: 49-61.
- Kim D-G, Christopherson GT, Dong XN, Fyhrie DP, Yeni YN. 2004. The effect of microcomputed tomography scanning and reconstruction voxel size on the accuracy of stereological measurements in human cancellous bone. *Bone* 35(6): 1375-1382.
- Kirkwood TB. 2005. Understanding the odd science of aging. *Cell* 120: 437-447.
- Kivell TL, Skinner MM, Lazenby R, Hublin J-J. 2011. Methodological considerations for analyzing trabecular architecture: an example from the primate hand. *Journal of Anatomy* 218(2): 209-225.
- Kivell TL. 2016. A review of trabecular bone functional adaptation: what have we learned from trabecular analyses in extant hominoids and what can we apply to fossils. *Journal of Anatomy* 228: 569-594.
- Klaus HD, Larsen CS, Tam ME. 2009. Economic Intensification and DJD: Life and Labor on the Postcontact North Coast of Peru. *American Journal of Physical Anthropology* 139: 204-221.
- Kneissel M, Roschger P, Steiner W, Schamall D, Kalchhauser G, Boyde A, Teschler-Nicola M. 1997. Cancellous bone structure in the growing and aging spine in a historic Nubian population. *Calcified Tissue International* 61(2): 95-100.
- Knopp E, Troiano N, Bouxsein M, Sun BH, Lostritto K, Gundberg, C, Dziura J, Insogna K. 2005. The effect of aging on the skeletal response to intermittent treatment with parathyroid hormone. *Endocrinology* 146: 1983-1990.
- Koch JC. 1917. The laws of bone architecture. *American Journal of Anatomy* 21:177-293.
- Kohrt WM. 2001. Aging and the osteogenic response to mechanical loading. *International Journal of Sport Nutrition and Exercise Metabolism* 11: S137-142.

- Kontulainen SA, Hughes JM, Macdonald HM, Johnston JD. 2007. The biomechanical basis of bone strength development during growth. In: Daly RM, Petit MA, editors. *Optimizing bone mass and strength*. Basel: Karger. pp. 13–32.
- Koyama E, Shibukawa Y, Nagayama M, et al. 2008. A distinct cohort of progenitor cells participates in synovial joint and articular cartilage formation during mouse limb skeletogenesis. *Developmental Biology* 316(1):62–73.
- Kraan PM, Berg WB. 2012. Chondrocyte hypertrophy and osteoarthritis: role in initiation and progression of cartilage degeneration. *Osteoarthritis and Cartilage* 20: 223-232.
- Kreisa PP. 1993. Oneota Burial Patterns in Eastern Wisconsin. *Midcontinental Journal of Archaeology* 18(1): 35-60.
- Krogman WM. 1962. *The Human Skeleton in Forensic Medicine*. Springfield: C.C. Thomas.
- Kronenberg HM. 2006. PTHrP and Skeletal Development. *Annals of the New York Academy of Sciences* 1068: 1-13.
- Kuhns LR, Finnstrom O. 1976. New standards of ossification of the newborn. *Radiology* 119:655-660.
- Kumar V, Abbas AK, Fausto N. 2005. *Robbins and Cotran's Pathological Basis of Disease*, 7th ed. W.B. Saunders Co.
- Lambers FM, Koch K, Kuhn G, Ruffoni D, Weigt C, Schulte FA, Müller R. 2013. Trabecular bone adapts to long-term cyclic loading by increasing stiffness and normalization of dynamic morphometric rates. *Bone* 55: 325-334.
- Lane NE, Beat M, Bjorkengren A, et al. 1993. The Risk of Osteoarthritis with Running and Aging: A 5-Year Longitudinal Study. *Journal of Rheumatology* 20: 462-468.
- Lanyon LE. 1992. Control of bone architecture by functional load bearing. *Journal of Bone and Mineral Research* 7(S2): S369-S375.
- Lanyon LE, Rubin CT. 1984. Static vs dynamic loads as an influence on bone remodeling. *Journal of Biomechanics* 17(12): 897-905.
- Larsen CS, Ruff CB, and Kelly RL. 1995. Structural analysis of the Stillwater postcranial human remains: behavioral implications of articular joint pathology and long bone diaphyseal morphology. In: Larsen CS, and Kelly RL, editors. *Bioarchaeology of the Stillwater Marsh: prehistoric human adaptation in the Western Great Basin*. New York: Anthropological Papers of the American Museum of Natural History No. 77. p 107-133.
- Larsen CS. 2015. *Bioarchaeology: interpreting behavior from the human skeleton* 2nd edition. Cambridge, UK: Cambridge University Press.

- Lajeunesse D. 2002. Altered subchondral osteoblast cellular metabolism in osteoarthritis: cytokines, eicosanoids, and growth factors. *Journal of Musculoskeletal and Neuronal Interactions* 2:504–506.
- Layton MW, Goldstein SA, Goulet RW, et al. 1988. Examination of subchondral bone architecture in experimental osteoarthritis by microscopic computed axial tomography. *Arthritis and Rheumatology* 31: 1400–1405.
- Lazenby RA, Skinner MM, Kivell TL, Hublin J-J. 2011. Scaling VOI Size in 3D μ CT Studies of Trabecular Bone: A Test of the Over-Sampling Hypothesis. *American Journal of Physical Anthropology* 144:196-203.
- Lereim P, Goldie I, Dahlberg E. 1974. Hardness of the subchondral bone of the tibial condyles in the normal state and in osteoarthritis and rheumatoid arthritis. *Acta Orthopaedica* 45:614–627.
- Leung VYL, Gao B, Leung KKH, Melhado IG, Wynn SL, Au TYK, et al. 2011. SOX9 Governs Differentiation Stage-Specific Gene Expression in Growth Plate Chondrocytes via Direct Concomitant Transactivation and Repression. *PLoS Genetics* 7(11): e1002356.
- Li G, Yin J, Gao J, Cheng TS, Pavlos NJ, Zhang C, Zheng MH. 2013. Subchondral bone in osteoarthritis: insight into risk factors and microstructural changes. *Arthritis Research and Therapy* 15(6): 223.
- Lieberman DE. 1996. How and why humans grow thin skulls: Experimental evidence for systemic cortical robusticity. *American Journal of Physical Anthropology* 101: 217-236.
- Lieto JR, O’Gorman JA. 2014. A Preliminary Analysis of Oneota and Mississippian Serving Vessels at the Morton Village Site, West-Central Illinois. *North American Archaeology* 35(3): 243-255.
- Liu P, Ping Y, Meng M, Zhang D, Liu C, Zaidl S, Gao S, et al. 2016. Anabolic actions of Notch on mature bone. *Proceedings of the National Academy of Sciences* 113(15): E2152-E2161.
- Long F, Ornitz DM. 2013. Development of the Endochondral Skeleton. *Cold Springs Harbor Perspectives in Biology* 5:a008334.
- Lories RJ, Luyten FP. 2011. The bone-cartilage unit in osteoarthritis. *Rheumatology* 7: 43-49.
- Lotz JC, Gerhart TN, Hayes WC. 1991. Mechanical properties of metaphyseal bone in the proximal femur. *Journal of Biomechanics* 24: 317–329.
- Lotz M, Loeser RF. 2012. Effects of aging on articular cartilage homeostasis. *Bone* 51: 241-248.

- Lovejoy CO, Russell KF, Harrison ML. 1990. Long bone growth velocity in the Libben population. *American Journal of Human Biology* 2: 533–541.
- Lyons TJ, Stoddart RW, McClure SF, McClure J. 2005. The tidemark of the chondro-osseous junction of the normal human knee joint. *Journal of Molecular Histology* 36: 207-215.
- Lyons TJ, McClure SF, Stoddart RW, McClure J. 2006. The normal human chondro-osseous junctional region: evidence for contact of uncalcified cartilage with subchondral bone and marrow spaces. *BMC Musculoskeletal Disorders* 7:52.
- Mackie EJ, Tatarczuch L, Mirams M. 2013. The skeleton: a multi-functional complex organ. The growth plate chondrocyte and endochondral ossification. *Journal of Endocrinology* 211:109-121.
- MacLatchy L, Müller R. 2002. A comparison of the femoral head and neck trabecular architecture of Galago and Perodicticus using micro-computed tomography (μ CT). *Journal of Human Evolution* 43(1):89-105.
- Madry H, van Dijk CN, Müller-Gerbl M. 2010. The basic science of the subchondral bone. *Knee Surgery, Sports Traumatology, Arthroscopy* 18: 419-433.
- Maga M, Kappelman J, Ryan TM, Ketcham RA. 2006. Preliminary observations on the calcaneal trabecular microarchitecture of extant large-bodied hominoids. *American Journal of Physical Anthropology* 129(3):410-417.
- Mahjoub M, Berenbaum F, Houard X. 2012. Why subchondral bone in osteoarthritis? The importance of the cartilage bone interface in osteoarthritis. *Osteoporosis International* 23 (Supplemental 8): S841-S846.
- Martel-Pelletier J, Lajeunesse, Reboul P, Pelletier J-P. 2007. The Role of Subchondral Bone in Osteoarthritis. In: Sherma L, Berenbaum F, editors. *Osteoarthritis: A Companion to Rheumatology*. 1st edition. Philadelphia: Mosby.
- Martin RB. 2007. The importance of mechanical loading in bone biology and medicine. *Journal of Musculoskeletal and Neuronal Interactions* 7(1): 48-53.
- Martin RB, Burr DB, Sharkey NA, Fyhrie DP. 2015. *Skeletal Tissue Mechanics*. 2nd edition. New York: Springer.
- Mankin HJ. 1982. The response of articular cartilage to mechanical injury. *Journal of Bone and Joint Surgery* 64: 460-466.
- Mays S. 2000. Linear and appositional long bone growth in earlier human populations: a case study from medieval England. In: Hoppa RD, Fitzgerald CM. editors. *Human*

Growth in the Past: Studies from Bones and Teeth. Cambridge: Cambridge University Press, p 290–312.

Mazurier A, Nakatsukasa M, Macchiarelli R. 2010. The inner structural variation of the primate tibial plateau characterized by high-resolution microtomography. Implications for the reconstruction of fossil locomotor behaviours. *Comptes Rendus Palevol* 9(6-7): 349-359.

McCammon RW. 1970. *Human Growth and Development*. Springfield: C. C. Thomas.

McKern TW, Stewart TD. 1957. Skeletal age changes in young American males, analyzed from the standpoint of age identification. Headquarters Quartermaster Research and Development Command, Technical Report EP-45. Natick, MA.

McKinley TO, Bay BK. 2001. Trabecular bone strain changes associated with cartilage defects in the proximal and distal tibia. *Journal of Orthopaedic Research* 19: 906-913.

Meulenbelt I. 2012. Osteoarthritis year 2011 in review: genetics. *Osteoarthritis and Cartilage* 20: 218-222.

Micheli LJ, Klein JD. 1991. Sports Injuries in Children and Adolescents. *British Journal of Sports Medicine* 25: 6-9.

Milner GR, Anderson E, Smith VG. 1991a. Warfare in Late Prehistoric West-Central Illinois. *American Antiquity* 56(4): 581-603.

Milner GR, Emerson TE, Mehrer MW, Williams JA, Esarey D. 1984. Mississippian and Oneota Period. In: Bareis CJ, Porter JW, editors. *American Bottom Archaeology*. University of Illinois Press: Urbana. p. 158-186.

Milner GR, Humpf DA, Harpending HC. 1989. Pattern matching of age-at-death distributions in paleodemographic analysis. *American Journal of Physical Anthropology* 80: 49-58.

Milner GR, Smith VG. 1990. Oneota Human Skeletal Remains. In: Santure S, Harn AD, Esarey D, editors. *Archaeological Investigations at the Morton Village and Norris Farms 36 Cemetery*. Springfield: Illinois State Museum. p. 111-148.

Milner GR, Smith VG, Anderson E. 1991b. Conflict, Mortality and Community Health in an Illinois Oneota Population. In: Gregg SA, editor. *Between Bands and Sands*. Center for Archaeological Investigations, Occasional Paper No. 9: South Illinois University. p. 245-264.

Milz S, Putz R. 1994. Quantitative morphology of the subchondral plate of the tibial plateau. *Journal of Anatomy* 185:103–110.

- Mirtz TA, Chandler JP, Eysers CM. 2011. The Effects of Physical Activity on the Epiphyseal Growth Plates: A Review of the Literature on Normal Physiology and Clinical Implications. *Journal of Clinical Medicine Research* 3(1): 1-7.
- Mitchell NS, Cruess RL. 1977. Classification of degenerative arthritis. *Canadian Medical Association Journal* 117: 763–765.
- Mitra E, Rubin C, Qin Y-X. 2005. Interrelationships of trabecular mechanical and microstructural properties in sheep trabecular bone. *Journal of Biomechanics* 38:1229-1237.
- Moore KL, Agur AMR, Dalley AF. 2011. Chapter 5: Lower Limb. *Essential Clinical Anatomy*. 4th edition. Baltimore: Lippincott Williams & Wilkins. p 316-404.
- Moorrees CFA, Fanning EA, Hunt EE. 1963a. Formation and resorption of three deciduous teeth in children. *American Journal of Physical Anthropology* 21: 205-213.
- Moorrees CFA, Fanning EA, Hunt EE. 1963b. Age variation of formation stages for ten permanent teeth. *Journal of Dental Research* 42: 1490-1502.
- Morgan EF, Bayraktar HH, Keaveny TM. 2003. Trabecular bone modulus-density relationships depend on anatomic site. *Journal of Biomechanics* 36: 897-904.
- Morse A, McDonald MM, Kelly NH, Melville KM, Schindeler A, Kramer I, et al. 2014. Mechanical Load Increases in Bone Formation via a Sclerostin-Independent Pathway. *Journal of Bone and Mineral Research* 29(11): 2456-2467.
- Morse DF, Morse PA. 1983. *Archaeology of the Central Mississippi Valley*. Academic Press: New York.
- Mow VC, Ateshian GA, Ratcliffe A. 1992. Anatomic form and biomechanical properties of articular cartilage of the knee joint. In: Finerman GAM, Noyes FR, editors. *Biology and Biomechanics of the Traumatized Synovial Joint: The Knee as a Model*. 2nd ed. Rosemont, IL: American Academy of Orthopaedic Surgeons. p 55-81.
- Müller-Gerbl M. 1998. The Subchondral Bone Plate. *Advances in Anatomy Embryology and Cell Biology* 141: III-XI. Berlin: Springer.
- Müller C, Khabut A, Dudhia J, Reinholt FP, Aspberg A, Heinegard D, Onnerfjord P. 2014. Quantitative proteomics at different depths in human articular cartilage reveals unique patterns of protein distribution. *Matrix Biology* 40: 34-45.
- Nikander R, Sievanen H, Heinonen A, Daly RM, Uusi-Rasi K, Kannus P. 2010. Targeted exercise against osteoporosis: A systematic review and meta-analysis for optimizing bone strength throughout life. *BMC Medicine* 8: 47.

- Nobel J, Alexander K. 1985. Studies of tibial subchondral bone density and its significance. *Journal of Bone and Joint Surgery*. 67(2): 295-302.
- Odgaard A. 1997. Three-dimensional methods for quantification of cancellous bone architecture. *Bone* 20: 315–28.
- Odgaard A, Gundersen HJ. 1993. Quantification of connectivity in cancellous bone, with special emphasis on 3-D reconstructions. *Bone* 14: 173–82.
- Odgaard A, Pedersen CM, Bentzen SM, Jorgensen J, Hvid I. 1989. Density changes at the proximal tibia after meniscectomy. *Journal of Orthopaedic Research* 7:744–753.
- Oginni LM, Badru OS, Sharp CA, Davie MW, Worsfold M. 2004. Knee angles and rickets in Nigerian children. *Journal of Pediatric Orthopaedics* 24(4): 403-407.
- Oliver H, Jameson KA, Sayer AA, Cooper C, Dennison EM. 2007. Growth in early life predicts bone strength in late adulthood: The Hertfordshire Cohort Study. *Bone* 41: 400–405.
- Oliveria SA, Felson DT, Reed JI, et al. 1995. Incidence of symptomatic hand, hip, and knee osteoarthritis among patients in a health maintenance organization. *Arthritis and Rheumatology* 38: 1134-1141.
- O’Rahilly R, Gray DJ, Gardner E. 1957. Chondrification in the hands and feet of staged human embryos. *Contributions to Embryology* 36:183-192.
- Ortner DJ. 2003. Identification of pathological conditions in human skeletal remains. 2nd ed. Amsterdam: Academic Press.
- Otsuki S, Taniguchi N, Grogan SP, D’Lima D, et al. 2008. Expression of novel extracellular sulfatases Sulf-1 and Sulf-2 in normal and osteoarthritic articular cartilage. *Arthritis Research and Therapy* 10(3): R61.
- Overstreet DF. 1981. Investigations at the Pipe Site (47Fd10) and Some Perspectives on Eastern Wisconsin in Oneota Prehistory. *The Wisconsin Archeologist* 62(4): 365-525.
- Overstreet DF. 1995. The Eastern Wisconsin Oneota Regional Continuity. In: Green, W. editor. *Oneota Archaeology: Past, Present, and Future*. Office of the State Archaeologist Report 20. Iowa City: Office of the State Archaeologist. p. 33-64.
- Pacifici M, Koyama E, Shibukawa Y, Wu C, Tamamura Y, et al. 2006. Cellular and Molecular Mechanisms of Synovial Joint and Articular Cartilage Formation. *Annals of the New York Academy of Sciences* 1968: 74-86.
- Paine RR, Brenton BP. 2006. Dietary Health Does Affect Histological Age Assessment: An Evaluation of the Stout and Paine (1992) Age Estimation Equation Using Secondary Osteons from the Rib. *Journal of Forensic Sciences* 51: 489-492.

- Pan J, Wang B, Li W, et al. 2012. Elevated cross-talk between subchondral bone and cartilage in osteoarthritic joints. *Bone* 51: 212-217.
- Pan J, Zhou X, Li W, Novotny JE, Doty SB, Wang L. 2009. In Situ Measurement of Transport between Subchondral Bone and Articular Cartilage. *Journal of Orthopaedic Research* 27(10): 1347-1352.
- Panush RS, Lane NE. 1994. Exercise and the Musculoskeletal System. *Bailliere's Clinical Rheumatology* 8: 79-102.
- Parfitt AM. 1983. The Physiological and Clinical Significance of Bone Histomorphometric Data. In: Recker RR, editor. *Bone Histomorphometry: Techniques and Interpretations*. Boca Raton: CRC Press.
- Parfitt AM. 1984. Age-related structural changes in trabecular and cortical bone: cellular mechanisms and biomechanical consequences. *Calcified Tissue International* 36: S123-128.
- Parfitt AM. 1990. Bone-forming cells in clinical conditions. In: Hall BK, editor. *Bone: A Treatise*, Vol. 1. Caldwell: Telford Press. p 351-429.
- Parfitt AM. 1994. Osteonal and hemi-osteonal remodeling: The spatial and temporal framework for signal traffic in adult human bone. *Journal of Cell Biochemistry* 55: 273-286.
- Parfitt AM. 2002. Targeted and Nontargeted Bone Remodeling: Relationship to Basic Multicellular Unit Organization and Progression. *Bone* 30(1): 5-7.
- Particelli F, Mecozzi L, Beraudi A, Montesi M, Baruffaldi F, Viceconti M. 2012. A comparison between micro-CT and histology for the evaluation of cortical bone: effect of polymethylmethacrylate embedding on structural parameters. *Journal of Microscopy* 245: 302-310.
- Paterson RS. 1929. A radiological investigation of the epiphyses of the long bones. *Journal of Anatomy* 64:28-46.
- Pearson OM, Buikstra JE. 2006. Behavior and the Bones. In: Buikstra JE, Beck LA, editors. *Bioarchaeology: The Contextual Analysis of Human Remains*. Oxford: Elsevier. p 207-227.
- Pearson OM, and Lieberman DE. 2004. The aging of Wolff's "Law": Ontogeny and responses to mechanical loading in cortical bone. *Yearbook of Physical Anthropology* 47:63-99.

- Peinado Cortest LM, Vanegas Acosta JC, Garzon Alvarado DA. 2011. A mechanobiological model of epiphysis structures formation. *Journal of Theoretical Biology* 287: 13-25.
- Peyrin F. 2011. Evaluation of bone scaffolds by micro-CT. *Osteoporosis International* 22: 2043-2048.
- Plochocki JH, Organ J. 2003. The effects of differential mechanical loading on articular surface area in miniature swine. *American Journal of Physical Anthropology Supplement* 36:169 [abstract].
- Plochocki JH, Ward CV, Smth DE. 2009. Evaluation of the chondral modeling theory using fe-simulation and numeric shape optimization. *Journal of Anatomy* 214(5): 768-777.
- Pontzer H, Lieberman DE, Momin E, Devlin MJ, et al. 2006. Trabecular Bone in the Bird Knee Responds with High Sensitivity to Changes in Load Orientation. *Journal of Experimental Biology* 209: 57-65.
- Pyle SI, Hoerr NL. 1955. *Radiographic Atlas of Skeletal Development of the Knee*. Springfield: C.C. Thomas.
- Radin EL. 1982. Mechanical factors in the causation of osteoarthritis. *Rheumatology* 7:46-52.
- Radin EL, Orr RB, Kelman JL, Paul IL, Rose RM. 1982. Effect of prolonged walking on concrete on the knees of sheep. *Journal of Biomechanics* 15:487-92.
- Radin EL, Rose RM. 1986. Role of subchondral bone in the initiation and progression of cartilage damage. *Clinical Orthopaedics and Related Research* 213: 34-40.
- Raichlen DA, Gordon AD, Foster AD, Webber JT, Sukhdeo SM, Scott RS, Gosman JH, Ryan TM. 2015. An ontogenetic framework linking locomotion and trabecular bone architecture with applications for reconstructing hominin lifehistory. *Journal of Human Evolution* 81: 1-12.
- Rauch F. 2012. The dynamics of bone structure development during pubertal growth. *Journal of Musculoskeletal and Neuronal Interactions* 12(1): 1-6.
- Reisinger AG, Pahr DH, Zysset PK. 2011. Elastic anisotropy of bone lamellae as a function of fibril orientation pattern. *Biomechanics and Modeling in Mechanobiology* 10: 67-77.
- Richmond BG, Nakatsukasa M, Ketcham R, Hirakawa T. 2004. Trabecular bone structure in human and chimpanzee knee joints. *American Journal of Physical Anthropology* S38:167.

- Robbins G, Sciulli PW, Blatt SH. 2010. Estimating body mass in subadult human skeletons. *American Journal of Physical Anthropology* 143(1):146-150.
- Robbins Schug G, Gupta S, Cowgill LW, Sciulli PW, Blatt SH. 2013. Panel regression formulas for estimating stature and body mass from immature human skeletons: a statistical approach without reference to specific age estimates. *Journal of Archaeological Science* 40(7): 3076-3086.
- Robling AG. 2009. Is bone's response to mechanical signals dominated by muscle forces? *Medicine and Science in Sports and Exercise* 41: 2044-2049.
- Robling AG, Castillo AB, Turner CH. 2006. Biomechanical and Molecular Regulation of Bone Remodeling. *Annual Reviews in Biomedical Engineering* 8: 455-498.
- Robling AG, and Stout SD. 2003. Histomorphology, geometry, and mechanical loading in past populations. In: Agarwal SC, and Stout SD, editors. *Bone loss and osteoporosis: An anthropological perspective*. New York: Kluwer Academic/Plenum Publishers. p 189-205.
- Robling AG, Stout SD. 2008. Histomorphometry of human cortical bone: Applications to age estimation. In: Katzenberg MA, Saunders SR, editors. *Biological anthropology of the human skeleton*. New York: Wiley Liss. p 149-182.
- Robling AG, Turner CH. 2009. Mechanical Signaling for Bone Modeling and Remodeling. *Critical Reviews in Eukaryotic Gene Expression* 19(4): 319-338.
- Roksandic M, Armstrong SD. 2011. Using the life history model to set the stage(s) of growth and senescence in bioarchaeology and paleodemography. *American Journal of Physical Anthropology* 145(3): 337-347.
- Rountree RB, Schoor M, Chen H, et al. 2004. BMP receptor signaling is required for postnatal maintenance of articular cartilage. *PLoS Biology* 2(11): e355.
- Roux W. 1881. *Der zuchtende Kampf der Teile, oder die Teilauslese' im Organismus (Theorie der 'funktionellen Anpassung')*. Leipzig: Wilhelm Engelmann.
- Rueckel J, Stockmar M, Pfeiffer F, Herzen J. 2014. Spatial resolution characterization of a X-ray microCT system. *Applied Radiation and Isotopes* 94: 230-234.
- Ruff CB. 2000a. Body size, body shape, and long bone strength in modern humans. *Journal of Human Evolution* 38: 269-290.
- Ruff C. 2000b. Biomechanical analyses of archaeological human skeletons. In: Katzenberg MA, Saunders SR, editors. *Biological Anthropology of the Human Skeleton*. New York: Wiley-Liss, p 71-102.

- Ruff CB. 2005. Mechanical determinants of bone form: Insights from skeletal remains. *Journal of Musculoskeletal Neuronal Interactions* 5(3): 202-212.
- Ruff CB. 2007. Body size prediction from juvenile skeletal remains. *American Physical of Physical Anthropology* 133(1): 698-716.
- Ruff CB, Holt B, Trinkaus E. 2006. Who's afraid of the big bad Wolff?: "Wolff's law" and bone functional adaptation. *American Journal of Physical Anthropology* 129: 484-498.
- Ruff CB, Scott WW, Liu AY. 1991. Articular and Diaphyseal Remodeling of the Proximal Femur with Changes in Body Mass in Adults, *American Journal of Physical Anthropology* 86: 397- 413.
- Ruff CB, Trinkaus E, Holliday TW. 1997. Body mass and encephalization in Pleistocene Homo. *Nature* 387: 173-176.
- Ryan TM, Ketcham RA. 2002. The three-dimensional structure of trabecular bone in the femoral head of strepsirrhine primates. *Journal of Human Evolution* 43: 1-26.
- Ryan TM, Krovitz GE. 2006. Trabecular bone ontogeny in the human proximal femur. *Journal of Human Evolution* 51: 591-602.
- Ryan TM, Milner GR. 2006. Osteological applications of high-resolution computed tomography: a prehistoric arrow injury. *Journal of Archaeological Science* 33(6):871-879.
- Ryan TM, Shaw CN. 2012. Unique Suites of Trabecular Bone Features Characterize Locomotor Behavior in Human and Non-Human Anthropoid Primates. *PLoS ONE* 7(7): e41037
- Ryan TM, Shaw CN. 2015. Gracility of the modern *Homo sapiens* skeleton is result of decreased biomechanical loading. *Proceedings of the National Academy of Sciences of the United States of America* 112(2): 372-377.
- Ryan TM, van Rietbergen B, Krovitz G. 2007. Mechanical adaptation of trabecular bone in the growing human femur and humerus. *American Journal of Physical Anthropology* 132: 205.
- Ryan TM, Walker A. 2010. Trabecular bone structure in the humeral and femoral heads of anthropoid primates. *Anatomical Record* 293: 719-729.
- Saers JPP, Cazorla-Bak Y, Shaw CN, Stock JT, Ryan TM. 2016. Trabecular bone structural variation throughout the human lower limb. *Journal of Human Evolution* 97: 97-108.

- Saini UC, Bali K, Sheth B, Gahlot N, Gahlot A. 2010. Normal development of the knee angle in healthy Indian children: a clinical study of 215 children. *Journal of Children's Orthopaedics* 4(6): 579-586.
- Salenius P, Vankka E. 1975. The development of the tibiofemoral angle in children. *Journal of Bone and Joint Surgery* 57(2): 259–261.
- Salmon PL, Ohlsson C, Shefelbine SJ, Doube M. 2015. Structure Model Index Does Not Measure Rods and Plates in Trabecular Bone. *Frontiers in Endocrinology* 6: 162.
- Sample SJ, Behan M, Smith L, Oldenhoff WE, Markel MD, Kalscheur VL, Muir P. 2008. Functional adaptation to loading of a single bone is neuronally regulated and involves multiple bones. *Journal of Bone and Mineral Research* 23: 1372-1381.
- Santure SK. 1990a. Bold Counselor Phase Oneota Habitation Component. In: Santure S, Harn AD, Esarey D, editors. *Archaeological Investigations at the Morton Village and Norris Farms 36 Cemetery*. Springfield: Illinois State Museum. p. 47-56.
- Santure SK. 1990b. Summary Excavations and Analyses. In: Santure S, Harn AD, Esarey D, editors. *Archaeological Investigations at the Morton Village and Norris Farms 36 Cemetery*. Springfield: Illinois State Museum. p. 160-161.
- Santure SK. 1990c. Norris Farms 36: A Bold Counselor Phase Oneota Cemetery. In: Santure S, Harn AD, Esarey D, editors. *Archaeological Investigations at the Morton Village and Norris Farms 36 Cemetery*. Springfield: Illinois State Museum. p. 66-74.
- Santure SK, Esarey D. 1990. Analysis of Artifacts From the Oneota Mortuary Component. In: Santure S, Harn AD, Esarey D, editors. *Archaeological Investigations at the Morton Village and Norris Farms 36 Cemetery*. Springfield: Illinois State Museum. p. 75-110.
- Santure SK, Harn AD, Esarey D. 1990. *Archaeological Investigations at the Morton Village and Norris Farms 36 Cemetery*. Springfield: Illinois State Museum.
- Saparin P, Scherf H, Hublin J-J, Fratzl P, Weinkamer R. 2011. Structural Adaptation of Trabecular Bone Revealed by Position Resolved Analysis of Proximal Femora of Different Primates. *Anatomical Record* 294: 55-67.
- Saunders SR. 2008. Juvenile Skeletons and Growth-Related Studies. In: Katzenberg MA, Saunders SR, editors. *Biology of the Human Skeleton*. 2nd edition. p 117-147.
- Saunders SR, Hoppa RD. 1993. Growth deficit in survivors and non-survivors: biological mortality bias in subadult skeletal samples. *Yearbook of Physical Anthropology* 36:127–151.

- Saunders SR, Melbye FJ. 1990. Subadult mortality and skeletal indicators of health in Late Woodland Ontario Iroquois. *Canadian Journal of Archaeology* 14: 61–74.
- Scheller S. 1960. Roentgenographic studies on epiphysial growth and ossification in the knee. *Acta Radiologica Scandinavica* 195 (Suppl.).
- Scherf H, Harvati K, Hublin JJ. 2013. A comparison of proximal humeral cancellous bone of great apes and humans. *Journal of Human Evolution* 65: 29-38.
- Scheuer L, Black S. 2004. *The Juvenile Skeleton*. London: Elsevier.
- Schipilow JD, Macdonald HM, Liphardt AM, Kan M, Boyd SK. 2013. Bone micro-architecture, estimated bone strength, and the muscle-bone interaction in elite athletes: An HR-pQCT study. *Bone* 56: 281-289.
- Schoenau E, Fricke O, Rauch F. 2003. The regulation of bone development as a biological system. *Homo* 54: 113-118.
- Schroeder S. 2004. Current Research on Late Precontact Societies of the Midcontinental United States. *Journal of Archaeological Research*. 12(4): 311- 372.
- Schulte FA, Ruffoni D, Lambers FM, Christen D, Webster DJ, Kuhn G, Müller R. 2013. Local mechanical stimuli regulate bone formation and resorption in mice at the tissue level. *PLoS One* 8: e62172.
- Schultz M. 2001. Paleohistopathology of bone: A new approach to the study of ancient diseases. *Yearbook of Physical Anthropology* 44: 106-147.
- Sciulli P. 1994. Standardization of long bone growth in children. *International Journal of Osteoarchaeology* 4:257–259.
- Seeman E. 2008. Structural basis of growth-related gain and age-related loss of bone strength. *Rheumatology* 47(Suppl 4): iv2-iv8.
- Seeman E. 2009. Bone modeling and remodeling. *Critical Reviews in Eukaryotic Gene Expression* 19(3): 219-233.
- Sharma AR, Jagga S, Lee S-S, Nam J-S. 2013. Interplay between Cartilage and Subchondral Bone Contributing to Pathogenesis of Osteoarthritis. *International Journal of Molecular Sciences* 14: 19805-19830.
- Sharma L, Song J, Dunlop D, Felson D, Lewis CE, Segal N, et al. 2010. Varus and Valgus Alignment and Incident and Progressive Knee Osteoarthritis. *Annals of the Rheumatic Diseases* 69(11): 1940-1945.
- Shaw CN. 2011. Is ‘hand preference’ coded in the hominin skeleton? An in-vivo study of bilateral morphological variation. *Journal of Human Evolution* 61(4): 480-487.

- Shaw CN, Ryan TM. 2012. Does skeletal anatomy reflect adaptation to locomotor patterns? Cortical and trabecular architecture in human and nonhuman anthropoids. *American Journal of Physical Anthropology* 147: 187-200.
- Stini WA. 1969. Nutritional stress and growth: sex difference in adaptive response. *American Journal of Physical Anthropology* 31:417–426.
- Sims NA, Martin TJ. 2014. Coupling: the activities of bone formation and resorption: a multitude of signals within the basic multicellular unit. *BoneKEy Reports* 2014 3: 481
- Skerry TM. 2006. One mechanostat or many? Modifications of the site-specific response of bone to mechanical loading by nature and nurture. *Journal of Musculoskeletal and Neuronal Interactions* 6(2): 122-127.
- Spector TD, MacGregor AJ. 2004. Risk Factors for Osteoarthritis: Genetics 12: S39-44.
- Stanford CM, Welsch F, Kastner N, Thomas G, Zaharias R, Holtman K, Brand RA. 2000. Primary human bone cultures from older patients do not respond at continuum levels of in vivo strain magnitudes. *Journal of Biomechanics* 33:63–71.
- Steadman DW. 1998. The population shuffle in the central Illinois valley: a diachronic model of Mississippian biocultural interactions. *World Archaeology* 30(2): 306-326.
- Steadman DW. 2008. Warfare Related Trauma at Orendorf, A Middle Mississippian Site in West-Central Illinois. *American Journal of Physical Anthropology* 136: 51-64.
- Steenvoorden MM, Huizinga TW, Verzijl N, et al. 2006. Activation of receptor for advanced glycation end products in osteoarthritis leads to increased stimulation of chondrocytes and synoviocytes. *Arthritis and Rheumatology* 54: 253-263.
- Stephens NB, Kivell TL, Gross T, Pahr DH, Lazenby RA, Hublin J-J, Hershkovitz I, Skinner MM. 2016. Trabecular architecture in the thumb of Pan and Homo: implications for investigating hand use, loading, and hand preference in the fossil record. *American Journal of Physical Anthropology* 161 (4): 603-619.
- Stewart TD. 1979. *Essentials of Forensic Anthropology*. Springfield: C.C. Thomas.
- Stock JT. 2006. Hunter-gatherer postcranial robusticity relative to patterns of mobility, climatic adaptation, and selection for tissue economy. *American Journal of Physical Anthropology* 131: 194-204.
- Stock SR. 2011. *MicroComputed Tomography: Methodology and Applications*. Boca Raton: CRC Press.
- Stoltman JB. 1986. The appearance of the Mississippian cultural tradition in the Upper Mississippi Valley. In: Stoltman JB, editor. *Prehistoric Mound Builders of the Mississippi Valley*. Davenport: The Putnam Museum. p. 26-34.

- Stone AC, Milner GR, Paabo S, Stoneking M. 1996 Sex determination of ancient human skeletons using DNA. *American Journal of Physical Anthropology* 99: 231-238.
- Stone AC, Stoneking M. 1993 Ancient DNA from a pre-Columbian Amerindian population. *American Journal of Physical Anthropology* 92: 463-471.
- Stone AC, Stoneking M. 1998 MtDNA analysis of a prehistoric Oneota population: implications for the peopling of the New World. *American Journal of Human Genetics* 62: 1153-1170.
- Stone AC, Stoneking M. 1999. Analysis of ancient DNA from a prehistoric Amerindian cemetery. *Philosophical Transactions of the Royal Society B* 354: 153-159.
- Storm EE, Kingsley DM. 1996. Joint patterning defects caused by single and double mutations in members of the bone morphogenetic protein (BMP) family. *Development* 122(12): 3969-3979.
- Stout SD. 1978. Histological structures and its preservation in ancient bone. *Current Anthropology* 19: 601-603.
- Stout SD. 1983. The application of histomorphometric analysis to ancient skeletal remains. *Anthropos* 10: 60-71.
- Stout SD. 1989. Histomorphometric analysis of human skeletal remains. In: Iscan MY, Kennedy KAR, editors. *Reconstruction of Life from the Skeleton*. New York: Wiley-Liss. p 41-52.
- Stout SD, Crowder C. 2012. Bone remodeling, histomorphology, and histomorphometry. In: Crowder C, and Stout SD, editors. *Bone histology: An anthropological perspective*. Boca Raton, FL: CRC Press, Taylor & Francis Group. p 1-22.
- Stout SD, Lueck R. 1995. Bone remodeling rates and maturation in three archaeological skeletal populations. *American Journal of Physical Anthropology* 98: 161-171.
- Stout SD, Simmons DJ. 1979. Use of histology in ancient bone research. *Yearbook of Physical Anthropology* 44: 263-270.
- Styles BW, King FB. 1990. Faunal and Floral Remains From the Bold Counselor Phase Village. In: Santure S, Harn AD, Esarey D, editors. *Archaeological Investigations at the Morton Village and Norris Farms 36 Cemetery*. Springfield: Illinois State Museum. p. 57-65.
- Su A. 2011. The functional morphology of subchondral and trabecular bone in the hominoid tibiotalar joint. PhD Dissertation: Stony Brook University.

- Su A, Wallace IJ, Nakatsukasa M. 2013. Trabecular bone anisotropy and orientation in an Early Pleistocene hominin talus from East Turkana, Kenya. *Journal of Human Evolution* 64: 667–677.
- Sugiyama T, Price JS, Lanyon LE. 2010. Functional adaptation to mechanical loading in both cortical and cancellous bone is controlled locally and is confined to the loaded bones. *Bone* 46:314-321.
- Suri S, Walsh DA. 2012. Osteochondral alterations in OA. *Bone* 51: 204-211.
- Szulc P, Delmas PD. 2007. Bone loss in elderly men: increased endosteal bone loss and stable periosteal apposition. The prospective MINOS study. *Osteoporosis International* 18(4): 495-503.
- Tanck E, Homminga J, Van Lenthe GH, Huiskes R. 2001. Increase in bone volume fraction precedes architectural adaptation in growing bone. *Bone* 28(6):650-654.
- Tanck E, Hannink G, Ruimerman R, Buma P, Burger EH, Huiskes R. 2006. Cortical bone development under the growth plate is regulated by mechanical load transfer. *Journal of Anatomy* 208: 73-79.
- Tanner JM. 1981. Catch-up Growth in Man. *British Medical Bulletin* 37: 233-238.
- Temple-Wong MM, Bae WC, Chen MQ, et al. 2009. Biomechanical, structural, and biochemical indices of degenerative and osteoarthritic deterioration of adult human articular cartilage of the femoral condyle. *Osteoarthritis Cartilage* 17: 1469-1476.
- Terhune CE, Kimbel WH, Lockwood CA. 2013. Postnatal Temporal Bone Ontogeny in *Pan*, *Gorilla*, and *Homo*, and the Implications for Temporal Bone Ontogeny in *Australopithecus afarensis*. *American Journal of Physical Anthropology* 151: 630-642.
- Teti A. 2011. Bone Development: Overview of Bone Cells and Signaling. *Current Osteoporosis Reports* 9: 264-273.
- Thoma KH, Goldman HM. 1960. *Oral Pathology*. St. Louis: Mosby.
- Thornton R. 1987. *American Indian holocaust and survival: a population history since 1492*. Norman: University of Oklahoma Press.
- Toriwaki J, Yonekura T. 2002. Euler number and connectivity indexes of a three dimensional digital picture. *Forma* 2002; 17: 183–209. 22
- Transeau EN. 1935. The Prairie Peninsula. *Ecology* 16(3): 423-437.
- Tsegai ZJ, Kiveli TL, Gross T, Nguyen NH, Pahr DH, Smaers JB, Skinner MM. 2013. Trabecular bone structure correlated with hand posture and use in hominoids. *PLoS One* 8: e78781.

- Tubbs RM. 2013. Ethnic Identity and Diet in the Central Illinois River Valley. Ph.D. dissertation, Michigan State University, East Lansing.
- Tubbs RM, O’Gorman JA. 2005. Assessing Oneota Diet and Health: A Community and Lifeway Perspective. *Midcontinental Journal of Archaeology* 30(1): 119-163.
- Turner CH, Pavalko FM. 1998. Mechanotransduction and functional response of the skeleton to physical stress: the mechanisms and mechanics of bone adaptation. *Journal of Orthopaedic Science* 3(6): 346-355.
- Turner CH, Robling AG. 2003. Designing exercise regimens to increase bone strength. *Exercise and Sport Sciences Reviews* 31(1):45-50.
- Turner CH, Robling AG. 2004. Exercise as an anabolic stimulus for bone. *Current Pharmaceutical Design* 10(21): 2629-2641.
- Turunen MJ, Saarakkala S, Helminen HJ, Jurvelin JS, Isaksson H. 2012. Age-Related Changes in Organization and Content of the Collagen Matrix in Rabbit Cortical Bone. *Journal of Orthopaedic Research*. 30(3): 435-42.
- Ubelaker DH. 1978. *Human Skeletal Remains: Excavation, Analysis, Interpretation*. Chicago: Aldine Publishing.
- Ubelaker DH. 1988. North American Indian population size, A.D. 1500 to 1985. *American Journal of Physical Anthropology* 77: 289-294.
- Ubelaker DH. 1992. Patterns of demographic change in the Americas. *Human Biology* 64: 361-379.
- Vanderoost J, van Lenthe GH. 2014. From histology to micro-CT: Measuring and modeling resorption cavities and their relation to bone competence. *World Journal of Radiology* 6(9): 643-656.
- Vercellotti G, Stout SD, Boano R, Sciulli PW. 2011. Intrapopulation Variation in Stature and Body Proportions: Social Status and Sex Differences in an Italian Medieval Population (Trino Vercellese, VC). *American Journal of Physical Anthropology* 145: 203-214.
- Vicencio JM, Galluzzi L, Tajeddine N, et al. 2008. Senescence, apoptosis or autophagy? When a damaged cell must decide its path – a mini-review. *Gerontology* 54: 92-99.
- von Meyer GH. 1867. Die Architektur der Spongiosa. *Archiv für Anatomie, Physiologie und Wissenschaftliche Medicin*. 34:615–28.
- Waldron T. 2007. *St. Peter’s Barton-upon-Humbert, Lincolnshire: a parish church and its community*. Vol. 2: The human remains. Oxford: Oxbow Books.

- Wallace IJ, Kwaczala AT, Demes JB, Carlson KJ. 2013. Physical activity engendering loads from diverse directions augments the growing skeleton. *Journal of Musculoskeletal and Neuronal Interactions* 13(3): 283-288.
- Wallace IJ, Middleton KM, Lublinsky S, Kelly SA, Judex S, Garland T, Demes B. 2010. Functional significance of genetic variation underlying limb bone diaphyseal structure. *American Journal of Physical Anthropology* 143: 21-30.
- Wang Q, Ghasem-Zadeh A, Wang X-F, Iuliano-Burns S, Seeman Ego. 2011. Trabecular Bone of Growth Plate Origin Influences Both Trabecular and Cortical Morphology in Adulthood. *Journal of Bone and Mineral Research* 26(7): 2577-1583.
- Ward FO. 1838. *Outlines of human osteology*. London: Renshaw.
- Weiss E. 2006. Osteoarthritis and body mass. *Journal of Archaeological Science* 33: 690–695.
- Weiss E, Jurmain R. 2007. Osteoarthritis revisited: a contemporary review of aetiology. *International Journal of Osteoarchaeology* 17: 437–450.
- Widmaier EP, Raff H, Strang KT. 2001. *Vanders, Sherman, and Luciano's Human Physiology*, 8th edition. Arlington: McGraw-Hill.
- Wolff J. 1892. *The Law of Bone Remodeling*. [Translation of Wolff's *Das Gesetz der Transformation der Knochen* Maquet P and Furlong R]. Berlin: Springer
- Wong M, Carter DR. 2003. Articular cartilage functional histomorphology and mechanobiology: a research perspective. *Bone* 33(1): 1-13.
- Woo SL, Kuei SC, Amiel D, Gomez MA, Hayes WC, White FC, Akeson WH. 1981. The effect of prolonged physical training on the properties of long bone: a study of Wolff's law. *Journal of Bone and Joint Surgery* 63: 780-787.
- Wu M, Fannin J, Rice KM, Wang B, Blough ER. 2011. Effect of aging on cellular mechanotransduction. *Ageing Research Reviews* 10(1): 1-15.
- Yammani RR, Carlson CS, Chen H, et al. 2006. Increase in production of matrix metalloproteinase 13 by human articular chondrocytes due to stimulation with S100A4: role of the receptor for advanced glycation end products. *Arthritis and Rheumatology* 54(9): 2901-2911.
- Yang Y. 2013. *Skeletal Morphogenesis and Embryonic Development*. In: Rosen CJ. Editor. *Primer on the Metabolic Bone Diseases and Disorders of Mineral Metabolism*. Ames: John Wiley & Sons. p 3-14.
- Yoo JH, Choi IH, Cho TJ, Chung CY, Yoo WJ. 2008. Development of tibiofemoral angle in Korean children. *Journal of Korean Medical Science* 23(4): 714-717.

Zamil Z, Brown KR, Tarlton JF, Adams MA, Torlot GE, Cartwright C, Cook WA, Vassilevskaja K, Sharif M. 2014. Subchondral Bone Plate Thickening Precedes Chondrocyte Apoptosis and Cartilage Degradation in Spontaneous Animal Models of Osteoarthritis. *BioMed Research International* 2014: 1-10.

Zamil Z, Brown KR, Sharif M. 2016. Subchondral Bone Plate Changes More Rapidly than Trabecular Bone in Osteoarthritis. *International Journal of Molecular Sciences* 17(9): 1496.

Zhang L-Z, Zheng H-A, Jiang Y, Tu Y-H, Jiang P-H, Yang A-L. 2012. Mechanical and Biologic Link Between Cartilage and Subchondral Bone in Osteoarthritis. *Arthritis Care and Research* 64(7): 960-967.

APPENDIX A: Supplemental Data Tables

Individual	Burial #	Catalog #	Tibia Side (R=right, L=left)	Age Estimate (Years)	Average Age (Years)	SEX (male=0, female=1)	Stature Estimation (cm)
1	209	821216	R	7-9	8	--	--
2	77	820686	L	8-10	9	--	--
3	113	821006	L	8-10	9	--	--
4	103	820732	R	8-11	9.5	--	--
5	89	820711	R	9-12.5	10.5	--	--
6	155	821078	L	10-12	11	--	--
7	95	820721	R	13-17	15	--	--
8	56	820608	R	14-17	15.5	0?	--
9	11	819915	R	15-17	16	1	166.773 +/- 3.27
10	42	819964	R	15-17	16	0	--
11	228	821246	R	15-17	16	--	--
12	170	821101	R	16-17	16.5	1?	158.647 +/- 3.27
13	20	819932	L	17-19	18	1	160.162 +/- 3.24
14	37	819957	L	18-21	19.5	1	154.664 +/- 3.18
15	66	820652	L	18-21	19.5	1?	156.380 +/- 3.24
16	69	820658	L	18-21	19.5	1	164.058 +/- 3.18
17	44	819977	R	20-23	21.5	0	160.398 +/- 3.18
18	49	819994	L	20-25	22.5	0	171.744 +/- 3.18
19	105	820735	R	25-28	26.5	0	163.720 +/- 3.18
20	132	821042	L	25-30	27.5	1	165.034 +/- 3.18

Continued

Table A.1: Demographic information for individuals in this study. Stature estimation is based on Trotter and Gleser (1958) "Mongoloid" formulae. "--" = no data

Table A.1 Continued

21	27	819941	L	30-35	32.5	1	162.838 +/- 3.18
22	33	819951	L	30-35	32.5	1	158.568 +/- 3.18
23	50	819996	L	30-35	32.5	0	171.500 +/- 3.18
24	63	820647	L	30-35	32.5	0	166.742 +/- 3.18
25	80	820696	R	30-35	32.5	1	163.814 +/- 3.18
26	216	821228	L	30-35	32.5	0	167.962 +/- 3.18
27	217	821230	L	30-35	32.5	0	169.304 +/- 3.18
28	90	820715	L	30-40	35	1	158.332 +/- 3.24
29	45	819983	L	35-40	37.5	0	174.306 +/- 3.18
30	71	820668	L	35-40	37.5	0	169.914 +/- 3.18
31	106	820740	L	35-40	37.5	0	170.768 +/- 3.18

Catalog #	Age (Yrs.)	Side (I_{min})	I_{min} (mm⁴)	I_{max} (mm⁴)	J (mm⁴)	Mean J (mm⁴)	Body Mass (kg)
821216	8	R	2085.018	2696.502	4781.521	4781.521	17.182
		L	--	--	--		
820686	9	R	5214.989	5745.356	10960.345	10960.345	26.786
		L	--	--	--		
821006	9	R	--	--	--	6534.055	20.152
		L	3094.351	3439.704	6534.055		
820732	9.5	R	1172.755	1368.279	2541.034	2541.033	12.802
		L	--	--	--		
820711	10.5	R	3841.802	4169.577	8011.379	8011.379	22.475
		L	--	--	--		
821078	11	R	3228.41	3515.047	6743.457	6738.253	20.481
		L	3223.398	3509.651	6733.049		

Table A.2: Body mass estimation calculations for individuals aged 8 to 11.99 years (see Chapter 5 for a complete description). I_{\min} = minimum bending moment; I_{\max} = maximum bending moment; J = polar second moment of area. "--" = no data

Catalog #	Age (Yrs.)	SEX male=0, female=1	FHD (mm)	E1	E2	E3 or E4	Body Mass (kg)
820721	15		35.96	40.61444	45.05728		33.68676
820608	15.5	0?	37.59	44.26401	48.75412	48.13419	36.5615
819915	16	1	36.47	41.75633	46.21396	53.37622	34.54931
819964	16	0	41.63	53.30957	57.91684	59.20783	44.90081
821246	16		38.94	47.28666	51.81592		39.14796
821101	16.5	1?	34.55	37.45745	41.8594	48.7183	31.40682
819932	18	1	37.55	44.17445	48.6634	55.9963	49.61138
819957	19.5	1	41.24	52.43636	57.03232	64.94824	58.13897
820652	19.5	1?	42.6	55.4814	60.1168	68.2476	61.28193
820658	19.5	1	38.97	47.35383	51.88396	59.4412	52.89299
819977	21.5	0	44.02	58.66078	63.33736	65.7588	62.58564
819994	22.5	0	50.47	73.10233	77.96596	83.43827	78.16885
820735	26.5	0	46.18	63.49702	68.23624	71.67938	67.80421
821042	27.5	1	39.6	48.7644	53.3128	60.9696	54.34893
819941	32.5	1	41.6	53.2424	57.8488	65.8216	58.97093
819951	32.5	1	41.82	53.73498	58.34776	66.35532	59.47935
819996	32.5	0	45.3	61.5267	66.2404	69.2673	65.67813
820647	32.5	0	42.16	54.49624	59.11888	60.66056	58.09189
820696	32.5	1	43.2	56.8284	61.4776	69.7032	62.66973
821228	32.5	0	48.72	69.18408	73.99696	78.64152	73.94085
821230	32.5	0	47.37	66.16143	70.93516	74.94117	70.67925
820715	35	1	43.59	57.69801	62.36212	70.64934	63.56982
819983	37.5	0	47.7	66.9003	71.6836	75.8457	71.47653
820668	37.5	0	45.79	62.62381	67.35172	70.61039	66.86197
820740	37.5	0	49.32	70.52748	75.35776	80.28612	75.39045

Table A.3 Body mass estimation calculations for individuals aged 15 to 37.99 years (see Chapter 5 for a complete description). FHD = femoral head diameter; E1 = 1st sex-pooled estimate; E2 = 2nd sex pooled estimate; E3 = male estimate; E4 female estimate

ID	Voxel Size (z) Proximal Scan	Voxel Size (z) Full Scan	Epiphyseal Condyle Breadth (mm)	VOI Cube Size (mm)	VOI Length (# of slices)	# of Slices FULL SCAN	# of Slices Lateral Condyle (ROI)	# of Slices Medial Condyle (ROI)
821216	0.04	0.081	46.95	4.72	119	2628	1104	1101
820686	0.05	0.094	58.43	4.4	89		1104	828
821006	0.04	0.081	50.61	5.16	130	3099	1071	1074
820732	0.04	0.081	44.82	4	101	2574	962	956
820711	0.05	0.094	55.38	5.5	111	2902	1126	1126
821078	0.05	0.094	51.35	5.7	115		1123	1119
820608	0.05	0.081	62.85	6.55	132	4478	830	799
819915	0.05	0.094	68.43	6.2	124	3870	1213	1215
819964	0.05	0.094	67.05	4.35	88	3573	1094	1126
820721	0.05	0.094	55.05	5.6	113	3336	1126	1126
821246	0.05	0.094	67	6.15	124	3833	1210	1211
821101	0.05	0.094	63.56	6.3	127	3522	911	914
819932	0.056	0.117	68.58	5.684	103		1078	1074
819957	0.057	0.117	67.53	5.015	89		1116	745
820652	0.056	0.117	70.02	6.322	114		992	992
820658	0.056	0.117	66.63	6.438	116		992	992
819977	0.057	0.117	76.72	7.772	137		1117	1117
819994	0.056	0.117	83.88	8.178	147		704	706
820735	0.056	0.117	79.14	8.12	146		992	992
821042	0.056	0.117	69.61	6.148	111		992	992
819941	0.056	0.117	75.42	6.902	124		992	992
819951	0.057	0.117	74.64	6.844	121		1116	1116
819996	0.057	0.117	80.27	5.684	101		1117	1117
820647	0.056	0.117	74.11	6.554	118		808	809
820696	0.056	0.117	69.51	6.264	113		992	992
821228	0.056	0.117	77.08	8.294	149		841	1051
821230	0.056	0.117	76.94	6.438	116		992	1110
820715	0.056	0.117	71.17	6.728	121		855	752
819983	0.057	0.117	81.66	7.328	130		1126	1126
820668	0.056	0.117	78.6	7.192	129		992	992
820740	0.056	0.117	82.48	7.598	137		831	671

Table A.4: VOI size and position data. Blank space = bone excluded. All measurements are in millimeters (mm).

Catalog#	Age (Yrs.)	Epiphyseal Condyle Breadth (mm)	Tibia Diaphyseal Length (mm)	Average Length by Age (mm)
821216	8	46.95	196.992	196.992
820686	9	58.43	279.838	251.416
821006	9	50.61	222.993	
820732	9.5	44.82	185.49	185.49
820711	10.5	55.38	241.862	241.862
821078	11	51.35	208.413	208.413
820721	15	55.05	278.052	278.052
820608	15.5	62.85	323.919	323.919
819915	16	68.43	318.284	313.365
819964	16	67.05	301.928	
821246	16	67	319.882	
821101	16.5	63.56	288.392	288.392
819932	18	68.58	339.768	339.768
819957	19.5	67.53	294.021	314.106
820652	19.5	70.02	283.725	
820658	19.5	66.63	364.572	
819977	21.5	76.72	--	--
819994	22.5	83.88	333.684	333.684
820735	26.5	79.14	327.132	327.132
821042	27.5	69.61	325.026	325.026
819941	32.5	75.42	360.126	332.564
819951	32.5	74.64	299.052	
819996	32.5	80.27	336.843	
820647	32.5	74.11	330.642	
820696	32.5	69.51	320.697	
821228	32.5	77.08	339.534	
821230	32.5	76.94	341.055	
820715	35	71.17	300.69	
819983	37.5	81.66	359.073	346.008
820668	37.5	78.6	339.183	
820740	37.5	82.48	339.768	

Table A.5: Postcranial metrics for all individuals in this study. "--" = no data. All measurements are in millimeters (mm).

Catalog #	Condyle	VOI #	Threshold	BV/TV	Tb.Th Mean (mm)	Tb.Sp Mean (mm)	SMI	Conn.D (mm ⁻³)	DA	Tb.N (mm ⁻¹)
821216	LAT	1	2951	0.259	0.434	1.047	0.751	2.15	0.507	0.59677419
		2	2822	0.217	0.329	1.116	0.858	2.606	0.532	0.65957446
		3	3180	0.473	0.492	0.705	1.408	3.087	0.119	0.96138211
		4	2817	0.174	0.229	0.888	1.251	4.567	0.422	0.759825328
	MID	5	2726	0.129	0.385	1.564	1.69	1.234	0.478	0.335064935
		6	2740	0.156	0.315	1.211	1.514	1.736	0.578	0.495238095
		7	2919	0.238	0.578	1.539	1.126	1.032	0.485	0.411764706
	MED	1	2868	0.164	0.222	0.959	1.118	3.284	0.743	0.738738739
		2	3102	0.356	0.481	0.903	1.208	3.009	0.426	0.74012474
		3	2922	0.191	0.244	0.986	1.023	4.535	0.697	0.782786885
		4	3021	0.292	0.396	1.142	1.325	3.459	0.359	0.737373737
	820686	LAT	1	3128	0.247	0.278	0.796	0.869	3.083	0.545
2			3105	0.21	0.267	0.874	1.07	3.054	0.794	0.786516854
3			3123	0.226	0.263	0.816	0.962	3.49	0.657	0.859315589
4			2962	0.166	0.243	0.993	1.333	2.666	0.689	0.683127572
MID		5	3064	0.104	0.334	2.219	1.471	0.508	0.94	0.311377246
		6	2973	0.129	0.307	1.634	1.553	1.024	0.565	0.42019544
		7	3298	0.166	0.349	1.448	1.387	0.957	0.75	0.475644699
MED		1	3242	0.178	0.279	1.254	0.95	1.441	0.785	0.637992832
		2	3137	0.183	0.257	1.073	0.874	1.796	0.813	0.712062257
		3	3272	0.153	0.294	1.268	1.388	1.403	0.591	0.520408163
		4	3176	0.199	0.257	0.973	0.861	2.038	0.761	0.774319066
821006		LAT	1	3300	0.173	0.208	0.834	1.172	4.637	0.593
	2		3228	0.192	0.219	0.754	1.162	5.598	0.554	0.876712329
	3		3227	0.182	0.243	0.819	1.172	5	0.538	0.748971193
	4		3233	0.21	0.214	0.683	1.007	6.291	0.66	0.981308411
	MID	5	3186	0.181	0.224	0.912	1.072	4.124	0.504	0.808035714
		6	3297	0.143	0.211	0.959	1.394	3.64	0.492	0.677725118
		7	3194	0.184	0.255	0.994	1.02	2.689	0.653	0.721568627
	MED	1	3777	0.269	0.274	0.682	0.667	5.224	0.632	0.981751825
		2	3464	0.235	0.274	0.768	0.79	4.765	0.717	0.857664234
		3	3856	0.294	0.287	0.671	1.17	5.686	0.563	1.024390244
		4	3399	0.204	0.233	0.797	0.876	4.907	0.738	0.875536481

Continued

Table A.6: Threshold and bone morphometric values for all VOIs in each condylar region for all individuals. LAT = Lateral Condyle; MID = Between Condyles; MED = Medial Condyle.

Table A.6 Continued

820732	LAT	1	3325	0.222	0.213	0.664	1.059	6.988	0.608	1.042253521
		2	3169	0.187	0.193	0.735	1.148	6.627	0.5	0.968911917
		3	3353	0.191	0.196	0.674	1.22	7.17	0.677	0.974489796
		4	3171	0.16	0.178	0.715	1.388	7.307	0.552	0.898876404
	MID	5	3229	0.139	0.201	0.89	1.52	4.143	0.301	0.691542289
		6	3065	0.163	0.209	0.827	1.369	4.576	0.535	0.779904306
		7	3359	0.155	0.2	0.836	1.459	5.141	0.363	0.775
	MED	1	3180	0.178	0.188	0.706	1.266	7.629	0.674	0.946808511
		2	3413	0.22	0.204	0.615	1.06	8.039	0.572	1.078431373
		3	3437	0.192	0.19	0.658	1.185	8.131	0.627	1.010526316
		4	3610	0.242	0.221	0.594	0.901	8.426	0.679	1.095022624
	820711	LAT	1	3108	0.264	0.258	0.636	0.876	5.683	0.544
2			3096	0.217	0.234	0.745	0.969	4.688	0.532	0.927350427
3			3159	0.232	0.237	0.679	0.971	5.807	0.594	0.978902954
4			3071	0.2	0.22	0.769	0.967	4.856	0.599	0.909090909
MID		5	2857	0.166	0.249	0.956	1.357	3.124	0.575	0.666666667
		6	2918	0.207	0.266	0.893	1.076	3.844	0.522	0.778195489
		7	2840	0.152	0.252	1.036	1.484	2.564	0.589	0.603174603
MED		1	3199	0.218	0.256	0.795	0.954	3.985	0.626	0.8515625
		2	3514	0.292	0.305	0.719	1.173	3.889	0.692	0.957377049
		3	3200	0.189	0.265	0.918	1.053	3.004	0.711	0.713207547
		4	3588	0.325	0.369	0.746	1.408	3.678	0.434	0.880758808
821078		LAT	1	2925	0.193	0.233	0.842	0.918	3.84	0.646
	2		3360	0.293	0.307	0.659	0.355	5.806	0.54	0.954397394
	3		3191	0.22	0.318	0.802	0.827	4.418	0.78	0.691823899
	4		3514	0.34	0.377	0.624	1.137	6.017	0.589	0.901856764
	MID	5	2857	0.195	0.294	1.028	1.046	1.993	0.75	0.663265306
		6	2852	0.22	0.295	0.976	0.875	2.18	0.659	0.745762712
		7	3374	0.209	0.545	1.062	0.583	1.9	0.617	0.383486239
	MED	1	3210	0.415	0.488	0.79	1.008	4.094	0.543	0.850409836
		2	2813	0.283	0.337	0.897	1.304	3.64	0.543	0.839762611
		3	3547	0.332	0.401	0.834	1.305	4.544	0.564	0.827930175
		4	3280	0.253	0.379	1.364	1.298	3.773	0.59	0.667546174

Continued

Table A.6 Continued

820721	LAT	1	3147	0.436	0.392	0.788	- 0.233	4.241	0.404	1.112244898
		2	2996	0.278	0.424	1.455	0.277	1.742	0.539	0.655660377
		3	3202	0.393	0.378	0.748	- 0.638	4.327	0.587	1.03968254
		4	3087	0.182	0.412	2.495	0.505	0.826	0.875	0.441747573
	MID	5	2831	0.16	0.39	1.559	1.489	1.173	0.367	0.41025641
		6	2949	0.253	0.463	1.325	0.767	1.296	0.704	0.546436285
		7	3007	0.22	0.472	1.297	1.153	1.167	0.542	0.466101695
	MED	1	3065	0.286	0.383	1.019	0.217	2.176	0.691	0.746736292
		2	3240	0.324	0.313	0.826	0.95	4.66	0.603	1.03514377
		3	3026	0.263	0.429	1.269	0.47	1.582	0.711	0.613053613
		4	3258	0.322	0.34	0.743	0.335	3.933	0.718	0.947058824
	820608	LAT	1	3506	0.468	0.477	0.734	0.935	1.404	0.632
2			3051	0.303	0.39	0.888	0.522	1.969	0.525	0.776923077
3			3383	0.4	0.369	0.702	0.653	2.555	0.688	1.08401084
4			3031	0.301	0.364	0.885	0.44	1.952	0.672	0.826923077
MID		5	2569	0.149	0.269	1.188	1.459	1.739	0.611	0.553903346
		6	2535	0.186	0.259	1.04	1.738	2.267	0.755	0.718146718
		7	2714	0.182	0.305	1.007	1.453	2.198	0.399	0.596721311
MED		1	3013	0.275	0.301	0.795	0.549	3.653	0.614	0.913621262
		2	3145	0.353	0.33	0.683	0.776	4.048	0.637	1.06969697
		3	3284	0.334	0.347	1.128	0.449	3.632	0.434	0.962536023
		4	3299	0.364	0.396	2.287	0.239	2.957	0.336	0.919191919
819915		LAT	1	2865	0.263	0.253	0.647	0.768	6.114	0.426
	2		2960	0.238	0.242	0.702	0.847	4.932	0.644	0.983471074
	3		2998	0.242	0.243	0.696	0.838	5.672	0.585	0.995884774
	4		3049	0.235	0.231	0.713	0.741	5.273	0.637	1.017316017
	MID	5	2812	0.184	0.269	1.01	1.266	2.544	0.473	0.68401487
		6	2845	0.228	0.275	0.818	0.997	2.665	0.821	0.829090909
		7	2859	0.195	0.27	1.011	1.098	2.737	0.638	0.722222222
	MED	1	3628	0.339	0.341	0.655	0.914	4.439	0.691	0.994134897
		2	3187	0.272	0.273	0.694	0.527	5.162	0.649	0.996336996
		3	3617	0.327	0.326	0.667	1.19	4.096	0.73	1.003067485
		4	3181	0.23	0.267	0.75	0.836	4.264	0.724	0.861423221

Continued

Table A.6 Continued

819964	LAT	1	2706	0.309	0.416	0.985	0.654	1.83	0.502	0.742788462
		2	2733	0.246	0.401	1.251	0.996	1.408	0.583	0.613466334
		3	2718	0.293	0.362	0.85	0.831	2.641	0.449	0.809392265
		4	2843	0.227	0.357	1.163	1.071	1.438	0.728	0.635854342
	MID	5	2724	0.133	0.26	1.29	1.521	1.498	0.535	0.511538462
		6	2771	0.176	0.263	1.125	1.004	1.724	0.783	0.669201521
		7	2888	0.168	0.299	1.275	1.287	1.427	0.544	0.56187291
	MED	1	3156	0.263	0.27	0.783	0.609	3.137	0.646	0.974074074
		2	3068	0.233	0.242	0.811	0.724	3.528	0.699	0.962809917
		3	3272	0.295	0.267	0.665	0.458	4.431	0.631	1.104868914
		4	3117	0.25	0.237	0.738	0.58	4.365	0.735	1.054852321
	821246	LAT	1	2578	0.206	0.279	0.811	1.228	3.223	0.505
2			2672	0.186	0.255	0.854	1.289	2.994	0.575	0.729411765
3			2544	0.16	0.23	0.955	1.279	3.03	0.739	0.695652174
4			2705	0.15	0.24	1.033	1.27	2.597	0.757	0.625
MID		5	3339	0.529	0.884	0.935	1.663	0.882	0.34	0.59841629
		6	2988	0.228	0.539	1.359	1.512	0.835	0.682	0.423005566
		7	3267	0.469	0.683	0.854	1.344	1.343	0.271	0.686676428
MED		1	2801	0.187	0.279	0.82	1.267	3.672	0.667	0.670250896
		2	2998	0.268	0.303	0.768	0.61	3.295	0.798	0.884488449
		3	2978	0.242	0.398	0.836	1.347	2.861	0.698	0.608040201
		4	3006	0.278	0.35	0.758	0.237	3.378	0.773	0.794285714
821101		LAT	1	3070	0.358	0.347	0.623	0.224	3.766	0.654
	2		3176	0.422	0.41	0.65	0.363	2.539	0.618	1.029268293
	3		2933	0.297	0.28	0.653	0.42	4.786	0.682	1.060714286
	4		2918	0.272	0.29	0.759	0.483	3.488	0.693	0.937931034
	MID	5	2630	0.198	0.305	0.988	1.24	2.351	0.54	0.649180328
		6	2836	0.301	0.492	0.926	0.925	1.941	0.354	0.611788618
		7	2470	0.186	0.255	0.902	1.245	3.233	0.48	0.729411765
	MED	1	3219	0.416	0.352	0.58	0.346	3.841	0.588	1.181818182
		2	3409	0.391	0.359	0.642	0.437	3.033	0.75	1.08913649
		3	3066	0.369	0.362	0.658	0.689	3.212	0.639	1.019337017
		4	3338	0.338	0.331	0.679	1.029	4.304	0.633	1.021148036

Continued

Table A.6 Continued

819932	LAT	1	2898	0.232	0.292	0.82	1.623	2.965	0.797	0.794520548
		2	3358	0.35	0.375	0.721	1.079	3.022	0.647	0.933333333
		3	3177	0.252	0.316	0.827	1.71	3.119	0.639	0.797468354
		4	3517	0.387	0.385	0.663	0.952	3.513	0.507	1.005194805
	MID	5	2632	0.197	0.309	1.102	2.024	1.782	0.566	0.637540453
		6	2593	0.21	0.312	1.065	1.949	1.812	0.682	0.673076923
		7	2780	0.236	0.301	0.863	1.79	2.964	0.631	0.784053156
	MED	1	2754	0.27	0.28	0.764	1.334	3.663	0.574	0.964285714
		2	2711	0.225	0.275	0.874	1.743	2.637	0.751	0.818181818
		3	2947	0.251	0.275	0.757	1.726	4.188	0.551	0.912727273
		4	2752	0.205	0.261	0.819	2.057	3.977	0.483	0.785440613
	819957	LAT	1	2839	0.234	0.3	0.923	1.727	2.169	0.74
2			2769	0.277	0.343	0.895	1.431	2.323	0.715	0.807580175
3			2958	0.236	0.309	1.077	1.252	1.594	0.688	0.763754045
4			2817	0.244	0.315	1.015	1.437	1.859	0.601	0.774603175
MID		5	2171	0.126	0.27	1.427	2.213	1.229	0.654	0.466666667
		6	2392	0.221	0.297	0.917	1.879	1.877	0.76	0.744107744
		7	2223	0.134	0.27	1.347	2.264	1.644	0.516	0.496296296
MED		1	3125	0.253	0.288	0.804	1.335	3.049	0.794	0.878472222
		2	2773	0.17	0.243	0.962	2.053	3.019	0.705	0.699588477
		3	3145	0.265	0.294	0.758	1.468	3.758	0.68	0.901360544
		4	2964	0.168	0.248	1.007	1.988	2.727	0.737	0.677419355
820652		LAT	1	2952	0.182	0.3	1.154	1.954	1.731	0.731
	2		2916	0.186	0.297	1.575	1.77	1.827	0.712	0.626262626
	3		3118	0.199	0.284	0.937	1.88	2.728	0.586	0.700704225
	4		3027	0.213	0.282	0.953	1.727	2.875	0.71	0.755319149
	MID	5	2375	0.196	0.301	1.027	1.845	2.097	0.562	0.651162791
		6	2709	0.244	0.354	1.057	1.54	1.471	0.778	0.689265537
		7	2608	0.208	0.299	1.013	1.768	2.046	0.468	0.695652174
	MED	1	2907	0.252	0.295	0.824	1.426	2.846	0.659	0.854237288
		2	2647	0.201	0.289	0.998	1.767	2.013	0.715	0.69550173
		3	3180	0.237	0.296	0.836	1.62	3.279	0.598	0.800675676
		4	2553	0.173	0.263	0.953	2.066	2.632	0.575	0.657794677

Continued

Table A.6 Continued

820658	LAT	1	3050	0.306	0.316	0.725	1.141	2.912	0.771	0.96835443
		2	3019	0.368	0.411	0.68	0.992	3.258	0.615	0.895377129
		3	3138	0.278	0.286	0.743	1.224	3.795	0.703	0.972027972
		4	3207	0.315	0.304	0.703	0.948	4.053	0.631	1.036184211
	MID	5	2620	0.231	0.292	0.889	1.655	2.588	0.704	0.79109589
		6	3062	0.332	0.379	0.796	1.117	2.337	0.693	0.875989446
		7	2724	0.211	0.322	1.039	1.77	2.03	0.641	0.655279503
	MED	1	3143	0.362	0.334	0.669	0.658	3.118	0.699	1.083832335
		2	2933	0.302	0.325	0.755	1.248	3.065	0.662	0.929230769
		3	3289	0.32	0.348	0.74	1.127	3.534	0.614	0.91954023
		4	2725	0.193	0.259	0.91	1.878	3.264	0.619	0.745173745
	819977	LAT	1	3126	0.372	0.421	0.723	1.06	2.517	0.582
2			3146	0.377	0.435	0.761	0.861	1.985	0.566	0.866666667
3			3066	0.278	0.313	0.779	1.341	2.846	0.648	0.888178914
4			3088	0.272	0.311	0.856	1.176	2.427	0.727	0.874598071
MID		5	2904	0.268	0.396	0.939	1.671	1.852	0.531	0.676767677
		6	2711	0.306	0.363	0.736	1.561	3.02	0.255	0.842975207
		7	3015	0.218	0.317	0.966	1.776	2.113	0.545	0.687697161
MED		1	2893	0.177	0.268	1.016	1.762	1.965	0.792	0.660447761
		2	3409	0.302	0.368	0.85	0.867	2.205	0.744	0.820652174
		3	3126	0.219	0.312	0.982	1.639	1.958	0.74	0.701923077
		4	3655	0.401	0.495	0.721	0.536	2.151	0.76	0.81010101
819994		LAT	1	2955	0.298	0.341	0.841	1.139	2.074	0.653
	2		2875	0.305	0.331	0.765	1.208	2.962	0.296	0.921450151
	3		3064	0.262	0.314	0.893	1.224	2.243	0.664	0.834394904
	4		3085	0.261	0.312	0.884	1.298	2.479	0.678	0.836538462
	MID	5	2803	0.184	0.336	1.358	1.709	1.027	0.63	0.547619048
		6	2658	0.219	0.344	1.252	1.422	1.283	0.674	0.636627907
		7	3056	0.249	0.412	1.175	1.348	0.935	0.78	0.604368932
	MED	1	3305	0.342	0.355	0.795	0.487	1.817	0.701	0.963380282
		2	2888	0.246	0.308	0.943	1.272	1.974	0.769	0.798701299
		3	3530	0.346	0.378	0.832	0.388	1.714	0.762	0.915343915
		4	3248	0.244	0.314	0.929	1.208	1.763	0.813	0.777070064

Continued

Table A.6 Continued

820735	LAT	1	2681	0.331	0.373	0.742	1.119	2.894	0.536	0.887399464
		2	2636	0.279	0.326	0.849	1.244	2.393	0.623	0.855828221
		3	2709	0.313	0.306	0.745	0.798	2.782	0.726	1.022875817
		4	2754	0.272	0.288	0.821	3.35	2.806	0.647	0.944444444
	MID	5	2562	0.24	0.37	1.038	1.472	1.872	0.641	0.648648649
		6	2501	0.284	0.328	0.837	1.224	2.494	0.577	0.865853659
		7	2643	0.229	0.344	1.047	1.486	1.739	0.564	0.665697674
	MED	1	2786	0.279	0.297	0.823	0.878	2.12	0.818	0.939393939
		2	3076	0.345	0.35	0.769	0.349	1.555	0.825	0.985714286
		3	2775	0.204	0.289	0.933	1.564	2.424	0.757	0.705882353
		4	3146	0.38	0.401	0.719	0.248	2.066	0.794	0.947630923
	821042	LAT	1	3020	0.284	0.307	0.799	0.785	2.386	0.773
2			2761	0.266	0.295	0.772	1.591	3.133	0.605	0.901694915
3			3025	0.258	0.289	0.793	1.398	3.255	0.6	0.892733564
4			2993	0.295	0.299	0.71	1.225	3.523	0.689	0.986622074
MID		5	2531	0.203	0.311	0.972	1.997	2.089	0.65	0.652733119
		6	2555	0.245	0.315	0.914	1.594	2.163	0.665	0.777777778
		7	2374	0.192	0.29	0.935	2.114	2.462	0.329	0.662068966
MED		1	3144	0.327	0.325	0.685	1.129	3.673	0.77	1.006153846
		2	2553	0.219	0.272	0.78	1.929	3.252	0.616	0.805147059
		3	3522	0.347	0.366	0.779	1.798	3.57	0.642	0.948087432
		4	2858	0.169	0.285	0.956	2.37	2.617	0.646	0.592982456
819941		LAT	1	2969	0.239	0.317	0.907	1.512	1.764	0.793
	2		2897	0.248	0.379	0.969	1.771	2.004	0.577	0.654353562
	3		2976	0.207	0.313	1.069	1.718	1.899	0.667	0.661341853
	4		3060	0.255	0.305	0.928	1.109	2.064	0.746	0.836065574
	MID	5	2320	0.158	0.282	1.17	2.065	1.606	0.601	0.560283688
		6	2391	0.235	0.298	0.836	1.734	2.796	0.469	0.788590604
		7	2337	0.116	0.278	1.436	2.371	1.226	0.52	0.417266187
	MED	1	2912	0.243	0.306	0.878	1.51	2.177	0.713	0.794117647
		2	2450	0.182	0.29	1.039	1.947	1.997	0.728	0.627586207
		3	3048	0.224	0.311	0.939	1.597	2.091	0.691	0.720257235
		4	2562	0.135	0.274	1.254	2.202	1.388	0.755	0.49270073

Continued

Table A.6 Continued

819951	LAT	1	3043	0.302	0.499	1.08	1.298	1.271	0.664	0.605210421
		2	3105	0.28	0.344	0.938	1.017	1.625	0.747	0.813953488
		3	3104	0.268	0.4	1.054	1.203	1.473	0.851	0.67
		4	3118	0.251	0.324	1.058	0.954	1.409	0.848	0.774691358
	MID	5	2464	0.149	0.469	1.836	2.417	0.647	0.638	0.317697228
		6	2390	0.146	0.37	1.684	2.115	0.919	0.541	0.394594595
		7	2606	0.156	0.372	1.698	2.042	0.713	0.618	0.419354839
	MED	1	2733	0.225	0.404	1.352	1.281	0.816	0.771	0.556930693
		2	2709	0.216	0.51	1.447	1.871	0.631	0.747	0.423529412
		3	2882	0.212	0.397	1.27	1.412	1.035	0.757	0.534005038
		4	2686	0.177	0.416	1.521	2.043	0.717	0.479	0.425480769
	819996	LAT	1	3209	0.29	0.332	0.888	1.04	1.689	0.756
2			2944	0.284	0.306	0.787	1.342	2.798	0.638	0.928104575
3			3066	0.255	0.274	0.826	1.288	3.099	0.746	0.930656934
4			3014	0.281	0.286	0.753	1.2	3.135	0.73	0.982517483
MID		5	2630	0.24	0.325	1.039	1.531	2.01	0.478	0.738461538
		6	2860	0.346	0.345	0.722	1.049	2.862	0.49	1.002898551
		7	2565	0.192	0.3	1.237	1.79	1.839	0.583	0.64
MED		1	3184	0.336	0.323	0.748	0.569	1.882	0.844	1.040247678
		2	2990	0.309	0.301	0.762	0.867	2.323	0.755	1.026578073
		3	3251	0.333	0.309	0.716	0.644	2.851	0.694	1.077669903
		4	2942	0.263	0.272	0.794	1.136	2.85	0.747	0.966911765
820647		LAT	1	3089	0.296	0.323	0.825	1.067	2.141	0.751
	2		3095	0.339	0.342	0.723	0.991	3.07	0.369	0.99122807
	3		3158	0.284	0.29	0.785	1.119	3.307	0.676	0.979310345
	4		3279	0.313	0.308	0.789	0.78	2.903	0.685	1.016233766
	MID	5	2809	0.255	0.364	1.123	1.385	1.649	0.647	0.700549451
		6	3687	0.171	0.338	1.254	2.141	0.995	0.739	0.50591716
		7	2817	0.228	0.351	1.262	1.432	1.447	0.42	0.64957265
	MED	1	3423	0.386	0.357	0.726	0.209	2.228	0.839	1.081232493
		2	3039	0.317	0.386	0.852	0.975	2.108	0.689	0.821243523
		3	3759	0.374	0.402	0.74	0.55	2.804	0.716	0.930348259
		4	3097	0.241	0.313	0.956	1.337	2.213	0.751	0.769968051

Continued

Table A.6 Continued

820696	LAT	1	3718	0.23	0.289	0.827	1.94	2.744	0.611	0.795847751
		2	3437	0.258	0.282	0.701	2.129	4.134	0.553	0.914893617
		3	3750	0.264	0.315	0.791	1.73	3.147	0.665	0.838095238
		4	3448	0.216	0.296	0.888	1.958	2.765	0.705	0.72972973
	MID	5	3289	0.095	0.242	1.474	2.639	1.404	0.511	0.392561983
		6	3377	0.094	0.253	1.817	2.736	1.342	0.607	0.371541502
		7	3056	0.169	0.307	1.186	2.175	1.553	0.554	0.550488599
	MED	1	3343	0.193	0.27	0.95	1.872	2.311	0.712	0.714814815
		2	3385	0.32	0.394	0.855	1.191	1.831	0.733	0.812182741
		3	2732	0.282	0.348	0.945	1.086	2.468	0.722	0.810344828
		4	3586	0.314	0.353	0.776	1.118	2.542	0.745	0.889518414
	821228	LAT	1	3941	0.103	0.256	1.498	2.434	1.099	0.505
2			3952	0.217	0.388	1.175	2.096	1.607	0.333	0.559278351
3			3381	0.359	0.351	0.761	1.044	4.868	0.494	1.022792023
4			3847	0.209	0.31	1.052	1.666	2.009	0.695	0.674193548
MID		5	3445	0.102	0.239	2.801	2.679	2.262	0.372	0.426778243
		6	3519	0.192	0.269	1.226	2.229	4.079	0.424	0.713754647
		7	3421	0.122	0.271	1.932	2.648	2.177	0.424	0.450184502
MED		1	2760	0.254	0.356	1.179	0.695	0.719	0.826	0.713483146
		2	3270	0.341	0.373	1.025	0.852	5.268	0.434	0.914209115
		3	2909	0.274	0.36	1.082	0.611	1.093	0.805	0.761111111
		4	3548	0.184	0.249	1.103	2.286	4.242	0.572	0.738955823
821230		LAT	1	2646	0.232	0.283	0.963	1.508	2.421	0.728
	2		2643	0.266	0.288	0.772	1.46	3.198	0.518	0.923611111
	3		2621	0.236	0.258	0.887	1.532	4.053	0.733	0.914728682
	4		2791	0.291	0.281	0.718	1.096	3.392	0.729	1.035587189
	MID	5	2398	0.182	0.306	1.128	1.917	1.739	0.622	0.594771242
		6	2412	0.213	0.31	1.035	1.667	1.854	0.657	0.687096774
		7	2339	0.16	0.298	1.312	1.997	1.362	0.663	0.536912752
	MED	1	2981	0.318	0.34	0.795	0.923	2.149	0.712	0.935294118
		2	2740	0.291	0.353	0.824	1.227	2.222	0.773	0.824362606
		3	3410	0.249	0.271	0.756	1.556	3.682	0.783	0.918819188
		4	3422	0.316	0.35	0.771	2.28	3.158	0.651	0.902857143

Continued

Table A.6 Continued

820715	LAT	1	3071	0.36	0.458	0.857	1.068	1.865	0.557	0.786026201	
		2	4070	0.205	0.27	0.985	1.987	3.584	0.376	0.759259259	
		3	3138	0.293	0.307	0.752	1.137	3.165	0.688	0.954397394	
		4	3598	0.282	0.299	0.721	1.336	3.431	0.686	0.943143813	
	MID	5	2607	0.229	0.353	1.034	1.934	1.785	0.41	0.648725212	
		6	2648	0.271	0.361	0.891	1.789	2.276	0.451	0.750692521	
		7	2518	0.204	0.316	1.064	1.837	1.797	0.472	0.64556962	
	MED	1	3352	0.314	0.347	0.793	0.892	2.424	0.706	0.904899135	
		2	2903	0.272	0.305	0.782	1.348	2.688	0.682	0.891803279	
		3	3456	0.31	0.353	0.773	1.051	2.99	0.696	0.878186969	
		4	2853	0.202	0.282	0.935	1.757	2.358	0.731	0.716312057	
	819983	LAT	1	2763	0.352	0.352	0.694	0.995	2.901	0.485	1
2			2796	0.353	0.34	0.611	1.343	4.134	0.47	1.038235294	
3			2830	0.33	0.307	0.704	0.752	2.94	0.701	1.074918567	
4			2869	0.339	0.33	0.688	0.976	3.216	0.545	1.027272727	
MID		5	2468	0.222	0.314	0.97	1.714	1.867	0.63	0.707006369	
		6	2362	0.239	0.302	0.883	1.653	2.309	0.751	0.791390728	
		7	2632	0.293	0.353	0.814	1.383	2.428	0.463	0.830028329	
MED		1	3246	0.369	0.347	0.678	0.443	2.85	0.749	1.063400576	
		2	2756	0.244	0.28	0.827	1.329	2.596	0.8	0.871428571	
		3	3185	0.379	0.354	0.651	0.516	3.416	0.639	1.070621469	
		4	2809	0.247	0.314	0.881	1.437	2.235	0.742	0.786624204	
820668		LAT	1	2591	0.258	0.281	0.777	1.376	2.584	0.644	0.918149466
			2	2451	0.284	0.273	0.661	1.412	4.303	0.58	1.04029304
			3	2647	0.238	0.256	0.732	1.588	4.164	0.757	0.9296875
			4	2673	0.277	0.263	0.632	1.421	4.662	0.753	1.053231939
		MID	5	2292	0.215	0.288	0.889	1.876	2.499	0.574	0.746527778
	6		2416	0.249	0.314	0.858	1.56	1.968	0.669	0.792993631	
	7		2341	0.205	0.3	0.938	2.001	2.496	0.444	0.683333333	
	MED	1	2865	0.322	0.31	0.694	0.856	3.002	0.741	1.038709677	
		2	2637	0.266	0.283	0.767	1.27	2.707	0.761	0.939929329	
		3	2885	0.274	0.297	0.716	1.432	4.007	0.68	0.922558923	
		4	2599	0.209	0.254	0.784	1.9	4.096	0.673	0.822834646	

Continued

Table A.6 Continued

820740	LAT	1	2718	0.254	0.303	0.964	1.032	1.772	0.598	0.838283828
		2	2634	0.27	0.3	0.819	1.312	2.73	0.556	0.9
		3	2861	0.237	0.282	0.962	1.079	2.084	0.732	0.840425532
		4	2855	0.285	0.287	0.829	0.814	2.725	0.716	0.993031359
	MID	5	2389	0.166	0.295	1.269	1.834	1.345	0.58	0.562711864
		6	2457	0.19	0.295	1.193	1.542	1.454	0.728	0.644067797
		7	2495	0.218	0.297	1.041	1.581	2.164	0.623	0.734006734
	MED	1	3393	0.364	0.338	0.716	0.235	2.525	0.73	1.076923077
		2	3023	0.24	0.292	0.944	1.147	2.363	0.793	0.821917808
		3	4198	0.409	0.415	0.643	1.901	2.904	0.707	0.985542169
		4	3265	0.304	0.336	0.848	0.639	2.039	0.754	0.904761905

Catalog #	Age (Yrs.)	Condyle	BV/TV	Tb.Th Mean (mm)	Tb.Sp Mean (mm)	SMI	Conn.D (mm ³)	DA	Tb.N (mm ⁻¹)
821216	8	LAT	0.281	0.371	0.939	1.067	3.103	0.395	0.757412399
		MID	0.174	0.426	1.438	1.443	1.334	0.514	0.408450704
		MED	0.251	0.336	0.998	1.169	3.572	0.556	0.74702381
820686	9	LAT	0.212	0.263	0.87	1.059	3.073	0.671	0.80608365
		MID	0.133	0.33	1.767	1.47	0.83	0.752	0.403030303
		MED	0.178	0.272	1.142	1.018	1.67	0.738	0.654411765
821006	9	LAT	0.189	0.221	0.773	1.128	5.381	0.586	0.85520362
		MID	0.169	0.23	0.955	1.162	3.484	0.55	0.734782609
		MED	0.251	0.267	0.73	0.876	5.146	0.663	0.940074906
820732	9.5	LAT	0.19	0.195	0.697	1.204	7.023	0.584	0.974358974
		MID	0.152	0.203	0.851	1.449	4.62	0.4	0.748768473
		MED	0.208	0.201	0.643	1.103	8.056	0.638	1.034825871
820711	10.5	LAT	0.228	0.237	0.707	0.946	5.259	0.567	0.962025316
		MID	0.175	0.256	0.962	1.306	3.177	0.562	0.68359375
		MED	0.256	0.3	0.795	1.147	3.639	0.616	0.853333333
821078	11	LAT	0.262	0.309	0.732	0.809	5.02	0.639	0.84789644
		MID	0.208	0.378	1.022	0.835	2.024	0.675	0.55026455
		MED	0.321	0.401	0.971	1.229	4.013	0.56	0.800498753
820721	15	LAT	0.322	0.402	1.372	- 0.022	2.784	0.601	0.800995025
		MID	0.211	0.442	1.394	1.136	1.212	0.538	0.477375566
		MED	0.299	0.366	0.964	0.493	3.088	0.681	0.816939891
820608	15.5	LAT	0.368	0.4	0.802	0.638	1.97	0.63	0.92
		MID	0.172	0.278	1.078	1.55	2.068	0.588	0.618705036
		MED	0.332	0.344	1.223	0.503	3.573	0.505	0.965116279
819915	16	LAT	0.245	0.242	0.69	0.799	5.5	0.573	1.012396694
		MID	0.202	0.271	0.946	1.12	2.649	0.644	0.745387454
		MED	0.292	0.302	0.692	0.867	4.49	0.699	0.966887417
819964	16	LAT	0.269	0.384	1.062	0.888	1.829	0.566	0.700520833
		MID	0.159	0.274	1.23	1.271	1.55	0.621	0.580291971
		MED	0.26	0.254	0.749	0.593	3.865	0.678	1.023622047
821246	16	LAT	0.176	0.251	0.913	1.267	2.961	0.644	0.701195219
		MID	0.409	0.702	1.049	1.506	1.02	0.431	0.582621083
		MED	0.244	0.333	0.796	0.865	3.302	0.734	0.732732733

Continued

Table A.7: Average bone morphometric values in each condylar region for all individuals. LAT = Lateral Condyle; MID = Between Condyles; MED = Medial Condyle.

Table A.7 Continued

821101	16.5	LAT	0.337	0.332	0.671	0.373	3.645	0.662	1.015060241
		MID	0.228	0.351	0.939	1.137	2.508	0.458	0.64957265
		MED	0.379	0.351	0.64	0.625	3.6	0.653	1.07977208
819932	18	LAT	0.305	0.342	0.758	1.341	3.155	0.648	0.891812865
		MID	0.214	0.307	1.01	1.921	2.186	0.626	0.697068404
		MED	0.238	0.273	0.804	1.715	3.616	0.59	0.871794872
819957	19.5	LAT	0.248	0.317	0.978	1.462	1.986	0.686	0.782334385
		MID	0.16	0.279	1.23	2.119	1.583	0.643	0.573476703
		MED	0.214	0.268	0.883	1.711	3.138	0.729	0.798507463
820652	19.5	LAT	0.195	0.291	1.155	1.833	2.29	0.685	0.670103093
		MID	0.216	0.318	1.032	1.718	1.871	0.603	0.679245283
		MED	0.216	0.286	0.903	1.72	2.693	0.637	0.755244755
820658	19.5	LAT	0.317	0.329	0.713	1.076	3.505	0.68	0.963525836
		MID	0.258	0.331	0.908	1.514	2.318	0.679	0.779456193
		MED	0.294	0.317	0.769	1.228	3.245	0.649	0.927444795
819977	21.5	LAT	0.325	0.37	0.78	1.11	2.444	0.631	0.878378378
		MID	0.264	0.359	0.88	1.67	2.328	0.444	0.735376045
		MED	0.275	0.361	0.892	1.201	2.07	0.759	0.761772853
819994	22.5	LAT	0.282	0.325	0.846	1.217	2.44	0.573	0.867692308
		MID	0.217	0.364	1.262	1.493	1.082	0.695	0.596153846
		MED	0.295	0.339	0.875	0.839	1.817	0.761	0.87020649
820735	26.5	LAT	0.299	0.323	0.789	1.628	2.719	0.633	0.925696594
		MID	0.251	0.347	0.974	1.394	2.035	0.594	0.723342939
		MED	0.302	0.334	0.811	0.76	2.041	0.799	0.904191617
821042	27.5	LAT	0.276	0.298	0.769	1.25	3.074	0.667	0.926174497
		MID	0.213	0.305	0.94	1.902	2.238	0.548	0.698360656
		MED	0.266	0.312	0.8	1.807	3.278	0.669	0.852564103
819941	32.5	LAT	0.237	0.329	0.968	1.528	1.933	0.7	0.720364742
		MID	0.17	0.286	1.147	2.057	1.876	0.53	0.594405594
		MED	0.196	0.295	1.028	1.814	1.913	0.722	0.66440678
819951	32.5	LAT	0.275	0.392	1.033	1.118	1.445	0.778	0.701530612
		MID	0.15	0.404	1.739	2.191	0.76	0.599	0.371287129
		MED	0.208	0.432	1.398	1.652	0.8	0.689	0.481481481
819996	32.5	LAT	0.278	0.3	0.814	1.218	2.68	0.718	0.926666667
		MID	0.259	0.323	0.999	1.457	2.237	0.517	0.801857585
		MED	0.31	0.301	0.755	0.804	2.477	0.76	1.029900332

Continued

Table A.7 Continued

820647	32.5	LAT	0.308	0.316	0.781	0.989	2.855	0.62	0.974683544
		MID	0.218	0.351	1.213	1.653	1.364	0.602	0.621082621
		MED	0.33	0.365	0.819	0.768	2.338	0.749	0.904109589
820696	32.5	LAT	0.242	0.296	0.802	1.939	3.198	0.634	0.817567568
		MID	0.119	0.267	1.492	2.517	1.433	0.557	0.445692884
		MED	0.278	0.341	0.882	1.317	2.288	0.728	0.815249267
821228	32.5	LAT	0.222	0.326	1.122	1.81	2.396	0.507	0.680981595
		MID	0.139	0.26	1.986	2.519	2.839	0.407	0.534615385
		MED	0.263	0.335	1.097	1.111	2.831	0.659	0.785074627
821230	32.5	LAT	0.256	0.278	0.835	1.399	3.266	0.677	0.920863309
		MID	0.185	0.305	1.158	1.86	1.652	0.647	0.606557377
		MED	0.294	0.329	0.787	1.497	2.803	0.73	0.893617021
820715	35	LAT	0.285	0.334	0.829	1.382	3.011	0.577	0.853293413
		MID	0.235	0.343	0.996	1.853	1.953	0.444	0.685131195
		MED	0.275	0.322	0.821	1.262	2.615	0.704	0.854037267
819983	37.5	LAT	0.344	0.332	0.674	1.017	3.3	0.55	1.036144578
		MID	0.251	0.323	0.889	1.583	2.201	0.615	0.777089783
		MED	0.31	0.324	0.759	0.931	2.774	0.733	0.956790123
820668	37.5	LAT	0.264	0.268	0.701	1.449	3.928	0.684	0.985074627
		MID	0.223	0.3	0.895	1.812	2.321	0.562	0.743333333
		MED	0.268	0.286	0.74	1.365	3.453	0.714	0.937062937
820740	37.5	LAT	0.262	0.293	0.894	1.059	2.328	0.651	0.894197952
		MID	0.191	0.296	1.168	1.652	1.654	0.644	0.64527027
		MED	0.329	0.345	0.788	0.981	2.458	0.746	0.953623188

Catalog #	Age (Yrs.)	Condyle	Voxel Size PROX (mm)	# of slices	Min 1	Max 1	Min 2	Max 2	Min 3	Max 3
821216	8	LAT	0.04	201	3200	7504	1926	2231	1	53
		MED	0.04	201	3200	7275	1893	2093	1	53
820686	9	LAT	0.05	301	3200	8074	1806	2000	1	53
		MED	0.05	300	3200	9691	1894	2040	1	53
821006	9	LAT	0.04	201	3200	8216	2100	2718	1	53
		MED	0.04	201	3200	8346	1945	2070	1	53
820732	9.5	LAT	0.04	201	3200	8361	2137	2954	1	53
		MED	0.04	204	3200	8762	1976	2305	1	53
820711	10.5	LAT	0.05	201	3200	7868	1833	2129	1	53
		MED	0.05	301	3200	8081	1762	1944	1	53
821078	11	LAT	0.05	220	3200	7719	1799	1973	1	53
		MED	0.05	224	3200	7725	1800	1916	1	53
820721	15	LAT	0.05	227	3200	6989	1694	1859	1	53
		MED	0.05	301	3200	7668	1704	1859	1	53
820608	15.5	LAT	0.05	300	3200	6917	1744	1931	1	53
		MED	0.05	300	3200	7035	1669	1788	1	53
819915	16	LAT	0.057	214	3200	8434	1965	3107	1	53
		MED	0.057	301	3200	8040	1994	3107	1	53
819964	16	LAT	0.05	300	3200	6463	1874	2068	1	53
		MED	0.05	327	3200	6722	1845	1977	1	53
821246	16	LAT	0.05	301	3200	6286	1862	2037	1	53
		MED	0.05	301	3200	6511	1887	2076	1	53
821101	16.5	LAT	0.05	301	3200	7971	1764	1960	1	53
		MED	0.05	301	3200	7711	1863	2120	1	53
819932	18	LAT	0.056	301	2920	7829	1677	1864	1	53
		MED	0.056	271	2915	7773	1700	1821	1	53
819957	19.5	LAT	0.057	301	2547	7997	1627	1840	1	53
		MED	0.057	301	2698	7894	1686	1889	1	53
820652	19.5	LAT	0.056	301	2593	7639	1681	1892	1	53
		MED	0.056	301	2581	7745	1649	1864	1	53
820658	19.5	LAT	0.056	301	2742	8364	1645	1988	1	53
		MED	0.056	301	2605	8364	1645	2125	1	53

Continued

Table A.8: Tibial threshold values used in the cortical masking procedure for steps 1-3 of dual thresholding/segmentation in Avizo Fire 8.1.1. LAT = Lateral condyle; MED = Medial condyle; PROX = Proximal Scan

Table A.8 Continued

819977	21.5	LAT	0.057	301	2904	7952	1728	1936	1	53
		MED	0.057	318	3116	7520	1693	1897	1	53
819994	22.5	LAT	0.056	301	3200	8222	1875	2163	1	53
		MED	0.056	331	2700	8268	1821	2172	1	53
820735	26.5	LAT	0.056	361	2615	7422	1696	1979	1	53
		MED	0.056	341	2508	8135	1627	1966	1	53
821042	27.5	LAT	0.056	351	2407	8596	1581	1856	1	53
		MED	0.056	351	2444	8800	1606	1955	1	53
819941	32.5	LAT	0.056	301	2921	7553	1639	1852	1	53
		MED	0.056	301	2669	7859	1705	2150	1	53
819951	32.5	LAT	0.057	301	2369	8368	1777	2221	1	53
		MED	0.057	301	2717	8530	1811	2189	1	53
819996	32.5	LAT	0.057	301	2564	8049	1780	2136	1	53
		MED	0.057	301	2738	7935	1800	2106	1	53
820647	32.5	LAT	0.056	309	3200	8920	1845	2200	1	53
		MED	0.056	331	2616	8895	1794	2242	1	53
820696	32.5	LAT	0.056	301	2937	7583	1776	2459	1	53
		MED	0.056	301	2992	7576	1846	2419	1	53
821228	32.5	LAT	0.056	342	3153	7950	1642	1905	1	53
		MED	0.056	381	3124	7484	1598	1889	1	53
821230	32.5	LAT	0.056	331	2412	8041	1608	1876	1	53
		MED	0.056	331	2503	7927	1599	1947	1	53
820715	35	LAT	0.056	341	2673	8493	1750	2123	1	53
		MED	0.056	353	2869	8986	1812	2341	1	53
819983	37.5	LAT	0.057	327	2744	7317	1829	2150	1	53
		MED	0.057	366	2769	7545	1661	2007	1	53
820668	37.5	LAT	0.056	301	2531	8055	1687	2000	1	53
		MED	0.056	343	2542	8499	1670	2034	1	53
820740	37.5	LAT	0.056	332	2420	8400	1708	2206	1	53
		MED	0.056	361	2558	8277	1655	2031	1	53

Catalog #	Age	Condyle	Voxel Size PROX (mm)	# of slices	Subchondral Plate Mean Thickness (mm)	Subchondral Plate Max Thickness (mm)
821216	8	LAT	0.04	201	0.528	0.973
		MED	0.04	201	0.567	1.6
820686	9	LAT	0.05	301	1.446	3.28
		MED	0.05	300	1.198	2.604
821006	9	LAT	0.04	201	0.534	1.052
		MED	0.04	201	0.666	1.815
820732	9.5	LAT	0.04	201	0.507	1.04
		MED	0.04	204	0.61	1.604
820711	10.5	LAT	0.05	201	0.79	2.229
		MED	0.05	301	0.952	2.216
821078	11	LAT	0.05	220	1.289	2.492
		MED	0.05	224	1.568	3.342
820721	15	LAT	0.05	227	1.31	3.169
		MED	0.05	301	1.372	3.523
820608	15.5	LAT	0.05	300	2.146	6.9
		MED	0.05	300	1.129	3.13
819915	16	LAT	0.057	214	0.821	1.887
		MED	0.057	301	0.822	1.961
819964	16	LAT	0.05	300	1.083	2.955
		MED	0.05	327	1.213	3.225
821246	16	LAT	0.05	301	0.995	2.737
		MED	0.05	301	1.219	3.348
821101	16.5	LAT	0.05	301	1.367	2.961
		MED	0.05	301	0.873	1.921
819932	18	LAT	0.056	301	2.429	5.813
		MED	0.056	271	2.584	6.105
819957	19.5	LAT	0.057	301	1.108	2.797
		MED	0.057	301	1.018	2.052
820652	19.5	LAT	0.056	301	1.192	2.897
		MED	0.056	301	1.158	2.636
820658	19.5	LAT	0.056	301	1.777	3.315
		MED	0.056	301	1.588	3.186

Continued

Table A.9: Subchondral plate mean thickness and max thickness for all individuals. All measurements are in millimeters (mm). LAT = Lateral condyle; MED = Medial condyle; PROX = Proximal Scan

Table A.9 Continued

819977	21.5	LAT	0.057	301	2.758	6.506
		MED	0.057	318	3.354	8.754
819994	22.5	LAT	0.056	301	1.314	3.248
		MED	0.056	331	1.654	3.495
820735	26.5	LAT	0.056	361	1.79	4.072
		MED	0.056	341	1.695	3.936
821042	27.5	LAT	0.056	351	1.572	3.829
		MED	0.056	351	1.573	4.021
819941	32.5	LAT	0.056	301	1.327	2.607
		MED	0.056	301	1.659	5.688
819951	32.5	LAT	0.057	301	1.237	2.861
		MED	0.057	301	1.24	2.843
819996	32.5	LAT	0.057	301	1.394	3.666
		MED	0.057	301	1.479	3.429
820647	32.5	LAT	0.056	309	6.041	12.477
		MED	0.056	331	2.373	7.074
820696	32.5	LAT	0.056	301	3.026	9.259
		MED	0.056	301	1.54	3.721
821228	32.5	LAT	0.056	342	2.163	5.279
		MED	0.056	381	2.119	6.032
821230	32.5	LAT	0.056	331	2	5.163
		MED	0.056	331	3.076	8.424
820715	35	LAT	0.056	341	2.223	6.077
		MED	0.056	353	1.876	4.313
819983	37.5	LAT	0.057	327	1.763	4.262
		MED	0.057	366	1.743	4.332
820668	37.5	LAT	0.056	301	1.257	2.709
		MED	0.056	343	1.39	4.56
820740	37.5	LAT	0.056	332	1.025	2.617
		MED	0.056	361	1.439	3.778

APPENDIX B: Supplemental Tables from SPSS Statistics

Variable (unit)	Statistic	df	Sig.
Age (years)	0.910	57	0.000
BV/TV (%)	0.992	57	0.977
Tb.Th (mm)	0.983	57	0.625
Tb.Sp (mm)	0.902	57	0.000
SMI (-)	0.984	57	0.640
Conn.D (mm ⁻³)	0.937	57	0.005
DA (-)	0.966	57	0.110
Tb.N (mm ⁻¹)	0.979	57	0.429
Plate Ct.Th (mm)	0.982	53	0.588

Table B.1: Shapiro-Wilk Test for Normality Note: Bolded values are significant (non-parametric)

Variables (unit)	N	Minimum	Maximum	Mean	Std. Deviation
Age (years)	61	8.0	37.5	22.852	9.6843
BV/TV (%)	59	0.176	0.379	0.270164	0.0470426
Tb.Th (mm)	59	0.195	0.4020	0.313000	0.0456384
Tb.Sp (mm)	57	0.640	1.372	0.841175	0.1406745
SMI (-)	60	0.3730	1.939	1.168300	0.3695452
Conn.D (mm⁻³)	56	1.445	5.50	3.043298	0.8912423
DA (-)	58	0.5070	0.799	0.662810	0.0666419
Tb.N (mm⁻¹)	59	0.654412	1.079772	0.86349443	0.106614712
Plate Ct.Th (mm)	53	0.507	2.373	1.31994	0.450680

Table B.2: Descriptive Statistics for Variables in Lateral and Medial Condylar Regions

Test Statistics ^{a,b}								
	BV/TV	Tb.Th (mm)	Tb.Sp (mm)	SMI	Conn.D (mm ³)	DA	Tb.N (mm ⁻¹)	Plate Ct.Th (mm)
Chi-Sq	8.752	4.711	.547	5.418	17.345	10.934	.515	26.861
df	3	3	3	3	3	3	3	3
Asymp. Sig.	.033	.194	.908	.144	.001	.012	.916	.000
a. Kruskal Wallis Test								
b. Grouping Variable: Age Category								

BV/TV

Sample 1-Sam...	Test Statistic	Std. Error	Std. Test Statistic	Sig.	Adj.Sig.
1-4	-14.955	6.555	-2.281	.023	.135
1-2	-15.509	6.663	-2.328	.020	.120
1-3	-22.347	8.248	-2.709	.007	.040
4-2	.555	5.484	.101	.919	1.000
4-3	7.392	7.328	1.009	.313	1.000
2-3	-6.838	7.426	-.921	.357	1.000

Each row tests the null hypothesis that the Sample 1 and Sample 2 distributions are the same. Asymptotic significances (2-sided tests) are displayed. The significance level is .05. Significance values have been adjusted by the Bonferroni correction for multiple tests.

Conn.D

Sample 1-Sam...	Test Statistic	Std. Error	Std. Test Statistic	Sig.	Adj.Sig.
3-4	-4.631	6.896	-.672	.502	1.000
3-2	15.700	6.944	2.261	.024	.143
3-1	28.750	8.299	3.464	.001	.003
4-2	11.069	5.186	2.134	.033	.197
4-1	24.119	6.896	3.497	.000	.003
2-1	13.050	6.944	1.879	.060	.361

Each row tests the null hypothesis that the Sample 1 and Sample 2 distributions are the same. Asymptotic significances (2-sided tests) are displayed. The significance level is .05. Significance values have been adjusted by the Bonferroni correction for multiple tests.

DA

Sample 1-Sam...	Test Statistic	Std. Error	Std. Test Statistic	Sig.	Adj.Sig.
1-2	-10.357	6.664	-1.554	.120	.721
1-3	-18.494	8.249	-2.242	.025	.150
1-4	-20.409	6.556	-3.113	.002	.011
2-3	-8.137	7.426	-1.096	.273	1.000
2-4	-10.052	5.485	-1.833	.067	.401
3-4	-1.915	7.329	-.261	.794	1.000

Each row tests the null hypothesis that the Sample 1 and Sample 2 distributions are the same. Asymptotic significances (2-sided tests) are displayed. The significance level is .05. Significance values have been adjusted by the Bonferroni correction for multiple tests.

Plate Ct.Th

Sample 1-Sam...	Test Statistic	Std. Error	Std. Test Statistic	Sig.	Adj.Sig.
1-2	-6.458	5.898	-1.095	.273	1.000
1-4	-24.781	5.695	-4.352	.000	.000
1-3	-26.500	7.722	-3.432	.001	.004
2-4	-18.322	5.240	-3.497	.000	.003
2-3	-20.042	7.393	-2.711	.007	.040
4-3	1.719	7.232	.238	.812	1.000

Each row tests the null hypothesis that the Sample 1 and Sample 2 distributions are the same. Asymptotic significances (2-sided tests) are displayed. The significance level is .05. Significance values have been adjusted by the Bonferroni correction for multiple tests.

Table B.3: Age Category Independent Sample Kruskal-Wallis Test with Bonferroni correction

Variables	Age Category	N	Mean	Std. Deviation	Std. Error Mean
BV/TV	1	11	.234182	.0443031	.0133579
	2	20	.277500	.0562677	.0125818
	3	8	.290000	.0190338	.0067295
	4	20	.274700	.0329531	.0073685
Tb.Th Mean (mm)	1	11	.282364	.0681077	.0205352
	2	20	.319200	.0482271	.0107839
	3	8	.332750	.0239628	.0084721
	4	20	.315750	.0249671	.0055828
Tb.Sp Mean (mm)	1	11	.842455	.1546249	.0466212
	2	19	.858632	.1862377	.0427259
	3	8	.820250	.0455561	.0161065
	4	19	.831789	.1103734	.0253214
SMI	1	11	1.079909	.1219307	.0367635
	2	19	1.052474	.4748600	.1089404
	3	8	1.226500	.3547285	.1254155
	4	22	1.291364	.3286175	.0700615
Conn.D (mm ⁻³)	1	8	4.132500	.9539245	.3372633
	2	19	3.144474	.8382980	.1923188
	3	8	2.485375	.5140617	.1817483
	4	21	2.680476	.5735647	.1251621
DA	1	10	.615500	.0577163	.0182515
	2	19	.653947	.0473268	.0108575
	3	8	.686500	.0783527	.0277019
	4	21	.684333	.0713375	.0155671
Tb.N (mm ⁻¹)	1	10	.82582481	.096622620	.030554755
	2	20	.86980033	.123957639	.027717771
	3	8	.87333461	.052685707	.018627210
	4	21	.87167808	.111063898	.024236130
Subchondral Plate Mean Thickness (mm)	1	12	.88792	.390111	.112615
	2	16	1.15356	.240299	.060075
	3	6	1.59967	.162080	.066169
	4	19	1.64458	.389856	.089439

Table B.4: Mean Statistics for All Variables by Age Category

Ranks				
		N	Mean Rank	Sum of Ranks
BTVV MED - BTVV LAT	Negative Ranks	10 ^a	18.75	187.50
	Positive Ranks	19 ^b	13.03	247.50
	Ties	0 ^c		
	Total	29		
a. BTVV MED < BTVV LAT				
b. BTVV MED > BTVV LAT				
c. BTVV MED = BTVV LAT				

Test Statistics ^a	
BTVV MED - BTVV LAT	
Z	-.649 ^b
Asymp. Sig. (2-tailed)	.516
a. Wilcoxon Signed Ranks Test	
b. Based on negative ranks.	

Ranks				
		N	Mean Rank	Sum of Ranks
TBTH MED - TBTH LAT	Negative Ranks	12 ^a	15.13	181.50
	Positive Ranks	16 ^b	14.03	224.50
	Ties	1 ^c		
	Total	29		
a. TBTH MED < TBTH LAT				
b. TBTH MED > TBTH LAT				
c. TBTH MED = TBTH LAT				

Test Statistics ^a	
TBTH MED - TBTH LAT	
Z	-.490 ^b
Asymp. Sig. (2-tailed)	.624
a. Wilcoxon Signed Ranks Test	
b. Based on negative ranks.	

Continued

Table B.5: Pairwise Related Samples Wilcoxon Signed Ranks Test for All Structural Parameters

Table B.5 Continued

Ranks				
		N	Mean Rank	Sum of Ranks
TBSP MED - TBSP LAT	Negative Ranks	13 ^a	13.35	173.50
	Positive Ranks	13 ^b	13.65	177.50
	Ties	0 ^c		
	Total	26		
a. TBSP MED < TBSP LAT				
b. TBSP MED > TBSP LAT				
c. TBSP MED = TBSP LAT				

Test Statistics ^a	
TBSP MED - TBSP LAT	
Z	-.051 ^b
Asymp. Sig. (2-tailed)	.959
a. Wilcoxon Signed Ranks Test	
b. Based on negative ranks.	

Ranks				
		N	Mean Rank	Sum of Ranks
SMI MED - SMI LAT	Negative Ranks	17 ^a	14.71	250.00
	Positive Ranks	13 ^b	16.54	215.00
	Ties	0 ^c		
	Total	30		
a. SMI MED < SMI LAT				
b. SMI MED > SMI LAT				
c. SMI MED = SMI LAT				

Test Statistics ^a	
SMI MED - SMI LAT	
Z	-.360 ^b
Asymp. Sig. (2-tailed)	.719
a. Wilcoxon Signed Ranks Test	
b. Based on positive ranks.	

Continued

Table B.5 Continued

Ranks				
		N	Mean Rank	Sum of Ranks
CONND MED - CONND LAT	Negative Ranks	13 ^a	15.31	199.00
	Positive Ranks	13 ^b	11.69	152.00
	Ties	0 ^c		
	Total	26		
a. CONND MED < CONND LAT				
b. CONND MED > CONND LAT				
c. CONND MED = CONND LAT				

Test Statistics ^a	
CONND MED - CONND LAT	
Z	-.597 ^b
Asymp. Sig. (2-tailed)	.551
a. Wilcoxon Signed Ranks Test	
b. Based on positive ranks.	

Ranks				
		N	Mean Rank	Sum of Ranks
TBN MED - TBN LAT	Negative Ranks	17 ^a	13.24	225.00
	Positive Ranks	11 ^b	16.45	181.00
	Ties	0 ^c		
	Total	28		
a. TBN MED < TBN LAT				
b. TBN MED > TBN LAT				
c. TBN MED = TBN LAT				

Test Statistics ^a	
TBN MED - TBN LAT	
Z	-.501 ^b
Asymp. Sig. (2-tailed)	.616
a. Wilcoxon Signed Ranks Test	
b. Based on positive ranks.	

Continued

Table B.5 Continued

Ranks				
		N	Mean Rank	Sum of Ranks
DA MED - DA LAT	Negative Ranks	7 ^a	10.93	76.50
	Positive Ranks	21 ^b	15.69	329.50
	Ties	0 ^c		
	Total	28		
a. DA MED < DA LAT				
b. DA MED > DA LAT				
c. DA MED = DA LAT				

Test Statistics ^a	
DA MED - DA LAT	
Z	-2.881 ^b
Asymp. Sig. (2-tailed)	.004
a. Wilcoxon Signed Ranks Test	
b. Based on negative ranks.	

Ranks				
		N	Mean Rank	Sum of Ranks
CT TH MED - CT TH LAT	Negative Ranks	10 ^a	15.70	157.00
	Positive Ranks	16 ^b	12.13	194.00
	Ties	0 ^c		
	Total	26		
a. CT TH MED < CT TH LAT				
b. CT TH MED > CT TH LAT				
c. CT TH MED = CT TH LAT				

Test Statistics ^a	
CT TH MED - CT TH LAT	
Z	-.470 ^b
Asymp. Sig. (2-tailed)	.638
a. Wilcoxon Signed Ranks Test	
b. Based on negative ranks.	

Group Statistics

	Condyle No	N	Mean	Std. Deviation	Std. Error Mean
BV/TV	1	30	.265167	.0468498	.0085536
	2	29	.275345	.0449796	.0083525
Tb.Th Mean (mm)	1	30	.309133	.0505253	.0092246
	2	29	.317000	.0404713	.0075153
Tb.Sp Mean (mm)	1	31	.853839	.1623057	.0291510
	2	26	.826077	.1108169	.0217330
SMI	1	31	1.160677	.4054650	.0728237
	2	30	1.136500	.3943512	.0719984
Conn.D (mm ⁻³)	1	30	3.082600	1.0485846	.1914445
	2	26	2.942308	.6384574	.1252118
DA	1	30	.634067	.0577969	.0105522
	2	28	.693607	.0623398	.0117811
Tb.N (mm ⁻¹)	1	31	.86355597	.108360157	.019462059
	2	28	.86342629	.106633756	.020151886
Subchondral Plate Ct.Th (mm)	1	26	1.30046	.466891	.091565
	2	27	1.33870	.442581	.085175

Table B.6: Mean Statistics for All Variables by Condyle Region
Note: Lateral Condyle = 1, Medial Condyle = 2

Test Statistics ^a								
	BV/TV	Tb.Th Mean (mm)	Tb.Sp Mean (mm)	SMI	Conn.D (mm ³)	DA	Tb.N (mm ⁻¹)	Plate Ct.Th
Mann-Whitney U	113.00 0	130.000	163.000	100.00 0	149.000	172.50 0	124.000	116.00 0
Wilcoxon W	266.00 0	266.000	394.000	353.00 0	402.000	343.50 0	277.000	287.00 0
Z	-1.924	-1.361	-.153	-2.664	-.798	-.465	-1.784	-1.671
Asymp. Sig. (2-tailed)	.054	.174	.878	.008	.425	.642	.074	.095
Exact Sig. [2*(1-tailed Sig.)]	.056 ^b	.181 ^b	.892 ^b	.007 ^b	.438 ^b	.646 ^b	.077 ^b	.098
a. Grouping Variable: SEX								
b. Not corrected for ties.								

Table B.7: Mann Whitney Test Comparing Structural Parameters Between Sexes